Doctoral theses at NTNU, 2013:218

Tobias Danner

Reactivity of Calcined Clays

Doctoral Thesis

Tobias Danner

ISBN 978-82-471-4552-4 (printed version)
ISBN 978-82-471-4553-1 (electronic version)
ISSN 1503-8181

NTNU – Trondheim
Norwegian University of
Science and Technology

NTNU
Norwegian University of Science and Technology
Thesis for the degree of Philosophiae Doctor
Faculty of Natural Sciences and Technology
Department of Materials Science and Engineering

Doctoral theses at NTNU, 2013:211

NTNU

NTNU – Trondheim
Norwegian University of
Science and Technology

Tobias Danner

Reactivity of Calcined Clays

Thesis for the degree of Philosophiae Doctor

Trondheim, August 2013

Norwegian University of Science and Technology
Faculty of Natural Sciences and Technology
Department of Materials Science and Engineering

NTNU – Trondheim
Norwegian University of
Science and Technology

NTNU
Norwegian University of Science and Technology

Thesis for the degree of Philosophiae Doctor

Faculty of Natural Science and Technology
Department of Natural Sciences and Engineering

ISBN 978-82-471-4552-4 (printed version)
ISBN 978-82-471-4553-1 (electronic version)
ISSN 1503-8181

Doctoral theses at NTNU, 2013:218

Printed by Skipnes Kommunikasjon as

Preface

This thesis is submitted to the Norwegian University of Science and Technology (NTNU) in partial fulfillment of the requirements for the degree of Philosophiae doctor. The doctoral work has been performed at the Department of Materials Science and Technology at NTNU under supervision of adjunct Professor Harald Justnes (Chief Scientist at SINTEF Building and Infrastructure) and Professor Kjell Wiik. The work was financed by Saint-Gobain Weber and initiated by Geir Norden who was industrial supervisor of this thesis.

Initially the project started with investigations on the Søvind Marl from Denmark as pozzolana for cementitious based materials and was conducted within the COIN group (www.coinweb.no) for Saint-Gobain Weber. With increasing interest of the industrial partner in calcined clays and the conceivable great potential of own clay deposits for the production of pozzolanic materials, this project was outsourced from COIN and it was decided to carry out further studies within a PhD thesis at NTNU financed as a whole by Saint-Gobain Weber. As the outcome of the thesis is of great interest for Saint-Gobain Weber, the main results were not published at this point and rather written as a monograph.

Still, parts of the thesis have been presented at international conferences:

- Tobias Danner, Tone Østnor, Harald Justnes, "Calcined Marl as a Pozzolan for Sustainable Development of the Cement and Concrete Industry", 12th International Conference on Recent Advances in Concrete Technology and Sustainability Issues, Nov.2012, Prague, pp. 357-365

- Tobias Danner, Tone Østnor, Harald Justnes, "Thermally Activated Marl as a Pozzolan for Cementitious Based Products", 5th Conference on the Concrete Future, May 2013, Covilha

Acknowledgement

First and foremost I would like to express my gratitude to my main supervisor, Adjunct Professor Harald Justnes, for accepting me as his PhD student and his guidance throughout this work. His valuable and fast responses and comments on drafts of the thesis and papers, his motivation, ideas, broad knowledge and scientific skills are greatly acknowledged.
I also want to thank my co-supervisor, Professor Kjell Wiik, for his solid support, his contributions, insightful comments and help with all kinds of matters during the last 3 years.
Furthermore I would like to thank Saint-Gobain Weber for giving me the trust to accomplish this PhD study and for the financial support of the thesis. Special thanks go to my industrial supervisor, Geir Norden. His interest, support, enthusiasm and positive nature have been very encouraging. Thanks for great discussions and giving me an insight to the industrial life. I also want to thank Oddvar Hyrve for following my scientific development and progress with interest and his great input at several meetings.
I want to express my sincere gratitude to Tone Østnor, for being very supportive from the first day. Her immediate help with all kind of issues, all her contributions of time and energy, as well as her enthusiasm, encouragement and interest in the topic and the progress was much appreciated.

I am grateful for all colleagues, co-workers and employees at NTNU, SINTEF (the COIN-group) and Saint-Gobain who contributed in different ways to this work, for creating a great, inquiring and inspiring working environment. Many people contributed to my personal and professional time in Trondheim. The technical staff is acknowledged for being very helpful and providing instant assistance when help was needed with all kinds of practical matters, handling instruments or other scientific challenges. Especially the support with mortar tests by Stig Roar Rudolfsen and Knut Lervik was very helpful. Thanks to Julian Tolchard for assistance in the XRD lab, Morten Peder Raanes for help with EPMA investigations and Syverin Lierhagen for performing HR-ICP-MS measurements.

The last three years have been a great time and I am also very grateful for all the new friends amongst the colleagues and the social activities. Especially being part of the institutes football team (PolyCrystal Palace) was great fun.

Last but not least I want to express my gratitude to my family and friends for their support and patience, for listening and helping to recharge my batteries.

Abstract

With 3-5 billion tons cement-produced every year, the cement industry is today the third largest emitter of CO_2 in the world after fossil-fuel based energy plants serving heating/cooling of buildings and combustion engines in the transport sector. In a short time, the easiest way to reduce CO_2 emission attributed to cement making is to replace a large portion of portland clinker in cement making blended cements, or to replace a part of portland cement in the concrete mixing operation with a suitable supplementary cementing material (SCM). However, with increasing trend of making "greener" construction materials, there is a need to look for unexploited pozzolan reserves. Common clays are a large, wide spread resource with great pozzolanic potential when calcined to serve not only the local but also the global cement market.

In this study the pozzolanic reactivity of common calcined clayey soils from different regions in Europe with varying mineralogy containing substantial amounts of non clay minerals was investigated by means of calcium hydroxide consumption and mortar strength tests with up to 65 % replacement of OPC. A clear correlation between mineralogy and reactivity was found showing that kaolinite rich clays (AB1080) are most reactive. However, also a smectite rich clay containing large amounts of calcium carbonate (Søvind Marl) showed good pozzolanic reactivity, while the actual origin of calcium carbonate seems to play an important role.
The compressive strength of mortars with a replacement of up to 50 % OPC by the calcined marl or the calcined kaolinite rich clay was equal or higher than the reference mortar with 100 % OPC at 28 days. The early strength was sufficient for demoulding concrete in-field practice.

For the main investigations the clays were burned in a pilot scale installation at IBU-tec in Germany at temperatures between 700-800 °C. To gain a better knowledge about the reactivity of calcined clays, e.g. due to structural modifications of the clay phases, phase transformations and microstructural changes, the raw and calcined state of the investigated clays was characterized with XRD, TG/DTG, BET, PSD, ICP-MS, SEM, FT-IR, ^{27}Al-MAS-NMR and Mössbauer Spectroscopy. The heat treatment upon complete dehydroxylation of the clay minerals accompanied with oxidation of iron in the clay minerals (if present) induces significant structural distortions leading to metastable reactive phases. In the presence of large amounts of calcium carbonate a reactive vitreous phase forms in the calcined state.

The early and long term hydration reactions occurring in calcined clay/lime and calcined clay/cement pastes were studied with XRD, TG/DTG, SEM and isothermal calorimetry. In reactive clays the pozzolanic reaction can start during the first 24 h. AFm phases especially hemi- and mono-carboaluminate hydrates are the favored hydration products formed, but also strätlingite was found in kaolinite rich clays. At long curing times or a higher hydration temperature hydrogarnet (katoite) was detected as well. Substitution of iron for aluminum in calcium aluminate hydrate phases and substitution of aluminum for silicon in C-S-H phases is very common.

The two most reactive clays of this study (AB1080 & Søvind Marl) were burned additionally in a lab scale electrical furnace to test the influence of cooling rate, retention time and particle size distribution on the pozzolanic reactivity by means of calcium hydroxide consumption in calcined clay/lime pastes. Retention time and cooling rate do not influence the reactivity while the particle size affects the reactivity considerably.

Moreover two full scale industrial trials were performed at existing and operating LECA-plants from Saint-Gobain Weber. The tests indicated that it is possible to produce calcined clay/marl of good homogeneous quality on an economically basis without changing the equipment.

The calcination temperature of highest reactivity depends on the mineralogy of the raw material and the atmosphere in the kiln. With good knowledge about the raw material, the measurement of the LOI of the respective calcined clay can serve as a quality test to assess the pozzolanic reactivity of the final material.

Table of Contents

Glossary – Notation

In parts of this work the cement chemist notation for the main oxides is used as simplification for the complex formulae of compounds present in cement chemistry.

Cement Notation:
Oxides that are frequently used in cementitious materials are abbreviated:

Notation	Actual Formula	Name
C	CaO	Calcium oxide
S	SiO_2	Silicon dioxide, silica
A	Al_2O_3	Aluminum oxide, alumina
F	Fe_2O_3	Ferrous Iron oxide
f	FeO	Ferric Iron oxide
T	TiO_2	Titanium oxide
M	MgO	Magnesium oxide
K	K_2O	Potassium oxide
N	Na_2O	Sodium oxide
H	H_2O	Water
$\bar{s}$	SO_3	Sulfur trioxide
$\bar{c}$	CO_3	Carbon dioxide

Common phases in cementitious systems with their cement notation and actual chemical formula:

Mineral Name	Cement Notation	Chemical Formula
Clinker Phases		
Alite (Hatrurite)	**C_3S**	Ca_3SiO_5
Belite (Larnite)	**C_2S**	Ca_2SiO_4
Aluminate (Tricalcium Aluminate)	**C_3A**	$Ca_3Al_2O_6$
Ferrite (Brownmillerite)	**$C_2(A,F)$**	$Ca_2(Al_xFe_{1-x})_2O_5$
Calcite	**$C\bar{c}$**	$CaCO_3$
Gypsum	**$C\bar{s}H_2$**	$CaSO_4 \cdot 2\ H_2O$
Bassanite	**$C\bar{s}H_{0.5}$**	$CaSO_4 \cdot ½\ H_2O$
Anhydrite	**$C\bar{s}$**	$CaSO_4$

Hydration Products		
Portlandite (Lime)	**CH**	$Ca(OH)_2$
Ettringite (AFt-phases)	$C_3A \cdot 3C\bar{s} \cdot H_{32}$ **($C_6A\bar{s}_3H_{32}$)**	$Ca_6[Al(OH)_6]_2(SO_4)_3 \cdot 26\ H_2O$
Mono-sulphoaluminate hydrate (AFm-phases)	$C_3A \cdot C\bar{s} \cdot H_{12\text{-}16}$ **($C_4A\bar{s}H_{12\text{-}16}$)**	$Ca_4[Al(OH)_6]_2SO_4 \cdot 10\text{-}14\ H_2O$
Mono-carboaluminate hydrate	$C_3A \cdot C\bar{c} \cdot H_{11}$ **($C_4A\bar{c}H_{11}$)**	$Ca_4[Al(OH)_6]_2(CO_3) \cdot 5\ H_2O$
Hemi-carboaluminate hydrate	$C_3A \cdot ½\ C\bar{c} \cdot ½\ CH \cdot\ H_{11}$ **($C_4A\bar{c}H_{12}$)**	$Ca_4[Al(OH)_6]_2(CO_3)_{0.5} \cdot 6\ H_2O$
Calcium-silicate-hydrate	**C-S-H**	$Ca_5Si_6O_{16}(OH)_2 \cdot 4H_2O$
Katoite (Hydrogarnet)	**C_3AH_6**	$Ca_3[Al[(OH)_6]_2$
Strätlingite	**C_2ASH_8**	$Ca_2Al_2(SiO_2)(OH)_{10} \cdot 2.5\ H_2O$
Gibbsite	**AH**	$Al(OH)_3$
Tetracalcium-aluminate hydrate	**C_4AH_{13}**	$Ca_4[Al(OH)_6]_2 \cdot 7\ H_2O$

Other mineral phases named in this work. The chemical formulae are according to **www.webmineral.com** and **www.mindat.org**:

Mineral Name	Chemical Formula
Clay Minerals:	
Kaolinite	$Al_2Si_2O_5(OH)_4$
Metakaolin	$Al_2Si_2O_5$
Illite	$(K,H_3O)(Al,Mg,Fe)_2(Si,Al)_4O_{10}[(OH)_2,(H_2O)]$
Smectite-Group:	
Montmorillonite	$(Na,Ca)_{0,3}(Al,Mg)_2Si_4O_{10}(OH)_2 \bullet n(H_2O)$
Nontronite	$Na_{0.3}\,Fe^{3+}{}_2(Si,Al)_4O_{10}(OH)_2 \bullet n(H_2O)$
Saponite	$(Ca_{0.5},Na)_{0,3}(Mg,\ Fe^{2+})_3(Si,Al)_4O_{10}(OH)_2 \bullet 4(H_2O)$
Beidellite	$Na_{0.5}Al_2(Si_{3.5}Al_{0.5})O_{10}(OH)_2 \bullet n(H_2O)$
Clinochlore (Chlorite)	$(Mg,\ Fe^{2+})_5Al(Si_3Al)O_{10}(OH)_8$

Non-clay Minerals:	
Akermanite	$Ca_2MgSi_2O_7$
Albite	$NaAlSi_3O_8$
Andalusite	Al_2SiO_5
Anorthite	$CaAl_2Si_2O_8$
Augelite	$Al_2(PO_4)(OH)_3$
Apatite	$Ca_5(PO_4)_3(OH,F,Cl)$
Barite	$BaSO_4$
Biotite	$K(Mg, Fe^{2+})_3[AlSi_3O_{10}(OH,F)_2$
Brucite	$Mg(OH)_2$
Calcite	$CaCO_3$
Cristoballite	SiO_2
Diopside	$CaMgSi_2O_6$
Dolomite	$CaMg(CO_3)_2$
Gehlenite	$Ca_2Al(AlSi)O_7$
Goethite	$Fe^{3+}O(OH)$
Hematite	Fe_2O_3
Ilmenite	$Fe^{2+}TiO_3$
Lepidocrocite	γ - $Fe^{3+}O(OH)$
Mullite	$Al_6Si_3O_{13}$
Muscovite	$KAl_2(Si_3Al)O_{10}(OH,F)_2$
Orthoclase	$KAlSi_3O_8$
Pyrite	FeS_2
Quartz	SiO_2
Rutile	TiO_2
Siderite	$FeCO_3$
Spinel (Common)	$MgAl_2O_4$
Tourmaline – Groupe	Na $Fe^{2+}{}_3Al_6(BO_3)_3Si_6O_{18}(OH)_4$ (Schorl)
Wollastonite	$CaSiO_3$
Zeolithe –Groupe	$NaAlSi_2O_6 \cdot H_2O$ (Analcim)
Zircon	ZrO_2

Methods used in this work:

XRD	X-Ray Diffraction
XRF	X-Ray Fluorescence Analysis
TG	Thermal Gravimetry
DTA/DTG	Differential Thermal Analysis/Gravimetry
PSD	Particle Size Distribution
BET	Specific Surface Area ("BET" Surface)
FT-IR	Fourier Transformed – Infrared Spectroscopy
HR-ICP-MS	High Resolution – Inductively Coupled Plasma – Mass Spectrometry
SEM	Scanning Electron Microscope
BEI	Backscattered Electron Image
EPMA	Electron Probe Micro Analyzer
MAS-NMR	Magic Angle Spinning – Nuclear Magnetic Resonance

Other abbreviations:

OPC	Ordinary Portland Cement
w/b	water to binder ratio
SCM	Supplementary Cementitious Material
GBFS	Granulated Blast Furnace Slag
MK	Metakaolin
M	Molecular Mass
° 2θ	diffraction angle
Å	Ångstrøm
LOI	Loss on Ignition
MIR	Mid Infrared
FWHM	Full Width of Half Maximum
SØ	Søvind Marl
H2-H4	3 Boreholes from Søvind Marl deposit
lime	calcium hydroxide (CH)
AIPEA	Association Internationale pour l'Etude des Argiles
CMS	Clay Minerals Society
EDTA	Ethylene diamine tetraacetic acid

1 Introduction

1.1 General

Concrete is the most important and fundamental building material for our society and will also remain the key material to satisfy global housing and future infrastructural needs. When it comes to volumes produced and annually consumed, concrete is only second to water [1-2]. Concrete is a mixture of sand, gravel and cement, whereas cement works as the binder between the other two. Cement is the essential material that solidifies the concrete due to a hydration reaction with water and is thus used in increasingly considerable volumes. In 2011 the worldwide cement production reached a value of about 3.4-3.6 billion tons [3-4].

For manufacturing cement, a homogenized and finely grained raw meal, mainly consisting of the components SiO_2, CaO, Al_2O_3 and Fe_2O_3 is burnt at temperatures of 1450 °C [5]. The raw material for this process is usually a mixture of limestone and clays or marl [6]. During the burning process the different components react with each other and form new crystalline phases through sintering processes. The resulting product is called the cement clinker. The main phases are Ca_3SiO_5 (C_3S), Ca_2SiO_4 (C_2S), $Ca_3Al_2O_6$ (C_3A) and a ferrite phase called Brownmillerite with the composition $Ca_4Al_2Fe_2O_5$ (C_4AF) [7]. Calcium sulphate is added to the cooled clinker to regulate the setting behaviour before grinding it to a fine powder.

However, accompanied with the popularity of this material in use for construction there is also an ever greater discussion emerging about environmental concerns regarding the cement industry. Only few know that as a consequence of the increasing demand for housing and buildings the cement industry is nowadays third biggest CO_2 emitter after housing and transport. Today the cement industry contributes 5-7 % of the worldwide carbon dioxide emissions [8-9]. Because of the ongoing upward trend in economical development especially in Asia the demand for cementitious materials will further increase in the future.

Manufacturing of cement is a highly energy intensive process taking into account all steps from raw material mining to the final product. For the production of one ton Portland cement clinker almost one ton of carbon dioxide is emitted, depending on the used technology (thermal efficiency of the kiln). In numbers the global average gross CO_2 emission per tonne of clinker was 866 kg CO_2 in 2006 [1]. The World Business Council for Sustainable Development provides ideas and approaches to reduce this level of CO_2 emissions to about 50 % up to 2050 [2].

About 60 % of the CO_2 emissions are due to the decomposition of limestone during firing (Eq. 1). A comparison of the molar masses shows that almost half of the mass of $CaCO_3$ is emitted as CO_2. The remaining 40 % are combustion related

emissions like the use of fossil fuels as well as the energy requirement during processes like drying or grinding [1-2].

(1) $CaCO_3$ (M = 100.09 g/mol) → $CaO + CO_2$ (M = 44.01 g/mol)

There are mainly four different possibilities today to reduce the carbon dioxide emissions during the cement production [2,8]:

- Energy Efficiency Improvement
- Replacing High-Carbon Fuels with Low-Carbon Fuels
- Carbon Dioxide removal from flue gases
- **Blended Cements - Make cement with less clinker content**

However due to an increasing economical and political pressure the cement and concrete industry was subject to an ongoing intensive modernization, equipping cement manufacturing plants with new, greener technologies and making them highly efficient. The upper limit for energy-efficiency is almost reached and the potential to improve the thermal energy efficiency of existing kilns through operational optimization is very small. In the years between 1990 and 2006 there was only little or no improvement in average thermal efficiency per kiln type [1]. Where possible, alternative fuels are used in the cement industry but there are a number of issues that should be considered. Alternative fuels can influence the clinker properties by incorporating unusual elements into the clinker and by having a different burning behaviour [10]. The use of waste-derived fuels is furthermore limited to political restrictions [2,8]. The use of natural gas is no option for the cement industry since it has a much greater reduction potential of CO_2 per unit of thermal energy when used in other sectors [1]. Carbon dioxide capture and storage is a relatively new technology with no practical experience in the cement industry. In the future this could help to reduce the emissions significantly. Nevertheless by now it is a not very cost-effective method and more research needs to be undertaken [2,8,10].
Consequently the biggest step towards further reducing CO_2 emissions in the future can be achieved by producing new cements, either by using other calcium sources than calcium carbonate or by reducing the clinker content with the addition of supplementary cementitious materials. The substitution of clinker with other materials in so called “Blended Cements” is the most effective way to reduce the specific CO_2 emissions in the short term [8,10-11].
Many natural as well as synthetic supplementary cementitious materials (SCM`s) are known to be suitable materials for reducing the clinker content and simultane-

ously maintaining or enhancing the properties of the product. For the long term the right choice of the replacing material is mainly a question of availability [12]. Popular replacement-materials in practice are industrial by-products like granulated blast furnace slag (GBFS) from the steel industry or fly ash from coal power plants. The availability of these materials is limited and cannot meet the future demand of the large cement industry on a sustained basis. Furthermore as they are derived from processes associated with CO_2 emissions themselves their supply may drop in the long run when coal fired power plants and blast furnace plants are replaced by less CO_2 intensive processes [10-11].
On the other hand the full potential of natural pozzolanic materials is not yet reached. Especially clays are abundant and widespread with huge deposits distributed all over the world. Mining and transportation costs would be rather low so that these materials are probably the only available to serve the cement industry sufficiently for a sustainable future [10-11].
Calcining clays at temperatures usually between 600-800 °C, depending on the mineral composition, leads to the formation of an active metastable state with high pozzolanic activity [13]. Many countries already start to investigate their local clay deposits and to assess their potential for the local cement industry since it could be shown that blended cements with 20 % or more calcined clay can reach, besides other positive side effects, a higher strength after 28 days as with no replacement. By using blended cements with calcined clay energy costs as well as the specific CO_2 emissions can be reduced considerably in the long term.

However clays are very complex materials regarding the chemical compositions and the crystal structures. It is less known about chemical and structural changes in the material upon heating and the effects that contribute to the high reactivity, making the calcined clays suitable as a pozzolanic material. To increase the use of calcined clays as supplementary cementitious materials more research is needed to understand the mechanisms of these materials and how they work together with cement.

1.2 Objectives of the thesis

The aim is to develop a pozzolana for cementitious based products by calcining ordinary “blue” clay. In order to utilize calcined clay as a pozzolana, and possibly to introduce it as a new product to the market, it must be understood how and why mixed “blue” clays work as a pozzolana when they are calcined. Therefore several issues like the following have to be solved and investigated in detail.

- What makes the calcined clay reactive to form cementitious binder in reaction with lime (CH)?
- What structural/microstructural alterations occur in the single minerals and the matrix upon heating?
- Which changes in the chemical and physical properties does the heating cause?
- Is the total integration between the different clay minerals and accessories responsible for the reactivity or is it just parts of the particle surfaces?
- Why are calcined mixed clays comparable to metakaolin in performance?
- Is there a minimum kaolinite or a maximum illite content to generate an effective pozzolana?
- Is there one mechanism, one universal feature to explain the reactivity of common calcined “blue” clays or is it several mechanisms for different clays?

Additionally the pozzolanic reactions of different calcined clays with calcium hydroxide or cement should be investigated for better understanding of:

- Which clay mineral forms which hydration product in combination with calcium hydroxide or cement
- Lime consumption of different clay minerals

In order to check the influence of atmosphere and different possible production conditions the clays were burned at different installations, lab-scale, pilot-scale and on industrial scale with varying parameters and the reactivity was compared.

After gaining detailed knowledge about the mechanism of calcined clays as pozzolana it is requested to develop easy testing methods to

- Identify or predict the reactivity
- Guarantee quality insurance and reproducibility of the material

1.3 Experimental approach

Clay fields from different parts of Europe with different clay mineral composition were chosen for this study (e.g. kaolinite, illite and smectite rich clays). The studied clays are in most cases located nearby existing Leca Plants of Saint-Gobain Weber with free capacity of a rotary kiln. Reason is the advantage in location in case one of the clays is suitable for the production of calcined clay as pozzolanic admixture for cementitious based products.
A sketch of the course of action for the first part of the work is shown in Figure 1-1. Details about the different methods will be described in chapter 3.

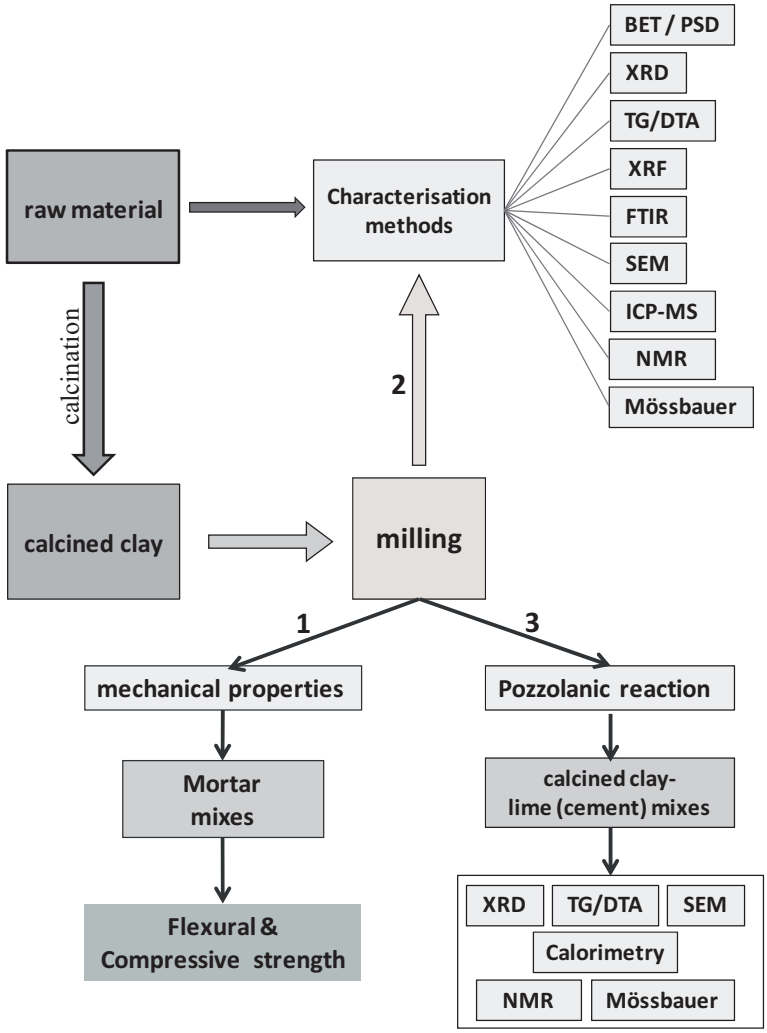

Figure 1-1: Methodical procedure for the first main chapter of the thesis

First of all it was important to obtain the exact chemical and mineralogical composition of the different clays (XRF, XRD). In the first part of the work all clays were send to IBU-tec (Weimar, Germany) for pilot production of calcined clay were they were fired at different temperatures in a small rotary kiln. The calcined clays were milled down to a $d_{50} < 10$ µm at UVR-FIA (Freiberg, Germany) before they were analysed at NTNU in Trondheim. First tests performed with the calcined clays were mortar tests with a replacement of 20 % OPC by calcined clay to check the compressive & flexural strength. It was crucial to find out if the mortars with calcined clay achieve higher strength than the reference mortar with no OPC replacement and at which temperature the different clays are most reactive. The reactivity of the different clays was then furthermore tested in clay/lime pastes with regard to their calcium hydroxide consumption (pozzolanic reaction). To work out why some clays are more reactive than others different spectroscopic methods were applied to detect any structural changes upon calcination. SEM was performed to get information about micro-structural changes in the clays with calcination. Furthermore BET and PSD was done to see the effect of particle size and specific surface on the reactivity. The clay/lime pastes for pozzolanic reaction were also investigated with regard to their hydration products applying methods like XRD, TG/DTA & SEM. To some extent the most reactive clays were investigated in more detail and methods like NMR, and Mössbauer spectroscopy were performed additionally.

In the second part, the most reactive clays were also calcined at laboratory scale in an electrical chamber furnace. Here the clays were burnt over a wider temperature range. Main aim was to check the influence of fast and slow cooling as well as retention time and particle size, on the reactivity of calcined clays and to compare the reactivity to the clays from pilot production, regarding lime consumption.

In the third big chapter the results of full scale industrial trials are discussed. The clays that showed the most promising results in the mortar tests were calcined on an industrial level to check if the material could be produced economically with homogeneous quality using existing Leca-plants from Saint-Gobain Weber without changing too much equipment.

2 Background

2.1 Clays and Clay Minerals

2.1.1 Definitions

A uniform definition of the term clay or clay materials does not exist yet, since it is very difficult to find a terminology that fulfils the specifications of all different disciplines working with clays as well as users and producers. The term clay can indicate a rock, a sedimentary deposit, and the alteration (weathering) products of primary silicate minerals [14]. Since the beginning of clay science many definitions were proposed and revised. In 1995 the Association Internationale pour l'Etude des Argiles (AIPEA) and the Clay Minerals Society (CMS) recommended the following definition:

"*Clay is a naturally occurring material composed primarily of fine grained minerals, which is generally plastic at appropriate water contents and will harden with dried or fired*" [15]. Plasticity refers to the ability of the material to be moulded to any shape. When talking about a fine grained material most geologists refer to particle sizes < 2 μm for the clay mineral fraction [16]. Nevertheless the particle size is also not a uniform property and differs between the disciplines. For example in sedimentology many engineers and soil scientist make use of the Wentworth scale which sets the limit to < 4 μm [17-18]. On the other hand 1 μm is the upper limit used in colloid science [14].

"Clay Minerals are phyllosilicates and minerals that impart plasticity to the clay and which harden upon drying or firing" [15]. This definition includes that clay minerals can be natural as well as synthetic phyllosilicates of any size. Besides these, other mineral phases like quartz, calcite, dolomite, feldspars, oxides and hydroxides of iron and aluminium, minor amounts of heavy trace minerals like ilmenite, rutile, tourmaline, zircon, apatite, barite, organic phases or non-crystalline phases like silica- or iron hydroxide gels and many more, maybe associated in the clay [14,19-20].

2.1.2 Geology and Genesis of Clays

The content given in this chapter is based on the information of Ref [19,21] if not mentioned otherwise.

The processes contributing to the formation of clays are primarily comminution of primary rocks by mechanical, physical or chemical weathering, transport and sedimentation, selection and differentiation processes as well as the new formation or

transformation of phases in an aqueous environment. Weathering of primary silicon and aluminium rich rocks is the main process leading to the formation of clay minerals. Involving physical disaggregation and chemical decomposition, the controlling factors are the original rock type, climate, time, topography and the presence of organic matter. The worldwide distribution of clays depends on prevailing climatic conditions. Illites and chlorites are favoured in cold (polar) climates while smectites are favoured in Mediterranean climates and tropical zones with seasonal differences. Kaolinites accompanied with Al-Fe oxides and hydroxides are the most common minerals forming under wet tropical and equatorial conditions. Clays can be found in many geological environments besides weathering crusts and soils, for example in continental and marine sediments, volcanic deposits, geothermal fields, wall-rock alterations and very low-grade metamorphic rocks (pelites). Most clay minerals are formed by incongruent dissolution of unstable silicates, but direct precipitation from the solution is also possible. This can lead to neoformed clay minerals differing significantly in composition from the parent minerals. The acidity and flow rate of the water play also an important role, since the hydrolysis generally involves the exchange of protons from solution for cations in the minerals. Granitic rocks or gneisses containing metastable mineral phases like micas are a typical example for alteration into clay minerals. Muscovite is degraded to illite while biotite and chlorite will be transformed to smectite minerals. The abundant feldspar minerals are also destabilized and primarily transformed into kaolinite (Equation 2) [22].

(2) $4\,K[AlSi_3O_8] + 4\,H^+ + 2\,H_2O \rightarrow Al_4[(OH)_8/Si_4O_{10}] + 8\,SiO_2 + 4\,K^+$
K-feldspar *Kaolinite*

In a classic soil profile kaolinite decreases towards the lower parts, while illite and smectite increase with depth, nearer to the bedrock where the accumulation of leached ions can form chemically more complex minerals. In general all common rock forming silicates, except quartz, can be destroyed under weathering conditions. Nevertheless clays can contain up to 40 % of quartz in the coarse clay fraction and the question, how a mineral with such a high chemical stability, high hardness and a missing cleavage can be crushed to grain sizes < 2 µm, arises. It is proposed that small grains of quartz are generated by the collision of bigger grains during aeolian or aquatic transport where edges and corners are chipped off from the surfaces. With decreasing grain size the quartz/feldspar ratio decreases in the clays. Feldspars are less stable towards chemical attack and possess a good cleavage along the (001) & (010) planes. But due to the higher solubility with decreasing grain size, also feldspars are mostly found in the coarse clay fraction. Micas

(e.g. muscovite) have an excellent cleavage and big platelets are easy to split up. However micas are not unlimited comminutable by mechanical means and behave very stiff against compressive and shear stresses at grain sizes around 1 mm. Micas are the most common accessory minerals in most clays so their origin in the clay fraction can not only be explained by mechanical processes. Investigations showed that micas are subject to structural changes like the loss of potassium in the interlayer sites with decreasing grain size. Such changes can be the reason for the almost open limit to smaller crystallites. Some clay minerals can also be formed by the action of hydrothermal activity and are then not related to sedimentary layers or weathering crusts [23-26].

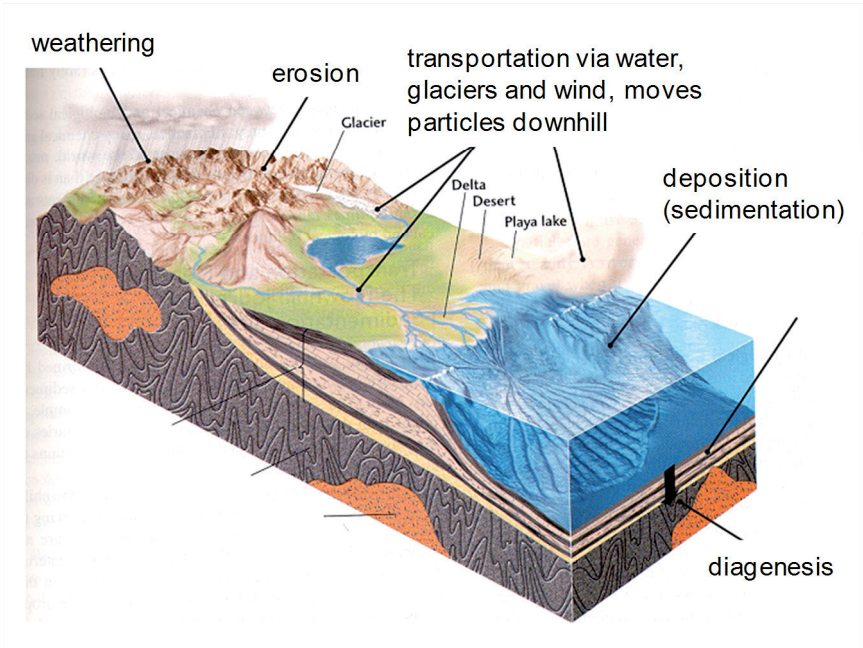

Figure 2-1: Schematic picture of the weathering of primary rocks and the transportation of sediments (modified according to Ref.[27])

Clay deposits can be formed on site as remaining deposits in soil (primary clays), or as secondary sedimentary deposits when the weathered and eroded material has been transported away from the original location. High amounts of clays can be found in lakes, rivers, estuaries and deltas as a part of the sediments and sedimentary rocks. The erosion of soils depends on the profile structure, the humidity, the slope and the climate conditions. The main transportation medium for clays is water (rivers, streams), but there are also deposits known that formed by Aeolian transport. Usually the time span of the transportation in rivers is very short leading

to particle size fractionation together with different mineral settings for example from the mouth of rivers to the interior. When the clays are deposited and buried under new sediments the free or weakly bonded water will be released and the porosity decreases with increasing depth. With ongoing diagenesis unstable soil clay minerals disappear and new clay minerals like chlorite/smectite mixed layer minerals or zeolithes are formed. Illite/smectite mixed layer minerals are the main indicator of diagenetic evolution of a sedimentary clay basin. The next step after diagenesis (compaction and cementation of sediments) is the metamorphosis (transformation) of the minerals under the influence of temperature and pressure (Figure 2-1).

2.1.3 Structural Principles of Clay Minerals

The clay minerals can be divided into three main classes [28]:

- Kaolin Group (e.g. Kaolinite, Dickite, Nacrite)
- Smectite Group (e.g. Montmorrilonite, Nontronite, Beidellite)
- Illite Group (e.g. Illite, Glauconite)

Although the structure and compositions of the three minerals are very different, the fundamental building blocks are the same. The two basic units describing the atomic structure of all clay minerals are an octahedral and a tetrahedral sheet.
The tetrahedral layer is composed of tetrahedras linked together by sharing three corners to form an infinite two-dimensional network of pseudo-hexagonal rings. The not-connected corners of the tetrahedras point all in the same direction. The tetrahedras contain a cation (Si, Al) coordinated by four oxygen or possibly hydroxyl ions [20,29].
The octahedral sheet consists of a hexagonal close-packed lattice of oxygen and hydroxyl ions ordered in an octahedral coordination around mainly aluminium or magnesium and iron atoms. The neighbouring octahedras are connected by sharing edges to form again a pseudo-hexagonal symmetry. Both layers are oriented along the *a, b* crystallographic directions. The tetrahedral layer is connected with the octahedral layer by linking the free tips of the tetrahedras to shared corners of the octahedras to build a 3-dimensional structure. The different layers are combined by sharing oxygen atoms. The non shared corners of the octahedras are occupied with anions, mainly OH^-, but also F^- and Cl^- are possible. These anions lie near to the centre of the pseudo-hexagonal rings formed by the tetrahedras. If one tetrahedral sheet is joined via the tips of the tetrahedras to the octahedral sheet we get a 1:1

clay mineral. By combining two tetrahedral sheets with one octahedral sheet a 2:1 clay mineral is formed [16,19-20,29] (Figure 2-2).
The unit cell of both layer minerals (1:1 and 2:1) is characterized by six octahedra. If the three valent aluminium is present in the octahedral sheets only two thirds of the three possible positions in the elementary cell are occupied in order to fulfill charge balance. In this case we talk about **di-octahedral** minerals. In the presence of divalent magnesium or iron atoms all possible positions are filled and the mineral is termed **tri-octahedral**.

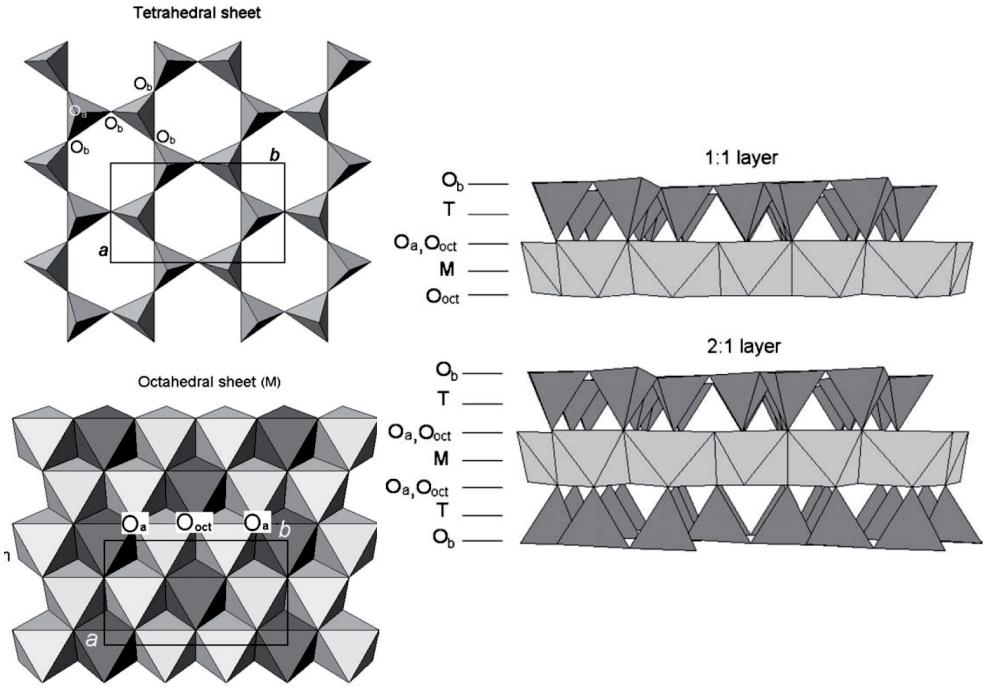

Figure 2-2: Tetrahedral and octahedral layer of common clay minerals, projection parallel to [001] (left). On the right side tetrahedral and octahedral layer are connected to basic 1:1 and 2:1 layer clay mineral structures. O_b and O_a stands for basal and apical oxygen atoms, O_{oct} are octahedral anionic positions, T & M are tetrahedral and octahedral cations, respectively. (Figure modified after Ref [29])

The lateral dimension of the tetrahedral sheet is usually slightly bigger than that of the octahedral sheet. This misfit needs to be adjusted in one or both layers by distorting or bending it. This distortion leads to a displacement of the ideal hexagonal symmetry to low triclinic or monoclinic symmetry [29].
The most typical minerals of the three clay mineral groups kaolinite, montmorillonite and illite are described below summarizing information from References [20,22,30]. The structures of these 3 minerals are shown in Figure 2-3.

Kaolinite:

Kaolinite is a di-octahedral 1:1 clay mineral with the chemical formula $Al_2Si_2O_5(OH)_4$. Since the 1:1 building units are electrically neutral, the weak bonding between the building units by Van der Waals bonds is responsible for the excellent cleavage. Crystals crystallize in the space group P1 of the triclinic pedial system with pseudo hexagonal habitus. Seldom are rhombic or trigonal forms. Kaolinite mainly originates from weathering of magmatic or metamorphic rocks rich in alumosilicates like feldspars.

The most important areas of application are the ceramic, building and paper industry.

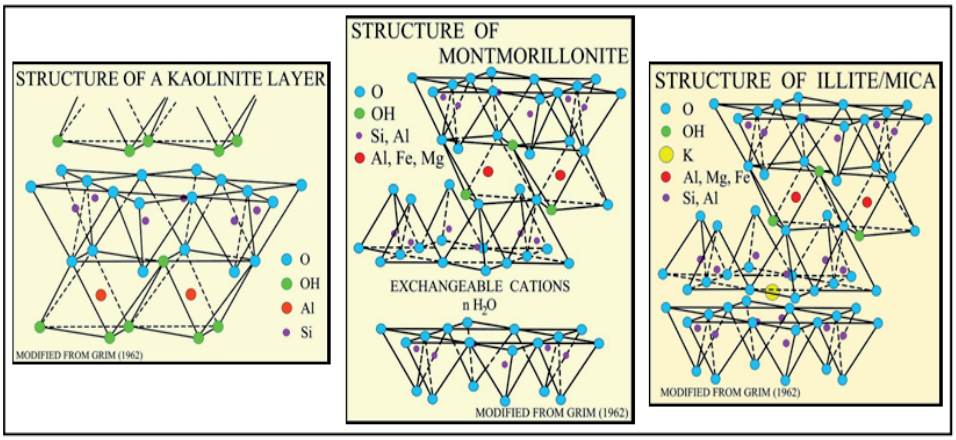

Figure 2-3: Structures of Kaolinite, Montmorrilonite and Illite (from USGS [31])

Montmorillonite:

This mineral belongs to the group of 2:1 dioctahedral (3-layer silicate) clay minerals, with water molecules incorporated between the 2:1 building units. Depending on the amount of water the d-value (c_0-spacing) changes and can vary between 12.4 – 21.4 Å. The chemical composition is very variable and can be estimated as $\sim(Al,Mg,Fe)_2[(OH)_2(Si,Al)_4O_{10}] \bullet Na_{0,33}(H_2O)_4$. The crystal system of montmorillonite is monoclinic with the point group 2/m. Montmorillonite is the predominant clay mineral in Bentonites forming through weathering of alkaline, magmatic rocks or volcanic ashes. Technically used are especially the enormous swelling properties and the ion exchange abilities. Thixotropic properties are in particular used in deep drilling installations.

Illite:
Illite is a di-octahedral 2:1 non-expansive clay mineral with muscovite structure, also called hydromuscovite with partly substitution of K^+ through H_3O^+-molecules. The chemical formula can be written as $(K,H_3O)Al_2[(H_2O,OH)_2/(Si,Al_4)O_{10}]$. Like muscovite, illite crystallizes in the monoclinic system. Substitution of potassium with other alkaline or earth alkaline ions is not possible since the K^+-ion is the only one that fits perfectly between the pseudo hexagonal rings of the tetrahedral sheet. The substitution with H_3O^+ ion which is a bit bigger than the K^+ leads only to a slight expansion of the structure.

2.2 Pozzolanic Materials

Supplementary cementitious materials, often referred to as mineral admixtures, can be divided into two main categories based on their type of reaction: latent hydraulic and pozzolanic. Latent hydraulic materials react, when activated, directly with water while pozzolanic materials react with calcium hydroxide in the presence of moisture to form calcium silicate- and calcium aluminate hydrates. The probably most used replacement material with latent hydraulic properties is ground granulated blast furnace slag (GGBS) [32-35]. Figure 2-4 shows the common cementitious materials in the ternary phase diagram $CaO - Al_2O_3 - SiO_2$ [36].

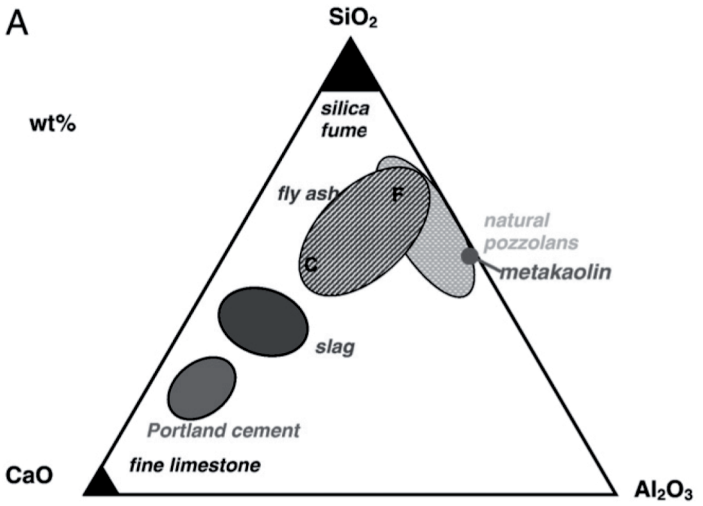

Figure 2-4: $CaO - Al_2O_3 - SiO_2$ ternary phase diagram of cementitious materials [36]

Pozzolanic materials can be of natural as well as of artificial origin. Natural materials can be volcanic tuffs, diatomaceous earth or bauxitic and clayey soils, whereas the most common synthetic materials are usually industrial by-products like fly ash (by-product of the combustion of pulverized coal in electrical power generating plants), rice husk ash or silica fume (result of the reduction of high purity quartz with coal in an electric arc furnace in the manufacture of silicon) [37-40]. The use of the latter has the positive side effect of getting rid of industrial wastes and reducing the CO_2 emissions at the same time.
Burned clays belong also to the group of artificial pozzolanas. In Figure 2-5 a graphical classification of pozzolanic materials is illustrated.
Economical and political reasons are pushing the research in this area forward and more and more materials are discovered to have pozzolanic properties like paper sludge waste [41]. Among the long list are also very exotic materials like sugar-cane bagasse ash [42] and bamboo leaf ash [43] which could serve the local markets in developing countries with a high housing demand.

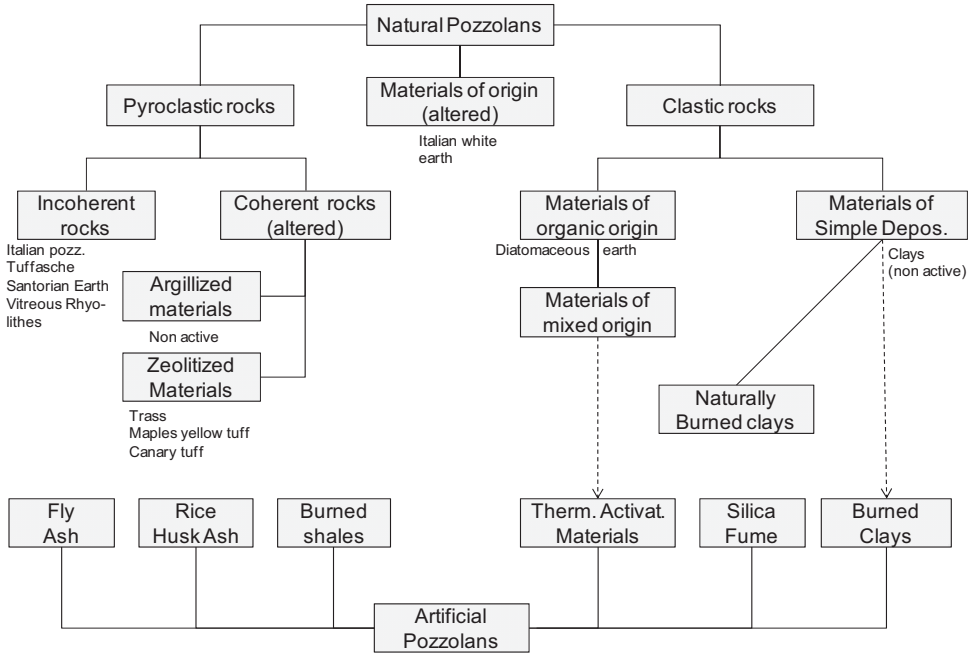

Figure 2-5: Classification of pozzolanas (modified from [39])

Today the term pozzolana is defined according to the **ASTM Standard C 618** [44] as "*siliceous or siliceous and aluminous materials, which in themselves possess little or no cementitious value but will, in finely divided form and in the presence of*

moisture, chemically react with calcium hydroxide at ordinary temperatures to form compounds possessing cementitious properties".

Actually the use of pozzolanas in construction is very old and can be dated back to the days of ancient Rome where it was discovered that finely graded alumina and silica rich powders can form cementitious binders with hydraulic properties when mixed with lime and water. The name pozzolan originates from a small town called Pozzuoli (Italy) near Naples located in the Flegraean fields, where volcanic ash or tuff was found as a suitable material [40]. Due to the mentioned environmental concerns regarding the cement and concrete industry pozzolanas experienced a renaissance as replacement material in blended cements.
Within the last years lots of studies about the pozzolanic activity of synthetic metakaolin have been published. The term metakaolin refers to calcined kaolin, resulting in an alteration to a metastable kaolinite structure of low cristallinity [45]. It was also some research carried out on other clay minerals [46], but it is little known about the interaction of all minerals together in one material. A comparative investigation on the pozzolanic activity of the three main minerals kaolinite, illite and montmorillonite was recently performed [13]. The same author also made investigations on Cuban clay composed of different minerals and could show that the pozzolanic activity is sufficient enough to be used in concretes. All authors agree that kaolinite is the most reactive clay mineral. Nevertheless, clays mainly composed of illite and smectite could also be a suitable raw material for the preparation of blended cements [47].
It seems that other mechanisms than that worked out for the single minerals might take place when a mixture of clay minerals is given. Since common mixed clays are widely distributed all over the world it is important to put more effort in the research of such materials instead of producing pure kaolinite/metakaolin products.

2.3 Clays as pozzolanic Materials

2.3.1 Natural (unburned) Clay Minerals

There are several typical physical and chemical properties of natural clay minerals, inhibiting their pozzolanic activity and excluding their utilization in blended cementitious formulations [48]. First of all clay minerals have very stable structures deriving from the weathering process of incongruently dissolving, primary feldspar minerals. The stability leads to a rather low chemical solubility of clay minerals like kaolinite or minerals from the smectite group compared to e.g. calcite or do-

lomite [49-50]. The resulting low release of aluminium and silicate ions, explains the low pozzolanic activity. Furthermore clay minerals are known for their small crystallite sizes (< 2 µm) and thus their high specific surface areas, up to 600 – 800 m^2/g in the case of smectite minerals [19]. The inner and outer surfaces of clay minerals are usually electrically charged. Negative charges can be caused by aluminium substitution in the tetrahedral layers. In aqueous solutions these surfaces are always covered by water molecules leading to a higher water demand in cementitious binders and concrete structures. In general, a higher amount of water results in a higher porosity, thus decreasing the density and the final strength of the product. The water demand can even be increased when swelling clay minerals are present. Montmorillonites can integrate up to four layers of H_2O in their interlayers and increase their d(001)-values from 9.6 to 18 Å [16]. The swelling properties of clay minerals are usually specified by using an expanding pressure. This pressure can be up to $3.92 \cdot 10^8$ N/mm^2 [51].

If the water absorption exceeds the pore and interlaying filling capacity, certain plasticity comes beside the expansion into effect [19]. This plasticity makes the clays deformable when facing external forces. Even with a low or even no water content the individual components of clay minerals are able to slide under high loads thus having a negative influence on the mechanical properties of cementitious binders. Moreover the high sorption capacities of raw clays can have a significant influence on the chemical composition of the aqueous phase.

There are hundreds of applications and industries for clay minerals and clayey soils where some of the mentioned properties are quite beneficial. Nevertheless, surprisingly during investigations on the interactions of uncalcined clay minerals with lime from a soil stabilization perspective, a real pozzolanic reaction forming small amounts of new hydration products after about a month could be observed [37]. The monitored reactions are however much too slow to be of interest for the cement and concrete industry where a certain early strength is demanded and necessary. As a result the research on blended cements is concentrated on calcined clays for the utilization as pozzolanic materials.

2.3.2 Activation of Clay Minerals

There are several ways to activate clays and clay minerals by changing their properties to make them more favorable as pozzolanic blends. Activation of clays implies the alteration of its original crystalline structure to make it more reactive to its environment. This can be achieved by mechanical, chemical or thermal action [13,52]. One example for mechanical activation is attrition milling leading to delamination of the clay, resulting in a more open structure [53]. Significant morphological and

structural alterations, accompanied with changes of the surface properties by physical disintegration of the clay minerals, can also be achieved with high-energy ball milling [54]. Prolonged milling produced amorphous alumina-silicate aggregates which are usually more reactive than the highly crystalline structures. Acid activation is also a common chemical modification of clays. Treating the clay with mineral acids causes a less crystalline, partly dissolved material of increased specific surface and porosity [55-57].

The most common technique to improve the quality of a natural pozzolana is the thermal activation by means of dehydroxylation/calcination of the minerals. Calcination has two main positive effects: It reduces the high water demand associated with the presence of clay minerals and increases the active phase content [58]. Upon heating the clays first loose the adsorbed water at temperatures < 200 °C (dehydration) and later on between 300 and 800 °C, depending on the nature of the clay mineral, the hydroxyl groups will be removed from the structure. Montmorillonite has the highest dehydroxylation temperature between 680-710 °C, whereas kaolinites and illites loose their OH^- between 550-600 °C [59]. The most reactive state is reached when the calcining temperature leads to a complete loss of hydroxyls and results in a collapsed and disarranged clay structure [45]. The removal of the OH-groups and the structural water can lead to a metastable state with lower cristallinity by destroying the layer structure of some clay minerals or by turning them into an amorphous state [60]. These metastable phases show often an increased pozzolanic reactivity.

Structural changes show up in a distortion of the tetrahedral sheets, a profound alteration of the octahedral sheets and an increased microporosity, in case of kaolinite. Whereas the structure of dioctahedral 2:1 clay minerals is preserved on dehydroxylation, with barely a collapse of the interlayer spaces, if water molecules were present. In the last years research focused mainly on calcined kaolinite forming the metastable metakaolin, because this is thought to have the highest reactivity and a lot of literature can be found about metakaolin blended cements [45,61-65]. In fact by using XRD and Al NMR-spectroscopy, a method to distinguish different coordination sites of aluminium, it could be shown that kaolinite undergoes the most significant structural changes upon calcination [13]. Figure 2-6 shows the XRD patterns and Al-NMR spectra of a standard kaolinite in the untreated and calcined state. As we can see in the XRD pattern the (001) peak of kaolinite disappears at 600 °C accompanied with an increased background in the diffractogram which indicates the formation of an amorphous phase. The background is even higher at 800 °C as the amount of the amorphous phase increases further.

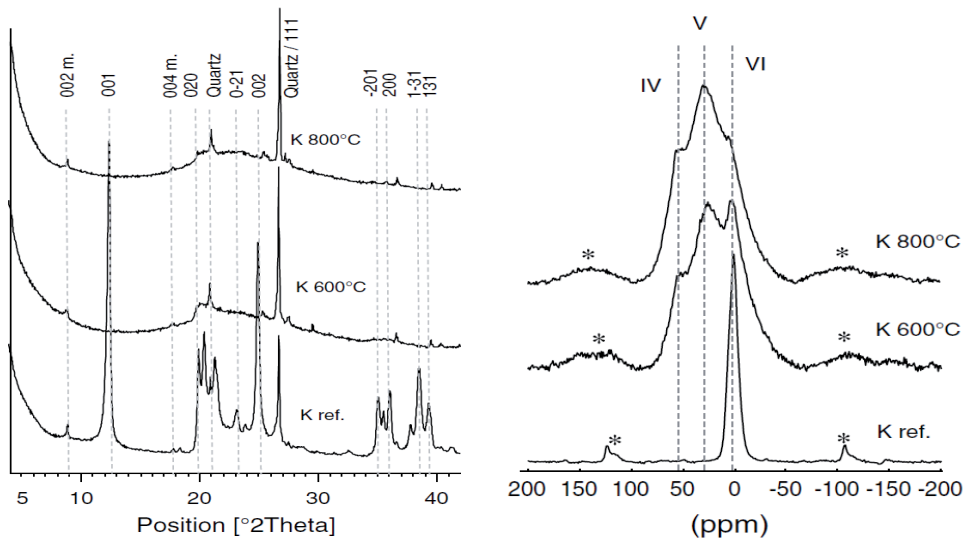

Figure 2-6: XRD patterns (right) and Al NMR (left) spectra of a standard kaolinite untreated and heated at temperatures of 600 and 800 degrees [13].

The loss in crystallinity is confirmed by having a look on the Al NMR spectra. The number of usually 6-coordinated Al in the octahedral sheets decreases with increasing temperature. The rising number of 5-coordinated Al supports the thesis of the presence of a low crystalline metastable phase at elavated temperatures.

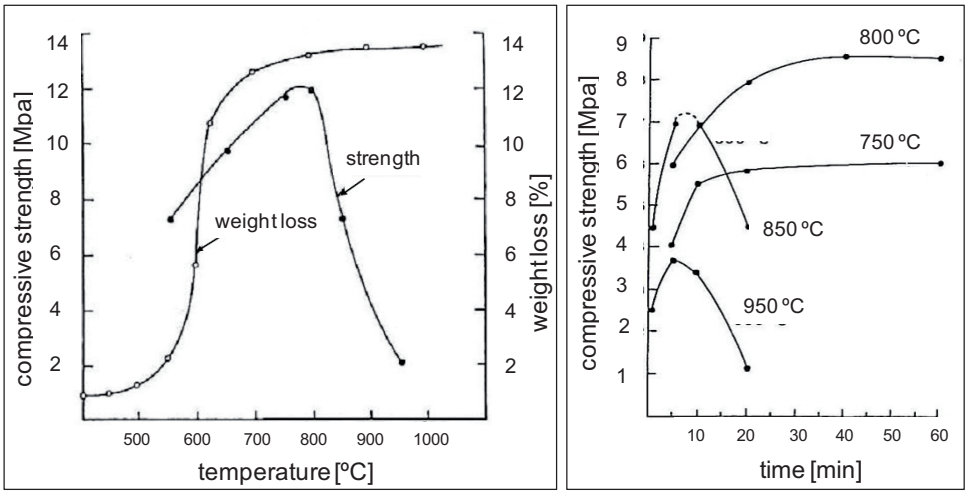

Figure 2-7: Weight loss and pozzolanic reactivity as a function of temperature (right diagram) and the effect of temperature and time of activation on the strength of lime-pozzolan mortars (left diagram) cured at 50 °C for 7days [66].

5-coordinated Al-atoms are seldom observed in nature but can occur for example in minerals like andalusite or augelite [22,67]. However the development of 5-coordinated structural sites due to heat treatment of a given material indicates in general a decrease in crystallinity.
Each clay mineral has a different optimum calcination temperature where it shows its highest reactivity. The optimum activation temperature for Ca-and Na-montmorillonite was assessed to be 830 °C [68]. The highest reactivity and pozzolanic activity of illite was evaluated for a temperature of 930 °C, while kaolinite revealed the highest reaction rates at 650 °C [69-70]. It is therefore crucial to find the optimum calcination temperature for clays containing a mixture of these minerals. The calcining temperature leading to the highest reactivity is not necessarily directly linked to the decomposition temperature whereas the time of calcination can be an important factor [66] (Figure 2-7).
The optimal temperature and duration depends on the mineralogy and chemical composition of the clay [71]. Heating to temperatures > 900 °C can lead to recrystallisation of high temperature phases and a decreasing reactivity of the material. In clays with high amounts of kaolinite, phases like mullite, cristoballite or hematite have been observed [72]. Calcium rich clays can produce assemblages of gehlenite, wollastonite and larnite. If Mg is present diopside, akermanite or spinel are more likely to form [73]. In the presence of sufficient silica, gehlenite and wollastonite become unstable to form anorthite [74]. The temperature range for the optimal temperature can be a narrow window of 50 °C below and above which the reactivity of the material is not high enough to serve as a pozzolanic material.

2.4 Cement Hydration and Pozzolanic Reaction

Mixing cement with water leads to a series of reactions of the different clinker phases causing the hardening and setting of cement pastes. The new phases formed during the hydration process are called the hydration products.
In the absence of calcium sulphates the interstitial phases C_3A and C_4AF react very fast with water to calcium aluminate hydrates. After an intermediate step forming a gel-like phase on the surface of the C_3A grains, this material transforms to hexagonal crystals of C_2AH_8 and C_4AH_{19}. The formation of these hexagonal phases slows down further hydration of C_3A as they function as a hydration barrier covering the C_3A surface. Finally the hexagonal phases convert to the thermodynamically stable cubic phase C_3AH_6, the diffusion barrier is disrupted and the hydration proceeds

again with a fairly high speed. The overall hydration process may thus be written as:

(3) $$2\ C_3A + 27\ H \rightarrow C_2AH_8 + C_4AH_{19} \rightarrow 2\ C_3AH_6 + 15\ H$$

In the presence of calcium sulphate (as in a Portland cement) the amount of hydration of C_3A in the initial state of hydration is distinctly reduced when compared to that consumed in the absence of $C\bar{s}$. Needle formed crystals of ettringite (trisulphate) are formed as the main product of hydration;

(4) $$C_3A + 3\ C\bar{s}H_2 + 26\ H \rightarrow\ C_6A\bar{s}_3H_{32}$$

The ettringite formation is accompanied by a significant liberation of heat. After a rapid initial reaction, the hydration rate is slowed down significantly. The length of this dormant period may vary and increases with increasing amount of calcium sulphate in the original paste. A faster hydration, associated with a second heat release maximum, gets under way after all the available amount of calcium sulphate has been consumed. Under these conditions the ettringite, formed initially, reacts with additional amounts of tricalcium aluminate, yielding calcium aluminate monosulphate hydrate (monosulphate) as the product of reaction;

(5) $$C_6A\bar{s}_3H_{32} + 2\ C_3A + 4\ H \rightarrow\ 3\ C_4A\bar{s}H_{12}$$

As ettringite is gradually consumed, hexagonal calcium aluminate hydrate (C_4AH_{19}) also starts to form. It may be present in the form of a solid solution with $C_4A\bar{s}H_{12}$ or as separate crystals.
The composition of the calcium aluminoferrite phase (ferrite phase), usually written as C_4AF, may vary between about $C_4A_{1.4}F_{0.6}$ and $C_4A_{0.6}F_{1.4}$. Under comparable conditions the hydration products formed in the hydration of the ferrite phase are similar in many respects to those formed by C_3A although the rates differ and the aluminium in the products are partially substituted by ferric ions. The reactivity of the ferrite may vary over a wide range, but seems to increase with increasing A/F ratio.

The hydration of the main clinker minerals alite (C_3S) and belite (C_2S) can be divided into 4 periods:

a) Pre-induction period. Immediately after contact with water, an intense, but short-lived hydration of C_3S gets under way. An intense liberation of heat may be

observed in this stage of hydration. The duration of this period is typically no more than a few minutes.

b) Induction (dormant) period. The pre-induction period is followed by a period in which the rate of reaction slows down significantly. At the same time the liberation of heat is significantly reduced. This period lasts typically a few hours.

c) Acceleration (post-induction) period. After several hours the rate of hydration accelerates suddenly and reaches a maximum within about 5-10 h. The beginning of the acceleration period coincides roughly with the beginning of the second, main heat evolution peak. The $Ca(OH)_2$ concentration in the liquid phase attains a maximum at this time and begins to decline while crystalline calcium hydroxide starts to precipitate. The initial set as determined by Vicat-needle is often just after the start of this period and the final setting time just before the ending of it.

d) Deceleration period. After reaching a maximum, the rate of hydration starts to slow down gradually; however, a measurable reaction may still persist even after months of curing. The reason is that the hydration reaction becomes diffusion controlled due to hydration products growing around the unhydrated cement core in increasingly thickness.

The overall alite hydration reaction may ideally be written as:

(6) $$2\ C_3S + 7\ H \rightarrow\ C_3S_2H_4 + 3\ CH$$

(7) $$2\ C_2S + 5\ H \rightarrow\ C_3S_2H_4 + CH$$

Belite essentially forms the same hydration products as alite, but it should be noted that belite reacts much slower and produces only about a third the amount of CH in the idealized reaction.
More detailed information about the cement hydration can be found in references [6,75-77].

The calcium hydroxide, CH, is crystalline, while the calcium silicate hydrate is microcrystalline and appears amorphous to X-rays. The CSH phase has a variable composition and is often simply denoted CSH-gel. The CSH-gel is the real hydraulic binder in concrete. Due to their morphology (microcrystalline needles or foil like) they are able to interlock with each other in the matrix of the cement paste and are thereby mainly responsible for the high strength development of cements and

concrete. On the other hand calcium hydroxide can be a source of weakness even though having a positive effect on concrete by serving as a buffer with high pH protecting steel against corrosion. But CH is highly soluble, can easily be attacked by acids and is the most unstable phase with respect to carbonation [6].

The pozzolanic reaction includes all the reactions occurring among the reactive phases of pozzolana, calcium hydroxide (lime) and water [39]. When cements are blended with pozzolanic materials, the reactive silica or alumina components from the pozzolana react with the calcium hydroxide formed during the cement hydration to produce further CSH or CASH phases. The result is in general a lower porosity with a higher amount of binding phases leading to an increased durability and in some cases to an increased strength of the final product. Figure 2-8 shows an illustration of the reduced porosity by producing more CSH at the cost of CH. The stochiometry of the reaction of metakaolin with lime is:

(8) $$5\ CH + AS_2 + 5\ H \rightarrow C_5AS_2H_5$$ [65]

"$C_5AS_2H_5$" represents an average composition between the phases CSH, C_4AH_{13}, C_3AH_6 and C_2ASH_8 [65]. C_3AH_6 usually forms only at higher temperatures as transformation product from other calcium aluminate hydrates like C_4AH_{13} [39]. This is also known from the hydration of calcium aluminate cements. The hydration products from the reaction of CA and water are highly temperature dependant.

At temperatures between 10 °C and 27 °C the phases CAH_{10} and C_2AH_8 form together, while at higher temperatures the cubic C_3AH_6 forms very fast [78].

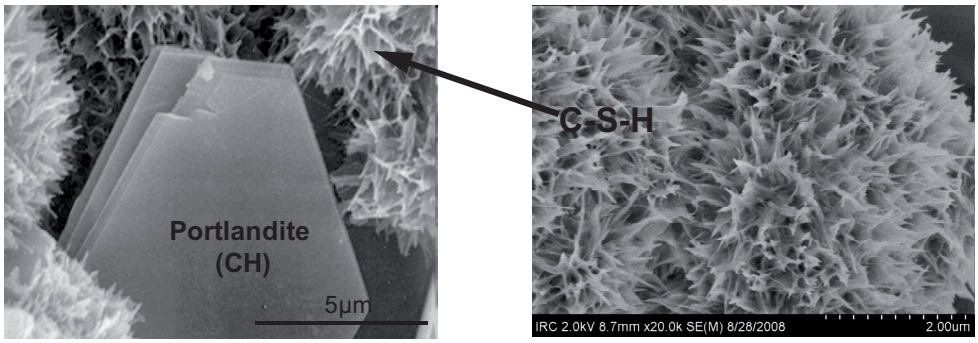

http://lebeton.free.fr/images/cim_gel_CSH.jpg&imgrefurl

www.cementlab.com/images/C3S-2week%2520L2_os.jpg&imgrefurl

Figure 2-8: SEM pictures of a hydrated cement paste with CSH phases and large CH crystals in the pore space (left). The right picture shows an increasing amount of CSH phase (needles). (The pictures are not taken from the same source, thus they should only serve to indicate the mechanism)

Reports on the amount of metakaolin required to completely consume the CH vary. Figure 2-9 shows the consumption of CH in metakaolin blended cement in relation to the curing time [79]. The authors show that there is still some CH present in the cement matrix when replacing 25 % of cement by metakaolin, while Kostuch et al. [80] state that CH is fully removed after 28 days with a replacement level of OPC of only 20 %.

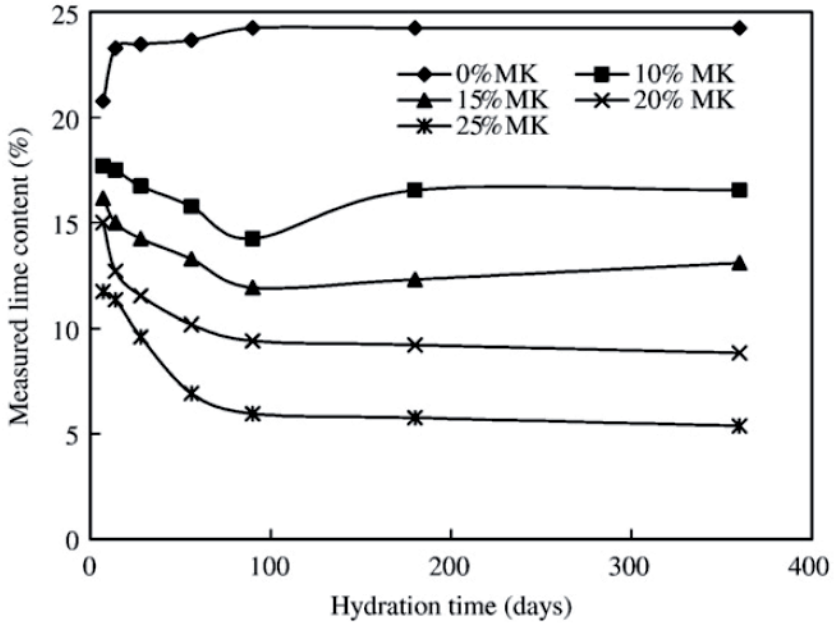

Figure 2-9: Effect of Metakaolin blended cement on the CH consumption [79]

The main hydration products forming during the pozzolanic reaction of clays and lime are CSH and C_4AH_{13}. C_2ASH_8 and C_3AH_6 are common with clays with higher aluminium content like kaolinite [46]. When calcium carbonate is present the formation of the AFm-phases mono- and hemi-carboaluminate hydrate can be expected.

2.5 Blended Cements with Calcined Clay

Besides the overall reduction of CO_2-emissions from the manufacturing process of cement, the partial replacement of cement clinker by calcined clays can have a number of additional beneficial effects in mortars and concretes. Most of them are as mentioned, linked to the pozzolanic reaction producing more binding phases and

reducing the pore space in the cement paste [45,58,81]. Due to the reduction in average pore size the diffusion rate of ions like Cl^- or Na^+ is significantly reduced. In general the use of pozzolanic materials as replacement for cement leads to an enhanced durability of mortars and concretes. The lower permeability makes the cement and concrete also more resistant to the action of aggressive waters like sea water or acidic solutions. Furthermore the reduced absorption of water can improve the durability under freezing and thawing conditions. Additionally the use of pozzolanas in concrete can be very effective in suppressing an alkali silica reaction. Compared to the hydration of cement, the pozzolanic reaction is a slow reaction which is dependent on the free available content of calcium hydroxide to react with. For concretes containing up to 30 % metakaolin as replacement for OPC, the pozzolanic reaction is reported to have its maximum effect between 7-14 days [82]. This causes a significant reduction in the heat of hydration during the first hours/days, depending on the replacement level, which makes pozzolanic cements very useful in the production of mass concrete. But the same effect is also responsible for a reduced compressive strength development of mortars and concretes at early ages, due to the lower reaction speed. However the long term compressive strength can be significantly improved with replacement levels up to 50 %.

One negative effect to mention is the influence of pozzolanas on the workability of mortar and concrete mixes. Calcined clays and many other pozzolanic materials show an increased water demand adversely affecting the mixing properties of pastes. This must be countered with the use of a superplasticizer to obtain the same water to binder ratio as in mixes with only OPC.

Metakaolin as a synthetic pure compound is investigated extensively in the literature as a pozzolanic additive for the cement industry. However in nature kaolin clays and other clay deposits are seldom pure but do always contain impurities of other minerals. Since there is a growing interest of applying calcined clays in the construction industry a lot of countries start to evaluate their local clay deposits and to assess the pozzolanic potential for the local cement and concrete industry.

The scientific and technological research council of Turkey (TÜBITAK) sponsored a study to investigate different kaolin clay deposits of different composition, crystallinity, morphology and purity in the Anatolian area of Turkey. The main impurity of the clays is quartz. Depending on the kaolinite content of the clays, the deposits were classified as high or medium quality clays for manufacturing of pozzolanic additives. The authors concluded that even the clay deposits with a average kaolinite content of only 40-65 % are suitable to produce pozzolanas of medium quality for the local industry [83].

Two kaolin clay deposits from Iraq showed good pozzolanic activity when calcined at temperatures between 600-700 °C for 45 min. Both claystones are of low grade

with kaolinite as the dominant clay mineral associated with an appreciable amount of iron oxides as well as quartz and calcite [84].

In Tunisia six local clays with different kaolinite content were investigated. The maximum burning temperature of the clays was 800 °C. All clays contained quartz as an accessory mineral. In some clay deposits illite, montmorillonite and calcite were present besides kaolinite. The clays with the highest amount of kaolinite showed the highest pozzolanic activity with potential to be used in the local construction industry [85]. The clays with impurities of illite, montmorillonite and calcite had a rather low pozzolanic activity. However it might be that the reactivity of these clays could be increased significantly if the calcination temperature would be chosen higher. Temperatures above 800 °C are necessary to destroy the clay mineral structures of illite and montmorillonite and to decompose calcite completely. However, our own investigations show that it may be smart to retain some calcite in the clay. The $CaCO_3$ can react with already formed AFm-phases to form further hydration products (carboaluminate hydrates) during the hydration of blended cements.

High quality kaolin clay deposits in Serbia with kaolinite contents > 80 % were determined, to have the highest pozzolanic activity when calcined at 650 °C for 90 min [86].

Tironi et al. [87] studied five natural kaolinitic clays from different regions of Argentine. The clays had different contents of kaolinite, with different impurities and different degrees of crystallinity. The calcining temperature was 700 °C. It could be shown that clays with at least 45 % kaolinite can perform very well as a pozzolanic material. In standard mortar tests, cubes with 30 % replacement of OPC by clays of medium kaolinite content, had a higher compressive strength after 28 days than the standard mortar cube with only OPC. However the clay with the highest kaolinite content performed worse than the clays with medium kaolinite content. But this clay had a more ordered structure before calcination and a lower total pore volume. The authors could show that not only the kaolinite content but also structural and physical parameters determine the rate of pozzolanic activity.

In Oman a research program was carried out focusing on potential local clay areas to produce artificial pozzolans for the building industry [88]. All clays were mixed clays containing a mixture of the clay minerals montmorillonite, illite and kaolinite accompanied with calcite and quartz in different amounts. Some samples also contained palygorskite and chlorite. The pozzolanic activity of the clays was very sensitive to the right heat treatment (temperature and time). In this study the chemical composition of the clays is a clear indicator for the behaviour as a pozzolana. A total silica, alumina and iron content greater than 50 % (Indian Standard) was suf-

ficient to produce a good pozzolanic material. The ASTM standard C 618-98 has set a minimum of 70 % for these three compounds.

The utilization of calcined clay soils as pozzolanic material is not a complete new idea, and it was already used in ancient pozzolan-lime mortars. Many authors have proven the potential of calcined clay, but only few tried to explain why and how calcined clay works. This thesis focuses on the mechanism behind the reactivity of calcined clay, by investigating clay deposits with a complete different mineralogy, to explain why some clays are more reactive than others.

3 Main Methods

3.1 Firing (Calcination) of clays

3.1.1 Pilot scale production

The thermal treatment of the raw clays for pilot scale production was executed at IBU-tec advanced materials AG (Weimar, Germany), using a direct heated rotary kiln (KDO)(Figure 3-1). The kiln is designed for a continuous thermal treatment and was used to simulate trials under industrial conditions. The key parameters are given in Table 3-1.

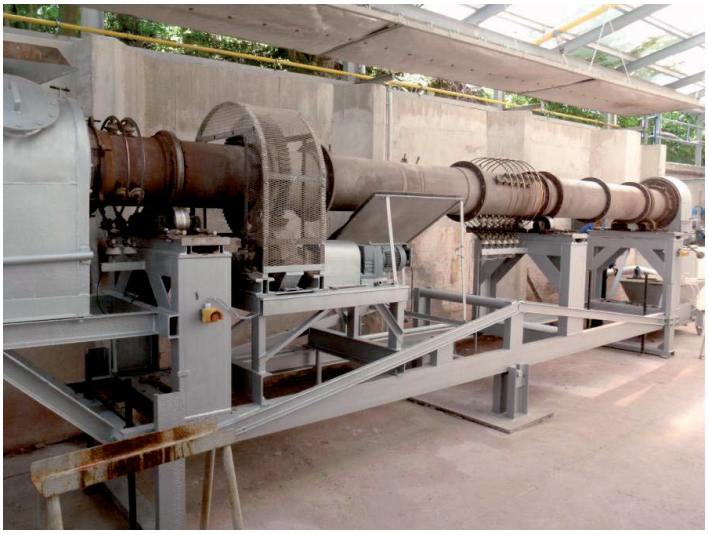

Figure 3-1: Direct gas heated kiln (HDO) from IBU-tec

Table 3-1: Technical key parameters of the rotary kiln

Inside diameter	0.3 m
Heated length	7 m
Feed throughput	20-30 kg/h
Heating	direct natural gas burner
Max. burning temperature	≤ 1500 ºC
Kiln atmosphere	air
Mode of operation	continuous operation
Exhaust gas flow	in parallel or counterflow to the material flow

Prior to feeding the kiln with the clay the material was homogenized, dried in a drying box and crushed to get feedable particles. Subsequently the rotary kiln was fed using a dosing belt. In earlier experiments on the reactivity of calcined clay

within the COIN-program (see www.coinweb.no), a retention time of 45 min gave the best results regarding the pozzolanicity of the then investigated clays [89]. To limit the parameters a retention time of 45 min was hence chosen for all investigated clays within this PhD study. The calcined clays were taken from the kiln outlet and filled into a metal drum where they were cooled with ambient air. To guarantee the correct temperature in the kiln, the temperature is monitored with several thermo-couples along the rotary kiln (Figure 3-2).

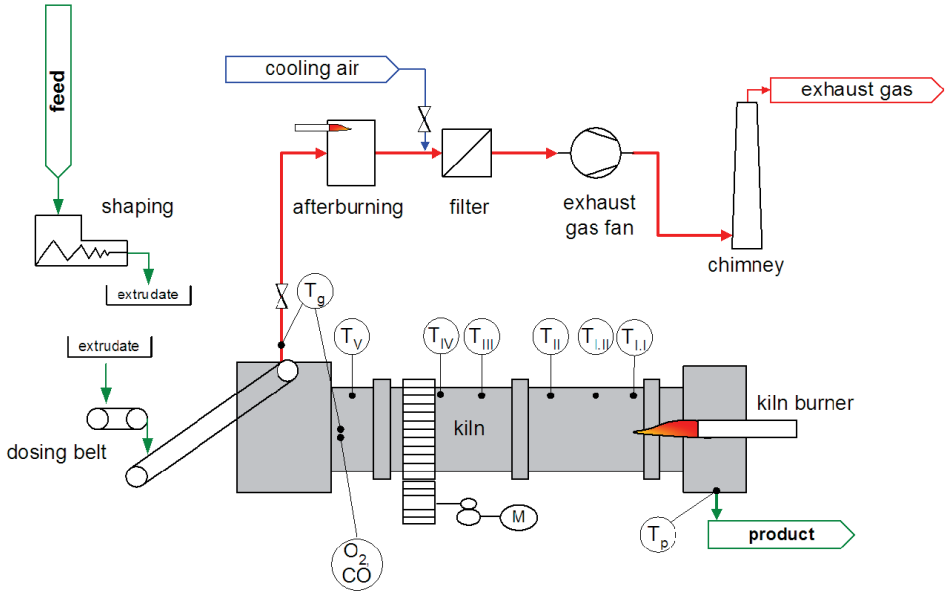

Figure 3-2: General process flow sheet of the rotary kiln

3.1.2 Calcination in the electrical furnace:

The parameters and numbers about the burning of the clays in the electrical lab furnace are given in chapter 6

3.1.3 Industrial scale calcination:

The execution of the industrial trials in Saint-Gobain Weber's rotary kilns is described in Chapter 7.

3.2 Milling of calcined clays from pilot scale production

The milling of the calcined clay lumps produced at IBU-tec was performed at UVR-FIA GmbH (Freiberg, Germany). The material was pre-crushed in a laboratory hammer mill equipped with a 1.6 mm grid applying a circumferential speed of 33 m/s, to obtain a material with d_{95} = 1 mm. The finish grinding to a d_{50} < 10 µm was performed with a discontinuous drum mill. The technical parameters of this mill can be found in Table 3-2.

Table 3-2: Technical parameters of the used mill at UVR-FIA

Mill dimensions	D = 0.66 m / L = 0.45 m
Lining	Steel
Grinding media	260 kg of steel cylpebs 12/16/18/20 mm
Driving conditions	35.5 rpm = 68.2 % $n_{crtitical}$
Amount of sample (loading)	20 kg

3.3 X-Ray Diffraction:

XRD was used for quantitative mineralogical analysis of the raw clays as well as qualitative analysis of the calcined clay materials.
X-Ray diffraction is a common used method to identify single crystalline phases in polyphase systems. The theory behind the method will not be addressed here but further informations can be found in several text books [16,90-91]. However, the analysis of clays and clay minerals is not a standard procedure and it requires a lot of experience for identifying and quantifying such samples. For that reason, a more detailed description about sample preparation and identification of clay minerals will be given in this chapter. The described procedures are according to the book from Moore & Reynolds [16].

3.3.1 Sample Preparation techniques:

Clays are very complex materials to analyze and may need certain pre-treatments to determine the exact mineralogy. X-ray diffraction of clays is a very difficult process and there are different preparation techniques known for different purposes in the analysis of raw clays. The first step is usually to grind a clay sample and make a random oriented powder sample of the bulk mineralogy to get a rough idea of the proportion of clay and non-clay minerals. Due to the weak *00l* clay mineral intensities you get in such preparations, it will be difficult to get much information

about the specific clay minerals. Therefore, clay mineral separation and fraction analysis can be performed in the next steps and are very helpful. Separation from clastic rocks can be achieved by crushing and mixing a suspension in a blender before decantation or centrifugation of the fine fraction. Ultrasonic disaggregation may be needed if the rock is hard or silica-cemented. Removal of carbonatic rocks is accomplished by heating a crushed sample in a sodium acetate-acetic acid buffer at pH 5 whereas sulfate rocks can be dissolved in the sodium salt of EDTA. Besides that there are variable chemical treatments for example for the removal of iron oxides or organics. Iron oxides can cause a high background in the diffractogram, which masks peaks, due to fluorescent X-rays from the iron. Before particle size separation, the suspension must be washed free of salts since these can cause flocculation. Particle size separation of the clay fraction (< 2 μm) is based on sedimentation following Stokes' law. But for the reason that clay minerals have no spherical particle shape it cannot be applied strictly. Centrifugation is the recommended method for gravity settling, but many clay laboratories still use tubes which can take days or even weeks to separate the clay fraction. To distinguish between different clay minerals it is important to get high intensities of the *00l* reflexes, deriving from the platy shape of the minerals. Thus oriented clay mineral samples are prepared using different techniques. The most common and only method that will be described here is the "Glass slide method" (Figure 3-3). The orientation of the sample is not as good as with other methods and particle size segregation can be a problem. The advantage however is its ease of application compared to other methods. The suspension of the material is put with an eyedropper on a glass slide mounted on a ceramic plate. The glass plate with the suspension is then dried for about 1 h at about 90 °C. The clay minerals settle down and orient themselves with the *a,b*-plane parallel to the glass slide.

However for some purposes like polytype studies or the differentiation between di- and trioctahedral species you need to see all reflexes, especially the (060). This is only possible when the minerals are randomly oriented in the sample. It is very difficult or even impossible to prepare a complete randomly oriented sample with most methods. The simplest of all methods is the so called back-loaded method. An inverted sample holder with a frosted glass plate held to its front is gently filled and packed with powder. Usually some kind of stamp is used to densify the powder carefully. The sample holder is then covered with the respective lid and turned around. After lifting the glass plate a flat homogeneous surface of the sample is revealed. Finally to avoid any misidentification most clay mineral samples should be, furthermore to the air-dried samples, be analyzed in the glycol-solvated state. This is particularly important for the identification of swelling clay minerals.

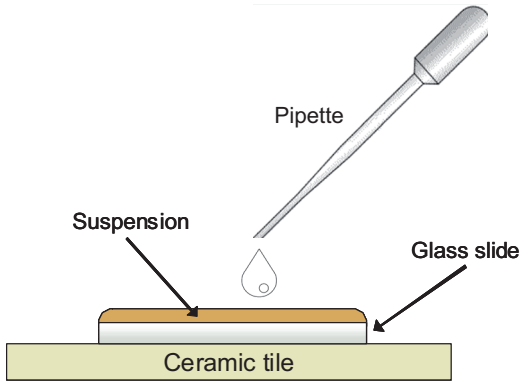

Figure 3-3: Glass slide method. Surface tension holds the suspension on the glass slide. (modified after [16])

3.3.2 Raw Clay Identification

In this chapter only the identification of the most common and important clay minerals for this study will be treated.

Clay minerals are identified in oriented samples by observing the *00l* reflections, because the atomic pattern along the z-axis is the most significant difference from one clay mineral to another. In poly-phase systems like clays, peak overlapping and interferences are not seldom and can complicate the analysis. In that case chemical treatments are necessary.

Illite and glauconite show a very distinct (001) peak at 8.9 °2θ and are in most cases easy to differentiate from other clay minerals. Compared to other minerals illite does not change upon heating up to 550 °C or when treated with glycol. The main distinctive feature between the diffraction patterns of illite and glauconite is the nonexistent (002) reflection of glauconite.

The differentiation between kaolinite and chlorite minerals is another major difficulty in XRD analysis. Chlorite is based on a first-order reflection of 14.2 Å, and kaolinite is based on a 7.1 Å structure, which means that most peaks of the two phases are overlapping. In case large amounts of both phases are present, the best way of identification is to have a look on the (003) reflections, since none of these peaks is interfered by reflections of the other phase. If only minor amounts are present these peaks are too weak to identify and heating of the sample is a better option for differentiation. By heating the sample to 550-600 °C, kaolinite will decompose and become amorphous to X-rays, while the chlorite structure only collapses due to dehydroxylation of the brucite layer starting at 500 °C. The (001) reflection of chlorite will still be present with even increased intensity, but shifted to lower d-values (higher 2θ angles). Another technique is to subject the sample to hydrochloric acid, which will not only dissolve carbonates but also most of the

chlorites. However Mg-chlorites may be unaffected leaving some doubts about the final results. The only definitive method to distinguish both phases is the expansion of kaolinite with certain reagents like dimethyl sulfoxide, shifting its peaks to higher d-values and thus eliminating the interference of peaks with chlorite.

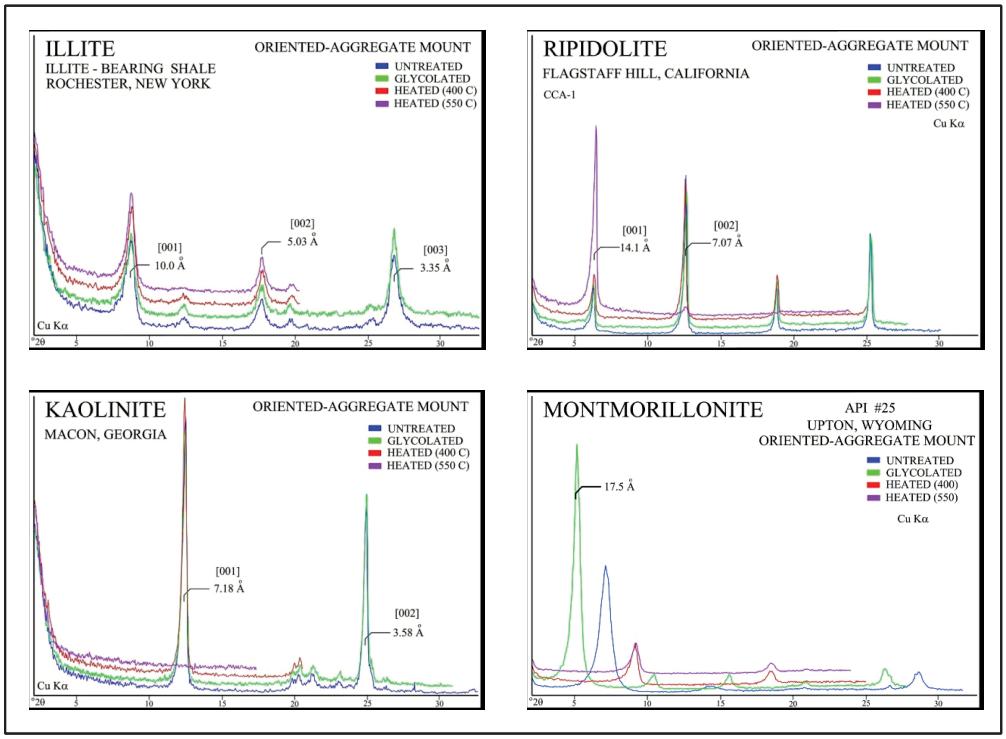

Figure 3-4: Diffraction patterns of Illite, Chlorite (Ripidolite), Kaolinite and Montmorillonite in the untreated, glycolated and heated state (USGS - www.usgs.gov/of/2001/of01-041/htmldocs/clay.htm)

Smectite minerals can be easily identified by comparing air-dried and glycol-solvated samples. In the glycol solvated state smectite will show a strong (001) reflection at about 5.2 °2θ which shifts to about 6 °2θ when dried in air. Confirmation can be achieved by saturating the sample with potassium and drying it at 300 °C. The result will be a similar diffraction pattern to that of illite with a (001) reflection at about 10 °2θ. The main problem that lies in the analysis is to decide whether a mixed layer structure with illite or only smectite is present. Small amounts of illite interstratifications can become visible in a shift of the (003) peak to higher diffraction angles. If the higher order reflections are not detectable, it is possible to get some information out of the (001) peak shape. With interstratified illite the peak will appear broader with a high shoulder at low angles. By treating

the sample with LiCl, montmorillonite can be distinguished from other smectite species like nontronite, saponite or beideleite. Li-ions are said to migrate into the octahedral sheet, neutralizing the layer charge. Thus montmorillonite will be converted into a pyrophyllite like structure accompanied with an irreversible collapse. The structure will not expand upon treatment with glycol, while the other named smectite minerals do. The 00l reflections of both smectite and chlorite can be taken to get information about the degree of Fe-substitution in the octahedral sheet.
To distinguish between di-and trioctahedral species the d-values of the (060) reflections are very important. These high order reflections become only sufficiently visible in random oriented sample preparations. Differentiating between species with help of this peak is possible because the *b* dimension is more sensitive to changes in the octahedral cation occupancy then the *a* and *c* dimension are.

3.3.3 Analysis of raw clays

The qualitative and quantitative analysis of the raw clays was performed by Ass. Prof. Ole Bjørslev Nielsen, at the University of Aarhus (Department of Earth Sciences). Ass. Prof. Nielsen and his group have very long experience in clay analysis and developed a standardized methodical procedure for this kind of problem. Bulk mineralogy of the clays was performed on dried and ground samples using the back-loading technique, which means on un-oriented and un-fractionized samples. Followed by that, the ≤ 2 μm fraction (clay fraction) was separated from the bulk sample by means of sedimentation. The ≤ 2 μm fraction was smeared on a glass plate and dried in air. As explained above the analysis of the clay fraction is performed on an oriented sample. The clay fraction was investigated under three different conditions.

- Untreated
- After treatment with ethylene glycol vapors in a desiccator for 24 h at 60 °C
- After heating at 500 °C for 1 h

The used diffractometer was a PANAnalytical X'Pert Pro MPD equipped with a X'Celerator RTMS detector and an automatic divergence slit. The samples were measured from 2-65 ° 2θ using a step size of 0.0170 ° 2θ and a step time of 20 sec. The used wavelength was Cu-Kα with 1.54060 Å. The qualitative and quantitative analysis was done with the software X'Pert High score from PANanalytical. Minerals are identified by the peak fitting part of the program using the JCPDS-ICDD database to assign the minerals. The quantification is based on the height of the selected reflections which are measured or read on a datasheet and corrected with

empirical calculated correction factors and then calculated to %-values, assuming that the sum of identified minerals are 100 %. Thus a possible amorphous content in the sample is neglected.

3.3.4 Analysis of raw & calcined clays

The calcined and ground samples were measured as received at NTNU in Trondheim. In addition, the bulk mineralogy of the raw clays was checked qualitatively to confirm the phase compositions. Except drying and grinding there was no further treatment of the raw clays. Due to a lack of other preparation techniques all samples (raw and calcined) were prepared using the front loading technique. The clay powder samples are pressed with a roughened glass plate into the sample holder and are densified by knocking the sample holder softly laterally on the table. This should reduce the orientation of the clay minerals. The surface is flattened by stripping off the excess material with the glass plate. The samples were measured with a D8 Focus diffractometer from Bruker equipped with a Lynx Eye detector. Measurements were taken from 5-65 ° 2θ with a step size of 0.2 ° 2θ and a step time of 1 sec. The used wavelength was Cu-Kα with 1.54060 Å.

3.3.5 In-situ XRD

The hydration of cement/clay pastes was monitored with in-situ XRD during the first 24 hours. The goal was to detect directly phase changes during the hydration and possible differences in the early hydration of pastes where cement is replaced with different levels of calcined clay.
The measurements were performed on a Bruker D8 Advance, equipped with Cu K-alpha radiation and a Våntec-1 position sensitive detector. The cement clay/pastes were mixed by hand for one 1 minute with a spatula in a plastic cup and smeared in the respective sample holder. The surface was flattened by stripping off the excess material with a glass plate. The sample was then put in an MRI Physikalische Geräte GmbH chamber, and data collected using electronic divergence slits to maintain a constant illuminated area of approx 12 x 15 mm on the sample. In the MRI sample chamber atmosphere and temperature can be controlled and measurements were taken at room temperature.
Samples were measured from 6-50 ° 2θ with a step size of 0.016 ° 2θ and a step time of 0.3 sec. This gives a total scan time of 15 min resulting in 96 scans during 24 h. These parameters were chosen as they are a good compromise between a sufficient resolution of the XRD spectra and fast enough scans to monitor the hydration in detail.

3.4 X-Ray Fluorescence Analysis (XRF)

XRF analysis was done for all the clays under investigation to obtain the exact chemical composition of the raw material.
The analyses were performed on a Bruker AXS S8 Tiger WDXRF with a 4 kW generator. In a first preparation step the dried and powdered samples were ignited at 850 °C. Then 0.5 g of the respective clay sample was added to 5.0 g of 66 % Lithiumtetraborate and 34 % Lithiummetaborate and 60 µl of Lithium iodide. The mixture was fused in a Pt crucible and moulded to a glass disk, to be ready for analysis.

3.5 Mortar Mix Designs

The mixing procedure of mortars was performed according to the Norwegian Standard NS-EN 196-1 [92].
The composition of control mix and test mixes is given in Table 3-3.

Table 3-3: Composition of the control and test mixes with 20 % replacement of OPC by calcined clay

	Control Mix [g]	Test Mix with 20 % replacement of OPC [g]
OPC (Portland Cement)	450	360
Pozzolan (Calcined Clay)	0	90
Graded standard sand	1350	1350
Distilled water	225	225

The aim was to obtain a w/b ratio of 0.5 in all mortars. In mortars with calcined clay this was done by varying the amount of superplasticizer (Dynamon SP 130, Rescon Mapei) to achieve a flow that was within ± 5 % of the reference mortar. The consistency of fresh mortar was determined using a flow table. The mortar mixes were cast in 3 40x40x160 mm moulds and stored in a cabinet for 24 hours at 23 ± 2°C and 90% RH. After 24 hours, the mortar prisms were removed from the moulds and stored in saturated lime water for 28 days. After 28 days storage, the compressive and flexural strengths were determined according to the Norwegian Standard NS-EN 196-1.

3.6 Particle Size Distribution (PSD)

Particle Size distribution of uncalcined and calcined clays was acquired by lasergranulometry using a Mastersizer 2000 equipped with a Hydro 2000 MU wet cell from Malvern Instruments. The measurement principle behind the technique is the Mie scattering of light on particles. The dry clay powders were dispersed in distilled water and treated with ultrasound for 2 minutes to deagglomerate the clay particles. Other dispersing agents were tested with no effect on the particle size distribution. Thus it was decided that distilled water together with ultrasonic displacement are sufficient to avoid possible wrong results by agglomeration of particles.

3.7 Specific Surface Area (BET-Surface)

For measuring the specific surface area of uncalcined and calcined clays, an apparatus from Micromeritics was used. The Tristar 3000 Surface Area & Porosity Analyzer is a gas-adsorption instrument which can measure three separate samples simultaneously. Prior to analysis the samples were degassed with a SmartPrep degasser (VacPrep 061) to remove adsorbed contaminants from the surface and pores of the samples.

3.8 Thermal Analysis

3.8.1 General

Thermo-gravimetric analysis and simultaneous differential thermal analysis (TGA/SDTA) were performed with a Mettler Toledo TGA/SDTA 851. TGA makes it possible to measure the weight loss of a sample in a specific temperature interval. In DTA any temperature change between a sample and an inert reference material is recorded while both undergo an identical thermal program. Thus any exothermic (structure transformations or crystallization, etc.) or endothermic (dehydration, melting, etc.) reactions are detected. The pure raw and calcined clays were analyzed with a heating rate of 10 °C/min between 40 – 1100 °C to determine the loss on ignition (LOI) of the material, characterize the type of clay minerals (and carbonates or other hydroxides) contained in the sample and estimating their amount. The ad- and absorbed water was determined with the weight loss between 40 – 100 °C. All measurements were performed in nitrogen atmosphere with a flow

rate of 30 ml/min. So any exothermic reactions like recrystallization of new phases in the high temperature area are not detected.

3.8.2 Pozzolanic-test by thermogravimetric analysis (TGA)

Calcined and ground clay samples were tested for their pozzolanic activity in pastes with calcium hydroxide. For that purpose pastes of about 40 ml were prepared by mixing calcined clay with laboratory grade $Ca(OH)_2$ in a ratio of 1:1. The mixing water was an alkaline solution with a pH of 13.2 and a KOH:NaOH ratio of 2:1 to simulate the pore water of ordinary Portland cement. To obtain mixable pastes the water to solid ratio had to be between 0.8 and 0.9 for the different calcined clays. Before adding the mixing water the two powders were homogenized by hand through stirring and rotating the cup. The samples were then mixed with the water in the plastic cup and stirred for about 1 min with a spoon. Four samples were taken and filled in glass bottles of 10 ml size, sealed with plastic lids and stored in climatized rooms of 20 and 38 °C for 28 days and 6 month. Some samples were stored for shorter times as well (1, 3, 7 days). To stop the hydration, the pastes were crushed and immersed in ethanol. The samples were washed with about 100 ml ethanol, before they were filtrated and dried at about 35 % RH in a closed desiccator upon $CaCl_2$ saturated water.

The resulting dry powders were analyzed by thermogravimetric analysis and simultaneous differential thermal analysis (TGA/DTA) with a Mettler Toledo TGA/SDTA 851. The samples were measured in two steps. They were dried again in the TGA apparatus at 40 °C for two hours before they were heated from 40 – 1100 °C with a heating rate of 10 °C/min. The purge gas was in both steps nitrogen (N_2) with a flow of 30 ml/min.

The decomposition of calcium hydroxide happens between 450-550 °C. By measuring the weight loss in this temperature interval the remaining calcium hydroxide content after 28 days and 6 month can be calculated relative to the content in the initial mixture. The exact boundaries for the temperature interval of $Ca(OH)_2$ are read from the 1st derivative curve (DTG). The weight loss calculated from the difference of the horizontal tangents in the TG signal is multiplied with the molar ratio 74/18 for $Ca(OH)_2$ and H_2O, respectively.

3.9 Isothermal Calorimetry

The heat of hydration of cement pastes with different amounts of calcined clay by mass as well as calcined clay-lime pastes over time was determined with isothermal calorimetry using a TAM Air apparatus from TA Instruments. The TAM Air is an eight channel Microcalorimeter designed for sensitive and stable heat flow measurements. All eight channels have a sample chamber connected to a reference chamber, each with a 20 ml volume. The reference material is inert quartz sand. All measurements were performed at an operating temperature of 20 ± 0.02 °C. Mixing of the pastes was done outside the calorimeter with a spatula in the device-specific glass ampoule for 1 minute, before transferring the ampoule into the calorimeter sample chamber.

3.10 Scanning Electron Microscope (SEM)

SEM investigations were done with uncalcined and calcined clay samples to investigate microstructural changes during the firing process. In the hydrated clay/lime and cement/clay pastes the hydration products were qualitatively and quantitatively analyzed with regard to their chemical composition, besides documenting the microstructure.
All samples were cast in epoxy resin, allowed to harden and plane polished in order to achieve a cross-section of the material. Polishing was performed in iso-propanol to avoid any reactions with water. Before analyzing, the samples were coated with carbon under vacuum to make the surface electrical conductive. All samples were investigated in the backscattered electron imaging (BEI) modus. Backscattered electron images were taken with an accelerating voltage of 15 kV. In this modus different phases can easily be distinguished visually due to the appearance in different grey shades. Phases containing heavy elements (e.g. FeS_2, $FeTiO_3$) or of high density will appear bright, while phases containing light elements (e.g. $CaCO_3$) will appear dark grey. Semi-quantitative EDS (energy dispersive spectrum) analysis was performed to check the chemical composition of mineral phases from the clay and in the pastes. For important phases like hydration products, quantitative WDS (wavelength dispersive spectrum) analysis was done to achieve the exact chemical composition.
The main instrument used was a JEOL JXA-8500F Electron Probe Micro analyzer (EPMA). The JXA-8500F is a high performance thermal field emission electron probe micro analyzer combining high SEM resolution with high quality X-ray analysis of submicron areas. The JEOL JXA-8500F instrument is equipped with 5

wavelength dispersive X-ray spectrometers (WDS) and an energy dispersive X-ray spectrometer (EDS). This combination can simultaneously analyze 5 elements WDS + 16 elements EDS plus collect image signals from backscatter and secondary electron detectors.

3.11 Fourier Transformed – Infrared Spectroscopy (FT-IR)

In this study Infrared Spectroscopy was used as a complementary method to XRD. IR spectroscopy is a very useful tool to characterize different clays and clay minerals and to investigate their structural features. Differentiation between di-and trioctahedral clay minerals and informations about the cation occupancy in the octahedral sheets for example, are much easier achieved with this method then with XRD. Besides that an IR-spectrum is obtained very fast and the equipment is fairly inexpensive. In theory this method is based on the fact that molecules absorb specific resonant frequencies that are characteristic for their structure. So the frequency of the absorbed radiation corresponds to the frequency of a molecule or group that vibrates.
Uncalcined and calcined clays were analyzed with this technique to characterize the raw clays and to get information about the degree of regularity or crystallinity within the structure of the calcined clays. Spectra were taken in the transmittance modus in the middle-IR (MIR) region. To record optimal spectra samples were prepared with the KBr (potassium bromide) pressed-disc technique since KBr shows no absorbance in the MIR region. Samples of 2 mg were dispersed in 200 mg of KBr and pressed to pellets with a 13 mm diameter using a mechanical hand press. Measurements were performed using a Bruker IFS 66v FTIR spectrometer equipped with an IR source, KBr beam splitter, and DTGS KBr detector for MIR measurements. For each sample, 200 scans in the 400 – 4000 cm^{-1} (MIR) spectral range were recorded with a resolution of 2 cm^{-1}. A spectrum of the atmosphere was recorded for background corrections of the samples.

3.12 High precision inductively coupled plasma mass spectrometry (HR-ICP-MS)

ICP-MS measurements were performed on raw and calcined clay samples to analyze the ion release of the samples into solution. The release of Al and Si especially can provide information about the reactivity of the different clays. Al and Si are the main elements released from the clay during the hydration with cement to react with $Ca(OH)_2$ to form CSH, CAH and CASH phases.
Suspensions of clay in distilled water or the alkaline solution used in other experiments were made in a ratio of 1:30. 3 g of clay were added to 90 ml solution and constantly moved (rotated) in a plastic bottle for 3 days. After 3 days the plastic bottle was standing still to enable the clay to settle down on the bottom of the bottle. About 15 ml of the clear solution were taken off with a pipette and given away to analyze. The same was done with a reference solution, composed of only the alkaline solution.
In general samples are introduced into argon plasma as aerosol droplets. The plasma dries the aerosol, dissociates the molecules, and then removes an electron from the components, thereby forming singly-charged ions, which are directed into a mass filtering device known as the mass spectrometer (www.perkinelmer.com). HR-ICP-MS analyses were performed using a Thermo Finnigan model Element 2 instrument. The samples were introduced using a SC-Fast autosampler with a peristaltic pump. The instrument was equipped with a concentric PFA-ST nebulizer connected to a Scott PFA spray chamber, aluminum sample and skimmer cones, a demountable torch and a quartz injector.

3.13 MAS-NMR – Spectroscopy:

Nuclear Magnetic Resonance spectroscopy is a method for investigations of the local environment of atoms and their interactions with neighboring atoms [93]. This high sensitivity to the local ordering and geometries around the spin nucleus under investigation stands in contrast to the long-range order detected by X-Ray diffraction. Thus it can provide information on the structural and dynamical aspects of solids, like bonding, bond length and bond angle, but is also extremely helpful in revealing the structural features of amorphous materials, where X-Ray diffraction is no longer applicable [94].
Atomic nucleus with a nuclear spin *I* possess a magnetic moment $\mu_n = (h/2\pi)\gamma_n$ (h = Planck constant, γ_n = magnetogyric ratio) as a rotating charge carrier. In an external

magnetic field B_0 the magnetic moment can only have certain orientations or energy levels characterized by the spin quantum number $2I + 1$. The interaction of the nuclear magnetic moment with an external magnetic field induces the splitting of these energy levels. If the sample is now irradiated with radio frequency it will absorb in the resonant energy between adjacent energy levels typical for each isotope [93].

Since the method is based on the magnetic moment of atomic nucleus only nuclides with an odd proton number are accessible for NMR-spectroscopy since these can have a magnetic atomic nucleus [95]. Examples are ^{27}Al with a spin number I = 5/2 and ^{29}Si with a spin number of I = 1/2. Changes in the atomic environment of these two elements can give essential information about structural changes in the clay minerals since we know they are mainly build up of layers of aluminum octahedra and silicon tetrahedra. The kind of condensation of silicon tetrahedra in silicate minerals can be distinguished with the isotropic chemical shift (variation in the resonance frequency) of ^{29}Si [96]. Following it can be distinguished between for example Neso (single tetrahedron)-, Soro (double tetrahedral)-, Ino (single chain)-, and Tectosilicates (3D framework), or Phyllosilicates (sheets) as in the case of clay minerals (Figure 3-5). On the other hand the signals of the isotropic chemical shift of ^{27}Al can be used to distinguish between Al in different coordination sites (octahedral, tetrahedral or 5-fold coordination) [97]. Together this can give crucial information about structural changes in the clay minerals upon calcination.

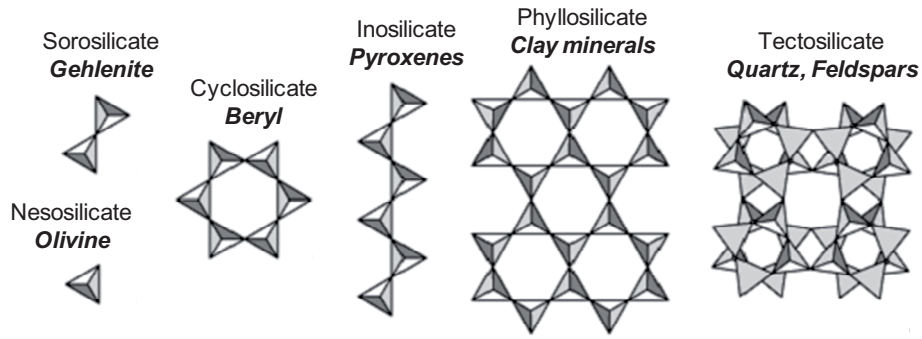

Figure 3-5: Building principles of silicate structures.

However the mobility of atoms in solids is severely limited, also hindering the molecular rotation. Furthermore neighboring atoms in slightly different local environments absorb photons of different frequency and can lead to anisotropic interactions like the mentioned chemical shift, dipolar or quadrupole interactions [98]. These effects generate narrower spectra of low resolution which had to be overcome in Solid State NMR techniques. In 1959 Andrew et al. [99] presented a technique based

on the rotation of the sample at high speed which improved the resolution of solid phase spectra significantly. The sample is usually rotated around an axis inclined at 54°44´ (the "magic-angle") with respect to the magnetic field B_0 [93]. This so called magic-angle spinning (MAS) technique became routine in solid state NMR experiments in the early 1980's.

All NMR measurements for this PhD were performed by Prof. Jørgen Skipsted at the University of Aarhus (Denmark) at the department of chemistry. The ^{27}Al MAS NMR spectra have been recorded at 14.1 T, using a 4 mm CP/MAS NMR probe, a spinning speed of νR = 13.0 kHz, a 0.5 μs excitation pulse, a 2 s relaxation delay, 1H decoupling during acquisition, and in between 6560 and 50300 scans.

3.14 Mössbauer Spectroscopy

Mössbauer Spectroscopy is nowadays an established method in clay science and regularly used in the characterization of clays and clay minerals. Using γ-rays with high-energy as radiation, Mössbauer spectroscopy is a method of high resolution revealing spectral details that would be inaccessible with other experiments. Most commonly it is used to determine the oxidation state and in some cases the coordination of iron. Another feature that can be measured is the magnetic properties induced by the presence of iron in the clay mineral structure. Many clayey soils contain substantial amounts of iron minerals, like hematite, goethite or lepidocrocite, and in these cases the method can be even used to identify the actual species [100].

Rudolf Mössbauer found that a γ-ray emitting radioactive isotope could be used as a source of gamma radiation of correct energy to be absorbed by non-radioactive isotopes of the same element. This however works only if the radioactive nucleus is bound in a solid. If that is not given the emitted γ-ray will lose too much energy due to the recoiling of the emitting nucleus in the opposite direction. This energy loss is larger than the width of a nuclear energy level and thus the produced γ-ray cannot be absorbed. Nuclear energy levels are very sharp defined and only γ-rays with the correct energy can be absorbed by the given nucleus of the same element [101]. In Mössbauer experiments to investigate the ^{57}Fe isotope the radioactive ^{57}Co isotope is used as the γ-ray producing source.

In general a mössbauer spectrum provides two signals that can give information about the material: The isomer shift and the quadrupole splitting parameters of the material. The isomer shift arises from the electrostatic interaction of the nucleus with the electric field due to the orbital s-electrons. Thus the effect is related to the

oxidation state of the element under investigation. Quadrupole splitting provides information about the distortion of Fe-sites and arises from the fact that the nucleus can have different shapes and does not have to be spherical [101]. More information about the theory behind this method can be found in several text books [102].
In this study the method was used to identify the oxidation state of iron in the raw and calcined Søvind (SØ) marl from Denmark and to check possible distortions of Fe-sites in the structure. A possible oxidation of iron during the firing process in the kiln can lead to severe distortions of the clay structure due to the introduction of one extra oxygen atom per 2 oxidized iron atoms [103].

(9) $$4\,Fe^{2+} + O_2 \quad \rightarrow \quad 4\,Fe^{3+} + 2\,O^{2-}$$

The experiments were performed by Lennart Häggström at the Department of Physics and Astronomy in Uppsala, Sweden. The Mössbauer measurements were carried out at room temperature on a spectrometer with a constant acceleration type of vibrator and a ^{57}Co*Rh* source. The samples were grounded, mixed with BN (boron nitride) and spread out to form absorbers. Calibration spectra were recorded using natural iron foil at room temperature as a reference absorber. Spectra obtained were folded and analyzed using the least-squares Mössbauer fitting program Recoil.

4 Materials

4.1 Raw Clays:

For the study different clay materials from different locations in Europe were used. The raw materials were chosen with regard to availability and locations close to production plants of Saint-Gobain Weber.
The two main materials used were a marl from Denmark and a kaolinitic clay from Portugal. Besides that different clays from Portugal with different compositions and a calcareous illite clay from Poland were investigated with different methods for comparison. Table 4-1 shows the main mineral phases of the different clays investigated in this thesis.

Table 4-1: Investigated raw clays with their main mineral phases

Name	Location	Main Minerals
AB 1080, Aldeia, Kal-Sorgila	Region of Avelar, Portugal	Kaolinite, K-feldspar, Quartz
Argila Rascoia		Illite, Chlorite, Quartz, Hematite
Argila Sorgila		Smectite, Quartz, K-feldspar
Søvind Marl	Hinge-Ølst, Denmark	Smectite, Calcite, Kaolinite, Illite, Quartz
Gniew	Gniew, Poland	Illite, Calcite, Kaolinite, Quartz

4.1.1 Clay deposits in Portugal

The deposits of the investigated clays from Portugal are all located in the vicinity of Avelar in central-western Portugal.
Kaolin deposits in Portugal have a diverse geological background. Besides the sedimentary deposits of fluvial origin with different ages, primary deposits formed by hydrothermal processes and weathering of granites, gneisses and acid porphyries are found as well. Source rocks are lower and upper Paleozoic granites and Precambrian gneisses [104]**.** Recently arkoses became an important resource, since they contain a high amount of kaolin besides k-feldspar and silica sands. Arkose is a detritical sedimentary rock, or rather a type of sandstone with an amount of feldspar > 20 %. In general arkoses are formed from the weathering of granitic rocks, which is why the feldspars can be occasionally highly kaolinised [22]. In fact the AB 1080 kaolinitic clay is a by-product from the washing of feldspar and quartz.
The kaolinitic clays from the Viana region (Figure 4-1) are formed by alteration of several types of granite and secondary kaolinitic terraces and were dated to be of

Plio-Pleistocene age (a geolical time scale is provided in the attachments). Primary kaolin deposits as they can be found in the Aveiro region are dated back to the Early Cretaceous were the climate was wet and warm favorable for intensive chemical weathering [105]. Kaolins from the Mondega Basin and the Pombal area were the studied clays are located, derive from Kaolinitic sands. The kaolins are recovered from washing the quartz and feldspar rich sands [106].
The investigated kaolinitic clays consist of up to 40 % kaolinite with quartz and feldspar comprising the rest, besides minor amounts of illite.
Smectite clays in Portugal are formed by weathering of volcanic, basaltic rocks under temperate mediterranean climatic conditions [107]. Typical deposits are the Lisbon (72 Ma) and the Runa Volcanic Complexes (100-70 Ma). The clay deposits should be not older than Tertiary age since the climate during the Cretaceous was hot and wet. In the Tertiary temperatures were decreasing and there was a change from tropical to temperate climate in the beginning of the Quaternary [107].
Common clays are very abundant and they are predominantly distributed in the western and southern mesocenozoic coastal zone. Common clays occur mainly in the areas of Chaves, Bragança, Aveiro, Coimbra, Leiria, Lisboa, Santarém and Faro.

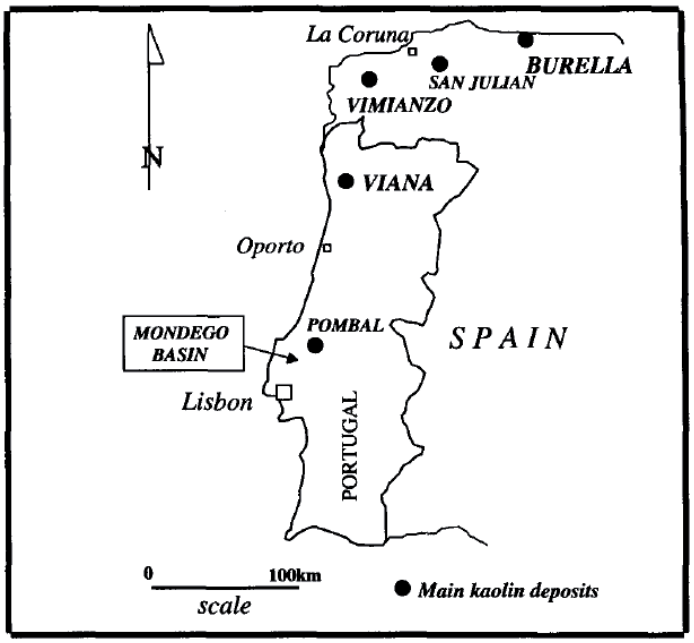

Figure 4-1: Location of main kaolin deposits of western Iberia [106]

4.1.2 Søvind Marl from Denmark:

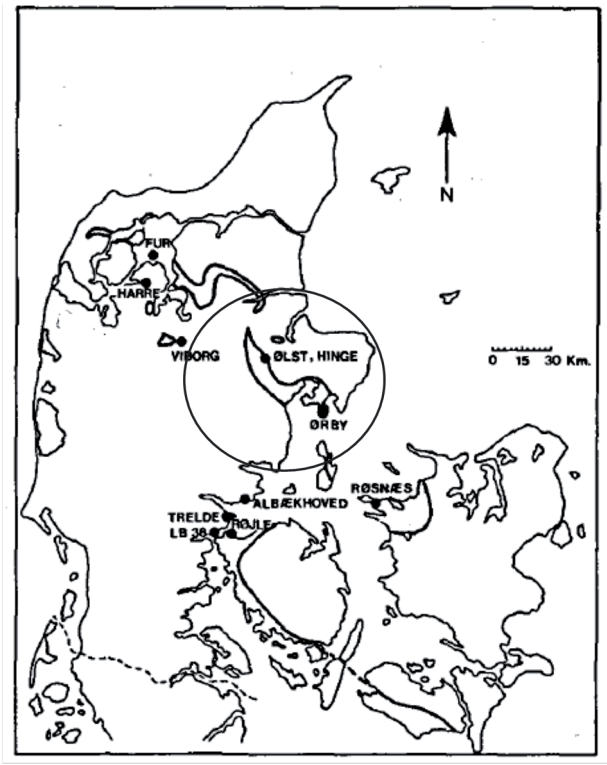

Figure 4-2: Card of Denmark showing the Hinge area and the Søvind Marl deposits [108] (circle)

The information given in the following paragraph are based on the articles of Hugget [109] & Clausen [108] if not mentioned otherwise.
The Søvind Marl is a stratigrafic term and the formation is exposed in several pits in Denmark. Saint-Gobain Weber is mining the marl close to one of their Leca production plants in Hinge, were the formation reaches a thickness of about 4.3 m. The thickness of the formation however varies a lot, and can be up to 20 m in some areas of Denmark. The name Søvind Marl derives from the village Søvind, north of Horsens Fjord. The color can vary from light grey to white over to a dark-green very fine-grained marl or calcareous clay. The marl formation is characterized through indistinct bedding and random fabric suggestive of bioturbation. The Søvind Marl is a tertiary sediment and was deposited between the middle and late Eocene in a marine depositional environment. During the Eocene the climate in Denmark was tropical to subtropical and the marl was deposited in a sea depth of 200-400 m in a period were the climate started to cool down gradually [110-111]. Rea-

sons for the high calcite content in the Søvind Marl formations compared to other stratigrafic units may be more oxygenated bottom water, indicated by the frequent burrows and the high temperature during deposition. The calcite content is variable and comes from coccoliths that lived when the marl was deposited. These coccoliths made it also possible to date the marl [111]**.** The high proportion of these calcareous microfossils and planktonic foraminifera confirms a deep shelf environment. The clastic fraction is build up of around 70 % clay minerals wherein smectite dominates, with kaolinite and illite in minor amounts. About 10% are silts consisting of mainly quartz. Main authigenic minerals are rare manganoan siderite, pyrite and calcite. The smectites are most likely a product from the weathering of volcanic ashes and/or basaltic glasses which are found in stratigrafic formations as several layers below the Søvind Marl due to high volcanic activity in the early Paleocene. It is possible that the smectite is both of detrital and authigenic origin in the marl formation.

4.1.3 Gniew Clay from Poland

This chapter is based on the information given in Ref. [112] if not mentioned otherwise.

The Gniew clays are located close to the towns Janiszewo, Lignowy and Gniew (about 75 km south of Gdansk) and cover an area of about 35 km^2 with an average thickness of 7 m. Locally the thickness can be up to 20 m. The area is north of the line of maximum ice extent of the Pomeranian phase of the late Vistulian (Weichselian) glaciations. The origin of the clays is connected with the retreat of the Pomeranian ice sheet which formed numerous proglacial lakes in front of the retreating ice sheet and among them the ice-dam lake at Gniew [113]. The sedimentological units of the Gniew clays were first described at the end of 19^{th} century and many different interpretations from several authors about their development can be found since then but it seems to be most likely that the deposition of the clays took place in a glaciomarginal/terminological lake.

Stratigraphically the Gniew clays can be subdivided into four facies.

Sedimentary facies A consists of laminated silts and clay that form silt/clay rhythmites. The maximum thickness is about 2 m. In the lower part of the facies a few intercalations of sandy diamicton can be found. The unit is the result from a deposition in the transitional zone between glacial and glaciofluvial environments. The average carbonate content of the silt is about 20-22 % whereas it is only about 13-18 % in the clays.

Facies B is a sand bed of 10-30 cm thickness erosionally overlying the silt/clay rhythmites.
Facies C is a massive clay unit of 4-18 m thickness containing diamicton clays and silt admixtures. The average carbonate content lies between 16-18 % and is probably the result of a clastic input of allochthonous carbonates, derived from carbonate rocks by the ice sheet. The homogeneous massive character of the clays shows that the clays could settle equally all over the lake resulting from suspension settling.
Facies D is composed of thick rhythmites, accumulated in a prodelta environment.

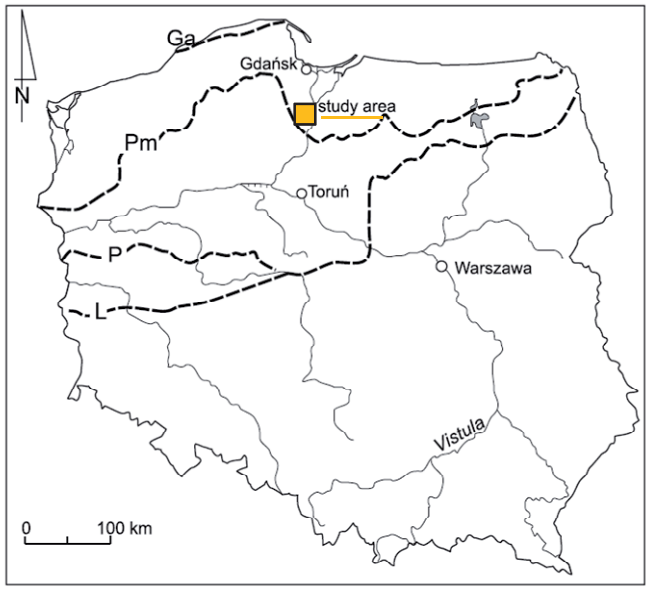

Figure 4-3: Map of Poland with the location of the Gniew clays (orange square) [112] L – Leszno phase, P – Poznan Phase, Pm – Pomeranian phase, Ga – Gardno phase

4.2 Other Materials

In mortar tests a commercial Metakaolin, Fly Ash and Slag were used to compare the performance of these SCM's with the investigated calcined clays. The chemical composition of the 3 materials and the used cement for mortar mixes and pastes is given in Table 4-2. The respective data sheets can be found in the appendix.

- Cement: Standard OPC (CEM I according to EN 197-1) from the Norwegian cement producer NORCEM, Brevik, Norway.
- Calcium Hydroxide: laboratory grade made by Merck Company of Germany
- Fly Ash: provided from NORCEM
- Metakaolin: Metaver N from Newchem
- Slag: from Tata-Steel

Table 4-2: Chemical Composition of OPC, Metakaolin, Fly Ash and Slag

	OPC CEM I EN 197-1 (Norcem)	Metakaolin Metaver N (Newchem)	Fly Ash (Norcem)	Slag (Tata-Steel)
SiO_2	19.9	52-54	50.0	33.9-36.1
Al_2O_3	4.8	41-44	23.9	11.9-14.3
Fe_2O_3	3.3	< 1.5	6.0	0.5-2.0
CaO	61.9	< 0.5	6.3	38.2-41.7
K_2O	1.0	< 2.0	1.4	0.4-1.0
Na_2O	0.5	< 0.1	0.6	<0.2-0.3
MgO	2.7	< 0.4	2.1	7.2-9.7
TiO_2		< 1.0		0.6-1.1
P_2O_5	0.2		1.1	0.0-0.1
SO_3	3.3		0.4	0.50-0.9
LOI	1.9		3.6	
Limestone	3.3			
Free Lime	1.5			
Alkali (Na_2O equ.)	1.2			
Tot. Chloride	0.05			

5 Clays from Pilot Scale Production – Results and Discussion

5.1 Mineralogical and chemical composition of the clays under investigation

Table 5-1 and Table 5-2 show the bulk mineralogy of crystalline phases before calcination and the chemical composition of the different clays studied in this thesis calcined at 800 °C.

Table 5-1: Bulk mineralogy of crystalline phases of the studied clays normalized to a total of 100 % (amorphous phases are not considered).

	Clays from Portugal					Denmark	Poland
Phase [%]	**AB 1080**	**Aldeia e Irmao**	**Kal-Sorgila**	**Argila Sorgila**	**Argila Rascoia**	**Søvind Marl ***	**Gniew** **
Kaolinite	46.7	33.8	27.6	1.0	5.2	8.4 ± 1.7	8.0
Smectite	—	—	—	42.5	0.2	53.5 ± 3.9	2.0
Illite	1.5	6.0	1.7	5.6	39.6	4.4 ± 0.8	33.0
Chlorite	—	—	—	1.0	9.1	—	—
Quartz	17.5	38.5	47.1	32.6	17.1	4.3 ± 1.2	22.0
K-feldspar	34.3	21.7	19.2	8.2	4.8	—	4.0
Plagioclase	—	—	—	—	6.5	—	4.0
Calcite	—	—	1.6	4.6	2.8	24.7 ± 1.9	15.0
Siderite	—	—	2.7	4.4	—	3.1 ± 2.7	—
Dolomite	—	—	—	—	—	—	4.0
Pyrite	—	—	—	—	—	1.3 ± 1.2	—
Hematite	—	—	—	—	14.7	—	—
Goethite	—	—	—	—	—	—	8.0

***Average composition of three different bore holes in the same deposit (H2-H4)**
**** Mineralogical composition determined at IBU-tec**

From Portugal 5 different clays as shown in Table 5-1 were investigated. AB 1080, Aldeia e Irmao and Kal-Sorgila are kaolinitic clays with the kaolinite content decreasing in the order AB1080 > Aldeia e Irmao > Kal-Sorgila. All three clays have

small amounts of illite as second clay phase. Quartz and orthoclase (K-feldspar) are the only accessory minerals and are therefore present in high amounts. The three clays are light reddish to yellow in color. Argila Sorgila is a smectite clay with minor amounts of other clay minerals. Besides that quartz is present in high amounts together with orthoclase and smaller amounts of calcium and iron-carbonate (Calcite and Siderite). The color of this clay can be described as red-brown. Argila Rascoia is a illite clay accompanied with chlorite and some kaolinite. Quartz, feldspars and small amounts of calcite were found as accessory minerals. Furthermore hematite is present in the clay with almost 15 %. The Rascoia clay has a dark brown color. The Søvind Marl comes from Denmark and is a mixed clay containing mainly smectite (> 50 %) and calcite (≈ 25 %). Besides that, minor amounts of quartz, siderite ($FeCO_3$) and pyrite (FeS_2) are present. The Søvind Marl formation has a light brown to grey color. Gniew is a calcareous clay too and comes from Poland, but with illite as the main clay mineral. The total clay and calcite content is lower but the quartz and feldspar content is significantly higher. Furthermore dolomite ($CaMg(CO_3)_2$) and goethite (FeOOH) are present. The color of the Gniew clay is darker brown to grey.

Table 5-2: Chemical composition of the calcined clays when normalized to 100 %.

	Clays from Portugal					Denmark	Poland
Oxide [%]	**AB 1080**	**Aldeia e Irmao**	**Kal-Sorgila**	**Argila Sorgila**	**Argila Rascoia**	**Søvind Marl ***	**Gniew**
SiO_2	61.7	64.5	67.6	62.3	57.0	49.6 ± 0.8	58.3
Al_2O_3	30.5	28.7	26.2	19.8	20.4	18.1 ± 0.1	15.9
Fe_2O_3	3.5	3.1	1.9	7.0	10.1	10.6 ± 0.2	8.1
CaO	0.1	0.1	0.1	3.2	1.1	14.1 ± 0.1	9.3
K_2O	3.3	2.6	3.3	3.1	5.1	2.4 ± 0.0	4.0
Na_2O	—	—	—	0.1	—	0.7 ± 0.1	0.2
MgO	0.4	0.4	0.3	3.1	5.1	2.9 ± 0.0	3.2
MnO	—	—	—	0.1	0.1	0.2 ± 0.1	0.1
P_2O_5	0.1	0.1	0.1	0.2	0.2	0.2 ± 0.1	0.2
TiO_2	0.4	0.5	0.5	1.1	0.9	1.0 ± 0.1	0.8
SiO_2 + Al_2O_3 + Fe_2O_3	95.7	96.3	95.7	89.1	87.5	78.3	82.3

***Average composition of three different bore holes in the same deposit (H2-H4)**

All clays from Portugal have a high amount of SiO_2 and Al_2O_3 due to their composition of mainly clay minerals, quartz and feldspars. The SiO_2 content increases from AB 1080 to Kal-Sorgila because of the increasing quartz content. Only minor amounts of iron minerals and maybe substitution of iron in the clay minerals makes the iron content of the three kaolinitic clays. Table 5-3 shows a comparison of the chemical analysis obtained with XRF to the oxides calculated from the pure phases of the mineralogical composition. The calculated iron content is derived by taking the phases illite, chlorite, siderite, pyrite, hematite and goethite into consideration. The difference in the iron content between the XRF analysis and the calculations can be seen as the substitution of Fe^{2+} and Fe^{3+} for Al or Si in the kaolinite and smectite minerals of the clays.
The rather high potassium content derives from illite and orthoclase (K-feldspar). Even though Aldeia e Irmao contains more illite than the other two, its orthoclase content is significantly lower showing in the lower K_2O content. The higher K_2O content in Kal-Sorgila does not fit the lower amounts of illite and K-feldspar. The excess of oxides from the calculations in Table 5-3 might give an idea of possible amorphous phases. Argila Sorgila and Argila Rascoia have a higher content of Fe_2O_3 than the other clays from Portugal. Argila Sorgila contains small amounts of Siderite ($FeCO_3$). However it can be seen from the calculations that about 3 % of iron are present as substitution for Al in the smectite. The iron rich end member of the smectite solid solutions is called nontronite which might be present in this clay. The high content of iron oxide in Argila Rascoia comes clearly from the mineral hematite (Fe_2O_3), present with 14.7 %. Nevertheless here again 14.7 % hematite do not fit with only 10 % Fe_2O_3 obtained with XRF. The higher CaO content of Argila Sorgila and Argila Rascoia compared to the other clay minerals comes from the small amounts of calcite. The main clay mineral in Argila Rascoia is illite which is reflected in the highest potassium content of all Portuguese clays. The high MgO content of Argila Rascoia derives from the high amounts of chlorite. Chlorite is a so called four layer clay mineral (2:1:1) with a brucite layer ($Mg(OH)_2$) between the packages of usual 2:1 clay minerals like smectites. In Argila Sorgila the MgO content comes mainly from solid solutions in the smectite and small amounts of chlorite. The chemical composition of the two calcareous clays Søvind Marl and Gniew is rather similar. The higher SiO_2 content in Gniew is due to the higher amount of quartz and feldspar minerals. The high amount of illite in Gniew is the reason for the higher K_2O content. Both clays are high in iron. In Søvind Marl the minerals siderite ($FeCO_3$) and pyrite (FeS_2) are present but about 7 % of iron derives from substitution in the clay minerals. In Gniew the iron mineral Goethite (FeOOH) is mainly responsible for the high iron content.

Table 5-3: Calculated oxides (Calc) from the minerals in Table 5-1 compared to the oxides obtained with XRF analysis for all investigated clays. For the calculations the pure phases where taken only. Cation substitution or solid solutions were not considered.

	AB1080 [a]		Aldeia [b]		Kal-Sorgila [c]		Argila Sorgila [d]		Argila Rascoia [e]	
	XRF	Calc.	XRF	Calc.	XRF	Calc.	XRF	Calc.	XRF	Calc.
SiO_2	61.7	66.8	64.5	75.8	67.6	77.9	62.3	75.5	57.0	55.2
Al_2O_3	30.5	26.7	28.7	19.4	26.2	15.6	19.8	13.7	20.4	15.1
Fe_2O_3	3.5	0.3	3.1	1.2	1.9	1.9	7.0	4.3	10.1	16.3
CaO	0.1		0.1		0.1	1.0	3.2	3.8	1.1	3.1
K_2O	3.3	6.3	2.6	4.3	3.3	3.6	3.1	2.3	5.1	4.1
Na_2O	—		—		—		0.1	0.6	—	
MgO	0.4	0.1	0.4	0.2	0.3	0.1	3.1		5.1	3.9
MnO	—		—		—		0.1		0.1	
P_2O_5	0.1		0.1		0.1		0.2		0.2	
TiO_2	0.4		0.5		0.5		1.1		0.9	

	Søvind [f]		Gniew [g]	
	XRF	Calc.	XRF	Calc.
SiO_2	49.6	50.9	58.3	58.6
Al_2O_3	18.1	21.0	15.9	13.6
Fe_2O_3	10.6	3.0	8.1	8.6
CaO	14.1	21.6	9.3	12.5
K_2O	2.4	0.5	4.0	3.7
Na_2O	0.7	0.9	0.2	0.1
MgO	2.9	0.2	3.2	2.3
MnO	0.2		0.1	
P_2O_5	0.2		0.2	
TiO_2	1.0		0.8	

a) Iron calculated from Illite
b) Iron calculated from Illite
c) Iron calculated from Siderite
d) Iron calculated from Siderite, Chlorite, Illite
e) Iron calculated from Hematite
f) Iron calculated from Siderite and Pyrite
g) Iron calculated from Goethite and Illite

According to the ASTM Standard C 618 [44] all clays are good pozzolanic materials with a sum of the oxides $SiO_2 + Al_2O_3 + Fe_2O_3$ higher than 70 %. However in natural pozzolans like clays this sum can be misleading as they can contain high amounts of quartz and feldspars which are not considered to be pozzolanic.

5.2 28 days compressive and flexural strength of standard mortars with 20 % replacement of OPC by calcined clay

In the following chapter the compressive and flexural strength of standard mortars containing different calcined clays as replacement for OPC are compared to each other. In all described tests 20 % of OPC was replaced by the respective calcined clay. Mixing and curing of the mortars was performed as described in Chapter 3.5.

5.2.1 Søvind Marl (SØ) from Denmark

This PhD study started off with investigations on the Søvind marl as potential pozzolanic material for the cement and concrete industry. Since its mineralogy is rather complex it was decided to calcine the marl between 700 and 1000 °C in steps of 50 °C in the first trial. Mortars were mixed by replacing cement with the marl calcined at all temperatures to assess the optimum calcination temperature with respect to reactivity reflected in the strength of mortar prisms. The results of the compressive and flexural strength after 28 days are shown in Figure 5-1.

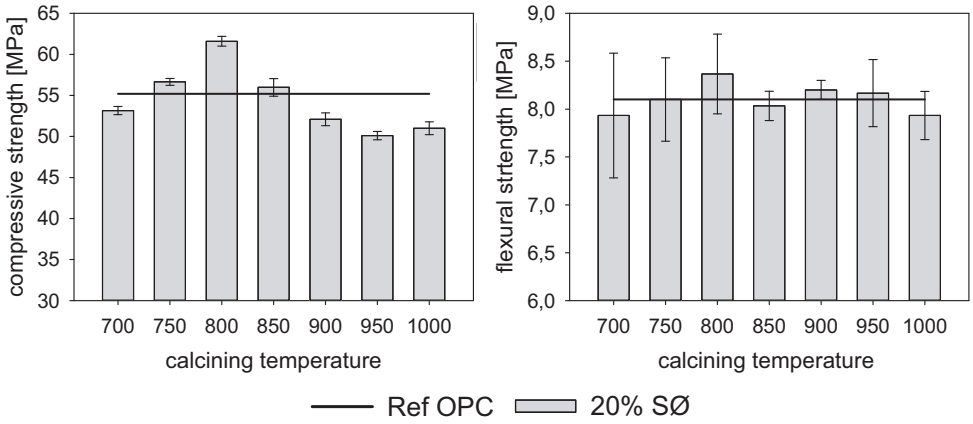

Figure 5-1: Compressive and flexural strength, after 28 days of curing at 20 °C, of standard mortars with 20 % replacement of OPC by Søvind Marl calcined at different temperatures.

The compressive strength of the mortars increases with increasing calcination temperature of the marl up to 800 °C. When calcined at temperatures higher than 800 °C the strength of the mortars decreases again. However in the temperature range

between 750-850 °C the mortars with 20 % replacement of OPC by calcined marl have a higher or equal strength than the reference with 100 % OPC. The highest compressive strength of 61.6 MPa was achieved with the marl calcined at 800 °C. This is about 10 % higher than the reference. The flexural strength shows the same trend as the compressive strength between 700 and 800 °C. At higher temperatures the strength development looks more even and in general it seems that the flexural strength is less sensitive to the calcination temperature, being about the same as the reference taking into account the error bars. The highest flexural strength with 8.4 MPa was also achieved with the mortar containing the marl calcined at 800 °C.
To assess the overall quality of the Søvind Marl deposit three bore holes from different places within the same deposit were taken and given to analysis. This was done because the mineralogy of the same clay can vary within a few meters by accumulation of special minerals. In different depth of the deposit the mineralogy can also change due to different climatic and environmental conditions during the sedimentation. The 3 additionally taken samples from the boreholes were named **H2, H3** and **H4**. From the first mortar tests it was known that the reactivity of the marl was too low to serve as a good pozzolanic material when calcined at temperatures higher than 850 °C. Therefore it was decided to calcine the three marl samples (H2, H3, H4) this time between 600 and 850 °C. Mortar mixes were prepared with all samples. The results of the compressive and flexural strength of the different mortars are given in Figure 5-2.

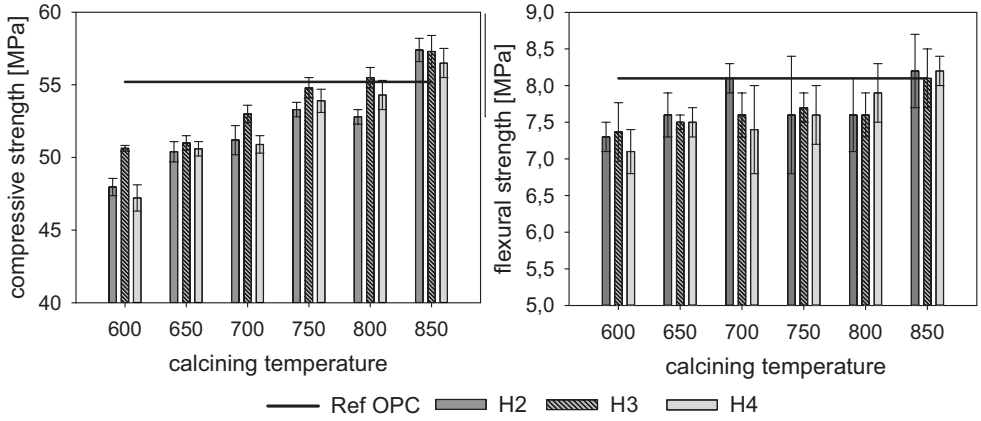

Figure 5-2: Compressive and flexural strength, after 28 days of curing at 20 °C, of standard mortars with 20 % replacement of OPC by H2, H3 and H4 calcined at different temperatures.

With increasing calcination temperature of the marl the compressive strength of the mortars increases for all three bore holes. In general the strength development of

the three samples is quit even with H3 gaining highest strength at all temperatures except at 850 °C. At a calcination temperature of 850 °C all calcined marl samples show their highest reactivity in mortars, gaining a higher 28 days strength than the reference mortar with 100 % OPC. When calcined at 800 °C only marl from the bore hole H3 seems to have enough reactivity to raise the compressive strength of the mortar above the value of the reference. The average strength after 28 days of the mortars containing marl calcined at 850 °C was 57.1 MPa.
In fact the mineralogy of the three bore holes differs slightly which can explain the small differences in the strength development of H3 compared to H2 and H4. A closer look on the bulk mineralogy of the samples from the three bore holes (Table 5-4) shows that there was no siderite and no pyrite detected in H3 and that the quartz content is lower compared to H2 and H4. On the other hand calcite, smectite and kaolinite were measured in higher amounts in sample H3. The higher calcite and smectite content is not in agreement with the lower CaO content measured with XRF in sample H3. In total H3 has the highest amount of clay minerals with 70.5 % compared to 63.1 and 66.5 % for H2 and H4 respectively. The chemical composition of all samples from the three bore holes is rather similar with no significant differences.

Table 5-4: Bulk Mineralogy and chemical composition of the three bore holes (H2, H3, H4) from the Søvind Marl deposit

Bulk Mineralogy				Chemical Composition			
Phase [%]	**H2**	**H3**	**H4**	**Oxide [%]**	**H2**	**H3**	**H4**
Kaolinite	8.9	9.7	6.5	**SiO_2**	48.32	49.19	48.67
Smectite	49.1	56.4	55.1	**Al_2O_3**	16.80	18.36	18.13
Illite	5.2	4.4	3.7	**Fe_2O_3**	10.16	10.39	10.71
Chlorite	—	—	1.2	**CaO**	15.33	12.78	13.34
Quartz	4.7	2.9	5.2	**K_2O**	2.51	2.42	2.29
K-feldspar	—	—	—	**Na_2O**	0.63	0.68	0.72
Plagioclase	—	—	—	**MgO**	2.71	2.80	2.82
Calcite	24.6	26.6	22.8	**MnO**	0.11	0.18	0.34
Siderite	5.3	—	3.9	**P_2O_5**	0.21	0.23	0.23
Pyrite	2.3	—	1.6	**TiO_2**	0.97	1.09	1.08

Regarding the flexural strength a similar trend as for the compressive strength is visible in Figure 5-2. Only the marl samples calcined at 850 °C have sufficient reactivity to increase the strength of mortars when 20 % of OPC is replaced by calcined marl, compared to the reference. When calcined at lower temperatures the

marl samples are less reactive. The mortars containing marl calcined between 600-800 °C have a lower strength than the reference mortar with 100 % OPC, while the strength development is more even compared to the compressive strength.

This calcination trial showed that the reactivity of the Søvind Marl deposit is very sensitive to the right temperature treatment, mainly due to its varying mineralogy. In the first trial the highest strength in mortars was achieved when the marl was calcined at 800 °C. Now the highest strength was achieved with marl samples calcined at 850 °C. Moreover it nearly looks like the compressive strength of mortars containing calcined marl from the bore holes H2-H4 increases linearly with increasing calcination temperature of the marl. So it is not known if the reactivity of the marl could have been even higher in this trial, when the marl was calcined at a higher temperature.
A third calcination trial was performed to narrow down the optimal temperature for the marl. Samples from the three boreholes were mixed together before calcination. The sample called **H2-H4 Mix** was then calcined between 775 and 875 °C with a reduced temperature interval of 25 °C. The results of the 28 days compressive and flexural strength of mortars where 20 % of OPC were replaced with the marl H2-H4 Mix calcined at the different temperatures are given below (Figure 5-3).

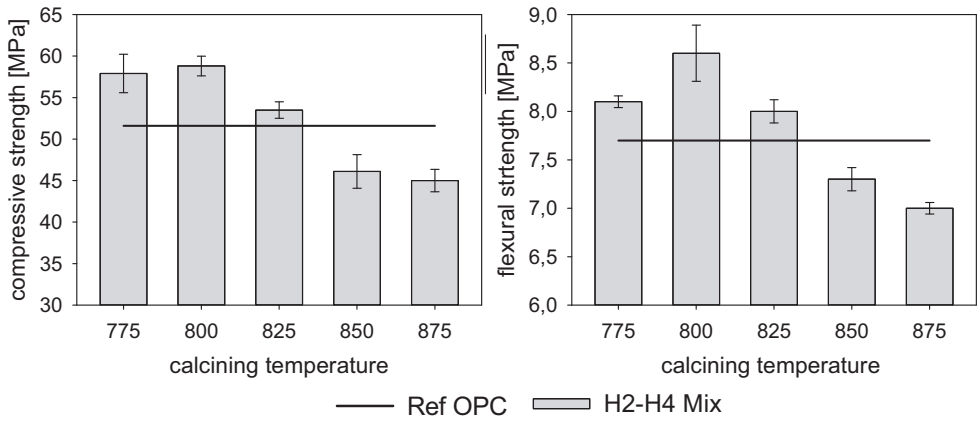

Figure 5-3: Compressive and flexural strength, after 28 days of curing at 20 °C, of standard mortars with 20 % replacement of OPC by H2-H4 Mix calcined at different temperatures.

From this trial it seems that the optimum calcinations temperature for the marl deposit is somewhere between 775-825 °C. In this temperature range the mixed marl is reactive enough to improve the 28 days strength of mortars when used as a replacement material for OPC. The highest compressive and flexural strength with

58.8 and 8.6 MPa respectively was now again obtained with mortars containing marl calcined at 800 °C. It should be noted again, that all clays were burned in the same oven under the exact same conditions. Strangely when calcined at 850 °C the mixture is by far not as reactive as the single samples H2, H3 and H4. The mortar with 20 % H2-H4 Mix calcined at 850 °C has a compressive strength of only about 45 MPa, significantly less than the reference mortar with 100 % OPC. This again confirms the difficulty of controlling the reactivity of the Søvind Marl deposit. Since the reactivity of the calcined marl can change significantly within a narrow window of 50 °C, good process and quality control in case of producing calcined Søvind Marl as pozzolana for the cement and concrete industry, is needed.

5.2.2 Calcined Clays from Portugal

The kaolin to metakaolin transformation starts at around 500 °C and it is known that kaolinite clays can be sufficiently reactive as pozzolana when calcined at temperatures higher than 600 °C [45,114-115]. To ensure a complete conversion to metakaolin it was decided to calcine the 3 kaolinitic clays from Portugal (AB1080, Aldeia e Irmao & Kal-Sorgila) between 700 and 800 °C in steps of 25 °C. The results of compressive and flexural strength of mortars with 20 % replacement of OPC by the respective calcined clays are given in Figure 5-4.

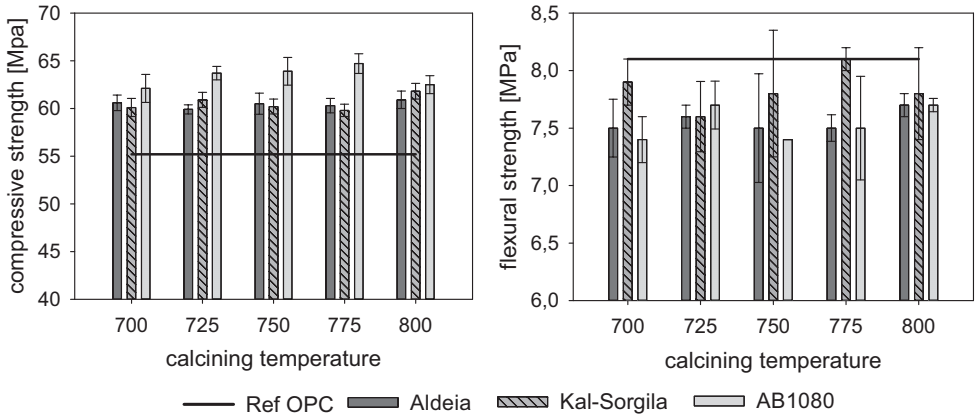

Figure 5-4: Compressive and flexural strength, after 28 days of curing at 20 °C, of standard mortars with 20 % replacement of OPC by AB1080, Aldeia e Irmao and Kal-Sorgila calcined at different temperatures.

In the whole temperature range all clays are reactive enough to act as a pozzolanic additive for cement and concrete. The 28 days compressive strength of mortars

with 20 % replacement of OPC by the calcined clays was for all samples higher than the reference mortar with 100 % OPC. There are only minor differences between the three clays and at the different calcination temperatures regarding the strength contribution. AB1080 gives the highest compressive strength at all temperatures but not the highest flexural strength when used as additive in mortars. The mortar containing AB1080 calcined at 775 °C has with 64.7 MPa (more than 15 % higher as the reference) the highest compressive strength of all. AB1080 has the highest kaolinite content and hence lower amounts of quartz and feldspar, which might explain the higher reactivity.
The average flexural strength of mortars containing calcined clay is slightly lower than the strength of the reference mortar after 28 days. Only the mortar with the clay Kal-Sorgila, calcined at 775 °C, could achieve the same strength as the reference mortar. It is interesting that the Kal-Sorgila clay in general achieves a higher flexural strength in mortars than the other two clays. Kal-Sorgila has with about 70 % the highest sum of Quartz + Feldspar in the bulk mineralogy, prior to calcination.

Since AB1080 showed the best performance regarding the 28 days compressive strength of mortars and because of the similar mineralogy and chemistry of the three kaolinitic clays, only AB1080 was used for further investigations.
On the basis of the good results obtained with the Søvind M
arl which has a clay mineral composition that was expected to be less reactive accompanied with the lowest sum of SiO_2, Al_2O_3 and Fe_2O_3 of all clays, it was tried to produce synthetic marl based on the AB1080 clay to check if this can further boost its already very good reactivity. For this trial simply 15, 20 and 25 % of AB1080 calcined at 750 °C were replaced by laboratory calcium carbonate. Calcium carbonate was added before (added to the raw clay and calcined together) and after calcination (added to the calcined clay) of the clay. Again standard mortars were mixed with 20 % replacement of OPC by the new synthetic “AB1080 marl” mixtures. The results of the 28 days compressive strength of the mortars are shown in Figure 5-5.
The results show that basically the strength of AB1080 when used as pozzolana in mortars did not increase by adding calcium carbonate. Furthermore there is no significant difference if the calcium carbonate is added before or after calcination of the clay, since the calcination temperature is below the decomposition temperature of calcite. However, it is also positive that by replacing 25 % of calcined clay with calcium carbonate the performance of the clay did not decrease, meaning that $CaCO_3$ can be considered to have the same “efficiency factor” as clay. This can

lower the overall costs of the material and additionally have a positive effect on the overall carbon dioxide footprint.

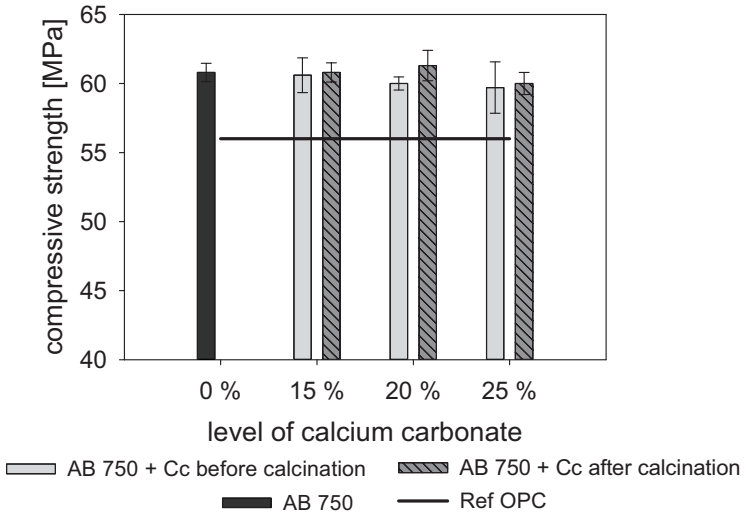

Figure 5-5: Compressive strength, after 28 days of curing at 20 °C, of standard mortars with 20 % replacement of OPC by AB1080 calcined at 750 °C and containing different amounts of calcium carbonate (Cc) added before and after calcination of the clay.

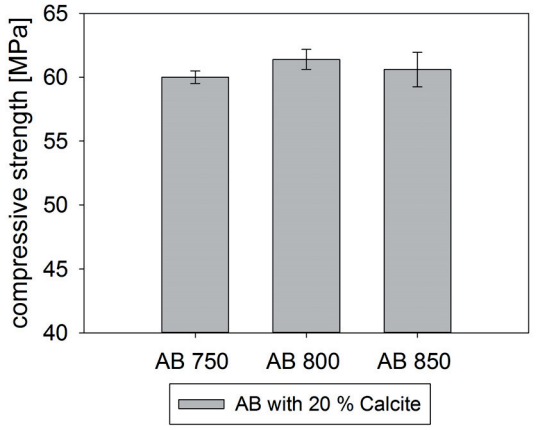

Figure 5-6: Compressive strength, after 28 days of curing at 20 °C, of standard mortars with 20 % replacement of OPC by AB1080 calcined at 750, 800 & 850 °C containing 20 % calcium carbonate that was added before calcination of the clay.

Additional tests were performed where 20 % of AB1080 were replaced by calcium carbonate before calcination at 3 different temperatures (750, 800 and 850 °C) to check if the decomposition of calcium carbonate has any effect on the reactivity

with regard to mortar strength. Mortars were prepared with 20 % replacement of OPC by the "AB1080 marl" and the compressive strength was tested after 28 days (Figure 5-6). Again the compressive strength of all mortars is around 60 MPa. XRD diffractograms and TG/DTG curves of the clay-calcium carbonate mixtures are given in the appendix. It is shown that the calcium carbonate is not completely decomposed even at 850 °C and from the weight loss in the TG curves a residual amount of ~ 6.5 % calcite was calculated. In the AB1080-calcium carbonate mix calcined at 750 °C an amount of ~ 18.6 % calcite was calculated from the TG curves. This shows that there is no difference in the performance if the calcium carbonate is decomposed with the clay or not. The flexural strength of the mortars showed also no difference for the different mixtures.

To assess the pozzolanic quality of non kaolinitic clays the clays Argila Sorgila and Argila Rascoia, containing smectite and illite as main clay minerals respectively, were chosen for additional investigations. Both clays were calcined at 700, 750 and 800 °C and tested in mortars by replacing 20 % of OPC with each sample. The compressive strength after 28 days of the mortars is shown in Figure 5-7 und Figure 5-8. The reference strength for both clays is lower compared to the mortar mixes with AB1080 because of the use of a different batch of cement.

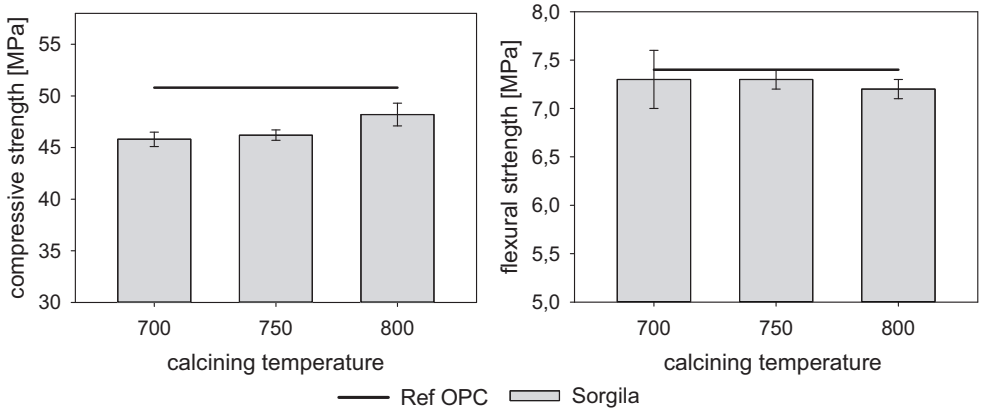

Figure 5-7: Compressive and flexural strength, after 28 days of curing at 20 °C, of standard mortars with 20 % replacement of OPC by Argila Sorgila calcined at different temperatures.

In the chosen temperature range both clays are less reactive than the kaolinitic clays. All mortars were 20 % of OPC was replaced with the calcined clays are lower in compressive strength after 28 days than the reference mortar made with 100 % OPC. Argila Sorgila shows highest reactivity at 800 °C and more reactivity than

Argila Rascoia regarding compressive strength in mortars. The compressive strength of the mortar containing Argila Sorgila calcined at 800 °C is 48.2 MPa. Mortars containing Argila Rascoia calcined at 700 and 800 °C achieve a compressive strength of 44.5 and 44.1 MPa respectively. The average flexural strength of mortars with calcined clay is also below the reference but in case of Argila Sorgila very close to it. In the chosen temperature range both clays could not be activated sufficiently to act as a good pozzolanic material.

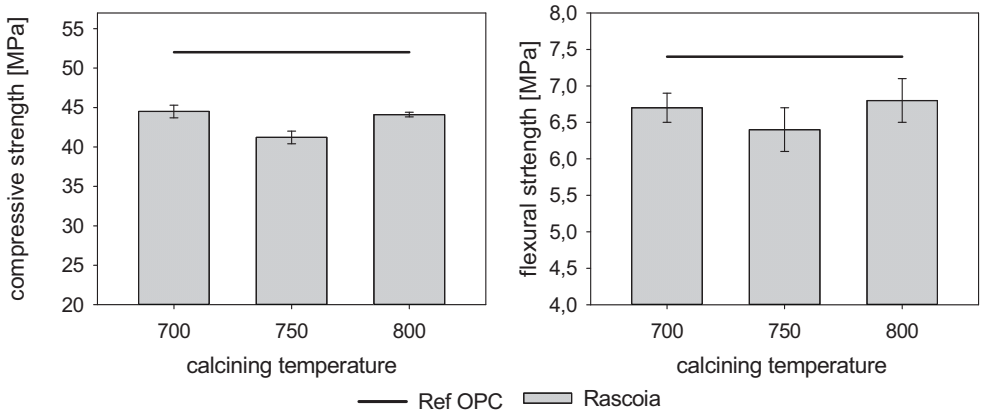

Figure 5-8: Compressive and flexural strength, after 28 days of curing at 20 °C, of standard mortars with 20 % replacement of OPC by Argila Rascoia calcined at different temperatures.

5.2.3 Clay Gniew from Poland

The calcareous clay from Gniew was calcined at the same time as the kaolinitic clays from Portugal and hence at the same temperatures between 700 and 800 °C. This is also the reason why the reference strength is back to the old level. AB1080 and Gniew mortar mixes were prepared at the same time with the same batch of cement. Figure 5-9 shows the results of the performed mortar tests. Mortars containing 20 % of Gniew clay calcined at 775 and 800 °C as replacement material for OPC gained about the same 28 days compressive strength as the reference with about 55 MPa. When calcined below 750 °C the pozzolanic reactivity is lower and mortars mixed with these clay samples have a lower compressive strength than the reference. The average 28 days flexural strength of mortars containing calcined Gniew clay is below the reference for all calcination temperatures. But the flexural strength is quite even for all samples and lies between 7.6 and 7.9 MPa. The reference mortar has a flexural strength of 8.1 MPa.

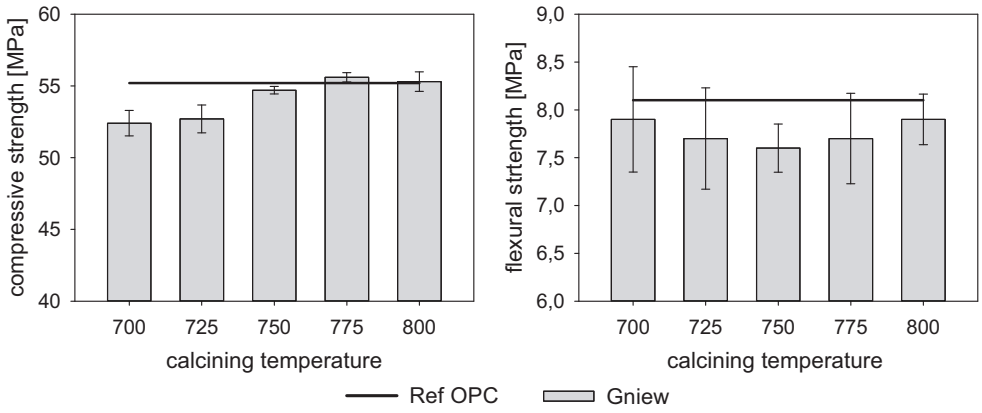

Figure 5-9: Compressive and flexural strength, after 28 days of curing at 20 °C, of standard mortars with 20 % replacement of OPC by the Gniew clay calcined at different temperatures.

5.2.4 Summary

When calcined around 800 °C all clays showed good reactivity regarding the compressive strength in mortar mixes with 20 % replacement of OPC. The optimum calcination temperature for AB1080 was 775 °C but it can be calcined at even lower temperatures (700 °C) with no significant loss in reactivity. Argila Rascoia and Argila Sorgila might need a higher calcination temperature or longer retention time to be made more reactive, but temperatures higher than 800 °C are not very economical. Therefore, to limit the parameters further down the clays burned at 800 °C will be compared to each other in the following chapters. Figure 5-10 shows the relative compressive strength of the mortars with 20 % replacement of OPC by the different clays calcined at 800 °C for 45 min. The reactivity of the clays in mortars increased in the following order:

$$\text{Rascoia} < \text{Sorgila} < \text{Gniew} < \text{Søvind Marl} \leq \text{AB1080}$$

Or expressed by using the main mineral phases:

(Illite, Quartz) < (Smectite, Quartz) < (Illite, Calcite, Quartz) < (Smectite, Calcite, Quartz) < (Kaolinite, Quartz, Feldspar)

A lot of studies were performed with pure clay minerals with the result that illite is only poorly reactive as a pozzolan while kaolinite usually shows the highest reactivity [13, 45-46]. Smectite however is a large mineral group with a wide variety of

chemical compositions and it could be shown that when calcined at optimum temperature Ca-montmorillonite achieved a higher to equal compressive strength in mortars, while Na-montmorillonite had a lower compressive strength than kaolinite. Nevertheless both clays showed higher reactivity than calcined illite [46]. Neglecting the calcareous clays or marls (Gniew and Søvind) and only considering the Portuguese clays, the reactivity increase Illite < Smectite < Kaolinite seems also to proof right in mixed natural calcined clays. The presence of calcium carbonate in Gniew and Søvind Marl seems to increase the pozzolanic activity of illite and smectite rich clays and thus the compressive strength of mortars containing these clays. However, also here the smectite rich Søvind Marl has a higher reactivity in mortars than the illite rich Gniew clay. Another explanation for the good performance of the Søvind Marl might lie in the overall high amount of clay minerals. Søvind Marl contains about 70 % clay minerals, about 20 % more clay minerals than the other clays.

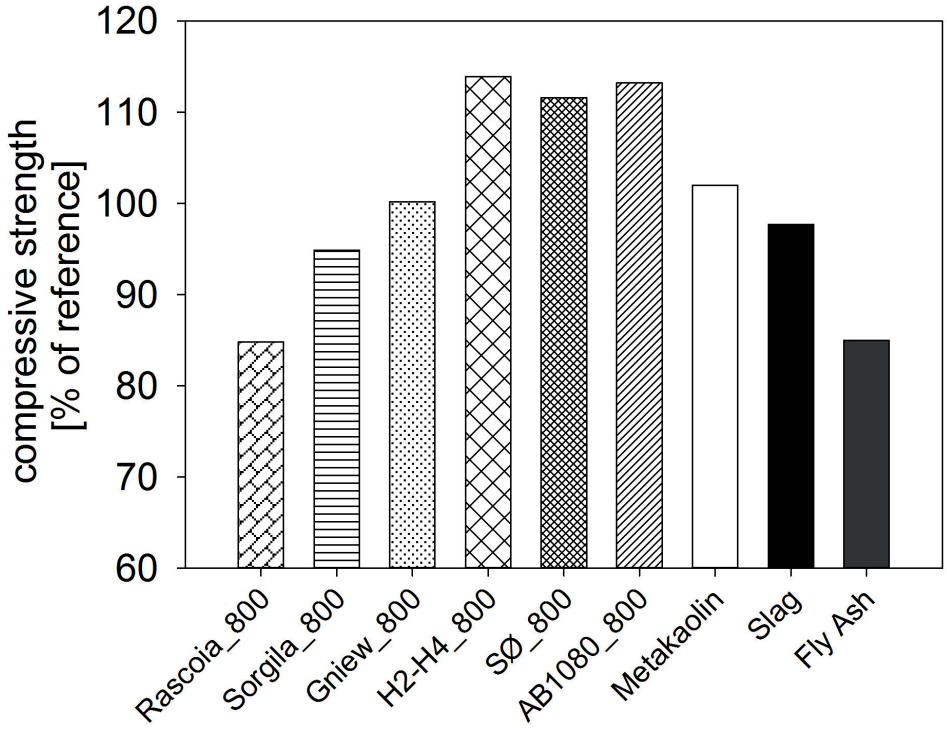

Figure 5-10: 28 day compressive strength of standard mortars with 20 % replacement of OPC by the different clays (Rascoia, Sorgila, Gniew, Søvind marl, AB1080) calcined at 800 °C for 45 min, compared to the 28 days compressive strength of mortars with 20 % replacement of OPC by Metakaolin, Slag and Fly Ash

To compare the performance of calcined natural clays with other popular synthetic pozzolanic materials, additional mortar mixes were prepared by replacing 20 % of OPC with Metakaolin, Slag and Fly Ash (Figure 5-10). After 28 days the Søvind Marl and AB1080 lead to higher compressive strength in the mortars than Metakaolin, Slag or Fly Ash. It is very interesting that the kaolinitic clay AB1080 which contains considerable high amounts of quartz and feldspar performs significantly better than pure metakaolin. When calcined at optimum temperatures AB1080 consists only of about 50 % metakaolin. In mortar mixes with 20 % replacement of OPC by AB1080 there is an actual metakaolin content of only about 10 % of the OPC mass. The high amounts of feldspar and quartz seem to play an important role to explain the reactivity of the calcined AB1080 clay. These non-clay minerals might act as nucleation sites for hydration products or contribute to a kind of filler effect promoting the strength of mortar prisms. In literature it can be even found that these in fact relative stable minerals can react at room to medium temperatures with calcium hydroxide to form calcium aluminate hydrates and thus contributing to the pozzolanic reaction [116]. However it can also be a matter of time. After 28 days not all of the metakaolin in the mortar mix has reacted with calcium hydroxide from the cement hydration. Assuming that for example only 5 % metakaolin of cement mass has reacted, it doesn't matter if the calcined clay contains 10 or 20 % metakaolin. At the same cement replacement level (20 %) both could give the same strength at a given time.
As mentioned in chapter 3.5 it was necessary to use a superplasticizer in the mortar mixes containing calcined clay to keep the w/b-ratio constant at 0.5 and to guarantee a flow of ± 5 % to the reference mix with 100 % OPC. The amount of superplasticizer used in the different mortar mixes can be seen in Table 5-5. When calcined at 800 °C Rascoia, Sorgila, Gniew and the Søvind Marl have a similar water demand. On the other hand AB1080 has a higher water demand and mortar mixes containing this material need more superplasticizer to achieve a good workability. This could indicate a higher surface and hence explain a higher reactivity. As we will see in chapter 5.3.3 AB1080 has in fact a slightly higher surface than the marl when calcined.

Table 5-5: Amount of superplasticizer (Rescon Mapei – Dynamon SP 130) in total % of dry weight of the mortar mixes, when 20% of OPC were replaced with the respective clay calcined at 800 °C for 45 min.

	Rascoia	Sorgila	Gniew	SØ	AB1080	Metakaolin
Amount of SP	0.3	0.3	0.3	0.3	0.7	0.6

5.3 Characterisation of raw and calcined clays

5.3.1 X-ray Powder Diffraction of the raw and calcined clays

5.3.1.1 Søvind Marl

In Figure 5-11 the phase changes and transformations during the calcination of the Søvind Marl between 700-1000 °C are presented.

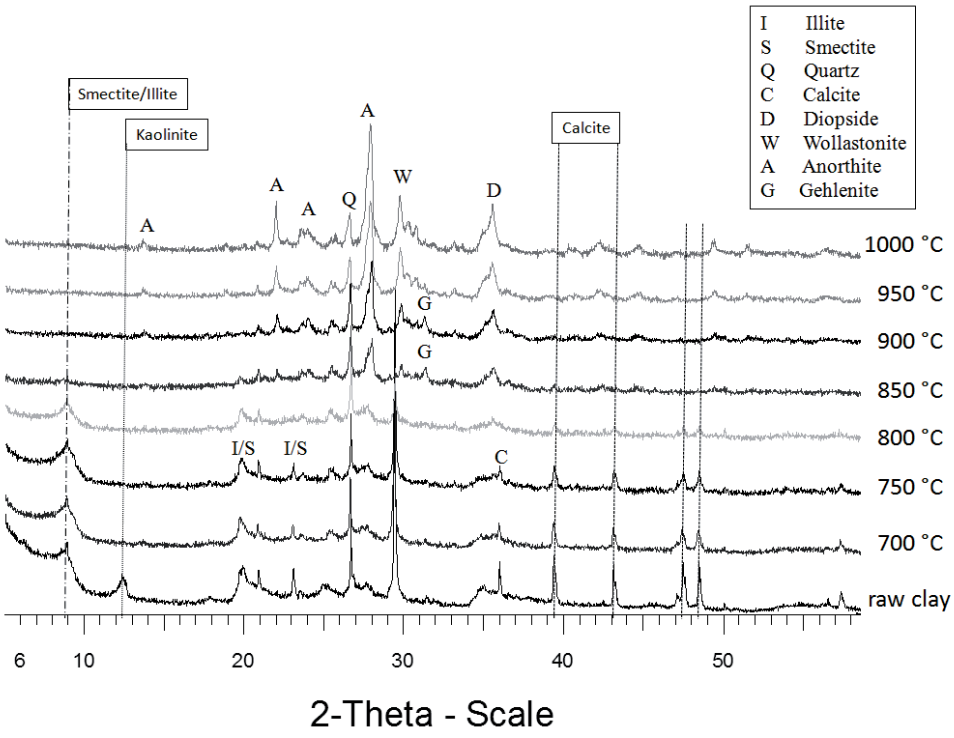

Figure 5-11: XRD of the unburned and calcined Søvind Marl between 700 and 1000 °C.

The raw clay was dried at 100 °C so that the clay mineral structure of smectite is already collapsed due to dehydroxylation of the interlayer space. This causes a shift of the (001) smectite peak from about 6 °2θ to 9 °2θ leading to a overlapping with the (001) illite peak at 8.9 °2θ. At a calcination temperature of 700 °C the (001) kaolinite peak at 12.4 °2θ is disappeared and kaolinite is already completely transformed to metakaolin. On the other hand calcite and the other clay phases (smectite

and illite) are not completely decomposed until 850 °C. Smectite and illite might be in a metastable state but still with some structural features intact. It is known for illite that has a dehydroxylation temperature of 540-580 °C, that its layer structure remains stable upon dehydroxylation until lattice destruction occurs at 890-910 °C [13, 117]. Regarding the elevated background in the clay sample burned at 850 °C it also seems that the highest amount of amorphous phase is present here. Simultaneously with the disappearing of calcite and smectite/illite, recrystallization of high temperature phases begins. Calcite reacts with the phyllosilicate (clay minerals) matrix transforming into Ca-bearing silicates with complete decomposition at 800-900 °C [118]. Due to the calcium, aluminium and silicon made available, mainly "secondary" anorthite ($CaAl_2Si_2O_8$) and wollastonite ($CaSiO_3$) forms at high temperatures. Diopside ($CaMgSi_2O_6$) or other pyroxene phases with similar structure than wollastonite but incorporating magnesium or iron from the clay could be detected as well. Gehlenite ($Ca_2Al_2SiO_7$) appears as an intermediate phase at 850 and 900 °C. Gehlenite is known to be an intermediate phase in the clay firing. When coexisting with quartz or other SiO_2 minerals it becomes unstable and reacts further to anorthite and wollastonite [73-74, 119]. The quartz peak at 26.6 °2θ decreases slightly in intensity above 900 °C, but remains stable until 1000 °C. At 1000 °C and higher temperatures the formation of spinel phases is possible [73, 120]. Especially hematite or magnetite is very likely to form as high temperature phases of the Søvind Marl due to the high iron content in the material. As a matter of fact the sample calcined at 1000 °C showed signs of magnetism, indicating the formation of magnetite (Fe_3O_4). When held next to a common ferrite magnet for whiteboards the powder was magnetically attracted. Nevertheless with XRD the presence of these phases could not be clearly identified.

With regard to the compressive strength results obtained in the mortar tests, the beginning recrystallization of new stable and unreactive phases at 850 °C explains the decreasing reactivity of the marl at temperatures above that and hence the decrease in compressive strength of the mortars. It is interesting that at 800 °C, the temperature of the highest marl reactivity, calcite is not completely decomposed (see chapter 5.3.2.2) and so are the clay phases smectite and illite. Smectite and illite are dehydroxylated but the structure is not destroyed yet. It becomes clear that the window of high reactivity of the marl is rather small between incomplete dehydroxylation/calcination and the beginning of recrystallization.

The samples taken from the three bore holes H2-H4 within the Søvind Marl deposit appeared very similar when measured with XRD. Only minor differences due to the presence of siderite and pyrite in some samples were visible. Figure 5-12 shows the XRD spectra of H4 calcined at 700 and 850 °C, respectively, representing the three bore holes. Beside the gradual decreasing intensities of the smectite/illite and

the calcite peaks there is no huge difference in the spectra between the calcination from 650-850 °C. However the background increases from 700 to 850 °C representing a higher amorphous phase content. Siderite is an iron carbonate that usually has a decomposition temperature between 500-600 °C [117, 121-122]. Therefore it can only be found in the diffractogram of the raw clay.

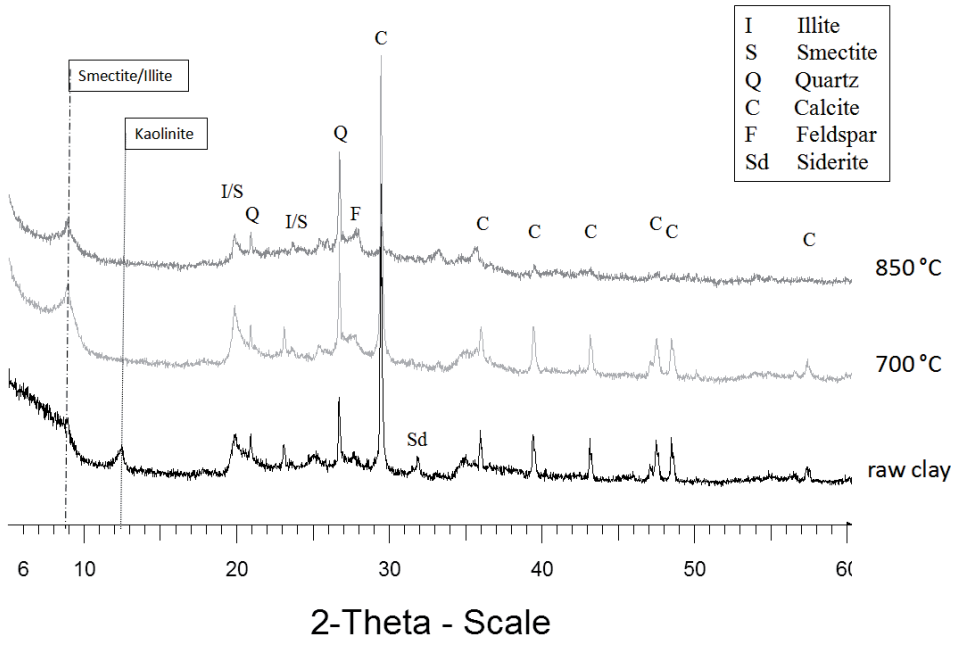

Figure 5-12: XRD of the raw and calcined clay H4 from the Søvind marl deposit

The diffractogram of H4 calcined at 850 °C looks very similar to the diffractogram of SØ calcined at 800 °C. At 850 °C calcite is not completely decomposed. We will confirm in chapter 5.3.2.2 that ~ 5 % calcite is left uncomposed in the sample calcined at 850 °C. The main calcite peak at 29.4 °2θ is still present which is difficult to see while the higher order peaks almost have disappeared. The clay mineral structure of smectite and illite is not completely destroyed and there are no new phases formed yet. To control the reactivity of the marl it seems very important to control the calcite decomposition. Some uncomposed calcite should be left in the marl since immediate recrystallization of new Ca-bearing phases begins with total decalcination. Besides, remaining $CaCO_3$ can become a reactive component for carboaluminate hydrates among the final products of the pozzolanic reaction. Likewise should the clay minerals not be completely destroyed but dehydroxylated and transformed into a metastable reactive state.

5.3.1.2 AB1080

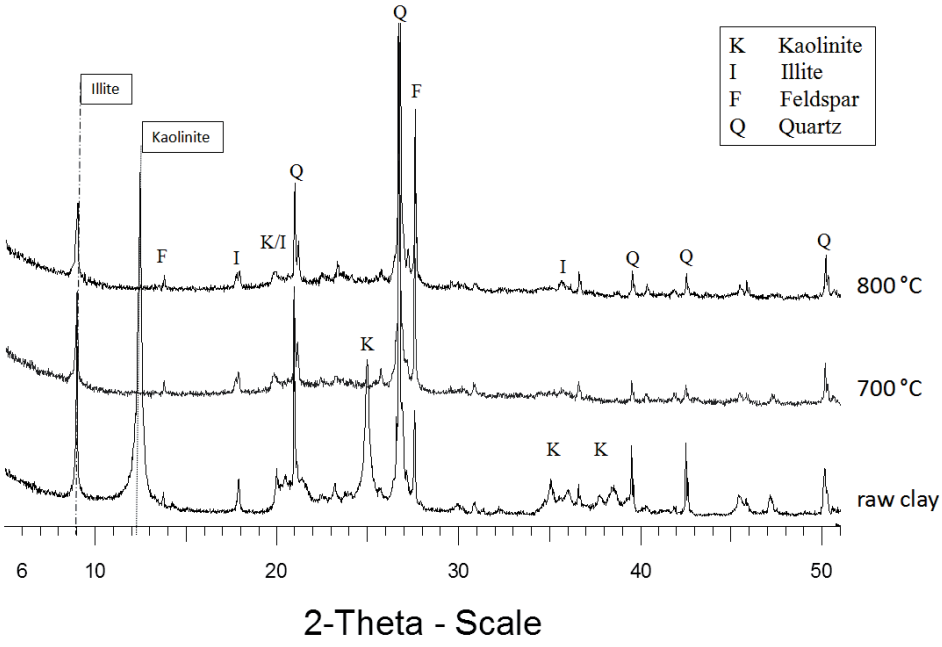

Figure 5-13: XRD of raw and calcined clay AB1080

AB1080 is a kaolinite rich clay containing no smectite minerals but some illite. There are no kaolinite peaks in the spectra of sample calcined at 700 °C which is a sign for complete kaolin to metakaolin transformation. The quartz and feldspars are not affected by the heat treatment. Illite is very crystalline and the peaks are quite sharp for a clay mineral. Sharp peaks at 8.9 °2θ are usually an indicator for the presence of illite. Smectite minerals have a lower crystallinity and often are present as a group of minerals with varying chemistry, thus creating a much broader peak shape. From 700-800 °C there is no difference in the XRD spectra observable except varying peak intensities. As mentioned before, the dehydroxylation of illite has only little effect on the *00l* reflections observed with XRD. The peak intensities are decreasing but there is no broadening and the FWHM (Full Width at Half Maximum) of the *00l* reflections did not change significantly. Parameters influencing the FWHM of illite crystals can be for example layer thickness or disorder in the crystal structure such as lattice strain [123]. The background curve in the spectra of the calcined samples is slightly increased compared to the raw clay. There is no recrystallization to expect in kaolinitic clays when burned at such low tempera-

tures. At temperatures above 1100 °C mullite usually forms as the stable phase in systems containing kaolinite [72, 124].

The almost stable reactivity of the AB1080 clay in mortar testing is coherent with the not changing XRD spectra in the temperature range between 700 and 800°C. The slightly increasing reactivity (strength development) from 700 to 775 °C may be explained with a more stressed metakaolin structure of even lower ordering with increasing calcination temperature. The background however did not increase in the XRD spectra from 700 to 800 °C.

5.3.1.3 Argila Sorgila and Rascoia

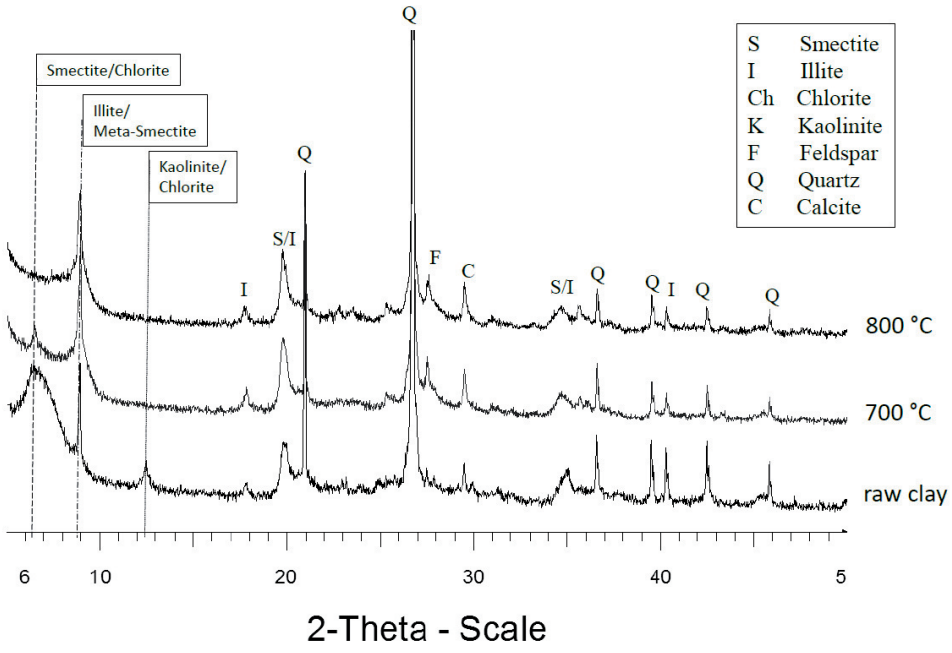

Figure 5-14: XRD of raw and calcined Argila Sorgila

The raw clay sample is dried only at room temperature, so that a clear differentiation between smectite (6 °2θ) and illite (8.9 °2θ) peaks is possible. At 6 and 12.4 °2θ chlorite overlaps with smectite and kaolinite respectively. Calcination at 700 °C leads to the decomposition of kaolinite and dehydration of the interlayer space in smectite minerals. The collapsed smectite structures are recognizable in a peak shift from 6-9 °2θ. Due to the overlapping (001) reflections of illite and smectite at

higher temperatures the illite peak appears more broad. Only the brucite layer in chlorite minerals is decomposed at 700 °C [117] explaining a small remaining peak at 6 °2θ. At 800 °C the mica layer of chlorite minerals is dehydrated as well and the chlorite peaks disappear. There are no further changes detectable in the diffractogram from 700-800 °C. The smectite structure as visible with XRD seems to be stable in the temperature range and so are the non clay minerals like quartz and feldspars. Even the small amounts of calcite show no sign of decomposition at 800 °C. In general the diffractogram of Sorgila looks more crystalline at 800 °C than the diffractogram of the Søvind Marl at the same temperature. The peaks are much sharper, the clay minerals and calcite are less affected by the heat treatment and the background curve is not getting significantly higher with temperature. There seems to be very little to no degree of amorphization.

Argila Rascoia is good example for the identification of chlorite minerals in mixed clays (Figure 5-15).

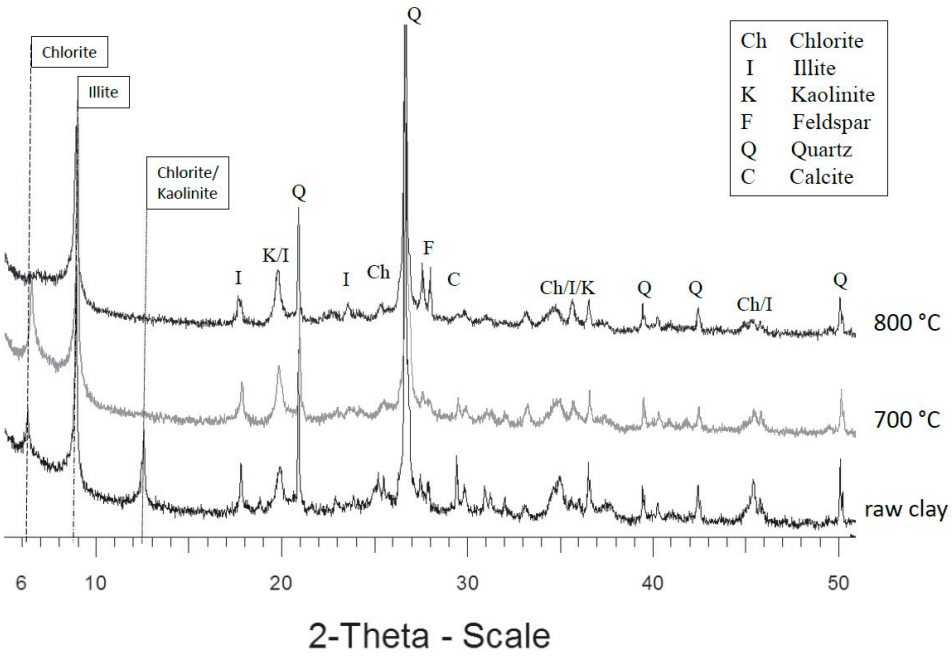

Figure 5-15: XRD of raw and calcined Argila Rascoia

This clay contains almost no smectite minerals, so that the peak at 6.3 °2θ belongs entirely to chlorite. When chlorite is heated up to temperatures above 500 °C the brucite layer in the structure dehydroxylates. This leads to an increased intensity of

the (001) reflection and a shift from about 6.3 to 6.4 °2θ, while the higher order peaks are significantly weakened [16]. This effect is clearly visible in the XRD spectra of Rascoia calcined at 700 °C. The (002) peak at 12.4 °2θ disappears completely, additionally pronounced due to the decomposition of kaolinite, while the (001) peak at 6.4 °2θ increased in intensity. At 800 °C the mica layers of the chlorite minerals are destroyed and the (001) reflection at 6.4 °2θ disappears as well. The small amounts of calcite present in the raw clay are decomposed at 800 °C in this clay. There is again only a small increase in background in the heated samples.

It is difficult to say why Argila Rascoia and Argila Sorgila are less reactive than the other clays when only looking at the XRD data of the raw and calcined clays. However these two clays appear more crystalline and stable when calcined, with less amorphization and less transformation of the present clay minerals to metastable phases. In general regarding the mineralogical composition, these clays were expected to be less reactive than the AB1080. Nevertheless a longer retention time in the kiln was not tested for these clays and might beneficiate a higher reactivity.

5.3.1.4 Gniew

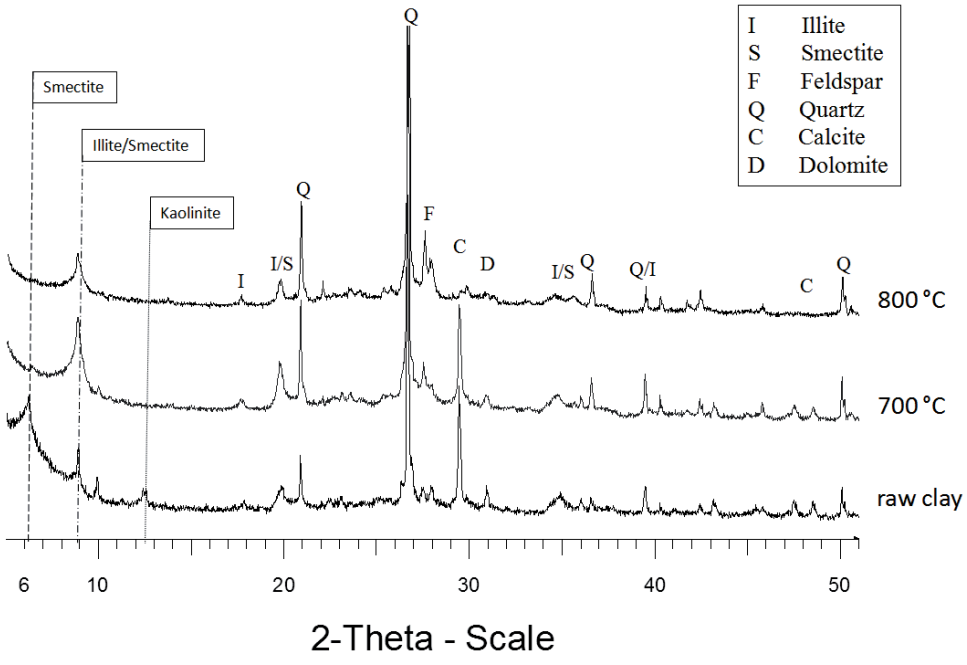

Figure 5-16: XRD of raw and calcined clay Gniew from Poland

In the XRD spectra of the raw clay from Gniew it looks like it is containing more smectite than given in the mineralogical composition. At 800 °C the overlapping peak for smectite and illite decreased in intensity due to complete dehydroxylation and a starting destruction of the structures. Kaolinite is transformed to metakaolin and calcite and dolomite seem to be completely decomposed at 800 °C. In the Gniew clay the present calcite seems to be less stable than in the Søvind Marl where some of the calcite was left uncomposed at temperatures around 800 °C. We have to keep in mind that the calcium carbonate of Gniew and Søvind Marl derives from two different sources. While the $CaCO_3$ in Gniew derives mainly from carbonate rocks the main $CaCO_3$ source of Søvind Marl are coccoliths. Different particle sizes and impurities of $CaCO_3$ in both clays may be responsible for the different thermal behavior and stability.
In the spectra of the raw clay a new peak at 9.8 °2θ is visible. This peak may either belong to the smectite phase or a zeolite phase. According to the search results obtained using the ICDD data base for qualitative XRD phase analysis it might be a sodium potassium containing aluminum silicate hydrate phase (zeolite LSX) [125].

5.3.2 Thermal Analysis of the raw and calcined clays

5.3.2.1 Characterization of the raw clays

With the help of thermal analysis the exact dehydroxylation or decomposition temperatures of different mineral phases can be determined. Since different types of carbonates or hydroxides and clay minerals possess different peak temperatures, thermal analysis can serve as a good supplementary method for the characterization of raw materials. In the calcined clay samples the degree of dehydroxylation and decomposition can be checked. This can give crucial information about the reactivity of the material.
Figure 5-17 shows the curves of the derivative thermogravimetry of the 5 analyzed raw clays. All raw clays were dried for 2 h at 40 °C prior to analysis.
Figure 5-17 can be divided into three 3 main regions, a low temperature region (100-250 °C), a mid temperature region (400-600 °C) and a high temperature region (600-850 °C). The weight losses of the different clays in these temperature regions are listed in Table 5-6. The DTG signals of all materials below 200 °C are due to the loss of adsorbed water, pore water or water in the interlayer space of clay minerals. The size and shape of this first peak depends on the type of clay mineral, the moisture content and the type and amount of exchangeable cations.

Among the clay minerals, montmorillonite shows the widest peaks in this temperature range [126]. The double peak (130 and 200 °C) or peak shoulder observed for Sorgila at around 200 °C is typical for the presence of smectite minerals containing bivalent cations [126]. From the chemical composition we know that Argila Sorgila contains significant amounts of CaO and MgO but only minor amounts of calcium carbonate and chlorite. Therefore the Ca^{2+} and Mg^{2+} must derive to a large content from the smectite mineral structure. The Gniew clay shows a similar peak shape. The Søvind Marl (H4) also contains smectite as the main clay mineral in the mineralogical composition. Nevertheless, it shows only a single peak at 130 °C. The reason for that is in general the presence of clay minerals with monovalent cations [126].

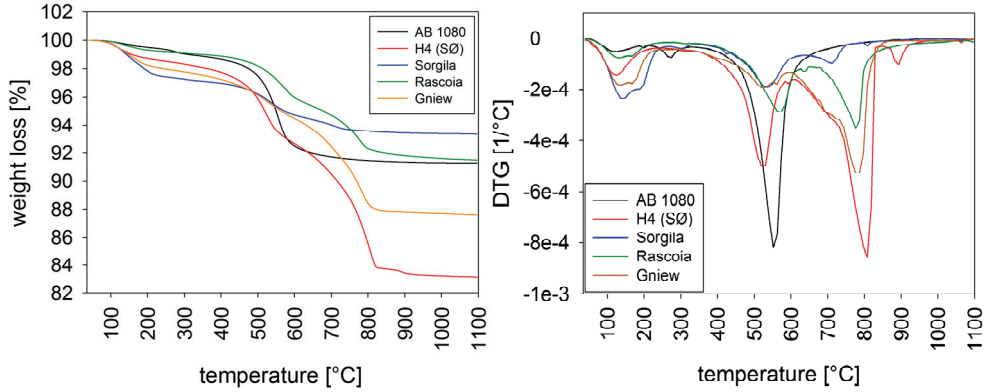

Figure 5-17: Thermogravimetry (left) and differential thermogravimetry (right) of the raw clays under investigations. All clays were dried for 2 h at 40 °C in the machine in nitrogen atmosphere prior to measurement.

Argila Rascoia and AB1080 show only small peaks below 200 °C. Typically kaolinite has no low temperature peak, so that the signals visible are due to the illite in these clays. Considering the weight loss of the clays in the different regions the amount of the different clay minerals can be estimated. Regarding the AB1080 clay and attributing the peak below 200 °C to the loss of water from illite a content of about 4.7 % illite can be recalculated from the mass loss. Additionally, regarding the peak between 400-600 °C as the dehydroxylation of kaolinite only, a kaolinite content of about 47.8 % can be recalculated from the mass loss and the molar masses. As illite also shows a signal in the same temperature region as kaolinite and considering this overlapping, the calculated values are not too far away from the real mineralogical composition.

AB1080 and Sorgila exhibit small peaks at 270 and 300 °C respectively. These peaks are probably due to the presence of small amounts of iron hydroxide phases

like limonite or goethite which were detected in the clay mineral fraction but were present in too small amounts to appear in the total bulk mineralogy [127].

Table 5-6: Weight loss of different clays in the 3 temperature regions, 0-250 °C, 400-600 °C and 600-850 °C, taken from the TG curves in Figure 5-16.

	weight loss in the 3 temperature regions in %		
Sample	**0-250 °C**	**400-600 °C**	**600-850 °C**
AB1080	0.56	6.67	——
H4 (SØ)	1.33	5.51	8.81
Sorgila	2.56	2.24	1.06
Rascoia	0.76	2.98	3.34
Gniew	1.95	2.78	6.56

The peaks in the mid temperature range are mainly associated with the loss of hydroxyls from the octahedral layer of clay minerals belonging to the kaolinite and illite group [59, 126-127]. These clay minerals are hard to distinguish when they are present together in the same clay since their dehydroxylation peaks overlap in this temperature region. AB1080 has the highest amount of kaolinite and hence shows the sharpest and most distinctive peak at 550 °C. This is because the magnitude of the dehydroxylation is much greater for kaolinite than for illite. The peak temperature of Søvind Marl in the mid temperature region is 525 °C. Conclusions about the crystallinity of kaolinite can be drawn from its dehydroxylation temperature, meaning the higher the dehydroxylation temperature the more ordered the kaolinite structure [128]. The illite rich Rascoia clay shows a peak temperature of about 575 °C. In this material the dehydroxylation of kaolinite, illite and the brucite layer of the chlorite, sum up in this one peak. In mixtures of illite and kaolinite the peak between 500-600°C looses in magnitude the higher the illite content in the mixture [129]. The same results are obtained with the raw clays were the intensity of the dehydroxylation peak decreases from AB1080 (Illite/Kaolinite = 3/97) to H4 (Illite/Kaolinite = 35/65) to Rascoia (Illite/Kaolinite = 90/10). The dehydroxylation of the illite and kaolinite contained in Gniew and Sorgila takes place at around 525 and 540 °C respectively. Sorgila shows one additional small peak in mid temperature range around 425 °C which is most likely the result of the decomposition of siderite.

The peaks in the high temperature range of the investigated clays can mainly be attributed to the dehydroxylation of smectite minerals and the decarbonation of calcite. Søvind Marl with the highest amount of smectite and calcite exhibits the largest peak between 600-800 °C. This peak can be separated in a sharp peak ranging from 730-830 °C and a shoulder between 600-730 °C. The shoulder can be assigned to the dehydroxylation of the octahedral layer of the smectite while the

sharp peak shows the decomposition of the calcite. At 900 °C the final breakdown of the illite and montmorillonite lattice is visible in a small peak [59, 127]. The Gniew clay shows a similar peak shape in this region but of smaller magnitude due to the lower amounts of the mentioned phases. The signal around 775 °C of Rascoia is probably due to the final dehydroxylation of the chlorite and the decomposition of the small amounts of calcite [59]. Sorgila has two signals at 700 and 800 °C owing to the smectite and minor amounts of calcite in the clay.

5.3.2.2 Calcined Clays

The TG/DTG curves of the Søvind Marl (H4) calcined between 600-850 °C are given in Figure 5-18. All samples show a small peak at 100 °C associated with the loss of adsorbed water from the atmosphere at the mineral surfaces during the storage of the clays. Already at a calcination temperature of 600 °C, the signals for the dehydroxylation of kaolinite and illite are almost completely disappeared. The peak in the high temperature region of the DTG curves still has the same shape as in the raw clay but with much smaller magnitude. With increasing calcination temperature from 700-850 °C this peak decreases in intensity and shifts to lower temperatures. At a calcination temperature of 800 °C the left hand shoulder representing the presence of smectite seems to level out. When calcined at 800 and 850 °C we can therefore assume that smectite is completely dehydroxylated and that the remaining peak belongs to the decarbonation of the calcite left in the sample. This is confirmed with FT-IR spectroscopy in chapter 5.3.5. Attributing this peak entirely to $CaCO_3$ and taking the weight loss between the horizontal tangents in the TG curves in this area, a remaining calcium carbonate content of about 7.7 % and 4.5 % can be recalculated in the sample calcined at 800 and 850 °C respectively.
The TG/DTG curves of the second calcareous clay Gniew are very similar to what can be seen in Figure 5-18. The curves are plotted in the appendix and confirm that the decomposition of calcium carbonate is a gradual process starting at 700 °C. At a calcination temperature of 800 °C there is a small peak left in the DTG curve around 700 °C which can be assigned to the decomposition of residual $CaCO_3$. From the weight loss in the TG curve a remaining calcium carbonate content of about 0.6 % can be recalculated for the sample calcined at 800 °C. The FT-IR spectra presented in Chapter 5.3.5 will confirm that there is an insignificant amount of $CaCO_3$ left at 800 °C.
Kaolinite and illite in AB1080 are completely dehydroxylated at 700 °C. As a result the TG/DTG curves show no significant difference for the samples calcined between 700-800 °C.

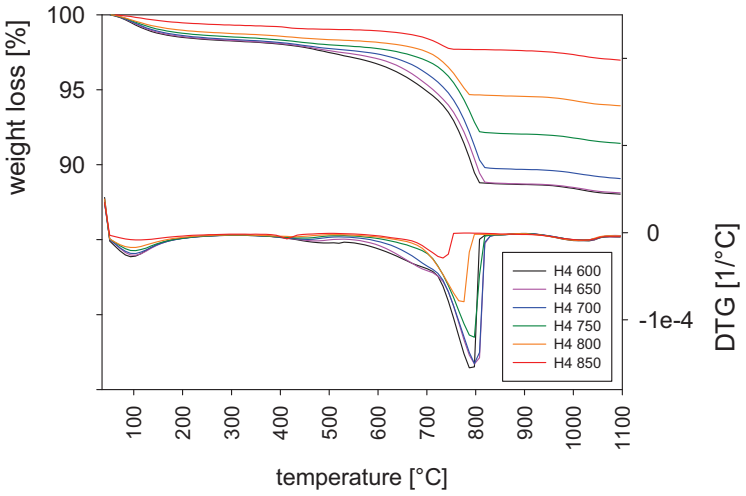

Figure 5-18: Thermogravimetry and differential thermogravimetry of Søvind Marl (H4) calcined between 600-850 °C.

In comparison, the smectite rich Sorgila and the illitic clay Rascoia are not as much dehydroxylated as the other clays in the temperature range between 700-800 °C. The TG/DTG curves of these two clays are shown in Figure 5-19.

Sorgila still contains about 2-3 % water in form of hydroxyls when burned at 800 °C compared to about 4-5 % in the raw clay. In the DTG curves the low temperature peak shifted for both clays to a lower temperature with disappearance of the shoulder. This means that the pore and interlayer water is removed from the clay minerals upon the calcination as expected. The single peak visible at 100 °C is now only due to adsorbed water molecules during the storage of the clays. In both clays the mid temperature peak decreased significantly in magnitude due to dehydroxylation of kaolinite and illite. While in Rascoia these two minerals seem to be largely decomposed, there is some more left in Sorgila. The smectite minerals and carbonates are in both cases not completely decomposed. For Sorgila the high temperature peak around 750 °C in the DTG even increased upon calcination. With increasing calcination temperature both clays gradually lose their hydroxyl groups, Rascoia in a greater magnitude. Especially Sorgila still contains a rather high amount of unhydroxylated clay minerals even at a calcination temperature of 800 °C. This is part of the explanation why these two clays are less reactive compared to AB1080 or the Søvind Marl. Possibly the clay minerals in these two clays are more stable and need a longer retention time to be as much decomposed as the others at the same temperature. One always has to keep in mind that there is a temperature profile and not a constant temperature in all areas of a rotary kiln. With a

total retention time of 45 min it is actually possible that the material is only for some minutes in the hot zone, exposed to 800 °C. In theory the clay minerals in Sorgila and Rascoia should be dehydroxylated when calcined at 800 °C.

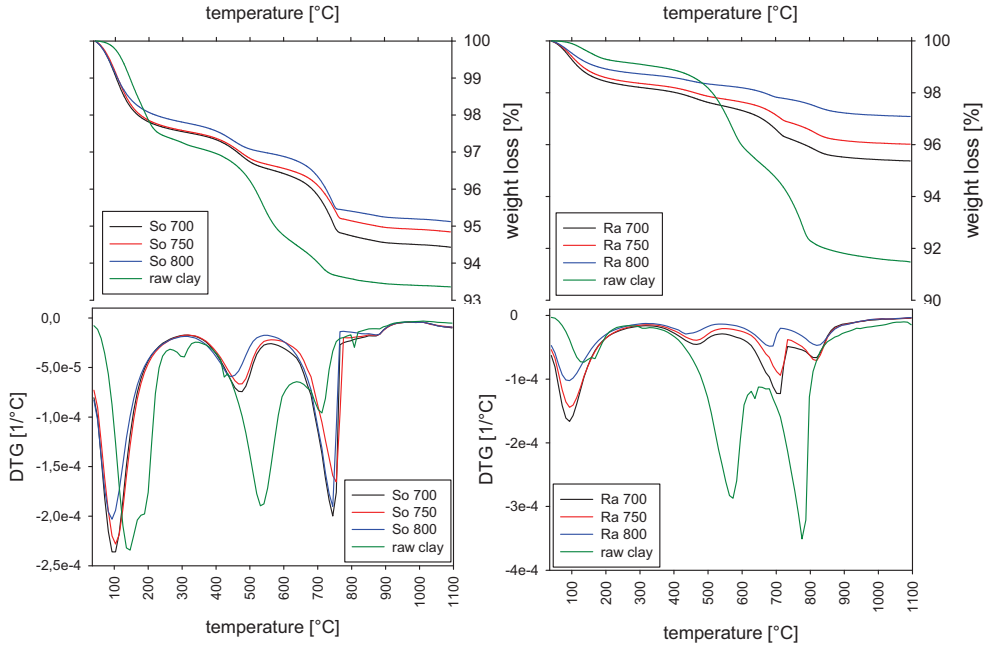

Figure 5-19: Thermogravimetry and differential thermogravimetry of raw and calcined Argila Sorgila (left) and Argila Rascoia (right)

5.3.3 Specific surface area (BET) and Particle size distribution (PSD) of raw and calcined clays

The BET surface based on nitrogen absorption and the particle size distribution (laser granulometry) was determined for all clays in the unburned but dried state as well as in the calcined state. The obtained results are given in Table 5-7. Figure 5-20 compares the behavior of Søvind Marl and the kaolinitic clay AB1080. The two clays behave completely different upon calcination. While the BET surface of the smectite rich Søvind Marl decreases with increasing temperature, the kaolinite rich AB1080 shows no significant change and the BET surface is almost stable. Similar trends as for AB1080 were observed for the single minerals illite and kaolinite or clays of similar composition [13, 40, 46].

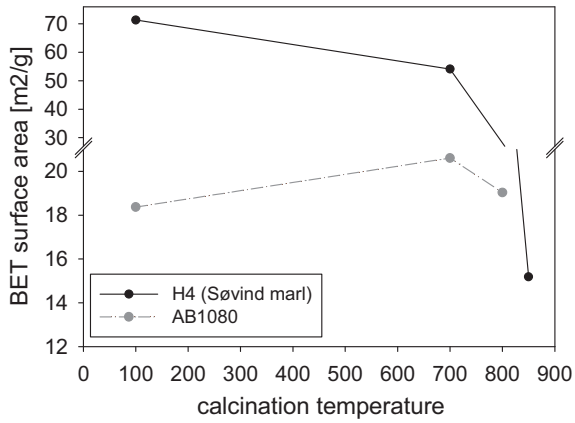

Figure 5-20: BET surface of Søvind Marl and AB1080 in the raw and calcined state

Clay minerals in general can have huge specific surfaces due to their layered structure with huge surfaces in relation to their grain size of < 2 µm. Swelling clay minerals like smectites have additional inner or intercrystalline surfaces, exceeding the outer surfaces in many cases by far. Therefore smectites usually possess bigger surfaces than the other clay mineral groups and can reach values of up to 600-800 m^2/g [19].

When calcined to 700 °C the specific surface of Søvind Marl falls from 71.3 to 54.1 m^2/g. This small decrease is the result of a first collapse of the structural 3 layer packages through dehydration of the interlayer spaces reducing the d-spacing of the mineral structure as observed with XRD. Upon further heating to 850 °C the specific surface drops significantly to 15.1 m^2/g. As a comparison silica fume has a

typical BET surface of 20 m^2/g [130]. A complete dehydration and dehydroxylation causes further decrease of the inner surfaces. Recrystallization of new phases can be excluded as it was not observed with XRD for H4 at 850 °C. Reduced pore sizes through a reorganization of the clay mineral structure upon dehydroxylation or sintering effects in the powder can however not be ruled out yet.
The specific surfaces of AB1080 are 18.4, 20.6 and 19.0 m^2/g at 100, 700 and 800 °C respectively. These values are probably within the real error of the equipment, so that the specific surface does not change much for AB1080 when calcined. Quartz and feldspar minerals do not undergo any significant changes when heated to these temperatures. The 2% change in volume which might occur due to the transformation of α- to β-quartz at a temperature of 575 °C is reversible when cooled down. Even the transformation of kaolinite to metakaolin has only a minor dependence on the specific surface of kaolinite [13, 46].

Table 5-7: BET surface and Particle Size Distribution (Laser) of all raw and calcined clays

Sample Name	BET [m^2/g]	PSD (laser granulometry) d_{10} [µm]	d_{50} [µm]	d_{90} [µm]
H4 (SØ) raw	71.3	1.5	5.7	17.7
H4 (SØ) 850	15.1	1.3	14.1	76.3
AB1080 raw	18.4	1.7	8.3	74.4
AB1080 800	19.0	1.7	10.8	46.1
Sorgila raw	20.8	2.1	10.4	82.2
Sorgila 800	29.1	1.4	9.0	33.9
Rascoia raw	40.5	2.0	12.0	46.1
Rascoia 800	22.9	1.4	8.6	40.8
Gniew raw	48.1	1.4	4.8	108.1
Gniew 800	8.9	0.9	9.1	51.7
Metakaolin	10.8	1.3	5.1	17.1
OPC	1.5	2.4	15.2	209.4

The calcareous clay Gniew shows a similar behavior as H4 with a significant drop in the specific surface from 48.1 to 8.9 m^2/g when calcined at 800 °C. Some authors propose the formation of a vitreous phase at temperatures around 800 °C in calcite rich clays [73, 131]. Upon fast cooling this can lead to the formation of larger glassy particles, decreasing the total surface of the clays. Sorgila is the only clay exhibiting a higher specific surface when calcined at 800 °C compared to the raw clay. Sorgila contains some calcite and siderite and in some cases the decomposi-

tion of carbonate phases can lead to a secondary porosity [132]. This might increase the surfaces here. The decreasing d_{50}-value of Argila Rascoia upon calcination is not in agreement with the decreasing BET surface.
In general the specific surface of the clays alone cannot explain the varying reactivity, since the least reactive clays in mortar tests exhibit the highest specific surfaces of the investigated clays.
Synthetic metakaolin and cement used in later experiments have a specific surface of 10.8 and 1.5 m^2/g respectively.
Particle size distribution shows less variation between the different calcined clays. All clays except H4 have a d_{50} of about 10 µm. H4 has the highest d_{50} and d_{90} values with 14.1 and 76.3 µm respectively.

It has to be kept in mind that both the BET measurement of the specific surface area and the particle size distribution based on laser diffraction can only provide estimates [133-134]. Both methods are associated with many uncertainties and a lack of accuracy for the determination of clay particles. The measured adsorption of nitrogen (BET) is strongly dependant on the preparation of the sample especially the degassing conditions. Some clay minerals have a narrow temperature window where only weakly adsorbed water is removed from the particles but no structural water is affected. Moreover micropores that are not completely filled by the gas, the surface heterogeneity of clay minerals, possible interactions between nitrogen and surface cations or other polar surface sites can further affect the results [134].
In PSD measurements based on laser diffraction, the Mie theory used to calculate the particle size distribution can only offer an exact solution to the scattering of light from a perfect sphere but not from an irregularly shaped particle. The averaged cross-sectional area over all particles is greater for layer silicate structures than for spheres which usually leads to an overdimensioning of the particle size and the number of particles in a coarser fraction [133].

5.3.4 HR-ICP-MS

3 grams of clay (raw and calcined) were dissolved in deionized water and in an alkaline solution (pH = 13.2) and the release of ions from the clay was measured after 3 days. Emphasis is put on the release of silicon and aluminum ions as these are the main elements contributing to the pozzolanic reaction to form C-S-H and C-A-S-H phases in reaction with calcium hydroxide. Furthermore the release of alkalis, especially K^+ is of particular interest. The possible formation of KOH in solution may help to activate the pozzolanic reaction and to accelerate it in blended cements. An increase in pH from 6 to 11 was measured when the calcined Søvind Marl was mixed with distilled water. Main sources of potassium in the investigated clays are illite and orthoclase (potassium feldspar). It is reported that the release of potassium from muscovite and feldspars increases significantly when these are heated to 700 °C [135-136]. Micas have the same structure and building units as illite, but not all micas behave in the same way. The release of potassium from biotite for example is retarded upon heating [136]. Investigations on clay-based geopolymeric binders recently showed that the release of aluminum and silicon from illite and smectite clays in alkaline solutions, increased with increasing burning temperature. Above a certain temperature when recrystallization of new stable phases occurred, the release of these ions declined again. Clays composed of mixtures of smectite and illite showed higher release rates than clays containing mainly illite [137]. Moreover it was shown that the release of silicon is at all times higher than the release of aluminum. This makes sense in 2:1 clay minerals where the tetrahedral silicon layers are more exposed to the environment than the octahedral layer. In case of smectite and illite the dissolution of the tetrahedral layer is the limiting element while in kaolinite it is the octahedral layer [49].
In Table 5-8 the ion release of raw and calcined Søvind Marl in deionized water is presented.

Table 5-8: Ion release of Søvind Marl in deionized water

	Si 30 [mg/l]	Al 27 [mg/l]	Ca 44 [mg/l]	Fe 56 [mg/l]	Na 23 [mg/l]	K 39 [mg/l]	Mg 25 [mg/l]	S 35 [mg/l]	Cl 35 [mg/l]
SØ raw	9.6	1.9	8.2	2.7	72.8	8.4	2.4	37.4	3.6
SØ 850	4.0	4.1	73.0	0.0	0.0	5.6	0.0	54.9	0.0

As expected the release of silicon ions from the raw clay is greater than the amount of released aluminum. Ca^{2+} is probably mainly derived from the dissolution of the calcium carbonate. However simple calculations using the solubility product of calcite ($K_{sp} = 3.3*10^{-9}$ mol/l [138]) result in a calcium concentration of about 2.3 mg/l for inorganic calcite (calculations are given in the appendix). This is considerably less than the measured 8.2 mg/l. As mentioned in chapter 4.1.2 and 5.3.6 the main source of calcium carbonate in Søvind Marl are coccoliths. Nevertheless the solubility of the calcite crystals from coccoliths should not differ noticeably from other inorganic calcites. The additional Ca^{2+} in solution may also derive from the smectite. Calcium and sodium ions located in the interlayer space are easily set free in solution. Magnesium and iron, most likely from the octahedral layer of the smectite, go into solution in about the same range as aluminum. Potassium is released from illite which is the major source of potassium in Søvind Marl. The highest values are obtained for sodium ions. Sodium is like calcium placed in the interlayer spaces of smectite minerals, only weakly bound and is probably set free in a cation exchange reaction. Sodium is maybe exchanged with calcium which is a typical process since the ionic radii of these two ions are very similar with 0.99 and 1.00 Å respectively. An explanation for the small sodium release in the calcined clay might be that the cation exchange capacity of the smectite is no longer provided. Upon calcination the smectite structure is collapsing due to dehydration and dehydroxylation. The interlayer spaces are consequently not longer present as they have been and the sodium might have diffused into the metaclay or another metaphase from which it is not set free in the dissolution process. With scanning electron microscopy (Chapter 5.3.6) we will later see the formation of a new vitreous phase with similar chemical composition as the whole Søvind Marl material. The sodium is probably stronger bound in this phase. The high release of calcium ions into solution from the calcined clay can be due to $Ca(OH)_2$ formed when CaO from the calcite decomposition reacts with water. The solubility of $Ca(OH)_2$ is significantly higher than that of $CaCO_3$ in pure water. Nevertheless again based on calculations using the solubility product of $Ca(OH)_2$ ($K_{sp} = 6.4*10^{-6}$ mol/l [138]) the concentration of Ca^{2+} should be about 744 mg/l if $Ca(OH)_2$ is present. This is ten times higher than the measured 73 mg/l. Moreover the presence of CaO or $Ca(OH)_2$ could not be identified with XRD or FT-IR methods for the calcined marl. None the less the higher calcium release in the calcined marl can be due to the non functioning cation exchange ability of the smectite. The detection of sulfide and chloride is typical for marine clay. The most common ions in seawater are Na^+, Cl^-, Mg^{2+} & SO_4^{2-}. The sulfate ions located in interstitial water of the marine sediments are usually reduced to sulfide by the action of sulfate-reducing bacteria. This leads to the formation of H_2S which reacts further with iron compounds to iron sulfides

as pyrite which is also present in the Søvind Marl [139]. The increase of dissolved sulfur in the calcined marl might be due to an oxidation of minor amounts of sulfide to sulfate upon calcination. Chloride is mainly located in the pore water of the clay and the chloride concentration in the pore water of Søvind Marl samples from Århus harbor were measured to be between 0.5 and 1.5 % in a depth from 12 to 27 m [140]. However in the calcined marl only very little to no chloride was released which is important for the application in concrete structures. An additional wet chemical test was performed with the calcined marl to proof the absence of dissolved Cl^- in solution. Marl was dissolved in water and later sedimented. The water with the solved ions was taken and filtrated and silver nitrate solution was dropped to the filtrate. In the presence of chloride, silver nitrate should react instantly to silver chloride and nitrate resulting in a clearly visible white precipitate of silver chloride.

(9) $$AgNO_3\,(aq) + Cl^- \rightarrow AgCl\,(s) + NO_3^-$$

This reaction is very sensitive, taking place already with very small amounts of available chloride ions. The same test was also performed for calcined AB1080 showing no reaction with $AgNO_3$ either.
In the calcined marl no release for magnesium and iron was measured while the release of aluminum from the clay minerals increased. Magnesium and iron seem to be fixed in the metastable clay structure or other amorphous phases. ^{27}Al-NMR results (Chapter 5.3.7) showed that Al changes from octahedral to tetrahedral coordination upon calcination causing immense structural distortions. This is expected to facilitate the release of octahedral cations. The liberation of silicon from the tetrahedral layer on the other hand is decreased in the calcined marl. With FT-IR (Chapter 5.3.5) it can be shown later that amorphous silica is forming in the calcined clay. Furthermore the potassium release of illite was also reduced. The reason might be again the new formed vitreous phase impeding the release of some ions.
Further tests were performed where all investigated clays were dissolved in an alkaline solution of pH = 13.2 (KOH/NaOH = 2/1, 0.132 M). The alkaline solution was chosen to simulate the conditions in a hydrating cement paste. Main emphasis is again on the release of silicon and aluminum for the pozzolanic reaction. The results are shown in Table 5-9.
It becomes clear that the alkaline solution attacks the clay minerals more effective. The release of silicon in the raw Søvind Marl is 7 times higher, while aluminum stayed on the same level. The tetrahedral layers of the smectite interact more intense with the solution while the octahedral layer is shielded between the tetrahe-

dral layers. Consequently the octahedra can still only react at the edges. This result could possibly also mean that there is not much substitution of aluminum for silicon in the tetrahedral layers. Calcined at 850 °C the same trend as in the marl dissolved in deionized water is obtained. The release of silicon decreases considerably while the release of aluminum increases significantly and in a much higher magnitude. In the metastable clay structural aluminum elements must be much more exposed than in the raw clay while the silicon is more trapped in the structure. FT-IR results (Chapter 5.3.5) will show the possible separation of octahedral and tetrahedral layer in the clay minerals accompanied with formation of amorphous silica.

Table 5-9: Ion release of raw and calcined clays dissolved in an alkaline solution (0.132 M, pH = 13.2, KOH/NaOH = 2/1)

	Si 30 [mg/l]	Al 27 [mg/l]	Ca 44 [mg/l]	Fe 56 [mg/l]	Na 23 [mg/l]	K 39 [mg/l]	S 35 [mg/l]	P 31 [mg/l]	Cl 35 [mg/l]
SØ raw	66.7	1.9	2.9	0.0	-13.0	-752.2	44.4	0.1	0.0
SØ 850	20.9	29.4	15.7	0.0	-40.7	-165.5	56.3	0.0	0.0
AB raw	41.9	43.9	1.0	0.0	-158.2	-1302	2.6	2.3	0.0
AB 800	106.2	154.1	0.0	0.2	-126.3	-798.3	2.8	6.0	0.0
Sorg. raw	17.2	4.7	16.4	0.0	-89.3	-1490	0.5	0.0	0.0
Sorg. 800	127.8	30.0	2.6	0.0	-100.1	-943.2	0.6	0.1	0.0
Rasc. raw	35.1	8.7	7.0	0.0	-92.4	-1317	3.9	0.0	0.0
Rasc. 800	105.3	42.5	1.5	0.1	-86.5	-587.6	3.0	1.5	0.0
Gn. raw	52.9	6.5	2.1	0.0	-36.7	-347.5	1.8	0.0	0.0
Gn. 800	64.6	33.8	2.4	0.0	-62.9	0.1	2.0	0.0	0.0
Meta-kaolin	106.2	91.3	0.0	0.3	-52.6	-1.6	0.2	4.5	0.0

Calcium carbonate and calcium hydroxide are less soluble at high pH values resulting in a lower release rate of calcium both in the raw and the calcined clay [50]. The

release of sulfide is not affected by the alkaline solution giving nearly the same values in both experiments.
The kaolinite rich AB1080 is the only clay with a higher release of aluminum in the raw as well as in the calcined state. In 1:1 clay minerals the octahedral layer is of course much more exposed to the environment as it is not packed between two tetrahedral layers. As mentioned before the octahedral layer is the rate of dissolution limiting element in kaolinite. Moreover the hydroxyl surfaces at the octahedral layer interact much stronger with the surrounding solution than the siloxan surfaces of the tetrahedral layer of unburned clays [141]. The total aluminum and silicon release are much higher than for the Søvind Marl in the calcined state and build up together the highest amount of all clays.
Sorgila, Rascoia and Gniew show all a higher release of silicon compared to aluminum as it is typical for smectite and illite clays. When calcined at 800 °C the amounts of dissolved aluminum and silicon increase in all cases except for Søvind Marl. Sorgila and Rascoia release a considerably higher amount of silicon than aluminum when calcined, that is in case of Sorgila even higher than for AB1080. The Si/Al ratio is 4.3 and 2.4 for Sorgila and Rascoia respectively. All clays contain carbonate phases like calcite or dolomite contributing to the release of calcium in the raw clays. Compared to the Søvind Marl the release of calcium decreases in Sorgila and Rascoia and does not change much in Gniew. From almost all clays small amounts of sulfide and phosphate were dissolved.
When clays were dissolved in alkaline solution lower levels of sodium and potassium were measured than in the reference alkaline solution without dissolved clay. The result is negative values in all clays for these two elements. One theory might be that the clays ad- and absorb more alkalis in total than they release. Especially potassium is reduced in much higher magnitude than sodium in the solution. The potassium ion with its bigger ionic radius of about 1.38 Å fits perfectly in the cavity of the pseudo-hexagonal rings of oxygens of the adjacent silica tetrahedral sheet of illite or smectite minerals [20]. The calcined metastable clay minerals are distorted and less ordered so that the ability to uptake potassium may be reduced. In case the numbers show the adsorption of potassium, it is reduced in all calcined clays. For sodium there is no big difference between the raw and calcined clays. However possible alkali adsorption of the clays can reduce the alkalinity in mortars or concrete when used in blended cements. Consequently there might be the possibility for the use of the clays in concrete with alkali reactive aggregate.
All clays (raw and calcined) have low levels of iron and magnesium release (not shown). Dissolution of chlorides could not be detected for the given clays in the alkaline solution.

To conclude it has to be said that the results shown cannot serve to explain the reactivity of the different clays without taking the other methods into account. First of all the measurements were performed after 3 days, so that any conclusions to the 28 days reactivity in mortars are very difficult. Iron for example might be released slower than silicon and aluminum, so that the element might be detected at later ages. Actually an additional measurement was performed were the alkaline solution was mixed with a 3-component accelerating admixture [142]. The clay dissolved in this mixed solution showed clear signs of iron release after 3 days. The amount of aluminum and silicon released from the clays after 3 days cannot be taken to compare the reactivity of the different clays. Sorgila and Rascoia performed bad in mortar tests but show a considerably higher release level than the Søvind Marl which performed very well in mortar tests. Nevertheless the method helps further to understand the behavior of clays in solution and shows trends that help to explain the pozzolanic activity.

5.3.5 Fourier Transformed – Infrared Spectroscopy (FT-IR)

Infrared Spectroscopy can be a very powerful tool to distinguish between different types of clay minerals or different species (di- or trioctahedral) within one clay mineral group. As a complementary method to XRD it can provide additional information about amorphous phases and phase transformations in the calcined state where XRD reaches its limits. Table 5-10 gives an overview over the measured absorbance bands in the FT-IR spectra of the investigated raw clays.

Table 5-10: Measured absorbance bands in the different raw clays and their assignments [143-144]; Mont = Montmorillonite; Kaol. = Kaolinite; Ill. = Illite

ν [cm^{-1}]	Phase	Assignment
3696-99	Kaolinite	OH stretching of inner-surface hydroxyl groups
3670	Kaolinite	OH stretching of inner-surface hydroxyl groups
3650	Kaolinite	OH stretching of inner-surface hydroxyl groups
~ 3620	Mont., Kaol.	OH stretching of inner hydroxyl groups
3415-50	Water	OH stretching of water
~ 3020	Organics (alkyl-groups)	C–H stretching of CH_3 and CH_2-group
~ 2920		C–H symmetrical stretching mode of $–CH_2$-group
~ 2850		C–H stretching of CH_3 and CH_2-group
2514	Calcite	symmetric C–O stretching mode
1878	Organics (carboxylic acids)	C═O stretching
~ 1800	Carbonates	bending modes of Aragonite, Siderite, Calcite
1635	Water	OH deformation of water
1493	Aragonite	asymmetric C–O stretching mode
~ 1430	Calcite	CO_3^{2-} stretching of calcite
1114	Kaolinite	perpendicular Si–O stretching
1030	Kaol., Mont., Ill.	in-plane Si–O stretching
1008	Kaolinite	in-plane Si–O stretching
~ 911	Kaol., Mont., Ill.	AlAlOH deformation
~ 875	Calcite	out-of-plane bending of calcite
~ 795	SiO_2	Si–O stretching of quartz and silica
778	SiO_2	Si–O stretching of quartz
755	Feldspar	Si–O, perpendicular
713	Calcite	in-plane bending of calcite
696	SiO_2	Si–O, perpendicular
~ 530	Kaol., Mont., Ill.	Al–O–Si deformation
~ 470	Kaol., Mont., Ill.	Si–O–Si deformation

The analysis of soils and phyllosilicates (e.g. clay minerals) in the mid-IR region allows the examination of the basic structural units in these materials. These are the hydroxyl groups, tetrahedral silicate ($[SiO_4]^{4-}$) and aluminate anions ($[AlO_4]^{5-}$), octahedral metal cations and interlayer cations. OH-stretching modes are typically in the region 3400-3750 cm^{-1}. Metal-OH bending modes are visible between 650 and 950 cm^{-1}. Si-O and Al-O stretching modes occur in the 700-1200 cm^{-1} range while Si-O and Al-O bending modes take place in the 150 and 600 cm^{-1} region [145]. Carbonate minerals like calcite usually show distinctive peaks in the 700-1500 cm^{-1} range which are not overlapping with clay mineral signals. Other accessory minerals like quartz and feldspars appear between 600-900 cm^{-1} and exhibit in many cases characteristic doublet peaks.

5.3.5.1 Søvind Marl

Figure 5-21 shows the FT-IR spectra of a raw and calcined sample from the Søvind Marl (H4).
Smectites show only one single band in the OH stretching region which exact position is dependent on the nature of the octahedral cation. The absorbance at 3620 cm^{-1} is typical for dioctahedral montmorillonites with a high amount of aluminum in the octahedra [146]. The absorption band at 3699 cm^{-1} reflects the presence of kaolinite and is related to the in-phase symmetric stretching vibration of inner-surface OH groups [144]. The OH stretching mode of H_2O molecules at 3439 cm^{-1} is found in almost all clay materials, especially when smectite is dominating. OH deformation bands related to water molecules occur at 1635 cm^{-1}. Common for all smectites is the broad complex Si-O stretching band at 1030 cm^{-1} [146]. At around 1100 cm^{-1} there is a shoulder in this wide peak which can be assigned to kaolinite. Kaolinite alone would show several Si-O stretching bands between 1120 and 1000 cm^{-1}. Nevertheless in the smectite dominating Søvind Marl these peaks are overlapped and not visible under the wide smectite peak. The AlAlOH deformation band at 911 cm^{-1} confirms the presence of dioctahedral smectite [146]. Trioctahedral minerals absorb at lower frequencies (e.g. MgMgOH at 600 cm^{-1}). Absorbance at 534 and 469 cm^{-1} is typical for all clay minerals and assigned to Al-O-Si and Si-O-Si deformation bands respectively. The former describing the connection of octahedral and tetrahedral sheet in the clay mineral structure and the second reflecting the bonding of tetrahedras in the tetrahedral sheet. Calcium carbonate absorption bands can be found at 713, 874, 1428 and 2514 cm^{-1}. The absorption peak at 1799 cm^{-1} is typical for a number of carbonate minerals and could possibly be due to the small amounts of siderite in the Søvind Marl. The presence of quartz in the material becomes visi-

ble in the Si-O stretching bands in the region of 796 cm^{-1} and the peak around 696 cm^{-1} left of the calcite signal at 713 cm^{-1}. Small amounts of organic material show absorbance at 2877 cm^{-1} and a number of smaller peaks at higher frequencies.

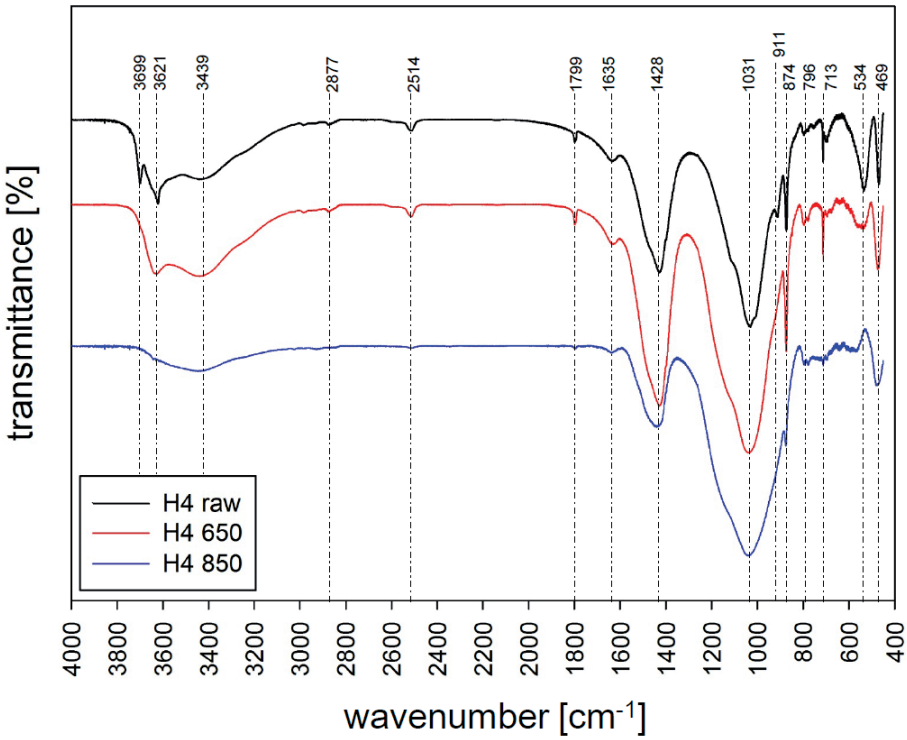

Figure 5-21: FT-IR spectra of Søvind Marl (H4), raw and calcined at 650 and 850 °C

When calcined at 650 °C the OH stretching band of kaolinite at 3699 cm^{-1} disappears while the OH stretching band of the smectite at 3621 cm^{-1} remains. At 850 °C smectite is also dehydroxylated. Complete dehydroxylation of the octahedra in the clay mineral structure can further be observed by the disappearing of the AlAlOH deformation band located at 911 cm^{-1}. The humps around 3440 and 1635 cm^{-1} are due to water molecules from the atmosphere absorbed at the KBr disks. With increasing calcination temperature the peak of the Si-O stretching bands around 1030 cm^{-1} widens up and becomes more and more a broad undefined peak. This wide peak with a slight shift to higher frequencies and the increasing intensity of the left shoulder are typical signs for the presence of amorphous silica [146]. Intense distortion in the clay sheets and modified bonding of the bridging oxygen atoms may be visible in the diminishing intensities of the Al-O-Si and Si-O-Si deformation bands at 534 and 469 cm^{-1}. The Si-O-Si deformation band gets broader, decreases in in-

tensity and shifts to higher frequencies. This confirms a decreased crystallinity in the tetrahedral sheet and distortions in the arrangement of the tetrahedra. The completely disappearing Al-O-Si deformation band can reflect a decreasing content of octahedral cations [146]. The conversion of octahedral Al to tetrahedral upon calcination is confirmed by Al MAS NMR as will be shown later. Additionally it might reflect a modified bonding between the tetrahedral and octahedral sheet in the clay minerals up to complete separation of the two units. The disappearance of the band at 534 cm^{-1} and the displacement of Si-O-Si band at 469 cm^{-1} are confirmed for kaolinite to metakaolin transformation in several papers as a sign for the presence of an amorphous reactive phase [87, 147]. Shifting signals can also imply a change in the bond length. Regarding the decomposition of calcium carbonate FT-IR spectroscopy is in agreement with XRD and thermal analysis. It is clearly visible that in the sample calcined at 850 °C, calcium carbonate is not completely decomposed. The main absorption band at 1428 cm^{-1} is still present and so are the bands at 874 and 713 cm^{-1}. The partly decomposition of calcite is reflected in a broadening of the peak and a decreasing intensity at 1428 cm^{-1}. All organic material present in the raw clay is burned out at 850 °C.
The higher intensities of some absorption bands in the sample calcined at 650 °C can be explained by a higher sample saturation in the KBr disk compared to the other samples.

5.3.5.2 Clays from Portugal

Kaolinite is the dominating clay mineral in the AB1080 clay resulting in a different IR spectrum of the raw clay. The region of the OH stretching bands as well as the Si-O stretching range is characterized by several distinctive peaks (Figure 5-22). The well crystallized kaolinite shows four OH stretching bands at 3696, 3670, 3670, 3620 cm^{-1}. Internal hydroxyl groups, lying between the tetrahedral and octahedral sheet are assigned to the absorption band at 3620 cm^{-1}. The other three bands arise from inner-surface hydroxyl groups located at the surface of the octahedral sheet. These are connected by weak hydrogen bonds with the oxygens of the tetrahedral sheet of the next layer [87, 146]. In less crystalline kaolinites the doublet at 3670 and 3650 cm^{-1} is replaced by a single broad band [87]. Furthermore the order/disorder of the kaolinite structure can be estimated by taking the so called P_0 index into account [87, 148]. This index describes the ratio between the intensities of the bands at 3620 and 3696 cm^{-1}. If this ratio is greater than 1 kaolinite has a well ordered structured [148]. Qualitatively it can be concluded that the kaolinite in AB1080 is well ordered since the OH stretching band at 3620 cm^{-1} has a higher

intensity than the OH stretching band at 3696 cm^{-1}. Three well resolved Si-O stretching bands at 1114, 1032, 1008 cm^{-1} are typical for kaolinite. The absorption band at 696 cm^{-1} can be assigned to Si-O stretching of kaolinite or quartz. At 912 cm^{-1}, the AlAlOH deformation band is present as it is in other clay minerals but with a sharper peak shape and higher intensity. Absorption bands at 538 and 469 cm^{-1} are again attributed to Al-O-Si and Si-O-Si deformation bands respectively. Quartz and feldspar minerals are detected through the absorption bands at 795 and 755 cm^{-1} respectively.

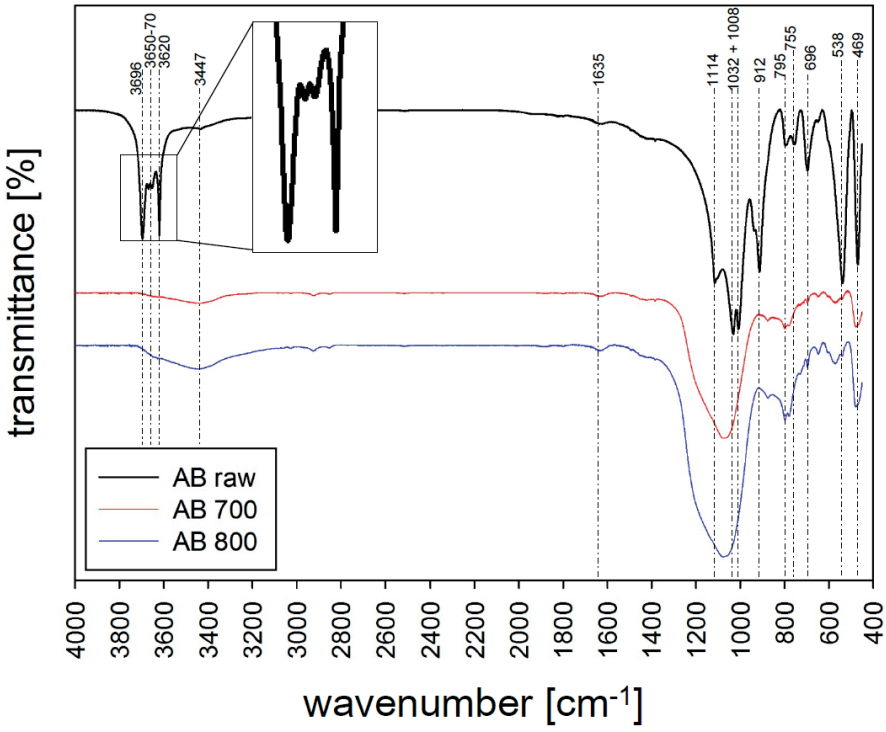

Figure 5-22: FT-IR spectra of AB1080, raw and calcined at 600 and 800 °C

Already at 600 °C the kaolinite is completely dehydroxylated as can be seen by the disappearing of the OH stretching bands between 3600-3700 cm^{-1} and the AlAlOH deformation band at 912 cm^{-1}. Absorption of water from the atmosphere is again reflected in the wide hump at about 3400 cm^{-1} and the small peak at 1635 cm^{-1}. The well resolved Si-O stretching peaks transformed into one wide peak with a maximum at about 1080 cm^{-1}. This is the result of the formation of a 3 dimensional amorphous silica network [146]. The disappearing of the Al-O-Si deformation band at 538 cm^{-1} and the shifting of the Si-O-Si deformation band at 469 to a higher wavenumber has been observed by several authors [87, 147]. Additionally new absorption

bands appear at 570 and 870 cm^{-1}. These belong probably to the new amorphous metakaolin structure. It is known from literature that calcination of kaolinite gives 5-coordinated Al [13]. Especially the disappearance of the Al-O-Si deformation band and the shift and broadening in the Si-O-Si deformation band must imply significant structural changes in the local environment of the Al/Si atoms in the octahedral and tetrahedral sheet. A lower degree of connectivity between the two different sheets within one layer can be expected from these results as well as a distorted tetrahedral silicon sheet. Increasing the calcination temperature from 600 to 800 °C does not result in a change of the FT-IR spectra obtained for the two samples. The higher intensities of most of the peaks are again due to a higher sample saturation in the KBr disk. Since the Si-O stretching band at 696 cm^{-1} also disappears with calcination it belongs to the kaolinite.

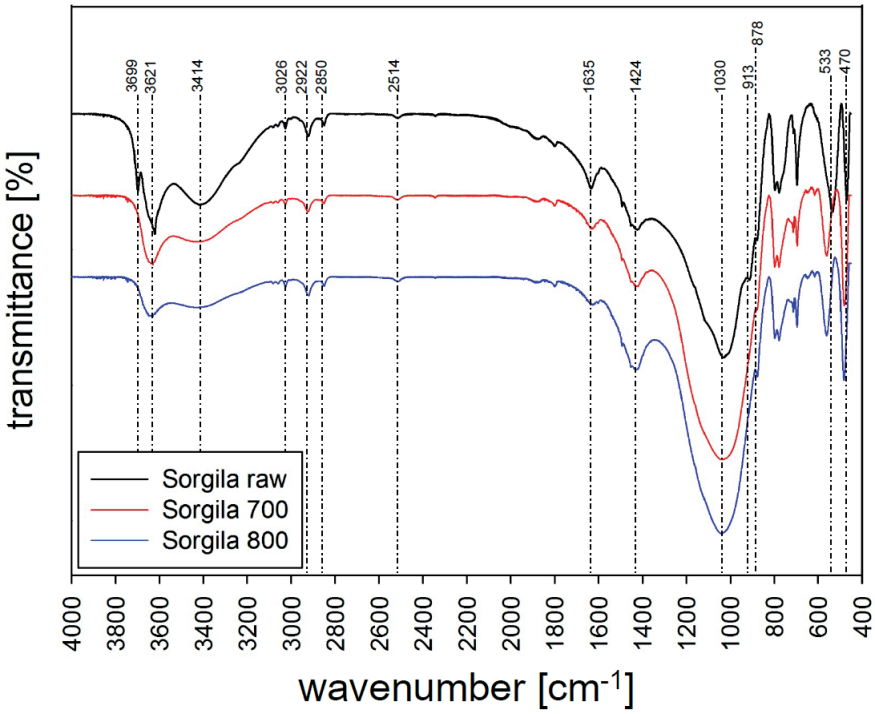

Figure 5-23: FT-IR spectra of Argila Sorgila, raw and calcined at 600 and 800 °C

Argila Sorgila containing large amounts of smectite is less affected by the heat treatment (Figure 5-23). Small amounts of kaolinite are dehydroxylated at 700 °C as can be seen in the disappearing of the OH-stretching band at 3699 cm^{-1}. In contrast to that the OH stretching band of smectite at 3621 cm^{-1} only decreases in i

ntensity and shifts to a higher wavenumber. Although the AlAlOH deformation band at 913 cm^{-1} seems to disappear with increasing temperature the smectite minerals are not completely dehydroxylated even at 800 °C. In agreement with XRD the calcium carbonate is also not much affected by the heat treatment and the deformation bands at 1424 and 878 cm^{-1} show no signs of decomposition. Not even all the organic material (absorption bands at 3026, 2922, 2850 cm^{-1}) is burned out. This clearly reflects that the heat treatment with the chosen parameters (retention time and temperature) is not effective enough to turn the clay in a quality pozzolanic material. Either a higher temperature and or a longer retention time in the kiln are necessary. Looking at the absorption bands between 1200 and 400 cm^{-1} we can furthermore observe that only minor changes in the clay mineral structure occurred upon the heating. The Si-O stretching band at 1030 cm^{-1} having some shoulders turned into one broad peak. This reflects a loss in the ordering to some extent. Nevertheless the peak tip did not shift significantly meaning there is only minor formation of amorphous silica. Additionally the peak shapes of the Al-O-Si and Si-O-Si deformation bands do not change. However both absorption bands show a shift from 533 to 570 cm^{-1} and 470 to 490 cm^{-1} respectively. Such frequency changes might imply small changes in the bond length [149]. Nonetheless all signals can still be found so there seems to be no change in the connectivity of the different units of a clay layer.
The FT-IR spectra of Argila Rascoia are similar to Argila Sorgila and show only minor changes from the raw to the calcined clay (Figure given in the appendix). The incomplete dehydroxylation, no significant changes in the ordering of the clay mineral structure and the non occurring formation of an amorphous phase are an explanation for the low pozzolanic reactivity in the performed mortar tests.

5.3.5.3 Gniew

The FT-IR spectra of raw and calcined Gniew clay are presented in Figure 5-24.
Besides the signals for the clay minerals, calcite and quartz are detectable in the raw material. One of the major differences to the other clays are the less resolved Al-O-Si and Si-O-Si deformation bands at 524 and 468 cm^{-1} which can be a distinctive feature of some illites which is the main clay mineral in Gniew [143]. The disappearing of the OH stretching bands at 3698 and 3620 cm^{-1} as well as the AlAlOH deformation band at 911 cm^{-1} reflect a complete dehydroxylation of the clay minerals at 800 °C. Only the absorption bands of adsorbed water are left. Most of the calcium carbonate is also decomposed at 800 °C. The absorption bands at

2514 and 875 cm^{-1} are not present any more and at 1433 cm^{-1} only a small, broad and diffuse peak is left. Accompanied with the decomposition of calcium carbonate some free CaO seems to form. A new small peak at around 3640 cm^{-1} at 800 °C can be attributed to $Ca(OH)_2$ from the reaction of CaO and atmospheric water [150]. The Si-O stretching band at 1030 cm^{-1} broadens significantly upon calcination with an enhancement of the area at higher wavenumbers. As mentioned before, this can be assigned to the formation of amorphous silica. At 700 and 800 °C the two deformation bands at 524 and 468 cm^{-1} merge together to one single absorption band. It looks like the Al-O-Si deformation band is decreasing in intensity, shifting to a higher wavenumber and only being visible as a small shoulder at 700 and 800 °C. Structural changes seem to be less significant than in the Søvind Marl and the AB1080 clay but to occur to a higher extent than in Sorgila and Rascoia. This reflects the reactivity of Gniew positioned between Sorgila/Rascoia and AB1080/Søvind Marl.

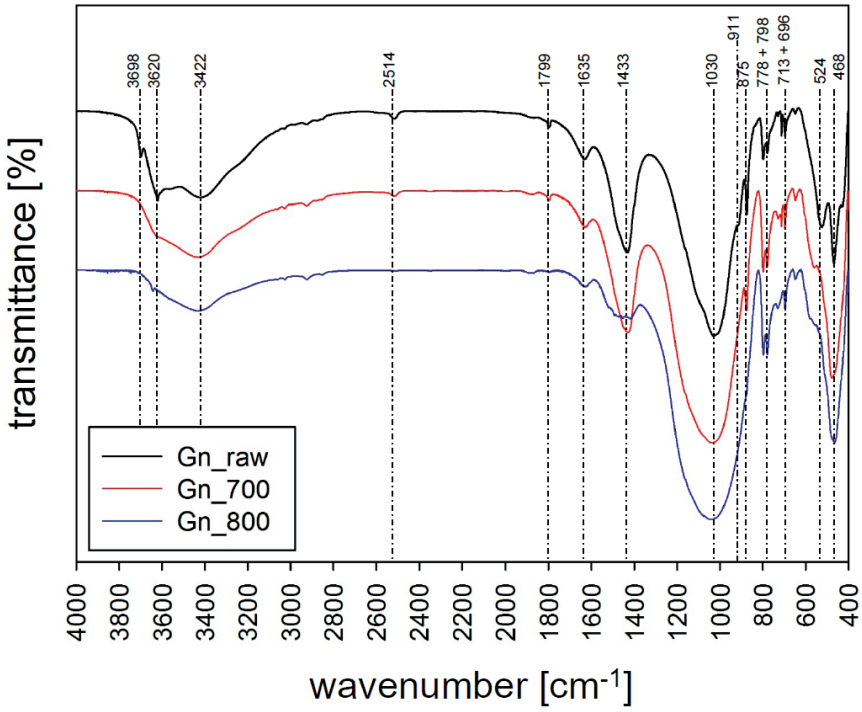

Figure 5-24: FT-IR spectra of raw and calcined Gniew clay

5.3.6 Scanning Electron Microscopy (SEM)

5.3.6.1 Søvind Marl

From chapter 4.1.2 we already know that the Søvind Marl contains a considerable amount of organic material in form of calcareous microfossils and planktonic foraminifera deposited together with the clay minerals as it is typical for marine sediments. The calcium carbonate content in the marl derives to a large extent from coccoliths. These are clearly visible from a top view and as cross sections in a close up to the matrix of the uncalcined Søvind Marl (Figure 5-25). Coccoliths are small calcite biominerals with a size between 1-10µm and a typical radial symmetry. They are the exoskeletons of a group of plant plankton called coccolithophores which belong to the algal division Haptophyta [151].

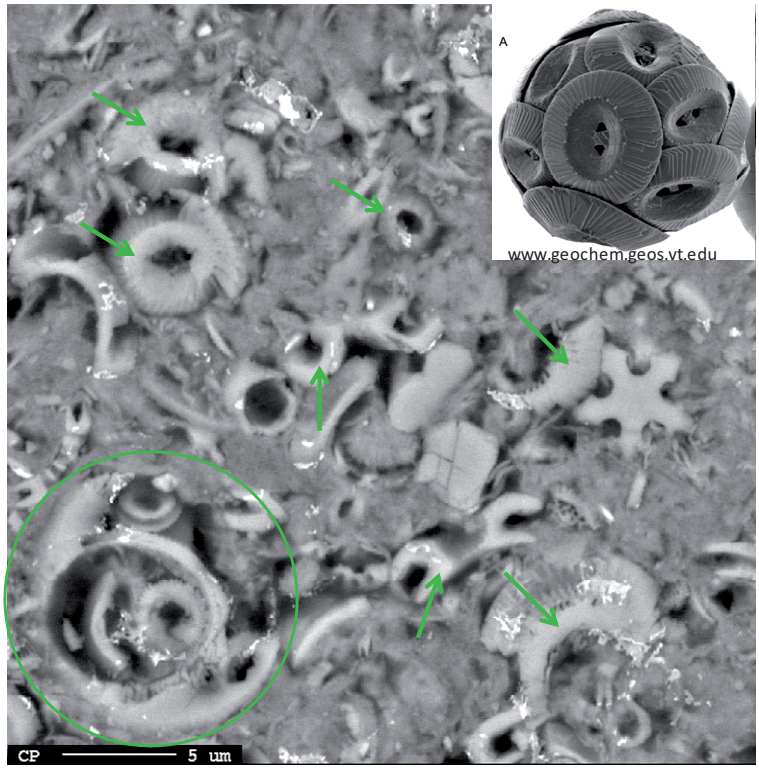

Figure 5-25: BSE image (3000 x) of unburned Søvind marl: Coccoliths and possibly Foraminifera in the matrix of the uncalcined marine Søvind Marl sediments. The picture in the top left corner is taken from Ref [151].

The coccolithophores lived in the marine environment after the glaciers retreated. With the dying of the planktonic plants their exoskeletons were left, thus deposited

in the sediments. At the left margin of Figure 5-25 a star like particle can be seen. From pentamerous symmetry one can assume something echinodermatic, like a seastar. But since the structure is very small, it is possible that this "star" is also part of a coccolith [152]. Fully grown foraminifera usually have a size greater than 100 µm and can be up to 20 cm long. However, coccoliths are an example for the theory of mesocrystal formation [153]. Their complex morphology is only possible through the connection of a number of smaller crystals to a big unit, appearing as a single crystal. Different forms of coccoliths may be built up of several hundred to a few thousand minute (ca. 0.1 µm) calcite crystals. Nucleation and growth of these crystals are regulated by organic molecules (here: complex acidic polysaccharides) [151]. As a biomineral alternating chemical compositions can be expected additionally, especially the incorporation of magnesium or phosphate [154]. In general, calcium carbonate from coccoliths should behave similar as "natural" calcite when exposed to heat but nevertheless the mentioned features may also influence the thermal decomposition behavior. The small crystallites may decompose at a slightly lower temperature than bigger calcite grains from limestone. This is partly confirmed in chapter 5.4.2.1. In the calcined marl coccoliths could not be found while inorganic calcite grains were randomly observed under the SEM. More pictures of the raw clay are shown in Figure 5-26 (a-c). Pyrite is only found in form of Pyrite framboids which are distributed all over the clay matrix (Figure 5-26a). The term framboid describes a micro morphological feature where small, mostly euhedral (idiomorph) crystals agglomerate to form a spherical aggregate. This framboidal structure is typical for certain sedimentary minerals and common to be found in marine sediments but also in coal. Therefore this feature was also found in Fly Ash [155]. Particularly for pyrite the phenomenon is extensively documented and described in the literature [156-158]. Figure 5-26 b shows an accumulation of anhedral siderite grains in the clay matrix. The distribution of siderite in the clay seemed to be very inhomogeneous under the SEM. This observation confirms the different siderite contents measured with XRD in the 3 boreholes H2-H3. While in H2 5.3 % Siderite were measured, nothing was detected in H3. WDX measurement of one of these particles gave a composition of Fe = 19.6 %, Mg = 3.1 %, Ca = 2.9 % and O = 74.1 %, showing that 6 % of the Fe in siderite are substituted with Mg + Ca. Siderite deposited in a marine environment, as it is the case for the Søvind Marl, usually shows extensive substitution of Mg and Ca for Fe in the lattice [159]. Picture 2c shows another picture of the raw clay with the coccoliths in the matrix. The clay calcined at 650 °C is presented in Figure 5-26d-f. It is visible that the coccoliths are not affected at this temperature and that no big micro morphological changes occurred in the clay. If any change is recognizable it seemed that the dense matrix started to widen up and different phases slightly separated from each other.

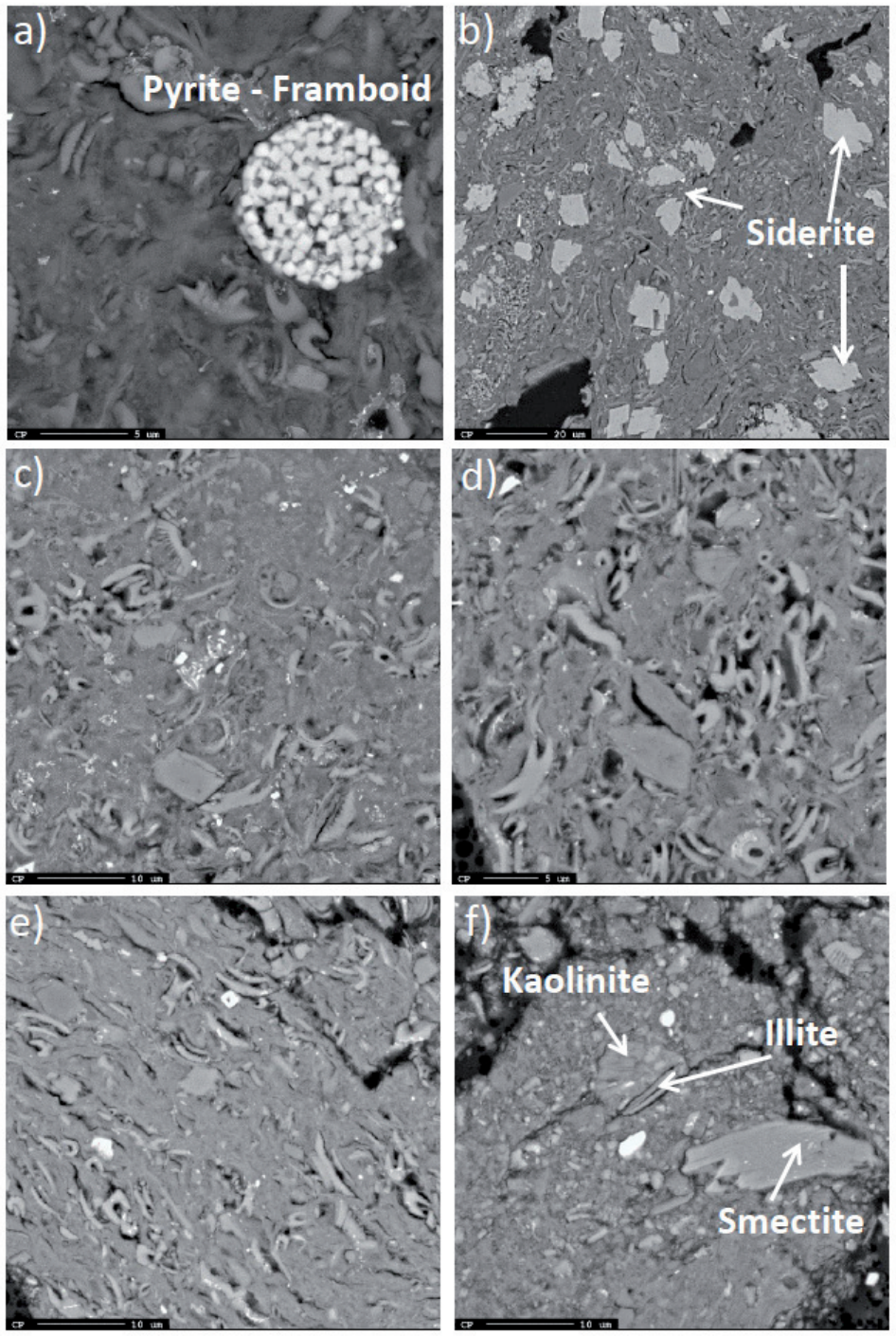

Figure 5-26: BSE images of Søvind Marl uncalcined (a: 4000x, b: 700x, c: 2000x) and calcined at 650 °C for 45 min (d: 2500x, e-f: 2000x)

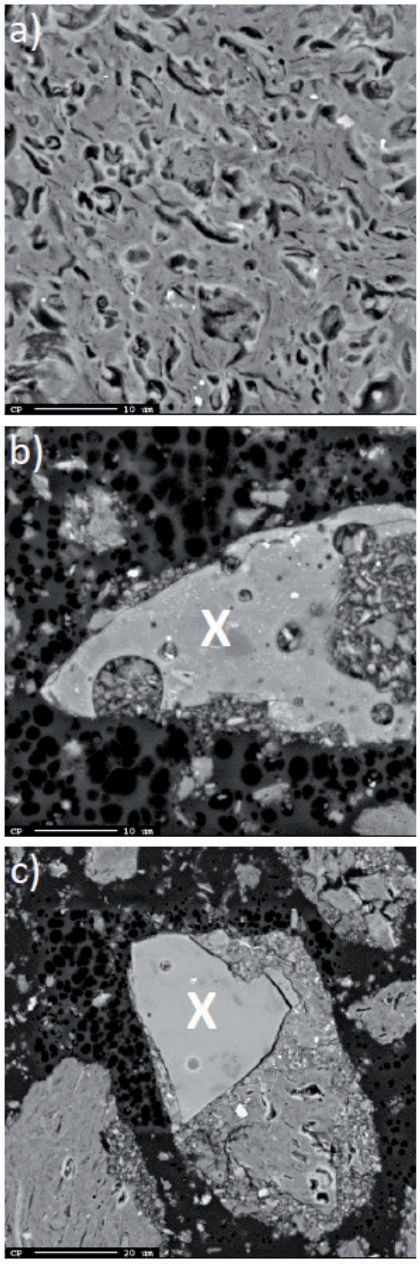

Average **WDX** composition of 3 similar phases marked with **X**:
Examples in picture b) & c)

	Atom %		Weight %
Si	18.9 ± 1.4	SiO_2	44.4
Al	8.1 ± 0.6	Al_2O_3	16.1
Fe	7.7 ± 0.8	Fe_2O_3	24.0
Ca	4.7 ± 2.1	CaO	10.3
Mg	1.5 ± 0.2	MgO	2.4
K	0.9 ± 0.2	K_2O	1.8
Na	0.8 ± 0.4	Na_2O	1.0
O	57.2 ± 1.5		

Figure 5-27: BSE pictures of Søvind Marl calcined at 850 °C for 45 min and average WDX composition of phases marked with X. Magnification a-b: 2000x, c: 1000x

In Figure 5-26 f the three different clay minerals contained in Søvind Marl could be found next to each other by EDX analysis. This is quite unusual as the smectite was hard to find in form of nice crystallites. Usually it was only measured in the dense

matrix. Illite and smectite appear still stable at this temperature with their layered morphology while kaolinite appears more damaged as it is already transformed to metakaolin.

When calcined at 850 °C the morphology is altered significantly (Figure 5-27 a-c). The coccoliths are completely decomposed leaving holes in the clay matrix while the surrounding matrix looks more vitreous. The whole matrix seems to fuse together leading to spongy morphology (Figure 5-27a). Moreover new larger phases were detected all over the clay that look like quenched glassy particles formed from the molten matrix (Figure 5-27b-c). The lower specific surface area measured in the calcined clay is most likely the result of these new formed glassy phases. The formation of a liquid phase in calcite bearing clays is in agreement with the observations made by other authors [73, 119, 132].
The composition of this new formed phase was measured with WDX analysis and the average composition of 3 particles in atom % is given in the table of Figure 5-27. The result obtained in atom % of the elements was recalculated in weight % of the respective oxides to have a comparison to the chemical composition of the whole clay measured by XRF (see Chapter 5.1). In fact the recalculated chemical composition of the new phase is very similar to the chemical composition of the initial raw clay. Only the Fe_2O_3 content is much higher in the new formed phase. It seems like all decomposed and disappearing phases (clay minerals and carbonates) contribute to the formation of the glassy phase without any significant preferred uptake of certain elements except iron. This glassy phase could be responsible for the high reactivity of the Søvind Marl at this temperature with higher solubility in alkaline solutions than the stable unburned clay minerals.

5.3.6.2 AB1080

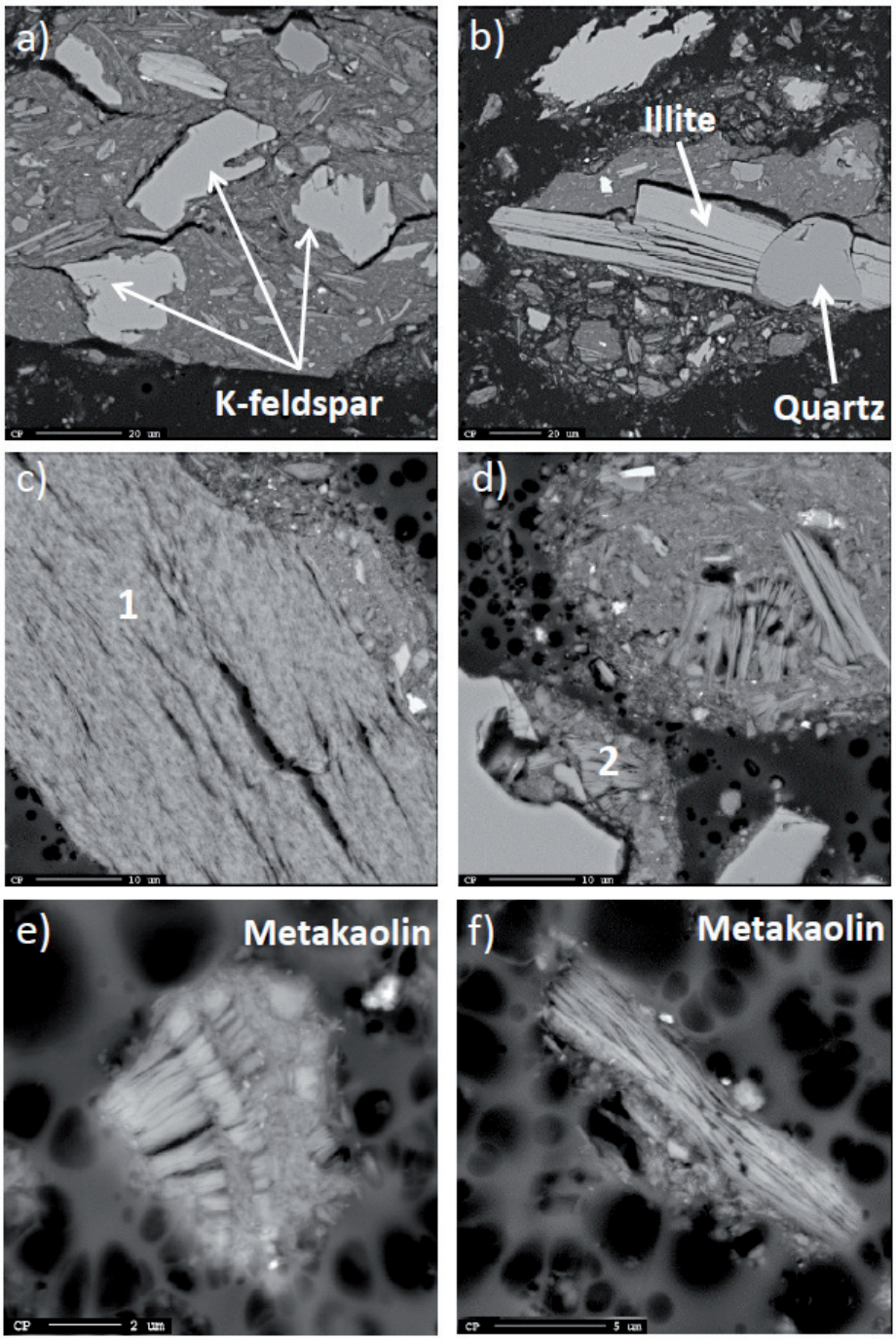

Figure 5-28: BSE images of AB1080 clay in the raw (a: 1000x, b: 600x) and calcined state (c-d: 2000x, e: 6000x, f: 4500x)

Figure 5-28 a-b shows images of the raw AB1080 clay. In the very fine grained grey kaolinite clay mineral matrix, bigger anhedral grains of K-feldspar and quartz could be identified without difficulty. Quartz and feldspar don't show well formed crystal faces. The edges are rounded and probably the result of the extensive weathering process the clay experienced. Due to the high surface area, created through the weathering process, these minerals can act as nucleation sites for cement hydration products as we will see later in chapter 5.4.1. This might help to enhance the early age strength in mortars using blended cements. It is even possible that K-feldspar and quartz take part in the pozzolanic reaction [116]. Furthermore it cannot be excluded that the feldspar and quartz grains may partly act as a filler in mortar or concrete, thus improving the strength development. Only small kaolinite crystallites with lamellar texture could be found in the matrix, but EDX measurements revealed that kaolinite is also the main constituent of the grey mass. In contrast to that big crystallites of illite with a size up to 50 µm were easier to find (Figure 5-28 b). When calcined at 700-800 °C the kaolinite matrix shows only a slightly modified microstructure (Figure 5-28 c-f). The clay minerals show its characteristic lamellar texture that seems to widen up upon calcination. In point 1 & 2 in Figure 5-28 c-d a WDX composition in atom % of Al = 19.0, Si = 21.4 and Al = 18.6, Si = 20.7 respectively was measured. The composition with a Al/Si ratio of about 1/1 is typical for metakaolin with the formula $Al_2Si_2O_5$. Figure 5-28 e-f shows a close up on two metakaolin particles with a size of about 5 µm.

5.3.6.3 Argila Sorgila

Figure 5-29 illustrates BSE images of the raw (a-b) and calcined (c-d) Argila Sorgila. In the finely crystalline clay mineral matrix consisting mainly of smectite larger quartz and feldspar grains are embedded. The non clay minerals exhibit all an anhedral shape with rounded edges and granular to columnar habitus. Distinct tabular clay mineral crystallites turned out to be illite in almost all cases. This actually accounts for all investigated clays. WDX measurement of the matrix in point 1 (Figure 5-29 b) gave the composition in atom % of Si = 19.5, Al = 10.6, Fe = 6.4, K = 1.5, Mg = 1.9, Ca = 0.5, Na = 0.2, O = 59.3. This is a typical composition of a clay mineral belonging to the smectite group with considerable amounts of substituted Mg and Fe for Al, alkali ions and a Si/Al ratio of about 2/1. Regarding the microstructure of the clay mineral matrix there are some changes recognizable from the unburned to the heat treated samples.
Figure 5-29 c shows a stressed illite crystallite on the left side. The microstructure in general appears undulated and more like flowing around the quartz and feldspar

grains. The partly dehydroxylated clay minerals seem to be moving apart instead of forming a dense matrix. An explanation could be an induced shrinkage of the clay minerals by dehydroxylation creating some space between the different phases.

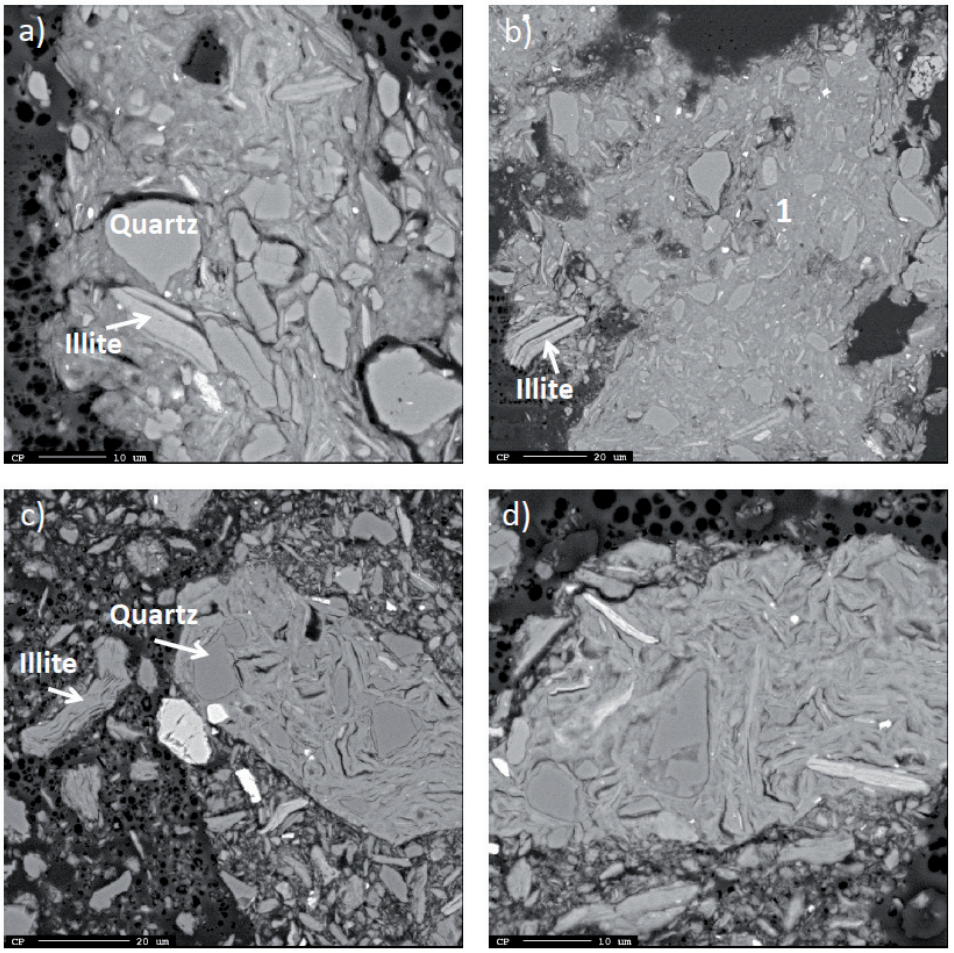

Figure 5-29: BSE images of Argila Sorgila unburned (a: 1500x, b: 700x) and calcined at 800 °C (c: 1000x, d: 1500x)

5.3.6.4 Argila Rascoia

Due to high content of illite and chlorite minerals the microstructure of Argila Rascoia differs from the other clays. The columnar to strip like crystals of illite and chlorite dominate the clay particles. In BSE images chlorite appears darker than illite.

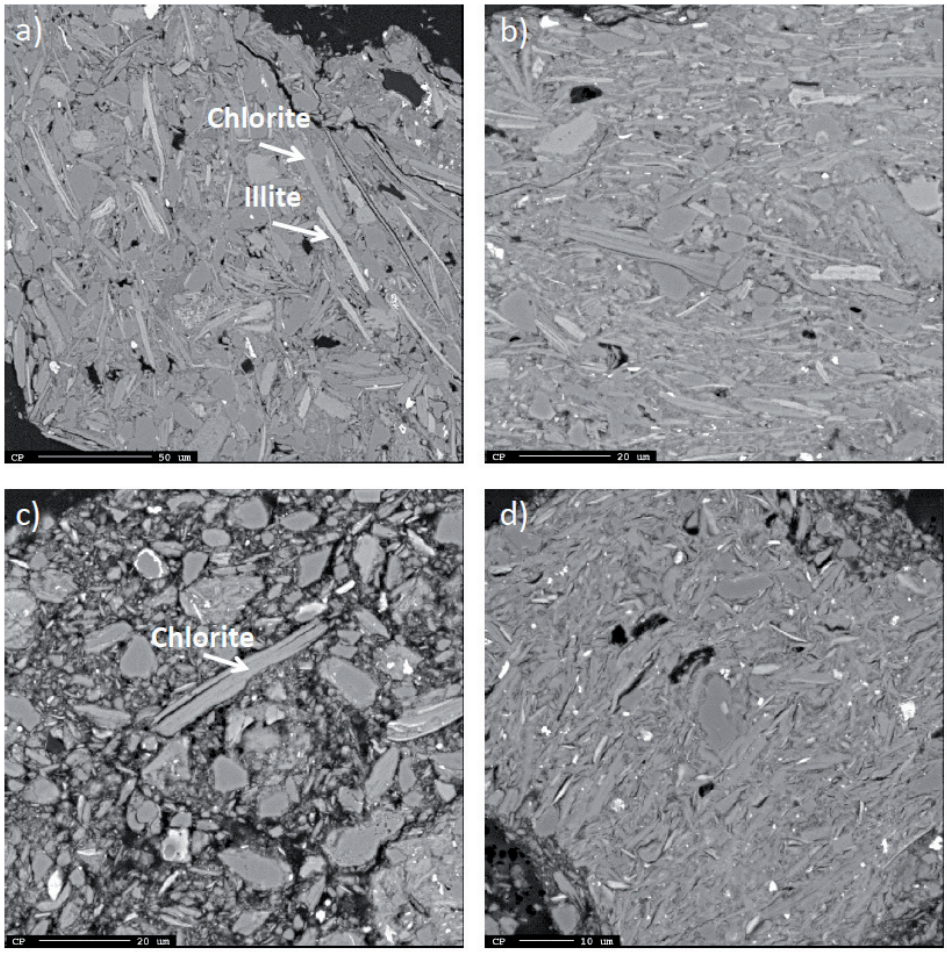

Figure 5-30: BSE images of Argila Rascoia raw (a: 500x, b:1000) and calcined at 800 °C (c: 1000x, d: 1200x).

With EDX measurements in some points these two minerals could be assigned and differentiated. The presence of K is a clear indicator for the presence of illite. In the darker phases Mg and Fe were measured besides Al and Si while K was missing.

Anhedral grains of quartz and feldspars are also visible in the clay matrix. Calcination at 800 °C for 45 min did not lead to any significant changes in the microstructure of the clay (Figure 5-30 c-d).

5.3.6.5 Gniew

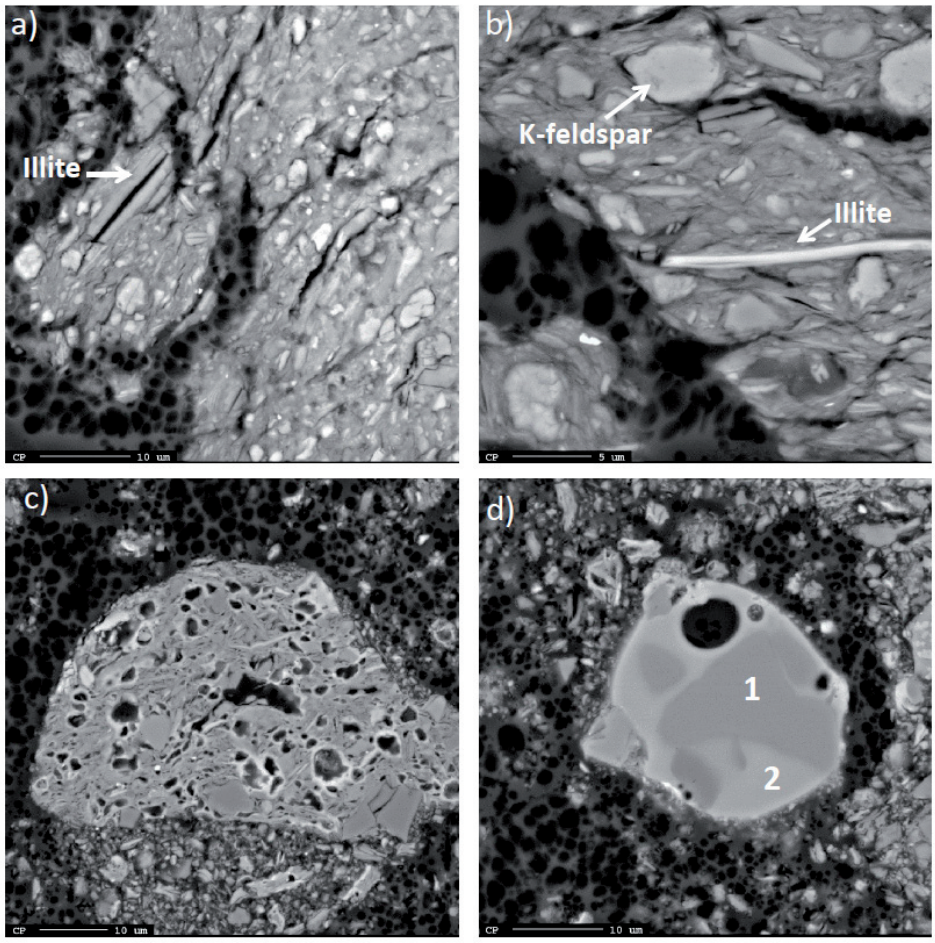

Figure 5-31: BSE images of the raw (a: 2000x, b: 3500x) and calcined (c: 1500x, d: 2000x) Gniew clay. Calcination temperature was 800 °C

The raw clay from Gniew (Figure 5-31 a-b) consists of anhedral feldspar and quartz crystals embedded in a fine crystalline clay matrix with some larger illite laths. The lighter grains in Figure 5-31 are calcium carbonate. In comparison to

Argila Rascoia which has a similar illite content, the illite in Gniew is not that easy to find and seems to have an average smaller crystallite size.
When calcined at 800 °C similar features as for the Søvind Marl can be observed. As explained before, clays containing calcium carbonate tend to form a fluid phase before recrystallizing new phases at higher temperatures. It can clearly be seen that the clay matrix starts to melt up while the feldspar and quartz grains remain stable. WDX composition was measured in 3 points of the matrix before and after calcination and the result is given in Table 5-11. The two average compositions are very similar, meaning that the clay mineral matrix is melting up homogeneously. Besides that amorphous, glassy particles formed that seem to show phase segregation (Figure 5-31 d). The WDX composition of point 1 & 2 is shown in Table 5-11. The dark areas of this particle are rich in Mg but contain no Al or Ca. The amount of Si and the alkalis is also lower in the dark area. Point 1 actually has a composition similar to olivine (Mg_2SiO_4 – Forsterite). However, this phase has a high melting point of about 1800-1900 °C which makes it very unlikely to be present as a glass at the given temperature. Moreover this phase could not be detected with XRD, so that the crystallization from a molten phase upon cooling can also be excluded.

Table 5-11: Average WDX composition of the clay matrix in the raw and calcined state and two points in the glass phase (Figure 5-31 d)

WDX Atom%	Si	Al	Ca	Fe	Mg	K	Na	O
Raw clay matrix	20.7	8.4	1.5	2.9	1.7	1.6	0.2	62.9
Calcined clay matrix	21.3	8.2	2.9	2.5	1.8	1.5	0.2	61.4
1 Glass phase	14.3	0.0	0.1	1.8	24.6	0.0	0.0	59.1
2 Glass phase	18.8	4.8	5.2	1.6	7.8	0.4	0.2	61.1

In Figure 5-31 c it can clearly be seen were the calcium carbonate is decomposed. The calcite decomposes upon calcination and leaves pores in the matrix. The rims of these pores appear very light in the BSE mode and EDX analysis revealed that these regions are rich in calcium. So this might be reaction zones were the decomposed calcium carbonate reacts with the clay matrix to form new phases.

5.3.7 ^{27}Al MAS NMR-Spectroscopy

^{27}Al MAS NMR spectroscopy was only performed for the two most reactive clays Søvind Marl and AB1080.

Due to the high iron content in the Søvind Marl satisfying ^{29}Si NMR could not be conducted. The noise to signal ratio for ^{29}Si was too high to get a quality spectra that allows interpretation. The paramagnetic Fe^{3+} in Fe_2O_3 interacts with the nuclear spins of atoms (Al,Si) in close proximity thus affecting the NMR signal intensity negatively [160]. ^{27}Al MAS NMR spectra of the uncalcined, raw Søvind Marl and a sample calcined at 850 °C is shown in Figure 5-32.

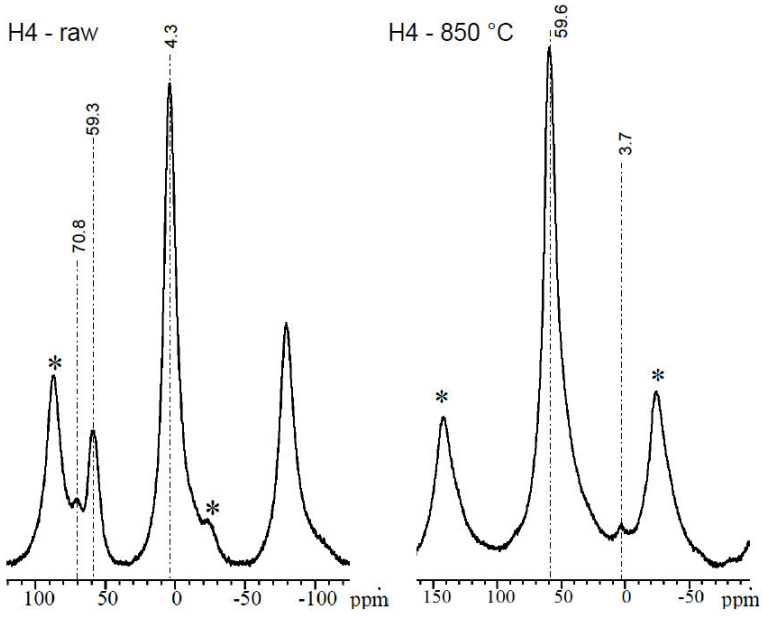

Figure 5-32: ^{27}Al MAS NMR spectra of raw and calcined Søvind marl (H4)

The spectral region for the ^{27}Al central transitions is roughly from 100 ppm to -20 ppm. The spectrum of the raw clay includes three centerband resonances in this region at 70.8 ppm, 59.3 ppm, and 4.3 ppm with the following relative intensities 5.4 %, 16.0 %, and 78.7 %, respectively. Note that the spinning sidebands closest to the central-transition region are marked by asterisks. These spinning sidebands reflect the coupling of the ^{27}Al spins to the spins of the unpaired electrons associated with the Fe^{3+} ions in the clay samples. The resonances at 70.8 ppm and 59.3 ppm originate from Al in tetrahedral coordination, with chemical shifts typical for Al sites in layered structures of clays (70.8 ppm) and fully condensed $Al(OSi)_4$

sites (59.3 ppm) [13, 161-164]. Al in tetrahedral coordination represents the substitution of Al for Si in the tetrahedral sheet typical for most clay minerals. The most intense resonance however at 4.3 ppm reflects Al in octahedral coordination, e.g., octahedral sheets in the clay.
The ^{27}Al NMR spectrum of the marl calcined at 850 °C allows identification of two resonances at 59.6 ppm and 3.7 ppm with the relative centerband intensities of 95.1 % and 4.9 %, respectively. This demonstrates that the main Al species in the uncalcined sample (octahedral Al) has been almost fully converted into Al in tetrahedral coordination. The uncalcined sample also includes a low-intensity resonance at 70.8 ppm and it cannot be excluded that the Al species for this resonance is also present in the calcined sample, since it may be situated below the dominating resonance at 59.6 ppm. In a comparing study about the thermal transformation of kaolinite, illite and montmorillonite when calcined at 800 °C, signs of octahedral aluminum were only found for the first two [13]. Since the Søvind Marl contains kaolinite and illite in smaller amounts besides smectite, the residual signal at 3.7 ppm in the calcined sample could be associated with one of these minerals. In contrast to that octahedral coordinated aluminum was found between 750-950 °C in a different study about thermal reactions of Ca-montmorillonite [162]. The authors even detected a small signal for 5-coordinated aluminum in the temperature range from 550-800 °C besides the signals for 4- and 6-coordinated Al. 5-coordinated Al is usually only found in metakaolin [13, 165-166].
The dehydroxylation accompanied with the change in coordination for Al must result in significant structural alterations not only in the Al environment. The reorganizing octahedral sheet will induce distortions in the tetrahedral silicon sheet as well, from changing bond lengths and angles up to a complete separation [160, 162]. This effect is in agreement with the results obtained by FT-IR spectroscopy where a disappearing Al-O-Si resonance peak could be observed upon calcination.

Figure 5-33 shows the ^{27}Al MAS NMR spectra of the raw and calcined AB1080 clay. The ^{27}Al MAS NMR spectrum of the AB – raw sample includes resonances from three distinct Al sites with chemical shifts of 71.4 ppm, 56.9 ppm, and 4.9 ppm, corresponding to two tetrahedral environments and Al in octahedral coordination (4.9 ppm) [167-168]. The peaks with lower intensities at 90 ppm, -23 ppm, and -77 ppm are spinning sidebands. A chemical shift in the range 55 – 60 ppm is characteristic for Al surrounded by SiO_4 tetrahedra, i.e., $Al(OSi)_4$ or $HOAl(SiO)_3$ sites [164]. The relative intensities are 2.6 % (71.4 ppm), 11.9 % (56.9 ppm) and 85.5 % (4.9 ppm), in accordance with that most of the aluminium is present in octahedral sheets of the clay mineral structure. The resonance at 56.9 ppm can be ascribed to Al substitutions in the layers of SiO_4 tetrahedra. However K-feldspars also contain Al

entirely in tetrahedral coordination and exhibit a chemical shift in the same region between 56-60 ppm [169]. Consequently, the chemical shift of K-feldspar which is contained with 34.3 % in AB1080 probably overlaps in this peak with tetrahedrally coordinated Al in kaolinite. This makes it hard to say if there is any substitution of Al for Si in the tetrahedral sheet.

The ^{27}Al MAS NMR spectrum of the AB1080 – 800 °C sample shows that this clay material contains Al in tetrahedral (57.2 ppm), five-fold (29 ppm) and octahedral (4.2 ppm) coordination [13, 165-166]. An estimation of the relative intensities for the different sites, by spectral integration, gives relative intensities of 37.3 % (57.2 ppm), 40.3 % (29 ppm), and 22.4 % (4.2 ppm). This indicates that 5-fold Al is the dominant coordination for the kaolinite clay calcined to 800 °C, which confirms the findings of Fernandez [13] for a standard kaolinite. An overlay plot of the spectra before and after calcination clearly reveals that the resonances at 57 ppm are identical in the two spectra and thereby originates from the same component [164]. 4-fold coordinated Al was observed before in calcined kaolinite [13] but it cannot be excluded that a significant amount of the intensity of this peak derives from the K-feldspar. The resonance from octahedral Al seems to be slightly broader in the spectrum of the calcined sample when overlaying the two plots of the raw and calcined clay [164]. It makes sense that the octahedral coordinated Al in the calcined sample has a different origin since the former octahedral sheet from the raw clay is completely dehydroxylated as was shown with previous methods like DTG, FT-IR, and XRD.

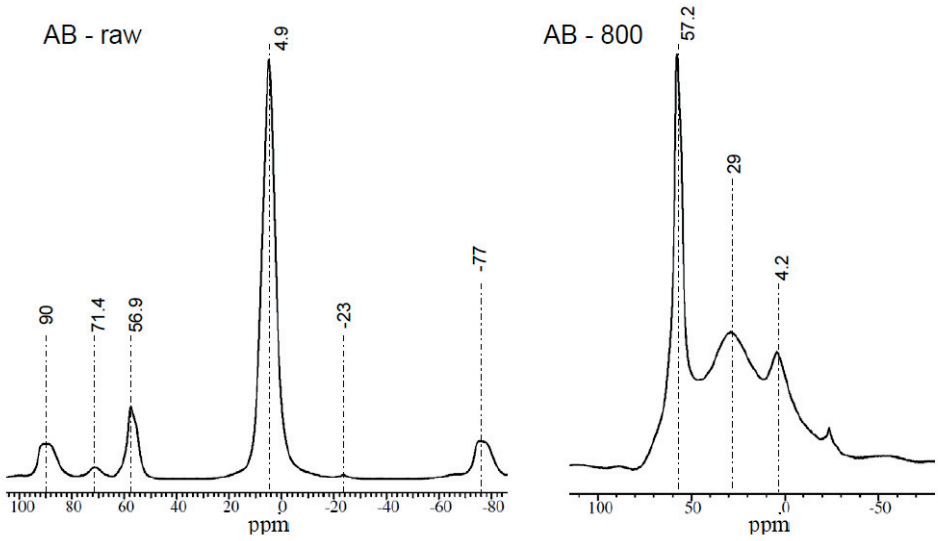

Figure 5-33: ^{27}Al MAS NMR spectra of raw and calcined AB1080 clay

The change in coordination and especially the presence of penta coordinated Al clearly indicates a disordering and loss in crystallinity of the original clay structure. 5 coordinated Al is very rare in stable minerals but can seldomly be found for example in the mineral andalusite (polymorph of Al_2SiO_5).
Taking into account the pure stoichiometry of the minerals kaolinite and montmorillonite it seems strange that in the dehydroxylated minerals 5 and 4 coordinated Al is the main species respectively (Figure 5-34). Regarding the simple equations of the dehydroxylation of pure phases it should be the other way around.

$$\underset{\text{Kaolinite}}{Al_2Si_2O_5(OH)_4} \rightarrow Al_2Si_2O_7 + 2\,H_2O$$

$$\underset{\text{Montmorillonite}}{(Na,Ca)_{0.33}(Al,Mg)_2(Si_4O_{10})(OH)_2} \rightarrow (Na,Ca)_{0.33}(Al,Mg)_2Si_4O_{11} + H_2O$$

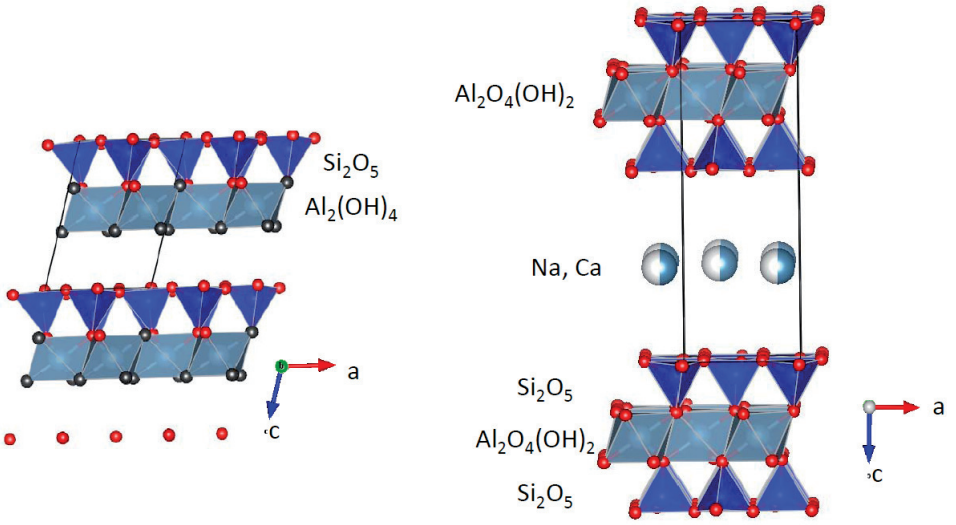

Figure 5-34: Visualized structures of kaolinite (left) and montmorillonite (right). Visualization performed with the software VESTA 3.1.2

In kaolinite 4 hydroxyls and two oxygen atoms are combined with one Al atom. Removal of these four hydroxyls as water molecules leaves in total four oxygen atoms with the Al which should lead to a 4-fold coordination mainly. On the other hand the removal of the two hydroxyls associated with the Al in montmorillonite as one water molecule should leave 5 oxygen atoms in total coordinated to Al in the structure. Thus one would expect 5-fold coordination in smectite minerals.

Moreover different structural models about the thermal transformation of montmorillonite were proposed that all predict 5 coordinated Al after the dehydroxylation [161]. Nevertheless a model is suggested in the same paper that can eliminate hydroxyls by producing 4- and 6-coordinated Al in addition to 5-coordinated. In Figure 5-32 it might actually be possible that the signal for 5-coordinated Al around 29 ppm lies under the main peak for 4-coordinated Al. The main peak at 59.6 ppm in the spectra of the calcined Søvind Marl shows a clear broadening to the right side.

The distorted structures of the dehydroxylates of both clay minerals kaolinite and smectite can not only be explained by the simple dehydroxylation of the octahedral sheet. Certainly this is the weakest part in the structure. Besides holding the hydroxyls the octahedra are connected via edges resulting in a weaker bonding than corner connected tetrahedra according to the Pauling rules of crystallography. The structural thermal transformations to metakaolin or metasmectite therefore are expected to start in the octahedral sheet. Nevertheless Si NMR analysis of calcined clays revealed that the dehydroxylation also has a major influence on the silicon tetrahedral sheet. Investigations on metakaolin indicated modifications in the short range order of the silicon tetrahedral sheet accompanied with the coexistence of Q^3 and Q^4 environments and different Q^m(nAl) sidebands [165]. The paper suggests a model to explain the coexistence of 4-, 5- and 6 coordinated Al in the metakaolin structure.

5.3.8 Mössbauer Spectroscopy

This method was only used to study the effect of iron in the Søvind Marl upon calcination. The other clays had either too low iron content in the clay minerals or did not show high enough reactivity to be interesting for investigation with this special method. As mentioned before the Søvind Marl has about 7 % iron in the clay mineral structures substituted for Al or Si.

The results presented are according to the report written by Lennart Häggström from the University in Uppsala, Sweden [170].

Representative Mössbauer spectra of the raw and calcined marl are shown in Figure 5-35. Data points and fitting are marked with crosses and black lines, respectively. The individual red and blue lines correspond to the absorption of the Fe^{2+} and Fe^{3+} components, respectively. The lines marked black in Figure 5-35a are the inner lines of the six-line patterns emanating from the magnetic part. In the fitting procedure both Fe^{2+} and Fe^{3+} are represented by two absorption lines with equal intensities (doublets). The isomer shift, δ, taken as the center of the doublet, is referred to α-Fe as standard absorber. The electric quadrupole splitting Δ, is the splitting of the doublet. In the fitting the isomer shift, quadrupole splitting, doublet intensity I and the line width Γ were kept as varying parameters.

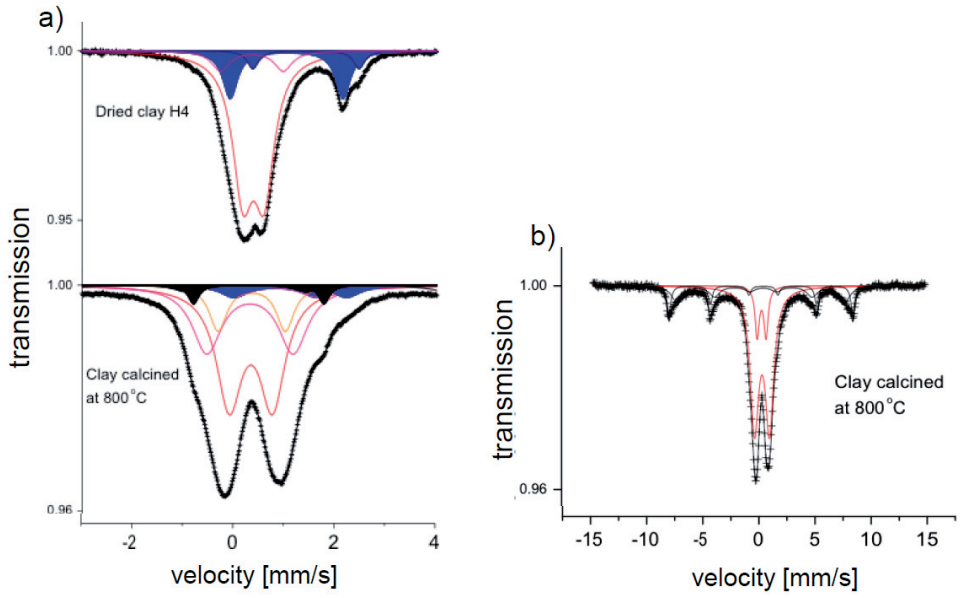

Figure 5-35: Room temperature Mössbauer spectra of the dried and calcined Søvind marl sample with low (a) and high (b) velocity scales

Both spectra show strong resonances at around 0 - 2 mm/s as it is typical for clay minerals [171]. The calcined sample displays furthermore resonances at higher velocities (Figure 5-35 b). These resonances are parts of six-line patterns originating from a magnetic part of the sample. These outer lines representing the magnetic phases are rather symmetric. The isomer shift is δ = 0.36 (1) mm/s and the quadrupole coupling constant is $\varepsilon \approx$ - 0.11 (3) mm/s. The high fields are representative for hematite (α-Fe_2O_3) while the lower field distribution also can derive from magnetite-maghemite ($Fe_{3-x}O_4$) solid solutions. The fact that the line distribution is symmetric for the outer lines in the six-line pattern makes it improbable that the signals come from magnetite and since maghemite is not stable above 400°C [172-173] the most probable explanation for the field distribution has to be from solid solutions of corundum-hematite (α-$Fe_{2-x}Al_xO_3$). Al atoms are present in the clay and can rather easily replace Fe^{3+} in hematite. However the substitution of Fe with Al results in a lowering of the field. With this interpretation the whole magnetic signal comes from Fe^{3+}. The intensities of these magnetic patterns were found, within error, equal to 30 (2) % for the calcined sample.
The analysis of spectra, recorded with lower velocity scale, (Figure 5-35a) are performed with varying number of quadrupole splitted doublets. For the spectrum of the raw sample the main part consists of a slightly splitted doublet and wider doublets (marked blue in the figure). From the fitting of the doublets in the raw marl Fe^{3+} and Fe^{2+} could be detected.
In Table 5-12 averaged hyperfine interaction values for the ferric and ferrous patterns are given. The same type of analysis was performed for the calcined sample, and the results are presented in Table 5-12.

Table 5-12: **Mössbauer averaged results. Isomer shift δ, quadrupole splitting Δ and line width at half maximum Γ are given in mm/s, while the intensities I are given in %. The errors in the parameters are: δ (± 0.01 mm/s), Δ (± 0.05 mm/s), I (± 1 %) and Γ (± 0.02 mm/s). For the calcined sample a magnetic signal with an intensity of 30% was also observed.**

	Fe^{3+}				Fe^{2+}			
Sample	δ	Δ	**I**	Γ	δ	Δ	**I**	Γ
dried clay	0.39	0.52	77	0.24	1.12	2.20	23	0.17
calcined clay	0.33	1.21	63	0.31	0.95	1.90	7	0.33

The isomer shifts and quadrupole splittings found are characteristic for clay minerals, like kaolinite, illite and montmorillonite [174]. The values for the isomer shift of Fe^{3+} and Fe^{2+} indicate both species to be in octahedral coordination [175]. Fe^{3+} and Fe^{2+} are thus substituted for Al^{3+} and Mg^{2+} in the octahedral layer of the clay miner-

al. All changes recorded for the iron species are therefore representative for any change in the octahedral layer of the clay structure, meaning also the Al environment.

The allowed quadrupole splitting versus isomer shift combinations for ^{57}Fe are shown in Figure 5-36. In dependence of the combinations Fe^{3+} and Fe^{2+} is present in different coordination. Reading the values from Table 5-12 into Figure 5-36 gives important information about the coordination state and possible distortions of Fe-sites in the clay mineral structure.

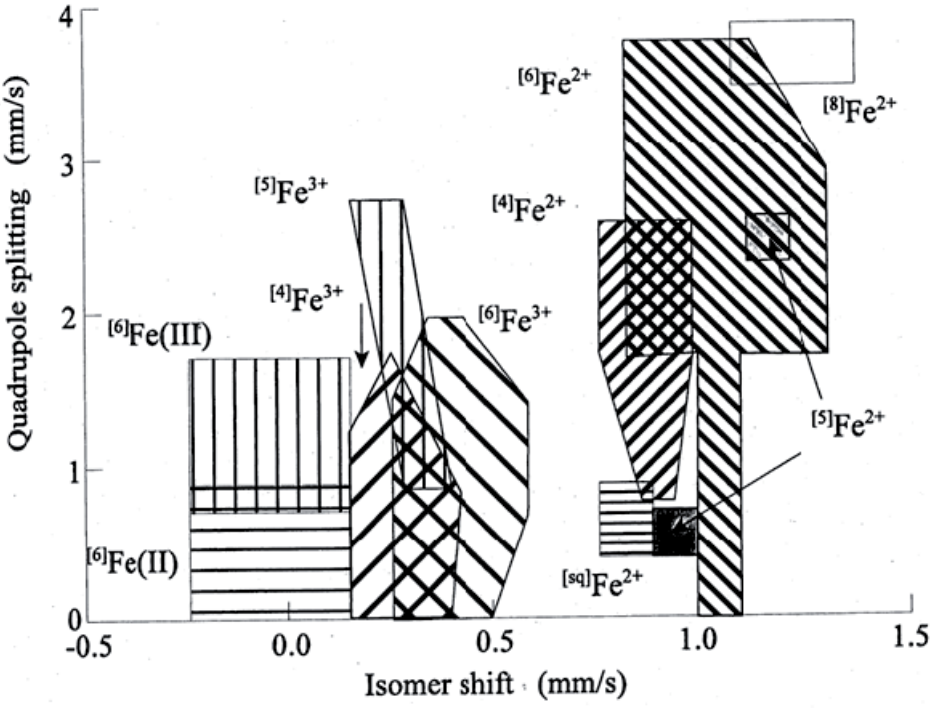

Figure 5-36: Allowed ^{57}Fe quadrupole splitting - isomer shift combinations for different valence states and coordination. The number in square brackets is the coordination number, with [6] indicating octahedral, [4] indicating tetrahedral and [sq] indicating square planar. High and low spin is indicated conventionally by the superscript valency or bracketed Roman numerals respectively. The isomer shift is referenced to α-Fe at room temperature [174].

The coordination of Fe^{3+} seems to change towards 5 and 6 upon calcination as the quadrupole splitting increases. Increasing quadrupole splitting may also be due to changes in the ligand structure for Fe caused by dehydroxylation. The isomer shift of Fe^{2+} is decreasing from the unfired to the calcined sample and so is the

quadrupole splitting, which may indicate a change in coordination towards 4. The values obtained for isomer shift and quadrupole splitting for the raw and calcined clay are in agreement with those of other authors and are interpreted as the result of strong distortions in the octahedral layer of the calcined clay mineral structures [175-176].

During the calcination process the Fe^{2+} is expected to be oxidized mostly to Fe^{3+} at 800 °C since the calcination takes place in air. The relative amounts of different Fe valences are presented in Table 5-13.

Table 5-13: Amounts in percent of iron ions in the samples. Errors 1%.

Sample	Fe^{3+} [%]	Fe^{2+} [%]
dried clay	77	23
calcined Clay	93	7

It can be seen that almost all the iron is oxidized in the calcined clay. Regarding a simple oxidation reaction of Fe^{2+} it must be noted that this oxidation not only affects the iron atom, but would lead to the inclusion of an extra oxygen atom somewhere in the structure for every second iron oxidized [103].

(10) $$4\,Fe^{2+} + O_2 \rightarrow 4\,Fe^{3+} + 2O^{2-}$$

Induced stresses and distortions leading to a highly disorganized calcined clay structure due to the oxidation of iron accompanied with increasing quadrupole splitting values is partly confirmed by several authors [177-179].

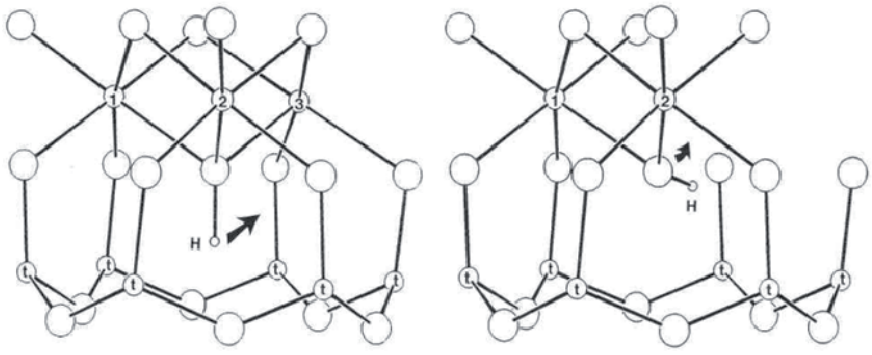

Figure 5-37: Schematic diagram of a portion of a tri-octahedral 2:1 layer (left) and a di-octahedral layer structure (right) showing the locations of octahedral cations (1,2,3), tetrahedral cations (t), and OH proton (H). Arrow indicates change in orientation of H upon heating-induced oxidation of Fe^{2+} (left) and relocation of hydroxyl oxygen toward the octahedral metal sheet upon heating-induced dehydroxylation [180].

It could also be shown that in tri-octahedral micas the oxidation of Fe^{2+} to Fe^{3+} upon heating causes a reorientation of the hydroxyls due to the redistribution of the octahedral charge. Dehydroxylation of then di-octahedral micas containing only Fe^{3+} results in a relocation of the residual oxygen in the octahedral plane (Figure 5-37) [180].

5.4 Pozzolanic Reaction of Calcined Clays

5.4.1 Calcium Hydroxide Consumption of Calcined Clays

The consumption of calcium hydroxide was tested in clay/lime pastes as described in chapter 3.8.2 and the amount of calcium hydroxide after 28 days and 6 month curing at 20 and 38 °C was measured with thermogravimetric analysis. First tests were performed on the Søvind Marl by preparing marl/lime pastes in the ratios 2/1 and 1/1.

Table 5–14: Calcium hydroxide consumption in calcined marl/lime pastes with a ratio of 2/1 and 1/1 cured for 28 days and 6 month at a temperature of 20 °C and 38 °C

	Clay/lime = 2/1		Clay/lime = 1/1	
	20 °C	**38 °C**	**20 °C**	**38 °C**
CH at 0 days [%]	30.9	30.9	47.1	47.1
CH at 28 days [%]	9.2	10.0	19.8	19.1
Consumed CH [%] 0-28 days	70.2	67.6	58.0	59.4
Consumed CH per gram clay	**0.31**	**0.30**	**0.52**	**0.53**
CH at 6 month [%]	6.7	7.1	15.1	13.8
Consumed CH [%] 0-6 month	78.3	77.0	67.9	70.7
Consumed CH per gram clay	**0.35**	**0.34**	**0.60**	**0.63**

From Table 5–14 it can be seen that marl/lime blend, in a ratio of 2/1, cured for 28 days at 20 °C and 38 °C consumed 70.2 and 67.6 % of the added calcium hydroxide, respectively. For marl/lime blend cured for 6 months the consumption of calcium hydroxide was 78.3 % and 77.0 %. Typical lime consumption for silica fume is 78 % under otherwise equal conditions [181]. The higher temperature of 38 °C which was expected to accelerate the reactions did not have much influence on the lime consumption. The tests with more lime (ratio 1/1) were performed to check if the maximum level of lime consumption is already reached or if there is a possibility for even more consumption. Curing for 28 days at 20 °C and 38 °C resulted in 58.0 and 59.4 % consumption of added calcium hydroxide, respectively. After 6 month curing 67.9 and 70.7 % lime were consumed, respectively. In these pastes more lime was consumed at the higher temperature, although the effect is still not as high as expected. Recalculated in absolute values of lime consumption per gram of clay, it can be shown that the level of lime consumption was almost double in the pastes with a ratio of 1/1. While in the 2/1 pastes 0.35 g lime per gram clay are consumed after 6 month curing at 20 °C, in the 1/1 pastes 1 gram of clay consumed 0.60 g of

lime. That could mean that the CH that is left in 2/1 and 1/1 pastes after hydration for 6 months has limited availability for further pozzolanic reaction. In chapter 5.4.2.1 it will be shown that some ill-dispersed lumps of CH from the mixing are present in the paste. These CH lumps probably have a more reacted outer layer, thus limiting the availability of "inner CH".
Further tests with the other calcined clays from Portugal and Poland were only performed for a clay/lime ratio of 1/1. The average results of the lime consumption for all calcined clays when cured at 20 and 38 °C are given in Table 5–15 and 5–16 respectively. The error for the values consumed lime per gram clay varies between 0.02-0.05 g.

Table 5–15: Calcium hydroxide consumption in calcined clay/lime pastes with a ratio of 1/1 cured for 28 days and 6 month at a temperature of 20 °C

Clay/lime = 1/1 (20 °C)	SØ	H2-H4	AB1080	Sorgila	Rascoia	Gniew
CH at 0 days [%]	47.1	46.2	47.1	47.9	46.5	46.3
CH at 28 days [%]	19.8	23.5	13.9	34.3	34.1	28.4
Consumed CH [%] 0-28 days	58.0	49.0	70.5	28.2	26.7	38.5
Consumed CH per gram clay [g]	**0.52**	**0.41**	**0.63**	**0.26**	**0.23**	**0.34**
CH at 6 month [%]	15.1	18.7	11.7	28.2	31.5	22.2
Consumed CH [%] 0-6 month	67.9	59.4	75.1	40.4	31.8	52.8
Consumed CH per gram clay [g]	**0.60**	**0.51**	**0.67**	**0.37**	**0.28**	**0.47**

At both temperatures AB1080 has the highest lime consumption of all clays after 28 days and 6 month. At 20 °C 75.1 % CH were consumed after 6 month. By increasing the curing temperature to 38 °C this value was already reached after 28 days. 6 month curing at 38 °C lead to a consumption of the initial added CH as high as 82.7 %. The maximum lime consumption of Søvind Marl reaches 70.7 % after 6 month curing at 38 °C. This is comparable to the value obtained with AB1080 after 28 days curing at 20 °C. The least reactive clay is Rascoia with a lime consumption of 31.8 and 39.6 % after curing for 6 month at 20 and 38 °C respectively.
The lime consumption after 28 days and 6 month increases in the following order:

Rascoia < Sorgila < Gniew < Søvind Marl < AB1080

Table 5–16: Calcium hydroxide consumption in calcined clay/lime pastes with a ratio of 1/1 cured for 28 days and 6 month at a temperature of 38 ºC

Clay/lime = 1/1 (38 °C)	SØ	H2-H4	AB1080	Sorgila	Rascoia	Gniew
CH at 0 days [%]	47.1	46.2	47.1	47.9	46.5	46.3
CH at 28 days [%]	19.1	19.7	11.7	28.4	31.3	24.8
Consumed CH [%] 0-28 days	59.4	57.4	75.1	40.6	32.7	45.5
Consumed CH per gram clay	**0.53**	**0.49**	**0.67**	**0.37**	**0.28**	**0.40**
CH at 6 month [%]	13.8	17.6	8.1	21.9	27.9	20.6
Consumed CH [%] 0-6 month	70.7	62.0	82.7	53.7	39.6	56.1
Consumed CH per gram clay	**0.63**	**0.53**	**0.73**	**0.48**	**0.34**	**0.50**

This order correlates directly to the 28 days compressive strength results of mortars were 20 % of OPC was replaced with the respective calcined clay. The compressive strength after 28 days followed the same increasing trend. All clays consumed more CH at higher curing temperature after 28 days as well as after 6 month. Nevertheless for the Søvind Marl including H2-H4 the difference is not very significant. However accelerated lime consumption could be possible at earlier ages (1-7 days) when cured at 38 °C. But the lime consumption at earlier ages was only tested at 20 °C for Søvind Marl and AB1080 (Table 5–17). The most significant difference in lime consumption, at different curing temperatures, shows Argila Sorgila where after 28 days and 6 month the lime consumption is increased about 0.1 g lime/g clay from 20 to 38 °C. In Table 5–17 it can be seen that already at 1 day the lime consumption of AB1080 is as high as the lime consumption of Argila Sorgila and Rascoia after 28 days. It also shows that the lime consumption of Søvind Marl and AB 1080 starts very early and reaches high values already after 7 days.

Table 5–17: Calcium hydroxide consumption in calcined clay/lime pastes with a ratio of 1/1 cured for 1, 3 and 7 days at a temperature of 20 ºC

Consumed lime [g] per gram clay	AB1080	H2-H4
1 day	0.24	0.13
3 days	0.28	0.21
7 days	0.44	0.33

Figure 5–38 plots the relative 28 days compressive strength of standard mortars with 20 % replacement of OPC by the respective calcined clay versus the lime consumption of the different calcined clays after 28 days cured at 20 °C in clay/lime pastes with a ratio of 1/1. The plot reflects a trend that at lower values a small increase in lime consumption has a much higher influence on the strength increase in mortars than at higher values. For Sorgila, Gniew and SØ (H2-H4) the compressive strength increases almost linear with the lime consumption. It can be assumed from this graph that a lime consumption above 0.7 g lime/g clay does not lead to any significant further strength increase in mortars, as long as other effects like additional "filler effect" are excluded. The graph also tells us that with the given clays the strength increase in mortars is mainly due to the pozzolanic reaction of the clays with calcium hydroxide and that a filler effect of non clay minerals like quartz and feldspars plays only a minor role. Assuming that quartz and feldspars do not take part in the pozzolanic reaction 44 % of kaolinite in AB1080 are able to consume more lime than the almost 70 % of total clay minerals in Søvind Marl. This confirms also again that the mineralogy of the clay has the highest influence on the lime consumption while the specific surface of the different materials has no big effect.

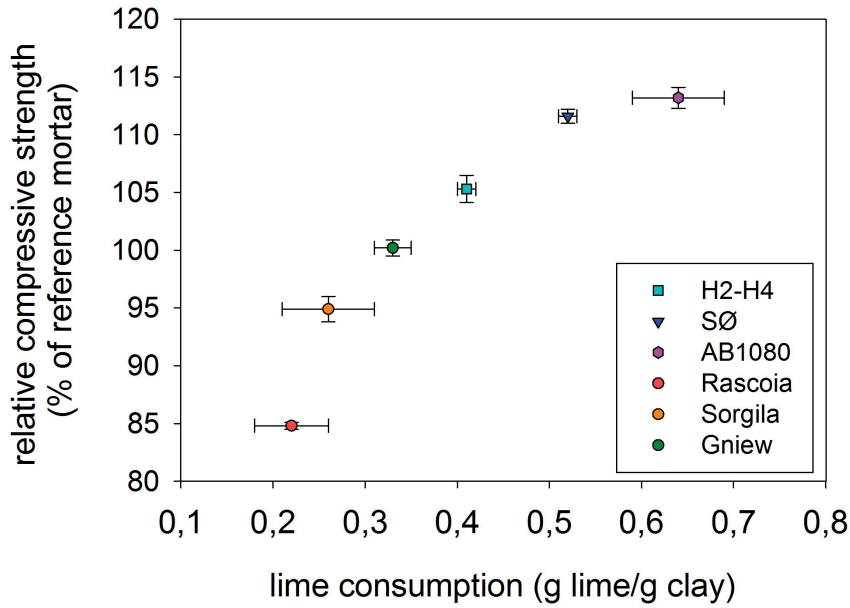

Figure 5–38: Relative 28 days compressive strength of standard mortars with 20 % replacement of OPC by calcined clay vs. lime consumption after 28 days of different calcined clays. The curing temperature of mortars and pastes was 20 °C.

Neglecting the non-clay minerals except calcium carbonate the lime consumption follows again the trend that illite is less reactive than smectite and smectite is less reactive than kaolinite. In combination with calcium carbonate however calcined illite and smectite rich clays are more reactive than illite and smectite alone.
If the lime consumption of clays at early ages correlates with the compressive strength at early ages in the same matter as shown in Figure 5–38, the data from Table 5–17 should be transferable to our graph. With a lime consumption of 0.44 g lime/ g clay after 7 days it can thereby be concluded that the 7 day compressive strength of a mortar where 20 % of OPC is replaced by AB1080 should be more than 5 % higher than the compressive strength of the reference mortar. Consequently the compressive strength of a mortar containing 20 % Søvind Marl should be about the same as the strength of the reference mortar after 7 days. In chapter 8 about the compressive and flexural strength of mortars with 20, 35, 50 and 65 % replacement of OPC by calcined clay cured for 1, 3, 7, 28, 90 and 365 days this assumption is confirmed.
In Figure 5–39 the lime consumption of calcined clays after hydration for 28 days at 20 °C versus the total and "real" sum of $SiO_2 + Al_2O_3 + Fe_2O_3$ of the clays is plotted. According to the standard C618 for pozzolanic materials, a material with a sum of $SiO_2 + Al_2O_3 + Fe_2O_3 > 70$ % of the total chemistry is a good pozzolana. The figure shows however that it cannot be concluded that the pozzolanic activity of natural calcined clays increases with increasing total sum of $SiO_2 + Al_2O_3 + Fe_2O_3$. As mentioned before the total sum of $SiO_2 + Al_2O_3 + Fe_2O_3$ can be misleading in natural pozzolans as many non reactive mineral phases as quartz and feldspars can be contained that raise this sum. For that reason the lime consumption is also plotted versus the "real" sum of $SiO_2 + Al_2O_3 + Fe_2O_3$ in Figure 5–39.

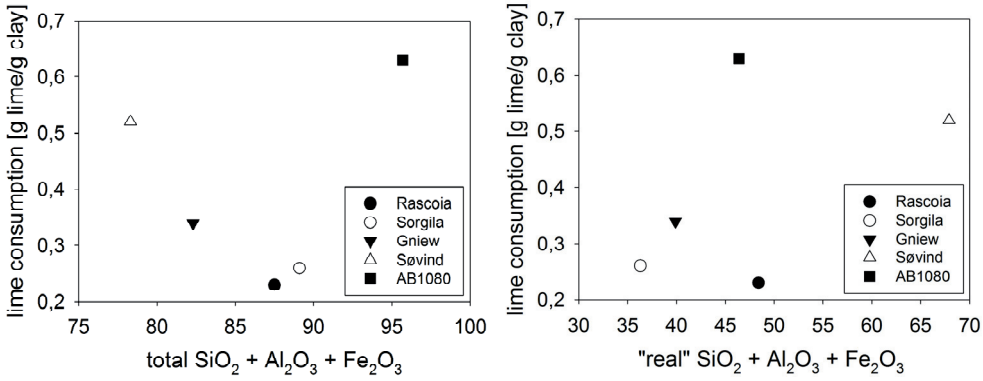

Figure 5–39: Lime consumption of calcined clays after hydration for 28 days at 20 °C versus the total (left) and "real" (right) sum of $SiO_2 + Al_2O_3 + Fe_2O_3$ of the clays

The "real" sum describes the sum of SiO_2 + Al_2O_3 + Fe_2O_3 that derives only from the clay minerals in the different clays itself and is calculated from the mineralogical composition considering the pure clay phases illite, smectite (montmorillonite), and kaolinite. Also here the lime consumption does not increase directly with increasing "real" sum of SiO_2 + Al_2O_3 + Fe_2O_3. It can be seen that Rascoia the clay with the lowest pozzolanic activity in lime consumption tests and reactivity in mortar tests has the second highest sum of "real" SiO_2 + Al_2O_3 + Fe_2O_3. Nevertheless all calcined clays reached a strength activity index of > 75 % meaning they are good pozzolanic materials in compliance with the standard C618. The strength activity index is defined as the ratio of the compressive strength for a mortar with 20 % pozzolan replacement for cement by mass to the compressive strength of a control mortar (see chapter 5.2.4).

5.4.2 Hydration Reactions of Calcined Clays in Clay/Lime pastes

5.4.2.1 Søvind Marl

The hydration products of the pozzolanic reaction of clays and marls are likely to be similar to those of siliceous fly ash (CSH, CAH and CASH), because fly ash is formed from clay impurities present in pulverized coal, which is often used as a fuel in thermal power plants. The diffractograms of pastes with different marl/lime ratios and curing temperatures showed no significant difference in the hydration products or intensities of single phases. Therefore the diffractograms of pastes with a clay/lime ratio of 1/1 are displayed only. Figure 5–40 shows diffractograms of the Søvind Marl pastes cured for 28 days and 6 month at 20 ºC.

The consumption of lime after 28 days and 6 month can easily be observed by the decreasing intensities of peaks at 47.4 º, 51 º and 54.6 º2θ. The wide peak around 9 º2θ is a peak of (meta)-smectite and illite minerals in clay. This peak almost disappears after 28 days of hydration and is completely gone after 6 month, which is a sign of the reaction between calcined clay minerals and calcium hydroxide. As expected, due to the high amount of calcium carbonate in the marl (~ 5 % at 850 °C), the formation of carboaluminate hydrate phases is correspondingly high [182]. If present, calcium aluminate hydrates react with any calcium carbonate present in the system to form calcium carboaluminate hydrates as documented for cementitious systems blended with calcium carbonate powder [183-185]. In a study about the pozzolanic activity of calcined Na-montmorillonite containing small amounts of calcite, carboaluminate hydrate ($C_4A\bar{c}H_{12}$) was also the main crystalline hydration

product to be found in hydrated pastes with lime [68]. Curing for 28 days leads mainly to the formation of hemicarboaluminate hydrate (peak at 10.8 º2θ). The excess of calcium hydroxide in the system interferes with the calcium carbonate, forming more hemicarboaluminate than monocarboaluminate hydrate (peak at 11.7 º2θ) after 28 days. After curing for 6 month and continuing lime consumption monocarboaluminate hydrate predominates. It is known that in general hemicarboaluminate forms first and converts to monocarboaluminate with time in the presence of calcite [186].

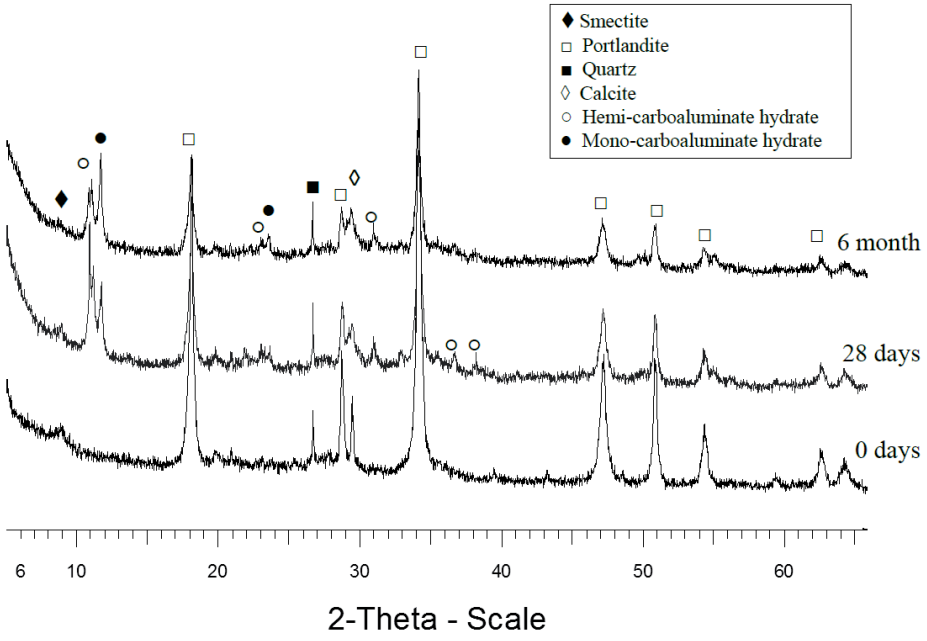

Figure 5–40: Diffractograms of calcined marl/lime pastes in the ratio 1/1 cured for 28 days and 6 month at 20 ºC

The transformation of hemi- into monocarboaluminate can furthermore be observed by the presence of two peaks, at 36.8 º and 38.3 º2θ. These two peaks belonging to hemicarboaluminate appear after 28 days and disappear again after 6 month. As early as 28 days, a second peak (11.1 º2θ) between hemi- and monocarboaluminate can be observed. This peak coincides with an iron substituted carboaluminate phase where iron from the clay is substituted for aluminum in the structure of the carboaluminates. In carboaluminate hydrate phases solid solutions between the Al and Fe- endmembers are not possible resulting in the extra peak at 11.1 º2θ. In fact Al- and Fe-substituted carboaluminate exist as two separate phases with different crystal structures. The incorporation of Fe ions into the structure

leads due to the greater ionic radius compared to Al to an enlarged a-unit cell parameter accompanied with a change in location of the carbonate ions in the structure [187]. This results in a rhombohedral structure for Fe-carboaluminate instead of a triclinic structure for Al-carboaluminate. The calcite peak at 29.4 º2θ is due to the presence of residual uncalcined calcium carbonate in the clay after the burning. After 28 days and 6 month of hydration this peak shows a clear loss of crystallinity due to the reaction between calcium carbonate and calcium aluminate hydrates resulting in the formation of carboaluminate hydrate phases. Other crystalline hydration products could not be detected by means of XRD. Hydration at a higher curing temperature did not result in any significant changes in the marl lime pastes. The same hydration phases were observed with XRD. However the equilibrium was in favor for monocarbolauminate already after 28 days and after 6 month only a small shoulder for hemicarboaluminate was visible. The diffractograms of the marl/lime paste in the ratio 1/1 hydrated for 28 days and 6 month at 38 °C is given in the appendix.

Figure 5–41 shows the DTG curves of the marl/lime pastes in the ratio 1/1 hydrated for 28 days and 6 month at 20 and 38 °C. The non-reacted marl/lime mixture shows two major peaks: the main peak at 450 ºC is due to the decomposition of calcium hydroxide, while the smaller peak at 730 ºC shows the final decarbonation of the residual 5.1 % calcium carbonate (calculated from weight loss in the TG curve). After 28 days curing, the peak for calcium hydroxide decreases, as seen in the XRD diffractograms. Additionally two signals between 100 and 200 ºC appear. The first peak at 130 ºC stands usually for the formation of a C-S-H like phase while the second reaction around 170 ºC can be attributed to the decomposition of carboaluminate phases [182, 188]. For synthesized monocarboaluminate a doublet dehydroxylation peak at ~ 120 and ~ 150 ºC was reported as well as a double or single peak around 240 ºC depending on the starting material of the synthesis (Gibbsite and Boehmite) [189]. The carboaluminate hydrate phases are therefore probably mainly responsible for the first three signals. The first two peaks increase in intensity from 28 days to 6 month as the calcium hydroxide peak decreases. Moreover, a smaller peak can be seen around 350 ºC, which possibly belongs to a hydrogarnet phase (C_3AH_6). When cured at 38 ºC this peak is already clearly visible after 28 days compared to a very weak signal in the paste cured at 20 ºC after 28 days. With XRD this phase was not clearly detected. The diffuse signals between 700 and 850 ºC appearing after 28 days and 6 month cannot be explained yet but are most likely due to the final dehydroxylation and decarbonation of the carboaluminate hydrates. A peak at 865 ºC was reported to represent the decarboxylation of monocarboaluminate [189]. Hemicarboaluminate and Fe-substituted

carboaluminate phases might show a slightly different decomposition behaviour explaining the different signals in the high temperature area.

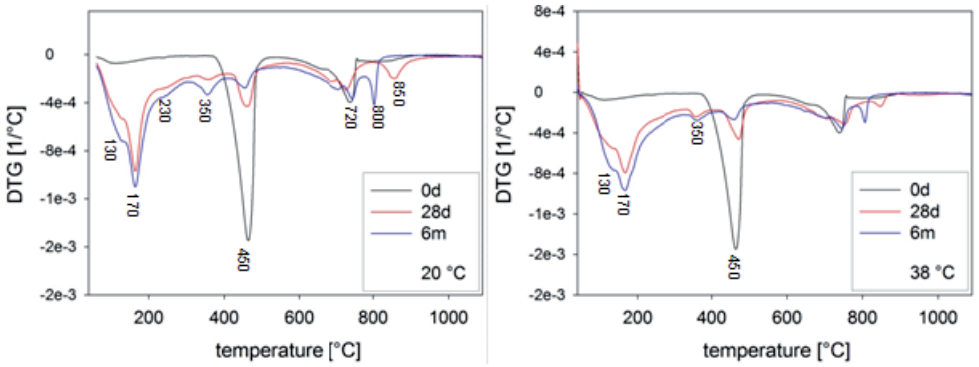

Figure 5–41: DTG curves of the calcined marl/lime pastes in the ratio 1/1 hydrated for 28 days and 6 month at 20 (left) and 38 °C (right)

^{27}Al MAS NMR was additionally performed on a marl/lime paste in the ratio 1/1 hydrated for 28 days at 20 ºC. With this technique more information about hydration products especially amorphous phases like C-S-H can be acquired. The ^{27}Al MAS NMR spectrum of the mentioned sample is given in Figure 5–42.

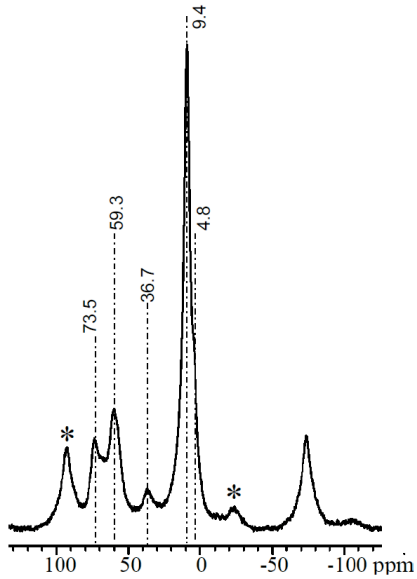

Figure 5–42: ^{27}AL MAS NMR spectra of a calcined marl/lime paste in the ratio 1/1 hydrated for 28 days at 20 °C

It includes two resonances from Al in tetrahedral coordination at 73.5 ppm and 59.7 ppm, a single-resonance from five-fold Al (36.7 ppm), and two resonances from Al in octahedral coordination (9.4 ppm and 4.8 ppm – shoulder). The peaks exhibit the following relative intensities 12.4 % (73.5 ppm), 19.4 % (59.7 ppm), 6.8 % (36.7 ppm), and 61.5 % (9.4 and 4.8 ppm). The resonances bear a clear resemblance to those observed in hydrated Portland cement, indicating the formation of a C-S-H like phase, probably with incorporation of Al as ^{27}Al-NMR cannot see pure C-S-H, and an AFm calcium aluminate hydrate phase [190]. The 73.5 ppm peak may reflect AlO_4 tetrahedra in a chain structure of silicate tetrahedra while the resonance at 36 ppm is typical for five-fold aluminum in the C-S-H phase. This resonance is assigned to Al^{3+} substituting for Ca^{2+} ions situated in the interlayer of the C-S-H structure [191-192]. The resonance at 9.4 ppm is typical for the $Al(OH)_6$ units in the structure of calcium aluminate hydrate AFm phases [190, 193]. Consequently this signal represents the presence of the carboaluminate species formed in our system as shown with XRD. Moreover, the shoulder at 4.8 ppm is very similar to a new aluminate hydrate phase detected in hydrated Portland cements [190]. The authors demonstrate that the resonance originates either from an amorphous or disordered aluminate hydroxide or a calcium aluminate hydrate. The species containing $Al(OH)_6^{3-}$ or $O_xAl(OH)_{6-x}^{(3+x)-}$ units can be produced as a separate phase or as a nanostructured precipitate at the surface of C-S-H particles. Since the resonance could not be assigned to any of the previous known aluminate phases in hydrated Portland cements, the phase was called the "third aluminate hydrate" [190].
The resonance at 59.7 ppm originates from the calcined clay as was shown in Chapter 5.3.7. Thus the relative intensities (19.4 %/95.1 %) indicate that about 80 % of the calcined clay minerals containing Al have reacted with water and lime during the 28 days of curing. In general it can be noted that Al changed from 6 to 4-fold coordination upon calcination. In the hydration reaction with calcium hydroxide the 4 coordinated Al from the metaclay changes back to mainly 6-fold coordination as a result of the AFm phase formation besides, the incorporation of Al ions in 4- and 5-fold coordination in the C-S-H structure.

The microstructure of hydrated lime/marl pastes was investigated under the SEM with BSE images. Furthermore WDX measurements were performed on interesting phases to get a better idea of the element distribution in hydration products in particular. The measured composition in atom % of the phases marked with numbers 1-12 in Figures 5–43 and 5–44 are given in Table 5–18. Figure 5–43 shows BSE images of marl/lime pastes hydrated for 28 days and 6 month at 20 °C. The first two pictures are close ups to the matrix revealing cloudy and elongated phases. The cloudy particles are most likely C-S-H phases while the elongated, needle like

phases are probably cross sections of platelets and can represent the AFm-phases which were observed with DTG and XRD. In most cases these particles were too small for the excitation volume of the X-Ray beam to be measured. That these phases are finely crystalline becomes clear with regard to the small scale of 5 µm in this picture. In point 1 & 2 in Figure 5–43a & b calcium rich phases with incorporation of some silicon and aluminum were measured showing most likely a reaction between calcium hydroxide lumps with silicon and aluminum ions in the pore solution. At the top of picture 5–43b one of the glassy particles observed in the calcined marl is visible. The typical microstructure of the marl/lime pastes observed all over the sample is presented in Figure 5–43c. Some unreacted and more reacted clay particles and big lumps with C-S-H gel composition (Point 3) lying in a matrix of finer particles described above. WDX analysis of Point 3 in Figure 5–43c gave the composition: 26.1 % Ca, 10.8 % Si, 4.5 % Al which is an Al-substituted C-S-H phase also observed with ^{27}Al MAS NMR spectroscopy. The Ca/Si+Al ratio is 1.7. These big lumps are probably grown pseudomorph of ill-dispersed calcium hydroxide lumps after diffusion of Si & Al into and Ca out of the particles. Figure 5–43d shows a close up to one of the C-S-H lumps surrounded by elongated particles. Attempts were made to analyze these and the composition at Point 4 is 14.4 % Ca, 1.3 % Si and 11.4 % Al. The composition represents a calcium aluminate hydrate but the Ca/Al ratio of 1.27 is too low for usual AFm phases. Maybe it is a calcium aluminate hydrate like C_2AH_8 (Ca/Al = 1) partly converted to C_3AH_6 (Ca/Al = 1.5) or another kind of pre-cursor phase of hydrogrossular. The picture shows a paste hydrated for 6 month and hydrogarnet was observed at this time with DTG. Hydrogarnet formation associated with the reaction of calcined clays and lime at longer curing times is confirmed in literature [58]. Figure 5–43e shows a calcined reactive clay particle with its open diffuse morphology in the matrix of finely crystalline hydration products. Point 5 and 6 in Figure 5–43f represent a C-S-H phase and an illite grain respectively. The C-S-H particle has some aluminum and minor amounts of sodium and potassium incorporation. Illite can be easily recognized due to the high potassium content, since orthoclase is not present in the marl. Such illite grains could be found all over the samples and show again how stable this clay mineral is upon heat treatment. Even after 6 month illite seems not to be reacted so that a contribution to the pozzolanic reaction cannot be expected.

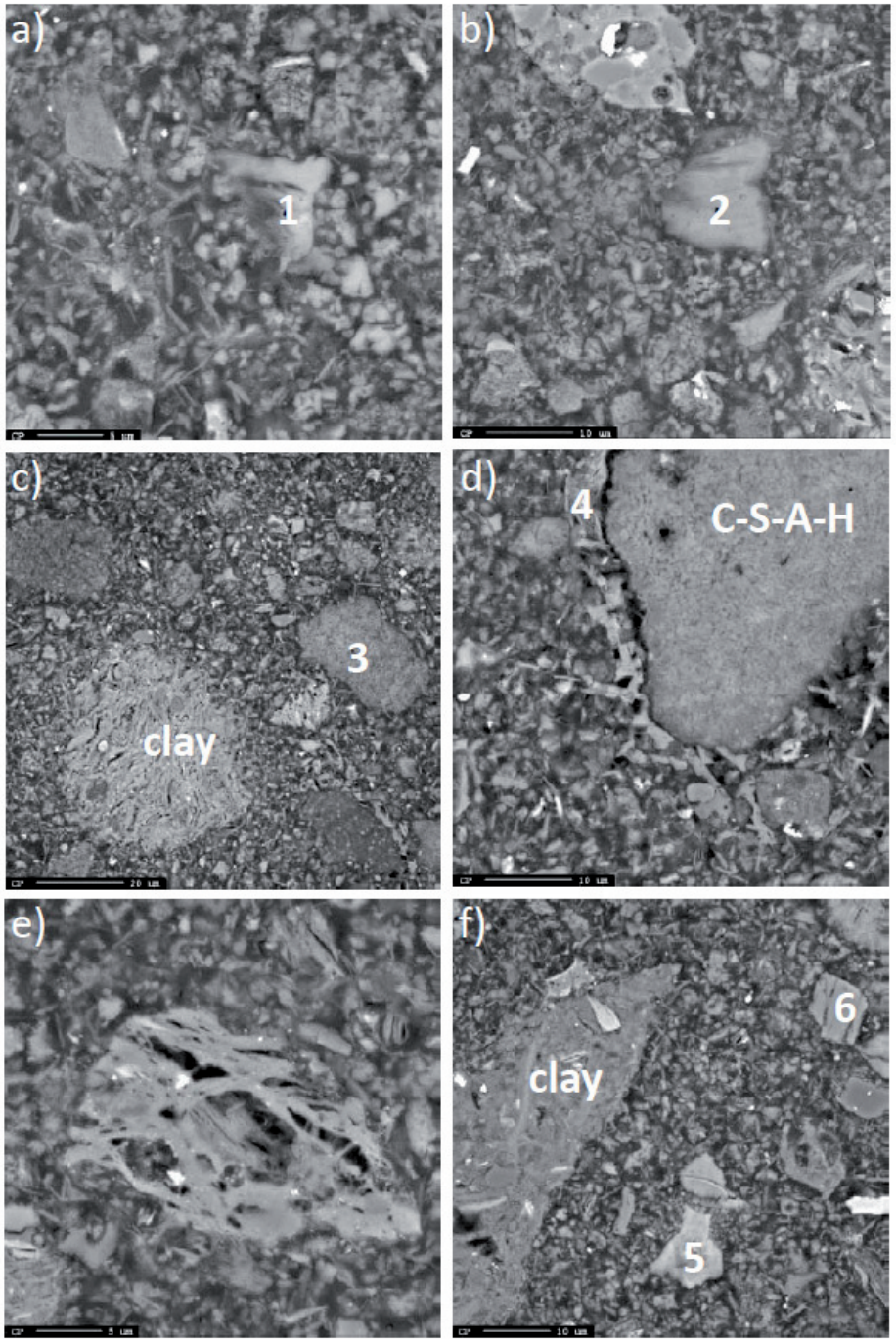

Figure 5–43: BSE images of calcined marl/lime pastes hydrated for 28 days (a: 3000x, b: 2000x) and 6 month (c-f, c: 1000x, d: 2000x, e: 3000x, f: 1500x) at 20 °C

When hydrated at 38 °C the matrix of the marl/lime pastes appeared to be somehow denser compared to the pastes hydrated at 20 °C. The BSE images of the lime/marl pastes cured for 28 days and 6 month at 38 °C are given in Figure 5–44. A reacting calcined clay particle in the dense matrix with a calcium aluminate hydrate phase in Point 7 is shown in Figure 5–44a. The composition in point 7 could represent an AFm phase with a Ca/Al ratio close to 2. There is some substitution with silicon and iron present in this phase. A glass particle from the calcined clay with a reaction rim is visible in Figure 5–44b. The glass particle (Point 8) and the reaction zone (Point 9) were measured with WDX. The composition of the glass particle is similar to the compositions measured in the pure calcined marl in Chapter 5.3.6.1. In the reaction zone the calcium content is significantly increased as a reaction of the calcium hydroxide with the silicon and aluminum ions released from the glass phase. The composition represents a calcium aluminate silicate hydrate with iron and magnesium substitution. This shows that the glassy particles are reactive with lime. Additionally a calcined clay particle with a reaction rim is shown in Figure 5–44c. The points marked with X at the edge of the calcined clay particle gave a calcium silicate hydrate composition that was measured with EDX. Massazza describes the pozzolanic reaction with natural pozzolans as the sum of topochemical reactions with dissolution and precipitation [58]. The alkaline solution attacks the surface of the pozzolana resulting in a dissociation of the surface to SiO_4^{4-} and H^+. Ca^{2+} can then adsorb on the negatively charged surface. Furthermore an unstable thin, amorphous Si and Al rich layer is formed on the surface by leaching alkalis from the pozzolana. The so dissolved SiO_4^{4-} and AlO_2^- will combine with the Ca^{2+} to form calcium silicate and calcium aluminate hydrate phases [58].
Pastes hydrated for 6 months are given in Figure 5–44d-f. The pictures d & f are close ups to the matrix where hydration products were tried to be measured. The composition in point 10 represents a calcium silicate hydrate with aluminum and iron substitution while in point 12 a calcium aluminate hydrate with silicon and iron substitution is present. Point 12 might represent a hydrogarnet phase where wide solid solutions with iron for aluminum in the octahedral and silicon tetrahedra for OH_4 tetrahedra are possible. In Figure 5–44e a larger calcite grain with a reaction rim is visible. The composition in point 11 is typical for an AFm phase with a Ca/Al ratio of about 2. Furthermore iron and silicon are present in considerable amounts. Consequently this might be one of the iron substituted carboaluminate hydrate phases observed with XRD, since it is close to a $CaCO_3$ particle.

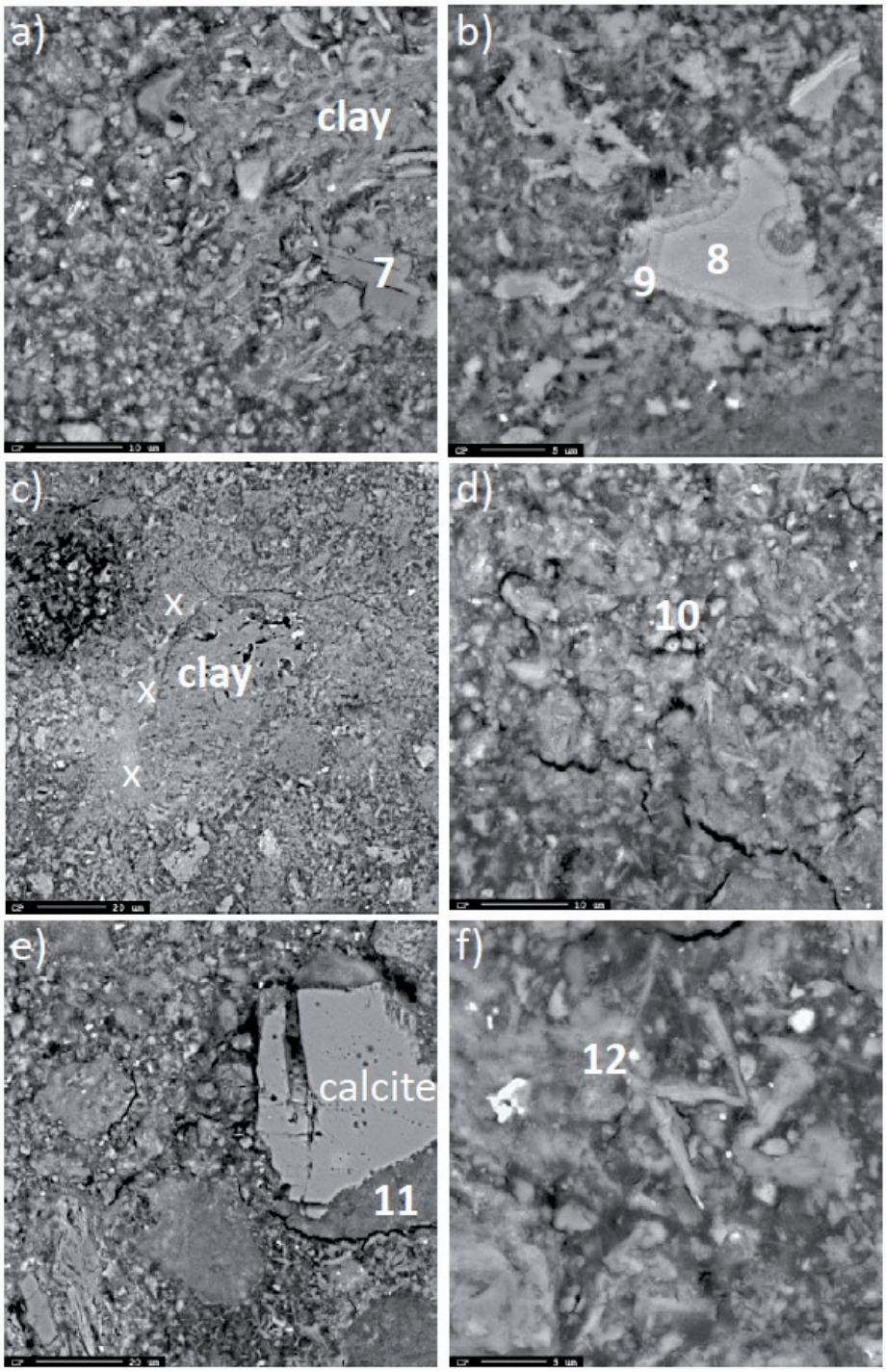

Figure 5–44: BSE images of calcined marl/lime pastes hydrated for 28 days (a: 2000x, b: 3000x, c: 800) and 6 month (d-f, d: 2000x, e: 1000x, f: 3000) at 38 °C

Table 5–18: WDX composition in Atom % of Points 1-12 marked in Figure 5–43 and 5–44

WDX_No.	Ca	Al	Si	Fe	Mg	K	Na	O
1	29.1	1.4	5.2	0.4	0.5	0.3	0.2	62.9
2	28.5	1.7	7.9	0.2	0.4	0.1	0.0	61.1
3	26.1	4.5	10.8	0.1	0.4	0.8	0.1	56.5
4	14.4	11.4	1.3	0.4	0.1	0.1	0.2	71.5
5	20.5	2.2	8.8	0.1	0.5	1.5	1.4	65.1
6	1.1	7.7	22.7	0.1	0.1	5.0	0.4	62.8
7	26.0	12.2	2.6	1.6	0.3	0.4	0.2	56.7
8	6.3	7.9	17.5	2.5	1.6	0.7	0.4	62.9
9	15.2	6.3	8.9	3.5	1.7	0.1	0.1	63.8
10	18.8	3.6	8.0	1.2	1.0	0.8	0.5	66.0
11	21.8	11.1	4.6	4.4	0.7	0.9	0.1	56.3
12	17.1	12.9	5.2	2.5	0.3	0.5	0.2	60.7

5.4.3.1 AB1080

The hydration products formed of metakaolin in combination with lime are slightly different compared to calcined smectite and illite clays. In metakaolin/lime pastes with a ratio of 1/1 hydrated for 28 days at 20 °C the main hydration product to be expected is strätlingite (C_2ASH_8) besides C-S-H and minor amounts of C_4AH_{13} [194]. This is exactly what we observe with XRD and DTG in our investigations with the impure kaolinite rich clay AB1080. The diffractograms of the pastes prepared by mixing calcined AB1080 with lime in a ratio of 1/1 hydrated for 28 days and 6 month at 20 °C are shown in Figure 5–45.

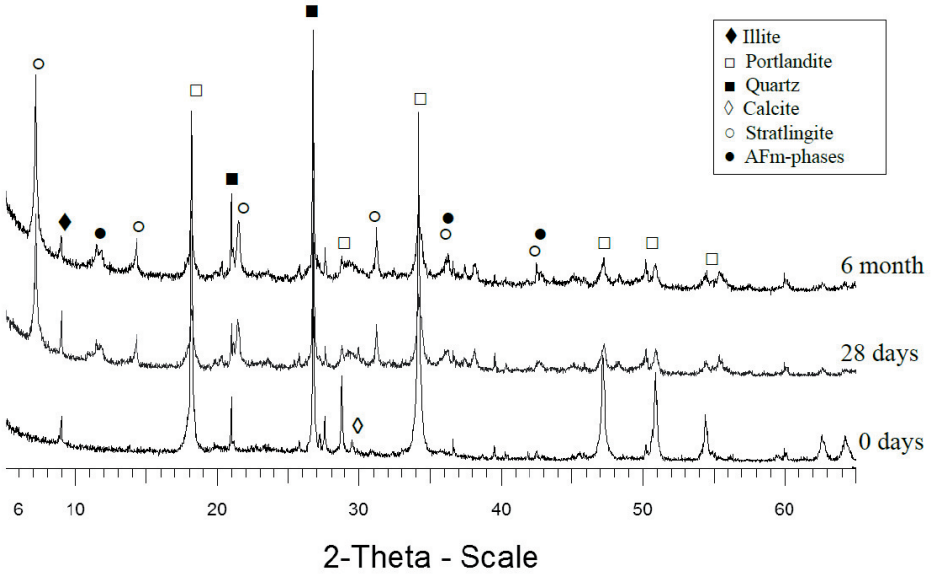

Figure 5–45: Diffractograms of calcined AB1080 clay/lime pastes mixed in a ratio of 1/1 and hydrated for 28 days and 6 month at 20 °C.

In the unhydrated sample (0 days) only peaks of portlandite and the minerals from the clay that were not affected by the heat treatment (quartz, feldspar, illite) are visible. Furthermore a small peak of calcite can be detected in the unhydrated mix deriving from the commercial portlandite. According to the manufacturer the material can contain up to 3 % calcite as impurity. The lime consumption of the calcined clay is again observable by the decreasing intensities of peaks at 47.4 º, 51 º and 54.6 º2θ. It becomes clear that also in this system the main consumption of lime takes place during the first 28 days. Strätlingite is the main hydration product after 28 days and 6 month with its 003 reflection at about 7.1 º2θ. The wide peak between 10-12 º2θ is probably due to a mixture of the AFm phases

monocarboaluminate ($C_4A\bar{c}H_{11}$) and tetracalciumaluminate hydrate (C_4AH_{13}). The small amount of calcite present in the mix reacts with the AFm phases and may have converted C_4AH_{13} partly to carboaluminate hydrate.
At a hydration temperature of 38 °C hydrogarnet (Katoite - C_3AH_6) can be detected after 28 days and 6 month as additional hydration product (Figure 5–46). The diffractograms look quite similar to the hydration at 20 °C with the major difference that the amount of strätlingite seems to decrease from 28 days to 6 month at the cost of katoite formation. The intensities of the strätlingite peaks decrease while the peaks of katoite e.g. at 17.3 º2θ increase in intensity.

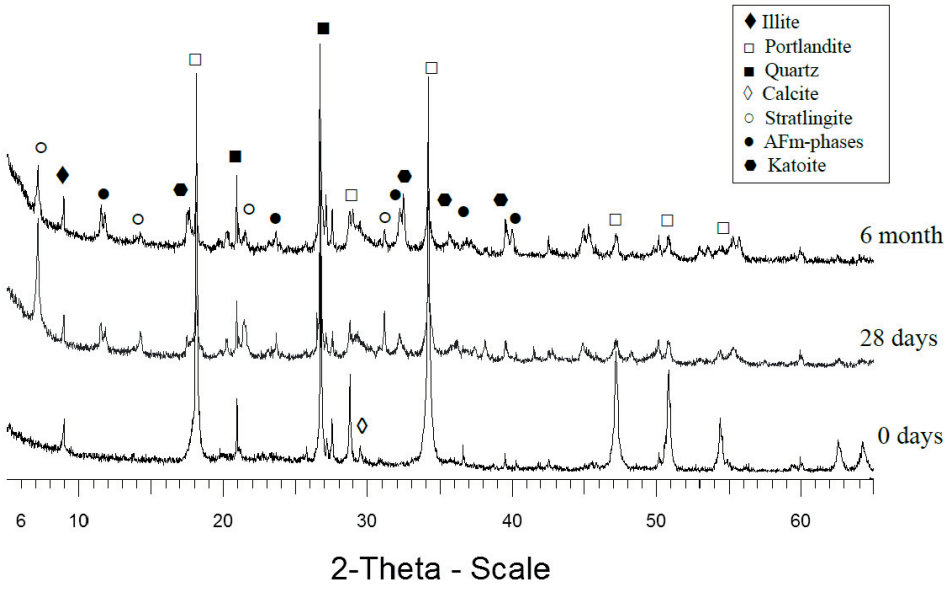

Figure 5–46: Diffractograms of calcined AB1080 clay/lime pastes mixed in a ratio of 1/1 and hydrated for 28 days and 6 month at 38 °C.

DTG confirms the results obtained by XRD. The DTG curves of the pastes hydrated for 28 days and 6 month at 20 and 38 °C are given in Figure 5–47. The unhydrated samples show only one major peak at 500 °C due to the decomposition of calcium hydroxide. The decreasing intensity of this peak after 28 days and 6 month accompanied with new signals between 100-400 °C reflects the lime consumption and formation of new hydration products from the reaction of the calcined clay with lime. It becomes clear that after 28 days further lime consumption proceeds very slowly. The hydration products exhibit 3 main peaks at 180-190 °C (C_2ASH_8) with a shoulder at 100-150 °C (C-S-H), 240 °C (C_4AH_{13}) and 340 °C (C_3AH_6). The small peaks between 700-800 °C are due to decarbonation of carboaluminate hydrates or calcite formed by eventual carbonation in contact with

the atmosphere. The mentioned hydration products were assigned to similar dehydration/dehydroxylation temperatures by several authors [194-198]. Hydration at 20 °C leads to the formation of C-S-H, C_2ASH_8 and C_4AH_{13} only, while at 38 °C a significant amount of hydrogarnet is formed already after 28 days. The decreasing amount of C_2ASH_8 and C_4AH_{13} from 28 days to 6 month with a simultaneous increase of C_3AH_6 suggests that the hydrogarnet phase is formed by a conversion reaction of strätlingite and calcium aluminate hydrate at elevated temperatures and longer curing times. The metastable nature of C_2ASH_8 and C_4AH_{13} at longer curing times and increased temperatures with a following conversion to hydrogarnet was reported before [199]. Nevertheless it was also suggested that hydrogarnet might be formed directly during the pozzolanic reaction of metakaolin and lime [195].

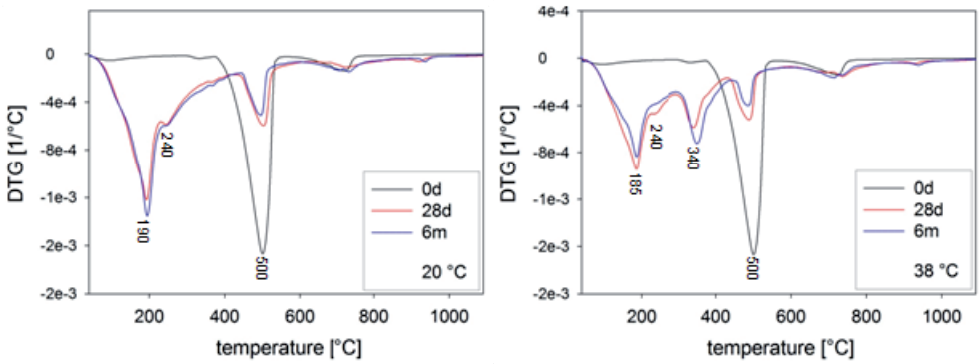

Figure 5–47: DTG curves of the unhydrated and hydrated calcined clay/lime pastes at 20 (left) and 38 °C (right)

As for the hydrated pastes with Søvind Marl ^{27}Al MAS NMR spectroscopy was additionally performed on the AB1080 clay/lime paste hydrated for 28 days at 20 °C. The ^{27}Al MAS NMR spectrum of the lime-cured sample in Figure 5–48 allows the identification of four different tetrahedral Al sites with chemical shifts at 74, 68, 61.5, and 57.2 ppm, along with a peak from penta-coordinated Al (26 ppm), and Al in octahedral coordination (10.5 ppm and 4.9 ppm). The resonances at 61.5 ppm is typical for 4-ccordinated Al in aluminosilicate anions in the interlayer of AFm phases [200]. Therefore this peak can be assigned to tetrahedrally coordinated Al in strätlingite while the resonance at 10.5 ppm probably represents the octahedrally coordinated Al ions in strätlingite [200-202]. The latter might overlap with resonances from octahedrally coordinated Al in the AFm phases C_4AH_{13} and carboaluminate hydrate [193]. Al substituted C-S-H phases can be ascribed to the resonances 74, 68 and 26 ppm. The first two represent AlO_4 tetrahedra in the chain structure of silica tetrahedra while the resonance at 26 ppm is responsible for 5

coordinated Al in the C-S-H structure [191-193, 200]. The resonances at 57 ppm and 4.9 ppm may originate from a small amount of the unreacted clay material. Thus, the major part of the clay material has reacted with lime and formed strätlingite and C-S-H. Subtraction of the spectrum for the calcined AB1080 clay from clay/lime spectrum reveals that at least 85 % of the clay material has reacted during the lime-curing process.

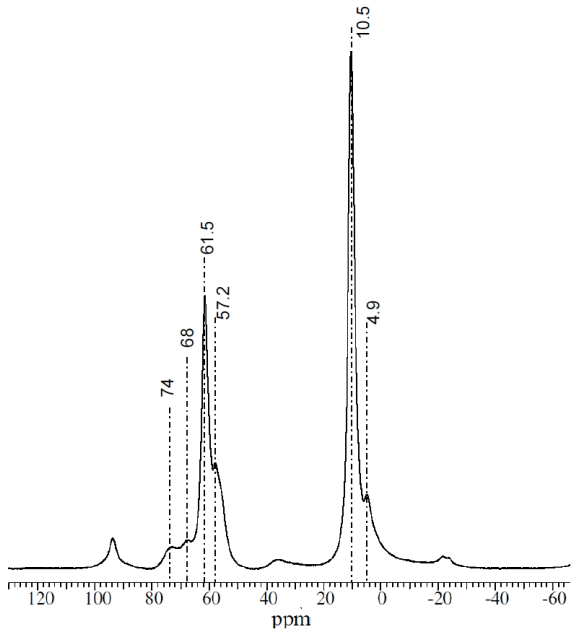

Figure 5–48: ^{27}Al MAS NMR spectrum of the AB1080 clay/lime paste hydrated for 28 days at 20 °C

The microstructure of the clay/lime pastes hydrated for 28 days at 20 °C is characterized by anhedral grains of feldspars and quartz in a matrix of finely crystalline hydration products. Figure 5–49 shows a selection of BSE images of the mentioned system. Again there are cloudy and needle like particles to find. In comparison to the microstructure of the hydrated pastes with Søvind Marl, needle like phases or cross sections of platelets are present in increased amount. These probably represent the strätlingite phase which was assigned as the main hydration product with the previous methods. The rounded edges of the feldspar and quartz grains might be a sign of a reaction/dissolution of the surfaces of these minerals in the alkaline solution. Nevertheless already in the raw clay quartz and feldspar had no sharp edges and a loss of original habitus due to the weathering process of the clay. Figure 5–49a shows a reacting metakaolin particle with quartz at its left-hand side

surrounded by hydration products. In Figure 5–49b a K-feldspar grain lies in the matrix of needles/platelets of AFm phases. On the right and left side of the picture bigger particles of C-S-H are visible. Quartz grains and a residual CH particle (left down corner) as well as an agglomeration of larger crystals of hydration products (right) are visible in Figure 5–49c. Figure 5–49d exhibits a close up to some of these clusters of the needle like phases. In point 1 these phases were analyzed with WDX and the result is given in Table 5–19. With Ca 9.3 %, Al 12.3 % and Si 7.3 % it is a calcium aluminate silicate hydrate. The shape of the crystals and the Ca/Al ratio of 0.8 might reflect the strätlingite detected with XRD, DTG and NMR. However the Ca/Si ratio of 1.3 is too small for this phase. Figure 5–49e & f show feldspar and quartz grains surrounded by hydration product. Especially in Figure 5–49f it looks like the hydration products are grown on to the feldspar grain or even that the edges of the feldspars have reacted. Moreover the needles in close proximity of the feldspar grains are larger than the needles in the matrix. This supports the suggestion earlier made that the quartz and feldspar may act as nucleation sites for early growth of hydration products thus enhancing the early and overall strength of mortars with AB1080 blended cements. On the other hand some feldpspar/quartz grains seem to have a thin reaction layer. It cannot be excluded that the surfaces of these minerals partly dissolve and that Al and Si ions react with Ca ions from CH to form hydration products. The pozzolanic activity of quartz and feldspar minerals is furthermore documented in literature [116, 203]. Nevertheless a loss in crystallinity of feldspars and quartz could not be detected by means of XRD. Tests with a local Tunisian crude kaolinitic clay and a purified sample of the same deposit (removal of secondary minerals as quartz) showed that the crude clay containing quartz achieved higher compressive strength in mortar tests than a purified (removal of quartz) clay. The increased mechanical properties of the crude clay are according to the authors attributed to both a filler and pozzolanic effect of quartz [203].

Table 5–19: composition in Atom % of Points 1-6 marked in Figure 5–49 and 5–50

WDX_No.	Ca	Al	Si	Fe	K	O
1	9.3	12.2	7.3	1.5	0.2	69.4
2	8.2	13.1	9.2	0.9	0.4	68.2
3	18.6	10.6	3.3	0.0	0.1	67.4
4	17.9	11.2	5.3	0.7	0.2	64.7
5	17.2	10.4	4.1	0.1	0.2	68.0
6	18.6	10.2	3.9	0.0	0.1	67.3

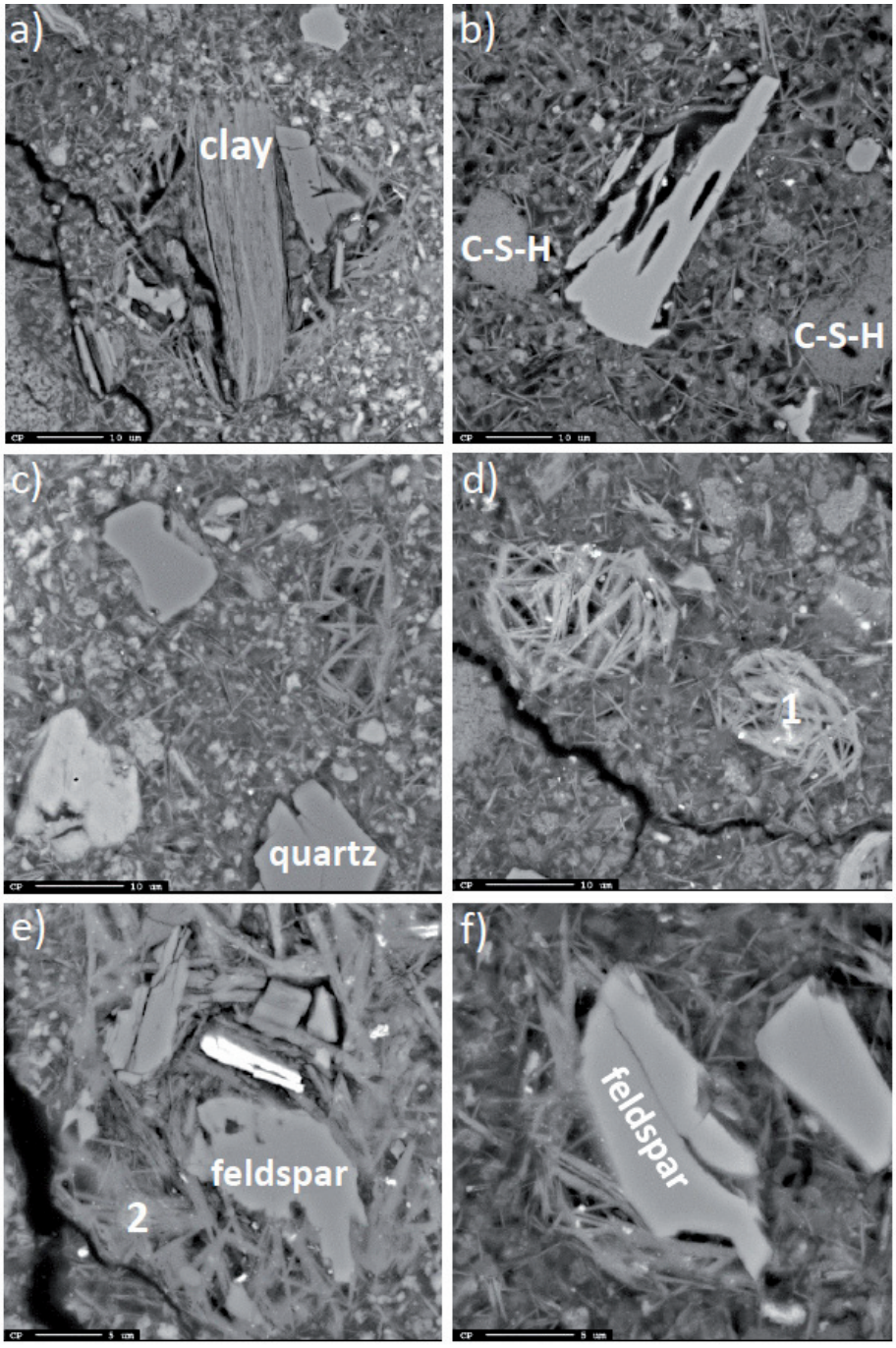

Figure 5–49: BSE images of calcined AB1080 clay/lime pastes hydrated for 28 days (a-b: 1500x, c-d: 2000x, e: 3000x, f: 4000x) at 20 °C

When hydrated at 38 °C the matrix of the clay/lime pastes appears denser compared to the hydration at 20 °C. Additionally new hydration phases are visible. The new formed phases appear all over the matrix as large clusters of dense light grey material. A selection of BSE images of the pastes hydrated for 28 days at 38 °C is given in Figure 5–50.

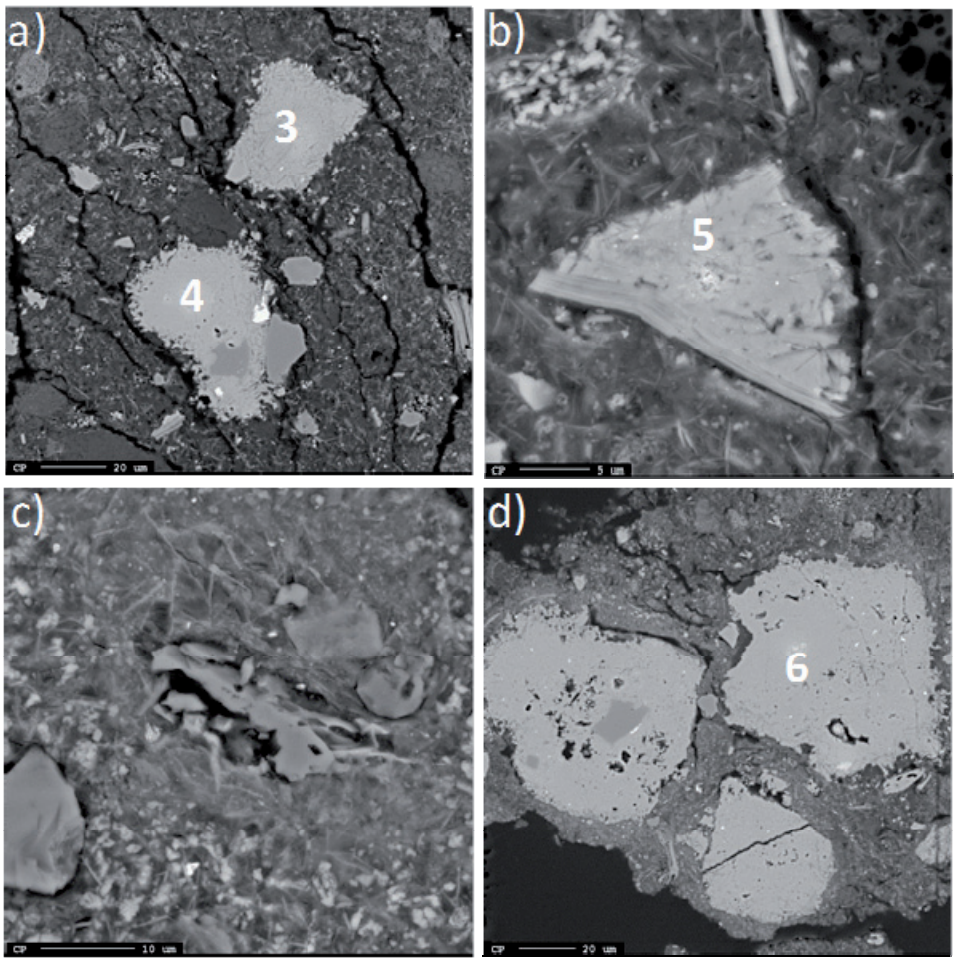

Figure 5–50: BSE images of calcined AB1080 clay/lime pastes hydrated for 28 days (a: 600x, b:3000x, c: 2000x, d: 600x) at 38 °C

The mentioned new phases were measured with WDX and are marked for example in the points 3-6. The composition of the single points is shown in Table 5–19. However the composition does not vary significantly and the average composition is Ca = 18.1 ± 0.7, Al = 10.6 ± 0.4, Si = 4.1 ± 0.8, O = 66.9 ± 1.5. The amount of Ca is considerably higher in these phases than in the hydration products measured

at 20 °C curing temperatures. The Ca/Al ratio varies from 1.8-1.6. Probably the new detected phase belongs to the hydrogarnet group with Si substitution. Hydrogarnets belong to a series of calcium aluminate garnets of the general formula $Ca_3Al_2(SiO_4)_{3-x}(OH)_{4x}$ with (OH) partially replacing silica (SiO_4). The endmembers of the hydrogarnet family (grossular, hibschite, and katoite) depend on the degree of substitution (x) [28].

grossular: $x = 0$
hibschite: $0.2 < x < 1.5$
katoite: $1.5 < x < 3$.

The measured average Al/Si ratio in points 3-6 of 4.1/10.7 = (3-x)/2 results in x = 2.2 meaning that katoite is present in the pastes hydrated at 38 °C.
In agreement with the results obtained from XRD and DTG it is imaginable that the agglomerated hydration products as visible in Figure 5–50 transform to katoite at higher curing temperatures. Figure 5–50c exhibits a fairly reacted feldspar in the centre in the very dense matrix of hydration products.

5.4.3 AB1080 with calcium carbonate

As for mortar tests, lime consumption tests were performed with AB1080 blended with calcium carbonate. 5 and 15 % of calcined AB1080 by weight were replaced with uncalcined laboratory grade calcium carbonate. The clay + calcium carbonate/lime ratio was kept at 1/1. Pastes were hydrated at 20 and 38 °C for 28 days and compared to the results obtained with the pastes containing no calcium carbonate. The results of the calcium hydroxide consumption are given in Table 5–20 and Table 5–21.

Table 5–20: Calcium hydroxide consumption in clay/lime pastes with a ratio of 1/1 cured for 28 days and 6 month at a temperature of 20 ºC with 5 and 15 % replacement of AB1080 by calcium carbonate

Clay+Calcite/lime = 1/1 (20 °C)	AB1080 (no Calcite)	AB1080 + 5% Calcite	AB1080 + 15% Calcite
CH at 0 days [%]	47.1	45.8	45.9
CH at 28 days [%]	13.9	12.7	13.5
Consumed CH [%] 0-28 days	70.5	72.3	70.6
Consumed CH per gram clay [g]	**0.63**	**0.61**	**0.60**
CH at 6 month [%]	11.7	10.5	10.0
Consumed CH [%] 0-6 month	75.1	77.1	78.1
Consumed CH per gram clay [g]	**0.67**	**0.65**	**0.66**

The values for consumed lime [g] per gram clay show no significant differences in pastes cured for 28 days and 6 month at 20 °C. 15 % replacement of calcined AB1080 by calcium carbonate has no influence on the lime consumption in the investigated pastes. This is in agreement with the strength results from mortar tests where neither a strength reduction nor an enhancement took place due to addition of calcium carbonate (Chapter 5.2.2.1). When hydrated at 38 °C the pastes containing calcium carbonate show slightly reduced lime consumption.
Nevertheless XRD analysis could demonstrate that the addition of calcium carbonate had direct influence on the type of hydration products formed during the pozzolanic reaction after 28 days. The diffractograms of the clay/lime pastes with different levels of calcite addition hydrated for 28 days at 20 °C are given in Figure 5–51.

Table 5–21: Calcium hydroxide consumption in clay/lime pastes with a ratio of 1/1 cured for 28 days and 6 month at a temperature of 38 ºC with 5 and 15 % replacement of AB1080 by calcium carbonate

Clay+Calcite/lime = 1/1 (38 °C)	AB1080 (no Calcite)	AB1080 + 5% Calcite	AB1080 + 15% Calcite
CH at 0 days [%]	47.1	45.8	45.9
CH at 28 days [%]	11.7	11.7	12.3
Consumed CH [%] 0-28 days	75.1	74.5	73.2
Consumed CH per gram clay [g]	**0.67**	**0.63**	**0.62**
CH at 6 month [%]	8.1	9.3	9.1
Consumed CH [%] 0-6 month	82.7	79.7	80.1
Consumed CH per gram clay [g]	**0.73**	**0.66**	**0.68**

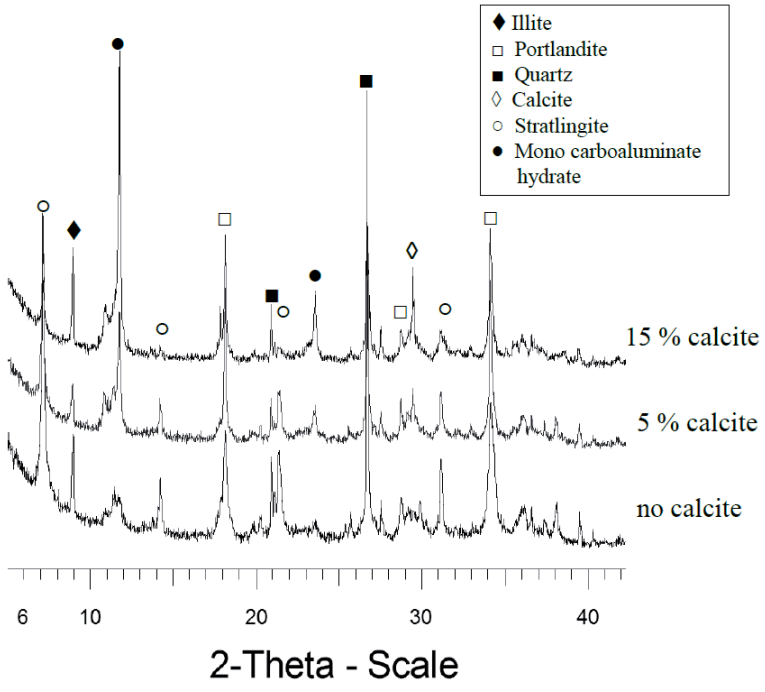

Figure 5–51: Diffractograms of the calcined clay/lime pastes hydrated for 28 days at 20 °C with 5 and 15 % replacement of AB1080 by calcium carbonate.

With increasing amount of calcium carbonate added to the pastes monocarboaluminate hydrate becomes the dominating hydration product after 28 days regarding the increasing intensities of the peaks at 11.7 and 23.5 º2θ. At the same time the intensities of the strätlingite peaks decrease. This shows either that by adding calcium carbonate the equilibrium is shifted towards the formation of carboaluminate hydrates from the very beginning or that the calcium carbonate is reacting with strätlingite leading to a transformation reaction. Hemicarboaluminate hydrate (10.8 º2θ) is formed in small amounts besides monocarboaluminate. When hydrated at 38 °C katoite could be detected as well but the diffractograms showed no significant differences in general.
Calcium carbonate participates indirectly to the pozzolanic reaction of AB1080 by changing the course of reaction and the type of hydration products formed. An additional filler effect of the mineral cannot be expected from the mortar results.

5.4.4.1 Argila Sorgila, Argila Rascoia and Gniew

The hydration products of calcined Argila Sorgila, Argila Rascoia and Gniew clay from Poland formed in combination with calcium hydroxide are similar to those observed in the Søvind Marl system. All clays contain more or less calcium carbonate as secondary minerals and therefore carboaluminate hydrates are the dominating hydration products after 28 days and 6 month. Besides that a C-S-H phase and small amounts of C_4AH_{13} and C_3AH_6 are formed. The diffractograms of calcined clay/lime pastes with Argila Sorgila and Argila Rascoia hydrated for 28 days and 6 month at 20 °C are shown in Figure 5–52. There was no difference recognizable in the diffractograms of the pastes hydrated at 38 °C regarding the phase compositions.
The intensity of the meta-smectite peak at 9 °2θ in the pastes with Argila Sorgila is decreasing with hydration time as a sign of a reaction of the clay minerals with calcium hydroxide. In comparison the intensity of the illite peaks of Rascoia barely change even after a hydration time of 6 month. Monocarboaluminate hydrate is the dominating hydration product with Argila Sorgila exhibiting a sharp peak at 11.7 °2θ. As with the Søvind Marl the small calcite peak at 29.4 °2θ looses crystallinity with hydration time as a reaction of calcium carbonate with the AFm phases. With Argila Rascoia small reflections at 10.8 and 11.3 are detectable after 28 days besides monocarboaluminate. These peaks can be assigned to either hemicarboaluminate hydrate or C_4AH_{13} and probably some Fe-substituted carboaluminate hydrate due to the almost 10 % iron oxide in the raw clay.

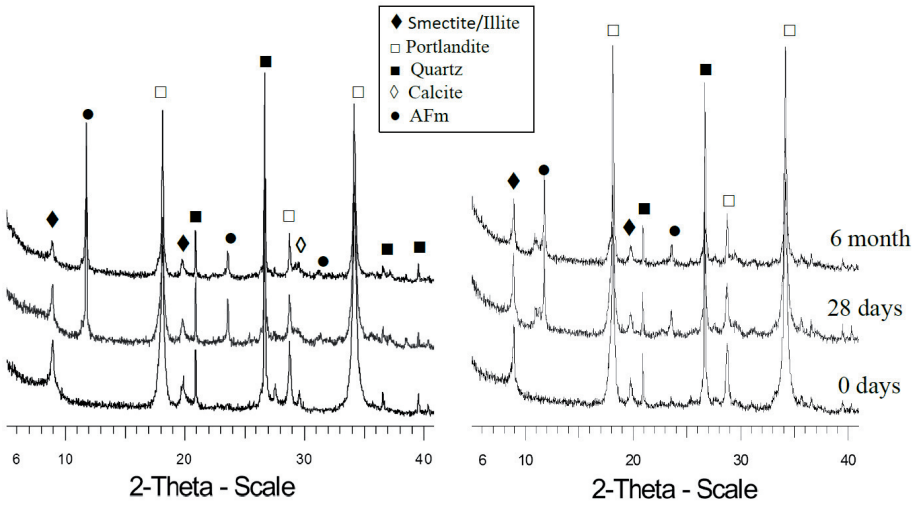

Figure 5–52: Diffractograms of calcined clay/lime pastes with Argila Sorgila (left) and Argila Rascoia (right) hydrated for 28 days and 6 month at 20 °C

With DTG C-S-H and small amounts of hydrogarnet could be found as well in both systems. The DTG curves of the calcined clay/lime pastes with Argila Sorgila and Argila Rascoia are given in Figure 5–53 and 5–54 respectively. In both cases there is no clear difference between the different hydration temperatures to notice. However a small acceleration in the system with Argila Sorgila might occur when hydrated at 38 °C. At 20 °C hydration temperature the amount of AFm phases (decomposition at 180 °C) increases slightly from 28 days to 6 month while at 38 °C no further formation can be observed. Here it seems a maximum of carboaluminate hydrate formation is already reached after 28 days although lime consumption still proceeds as visible in the decreasing intensity of the decomposition peak at 500 °C.

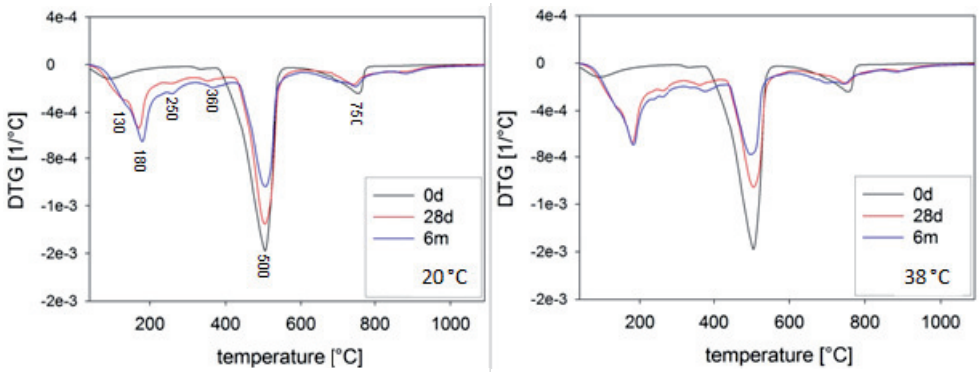

Figure 5–53: DTG curves of the calcined clay/lime pastes with Argila Sorgila hydrated for 28 days and 6 month at 20 °C (left) and 38 °C (right)

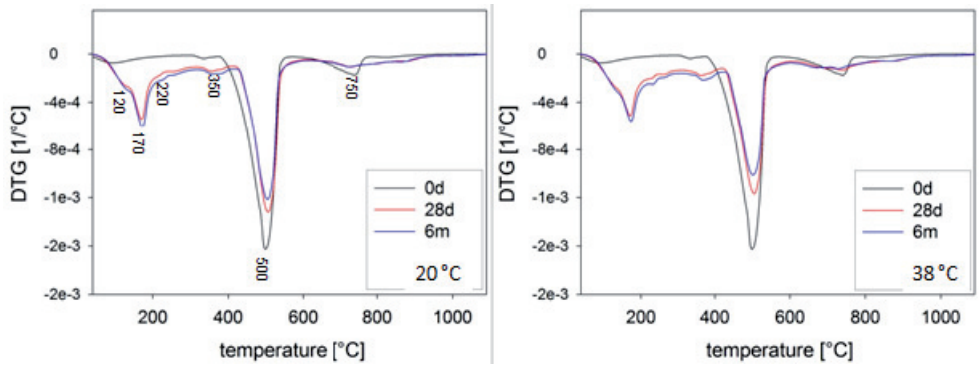

Figure 5–54: DTG curves of the calcined clay/lime pastes with Argila Rascoia hydrated for 28 days and 6 month at 20 °C (left) and 38 °C (right)

In general there are 4 signals observable in both systems that can be assigned to 4 different hydration products. 120-130 °C reflects the C-S-H phase, 170-180°C belongs to the carboaluminate hydrate, 220-250 is for C_4AH_{13} and 350-360 can be assigned to C_3AH_6. The lime consumption can be seen at the decreasing intensities of decomposition peaks at 500 °C. At 750 °C the unhydrated samples show another endothermic signal that is attributed to the decomposition of the small amounts of calcite present in the raw clay.

Due to the high calcite content of 15 % in the Gniew raw clay the hydration products formed in pastes with lime after 28 days are not expected to be different from those formed with the Søvind Marl as well as Argila Sorgila and Rascoia. Indeed the main hydration product after 28 days and 6 month for a hydration temperature of 20 and 38 °C is monocarboaluminate hydrate (Figure 5–55). Other crystalline hydration phases than carboaluminate hydrates could not be clearly identified with XRD. The direct formation of monocarboaluminate hydrate could indicate that the pozzolanic activity of illite is increased in the presence of calcium carbonate. Since illite itself has a rather stable mineral structure upon calcination and does not belong to a mineral group with large variations in the chemical composition like smectite, we can assume that the illite from Argila Rascoia and Gniew originally has the same reactivity. In this case both illites should have about the lime consumption. If the increased lime consumption of calcined Gniew compared to calcined Argila Rascoia would derive only from an additional reaction of a higher amount of uncomposed calcium carbonate with already formed calcium aluminate hydrates more hemicarboaluminate hydrate should be formed. The direct formation of monocarboaluminate reflects a pozzolanic reaction. This could indicate an increased pozzolanic activity of illite. However with XRD and other methods (DTG, FT-IR) it could be shown that most of the calcium carbonate is decomposed. Fur-

thermore we could observe under the SEM that the clay matrix is partly melting up. The clay minerals are forming a vitreous phase together with the decomposing calcite in the calcined state similar as it was observed for the Søvind Marl. The formation of an amorphous phase was also detected with FT-IR spectroscopy. Therefore it is more likely that this new amorphous phase is responsible for the higher lime consumption in the Gniew clay.

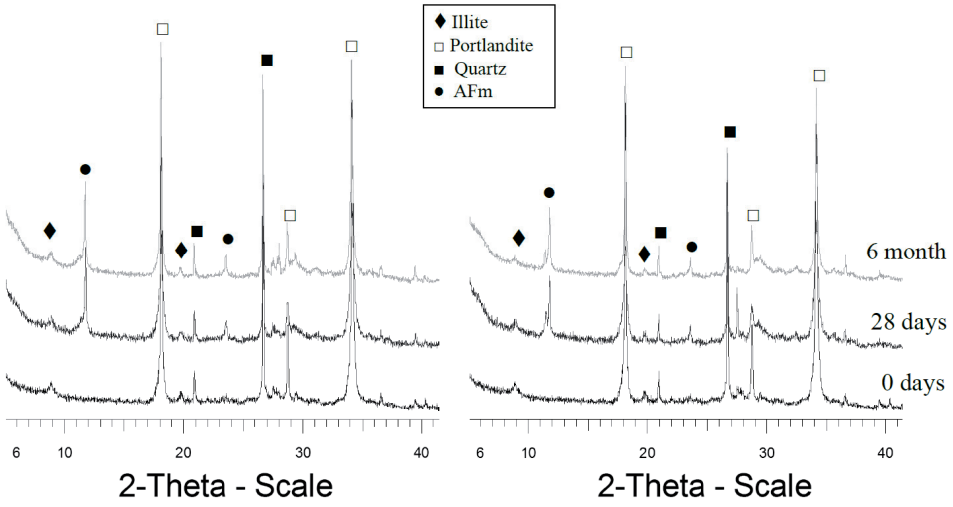

Figure 5–55: Diffractograms of calcined clay/lime pastes with Gniew hydrated for 28 days and 6 month at 20 °C (left) and 38 °C (right)

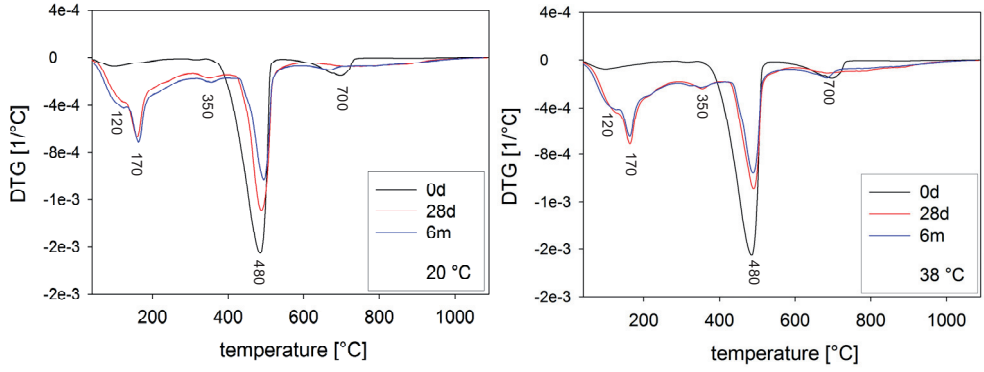

Figure 5–56: DTG curves of calcined clay/lime pastes with Gniew hydrated for 28 days and 6 month at 20 °C (left) and 38 °C (right)

However DTG (Figure 5–56) revealed the presence of a C-S-H phase and small amounts of hydrogarnet on the basis of two peaks at 120 and 350 °C respectively. The decomposition peak at 170 °C can be assigned as before to the carboaluminate hydrate. Hydrogarnet formation does not seem to be favored at a higher hydration

temperature of 38 °C in calcined clay/lime pastes with Gniew, Argila Sorgila and Rascoia. Transformation of the carboaluminate hydrates to hydrogarnet with higher temperature and longer curing times cannot be definitely assessed as it was the case for strätlingite in the system with the AB1080 clay.

5.4.3 Hydration of Cement pastes with Calcined Clays

Pastes of cement blended with the two most reactive clays (Søvind Marl & AB1080) were prepared to check if the hydration products formed in the reduced system with only calcium hydroxide differ from those formed in cement pastes.
Dry powder of OPC with 20, 35 and 50 % of calcined clay/marl by weight were homogenized before mixing with deionized water. The water to binder ratio was 0.5 and the pastes were hydrated for 28 days and 6 month at 20 and 38 °C.
The results show that the hydration products formed during the pozzolanic reaction of calcined clays in the cement pastes are the same as from the pozzolanic reaction of clay and lime only. Due to sulfate contained in the cement, ettringite is formed additionally. Figure 5–57 shows the diffractograms of OPC and the cement pastes blended with 20, 35 and 50 % calcined Søvind Marl hydrated for 28 days at 20 and 38 °C.

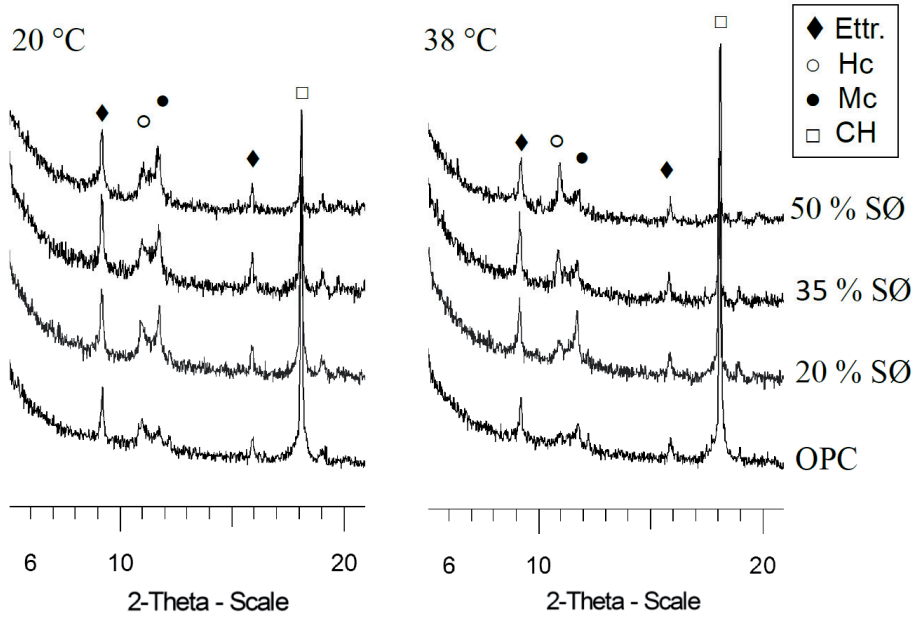

Figure 5–57 : Diffractograms of OPC and the cement/marl pastes containing 20, 35 and 50 % calcined marl hydrated for 28 days at 20 (left) and 38 °C (right). (Ettr = Ettringite, Hc = Hemi-carboaluminate hydrate, Mc = Mono-carboaluminate hydrate, CH = calcium hydroxide)

Crystalline hydration products of OPC hydrated for 28 days are mainly ettringite and CH besides small amounts of AFm phases (carboaluminate hydrates). With increasing amount of calcined marl in the pastes the amount of AFm phases formed

after 28 days increases. Due to the pozzolanic reaction the CH content decreases as the amount of carboaluminate hydrates increases.
A transformation of ettringite to monosulfate phases could not be detected. The favored formation of carboaluminate hydrates as the result of the high calcite content in the Søvind Marl seems to stabilize ettringite. Monosulfate phases may react with calcium carbonate to form further carboaluminate hydrates. Thus released sulfate ions are available even at long curing times to form ettringite [204-205].
The consequently overall higher amount of hydration products in pastes blended with calcined marl and the higher water binding by ettringite explain the higher compressive strength of mortars were 20 % of OPC are replaced by calcined marl.
After 6 month of hydration the only significant difference in the diffractograms was an increased background curve reflecting a higher amount of X-Ray amorphous C-S-H and C-A-S-H phases formed.
In Figure 5–58 the diffractograms of OPC and the cement/clay (AB1080) pastes containing 20, 35 and 50 % calcined clay hydrated for 28 days at 20 and 38 °C are given. Similar effects as for the pastes with Søvind Marl are observable in this system.

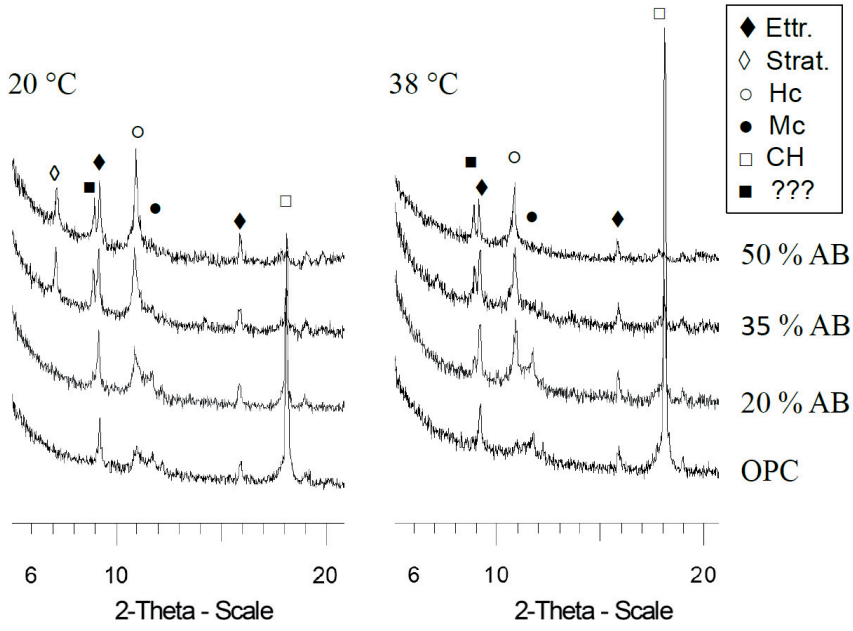

Figure 5–58: Diffractograms of OPC and the cement/clay (AB1080) pastes containing 20, 35 and 50 % calcined clay hydrated for 28 days at 20 (left) and 38 °C (right). (Ettr = Ettringite, Strat = Strätlingite, Hc = Hemi-carboaluminate hydrate, Mc = Mono-carboaluminate hydrate, CH = calcium hydroxide)

The hydration products produced of cement blended with calcined AB1080 clay are ettringite, carboaluminate hydrates and strätlingite. Strätlingite was first formed

in the paste containing 35 % calcined clay. Earlier investigations showed that at least 30 % of OPC have to be replaced by metakaolin to form crystalline strätlingite [61]. The amount of carboaluminate hydrate increases with increasing clay level in the pastes. It should be noted that the peak of Hc around 10.8 °2θ overlaps with C_4AH_{13} peak which also is a possible hydration product from the pozzolanic reaction of calcined clay and CH. Nevertheless the used cement contains about 3 % limestone and therefore the formation of carboaluminate hydrates is more likely. With 50 % calcined clay almost all calcium hydroxide is consumed after 28 days. Moreover with increasing clay content a new peak at 8.9 °2θ, to the left side of ettringite, appears. The peak might reflect a zeolite phase called Gismondine with the formula $CaAl_2Si_2O_8 \cdot 4H_2O$. This phase is described as an alteration product of feldspars which would support the thesis of feldspars taking actively part in the pozzolanic reaction. On the other hand the peak could also simply reflect the illite in AB1080. The mineral structure is not much affected by the heat treatment and becomes more and more visible with increasing clay content in the pastes. However the peak intensities do not increase proportionate from 20 to 35 % cement replacement. In contrast to the clay/lime pastes strätlingite could not be detected in the cement pastes hydrated at 38 °C. In the cement system strätlingite does not appear as a crystalline phase at the elevated hydration temperature. The different hydration behavior of metakaolin/lime pastes and metakaolin blended cements was reported before. Strätlingite was found to be the only hydration product from the pozzolanic reaction at a hydration temperature of 60 °C and 34 days of curing in metakaolin blended cements by the use of thermal analysis. Nevertheless, it was concluded that the strätlingite formed is of low crystallinity as it showed no XRD reflections [206]. In our investigations strätlingite was also detected with DTG to be present at 38 °C of hydration. A small peak at 17.3 °2θ (left of the main CH peak) in the diffractogram of the paste with 50 % AB1080 indicates the presence of small amounts of hydrogarnet (katoite).

The DTG curves of the cement pastes with Søvind Marl and AB1080 hydrated for 28 days at 20 °C are shown in Figure 5–59. Both systems show four major peaks at 130, 190, 490 & 700-800 °C. These peaks can be assigned to ettringite and C-S-H (130 °C), AFm-phases (190 °C), the decomposition of calcium hydroxide (500 °C) and the decarbonation from carboaluminate hydrates and calcite (700-800 °C). Both systems show furthermore a small peak around 370 °C reflecting the presence of hydrogarnet. It can be seen that the amount of AFm phases increases with increasing clay content in the pastes while the ettringite formation is rather stable. The CH content is significantly reduced after 28 days when calcined clays are mixed with cement and with 50 % AB1080 there is almost no CH left in the paste after 28 days of hydration.

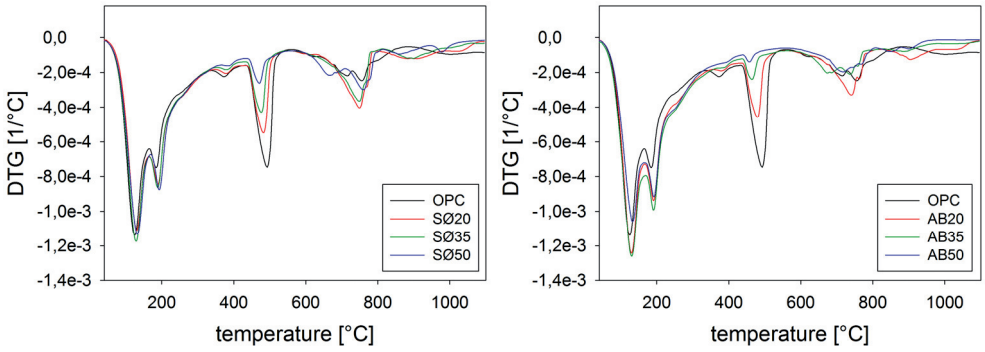

Figure 5–59: DTG curves of cement pastes containing 20, 35 and 50 % Søvind Marl (left) and AB1080 (right) hydrated for 28 days at 20 °C.

A small shoulder around 250 °C in the cement pastes blended with AB1080 can be assigned to C_4AH_{13}. The DTG curves of the cement pastes hydrated at 38 °C did not show any significant difference regarding the peak positions and the formed hydration products (Graphs are given in the appendix). The amount of CH in the paste after 28 days was calculated for the different pastes and is graphically presented in Figure 5–60.

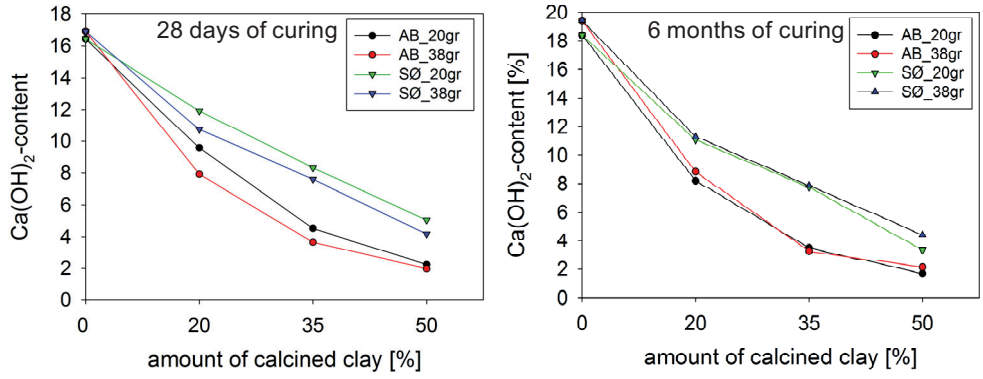

Figure 5–60: Amount of CH in cement pastes after 28 days (left) and 6 months (right) of hydration in dependence of the amount of calcined clay in the unhydrated cement paste.

Pure OPC (0 % calcined clay) produces between 16-17 % CH after hydration for 28 days at 20 and 38 °C. By replacing OPC with calcined clay the total CH content in the paste after 28 days is increasingly reduced the higher the replacement level. Both clays consumed more CH at the higher hydration temperature of 38 °C. Furthermore it is shown that AB1080 consumes significantly more CH in the cement paste than the Søvind Marl. With 50 % AB1080 only about 2 % CH are left in the paste after 28 days at 20 °C compared to about 5 % CH with the Søvind

Marl. Curing for 6 month did not lead to any significant further reduction in the overall CH content of the hardened paste. This confirms again that the main lime consumption takes place during the first 28 days in the cement pastes as it was stated before for the calcined clay/lime pastes. After 6 month of hydration the temperature dependency on the lime consumption is less pronounced.

BSE images of the cement pastes blended with the Søvind Marl and AB1080 clay were taken and in some points WDX measurements were performed to confirm the hydration products found with XRD and DTG and to get a better idea of substitutions in these phases. Figure 5–61 to Figure 5–63 show BSE images of the cement pastes blended with 20, 35 and 50 % calcined Søvind Marl after hydration for 28 days at 20 °C. BSE images of AB1080 blended cements hydrated under the same conditions are given in Figure 5–64 to Figure 5–66. The WDX compositions measured and marked with the numbers 1-8 are presented in Table 5–22. The microstructure of all pastes appears very dense showing some larger grains of quartz and feldspars deriving from the clays as well as grains of more or less hydrated clinker phases from the cement in a matrix of finer crystalline hydration products. The higher the clay content in the pastes the less CH could be found under the SEM. CH is easily recognizable by the light grey color and the shape in the microstructure (Figure 5–61). The long needles clearly visible in Figure 5–61 can probably be assigned to ettringite from the cement hydration. In voids of the matrix crystalline Ca-Al hydrates could be detected with a size large enough to be measured by WDX. Points 1-3 in Table 5–22 show the composition of these Ca-Al-hydrate phases measured in Figure 5–62 & 5–63. The Ca/Al ratio varies from 1.9 in point 1 to 2.8 in point 3. Point 1 & 2 represent AFm phases with iron and silicon substitution in the structure, while point 3 could be Fe-substituted ettringite. In the pastes with AB1080 strätlingite was the main hydration product to be detected. At higher replacement levels (Figure 5–66) cross sections of the strätlingite platelets were found all over the matrix. In the cement pastes blended with 20 % AB1080 strätlingite could be found in voids but seemed to be less crystalline (Figure 5–64) which is in agreement with XRD and DTG as observed before. The average composition of Points 4, 6, 7 & 8 is Ca = 11.9, Al = 9.9 and Si = 5.9. With a Ca/Al ratio of 1.2 and a Ca/Si ratio of 2.0 these points clearly can be assigned to strätlingite.

Table 5–22: WDX composition in Atom % of Points 1-8 marked in Figure 5–61 to 5–66

WDX_No.	Ca	Al	Si	Fe	K	O
1	16.9	9.1	0.8	1.5	0.1	71.1
2	16.7	6.9	2.8	0.5	0.3	72.2
3	16.1	5.8	0.9	1.6	0.0	75.2
4	12.9	9.4	5.3	0.8	0.3	70.8
5	16.5	8.9	1.1	0.5	0.1	72.1
6	11.3	9.4	5.9	0.6	0.2	72.5
7	11.5	10.1	6.7	0.5	0.2	70.9
8	11.7	10.6	5.5	0.5	0.1	71.4

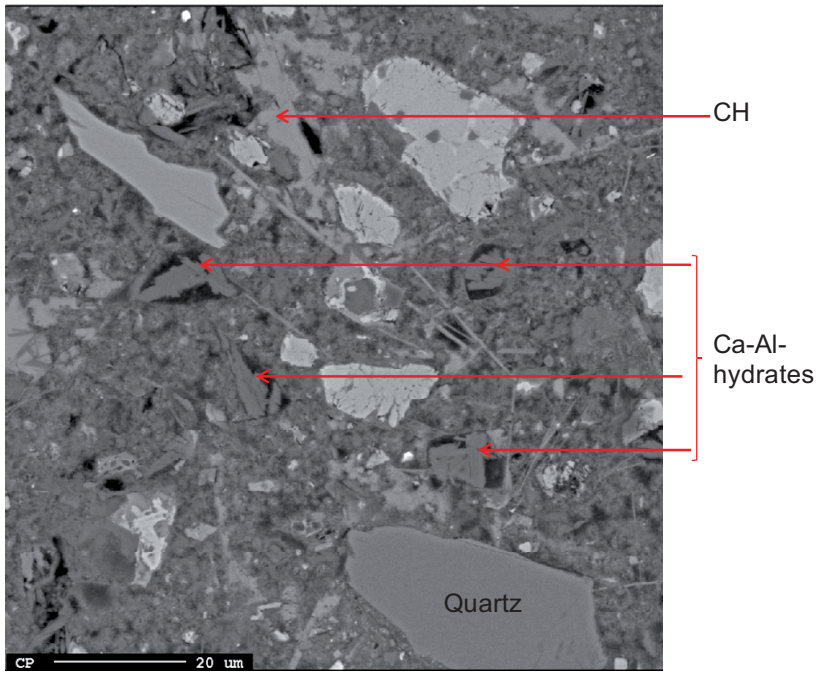

Figure 5–61: BSE image of cement paste with 20 % Søvind Marl, hydrated for 28 days at 20 °C (Mag.: 1000x)

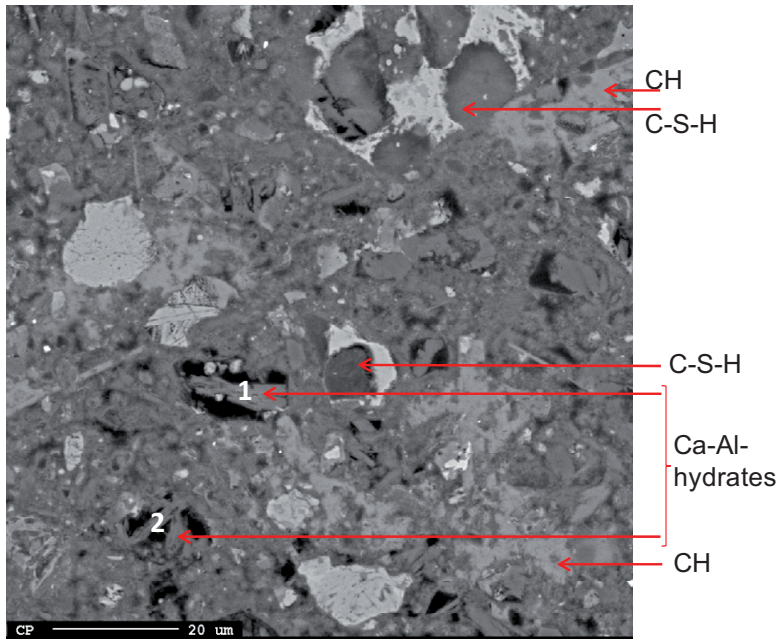

Figure 5–62: BSE image of cement paste with 35 % Søvind Marl, hydrated for 28 days at 20 ° (Mag.: 1000x)

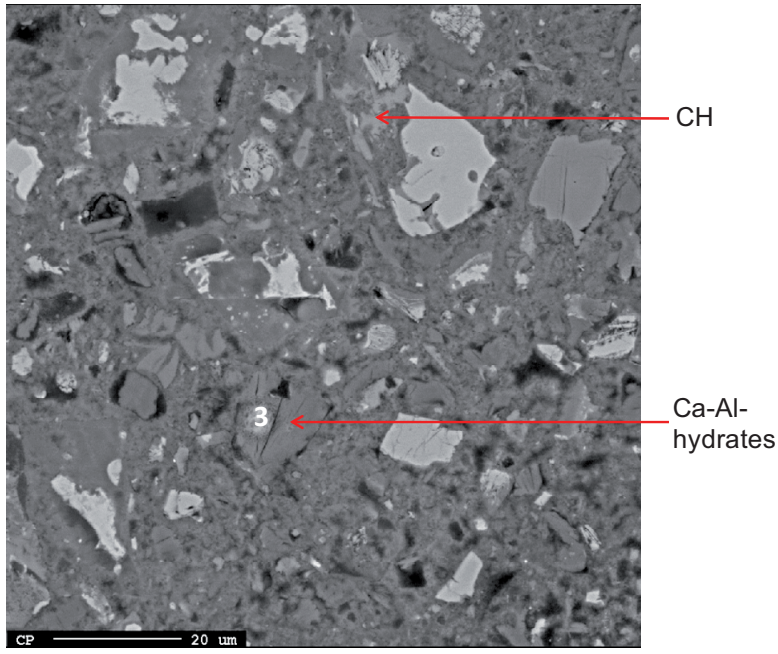

Figure 5–63: BSE image of cement paste with 50 % Søvind Marl, hydrated for 28 days at 20 °C (Mag.: 1000x)

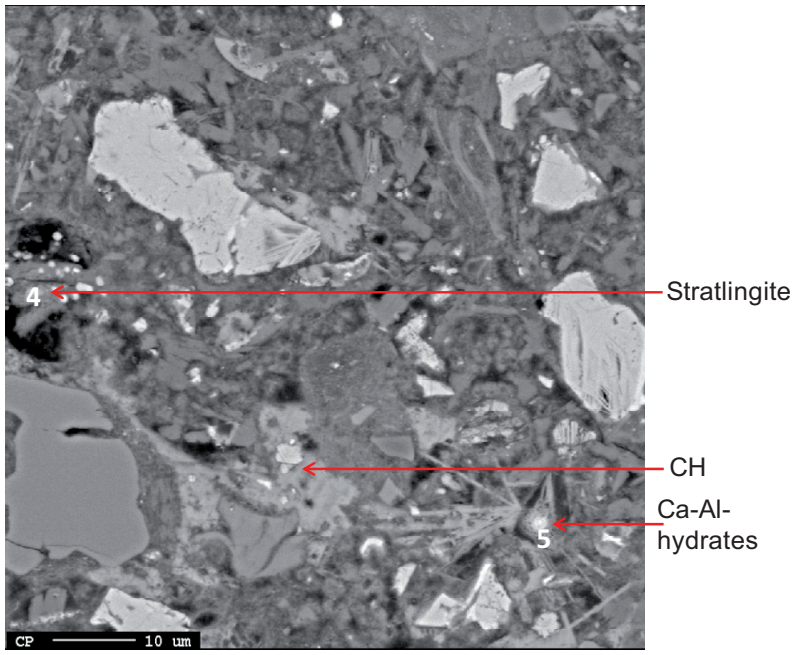

Figure 5–64: BSE image of cement paste containing 20 % AB1080, hydrated for 28 days at 20 °C (Mag.: 1300x)

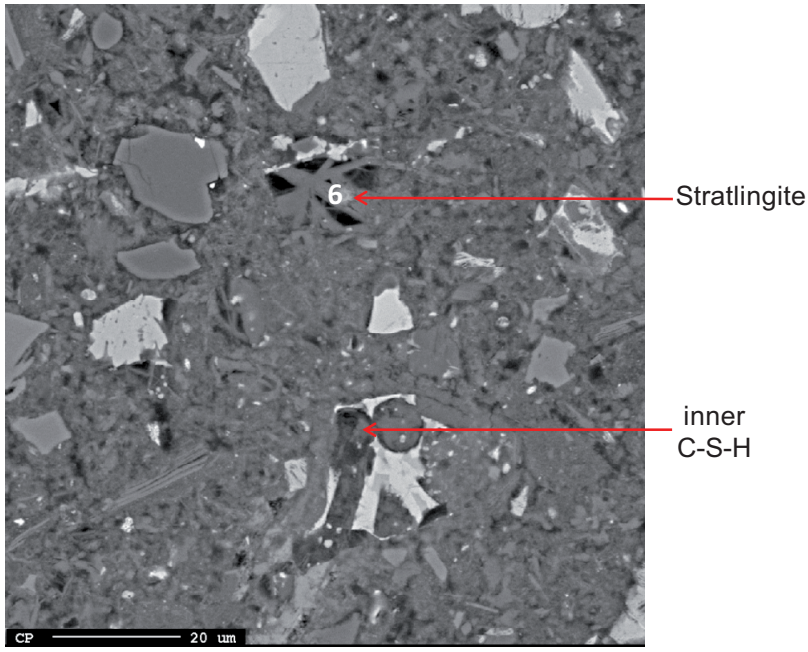

Figure 5–65: BSE image of cement paste containing 35 % AB1080, hydrated for 28 days at 20 °C (Mag.: 1000x)

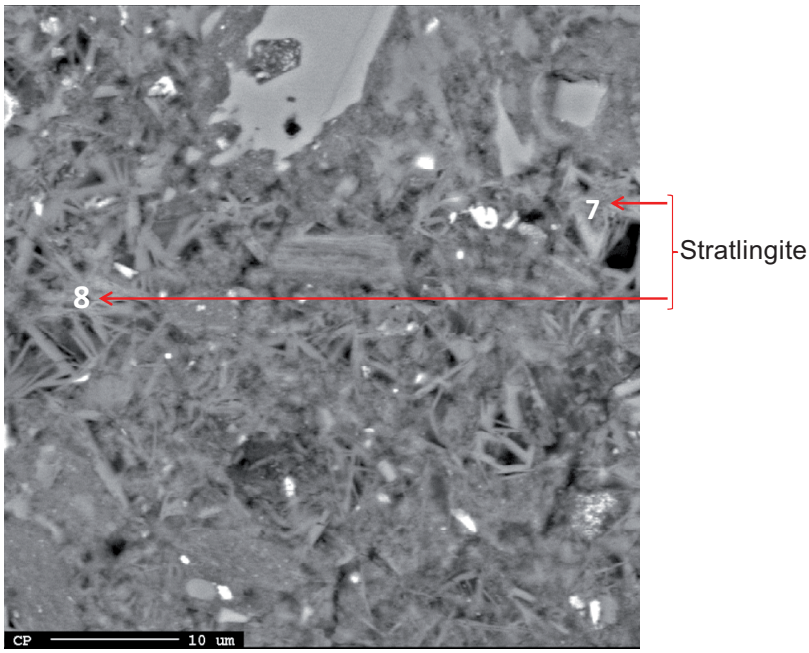

Figure 5–66: BSE image of cement paste containing 50 % AB1080, hydrated for 28 days at 20 °C (Mag.: 2000x)

5.4.4 Early Hydration of cement/clay pastes

Early hydration of cement pastes blended with different amounts of Søvind Marl and AB1080, especially in the first 24 h, was followed with isothermal calorimetry and in-situ XRD.

The heat flow curves and cumulative heat development up to 90 hours of the cement pastes blended with Søvind Marl and AB1080 are plotted in Figure 5–67 and Figure 5–68 respectively.

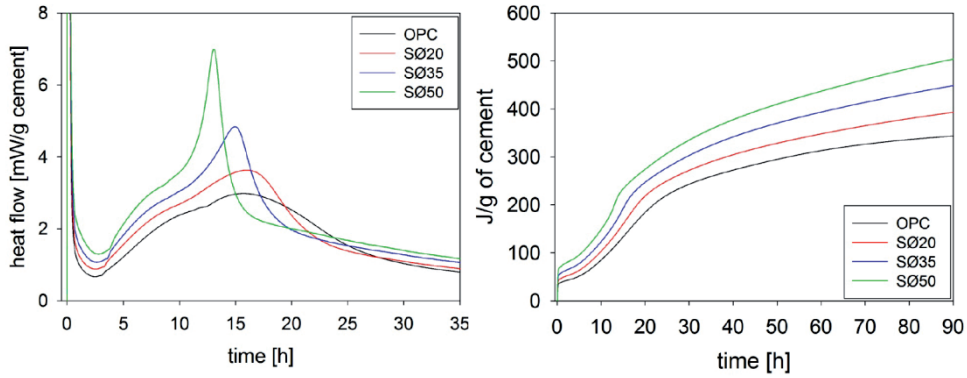

Figure 5–67: Heat flow (left) and cumulative heat (right) of hydrated OPC and cement blended with 20, 35 and 50 % calcined Søvind Marl

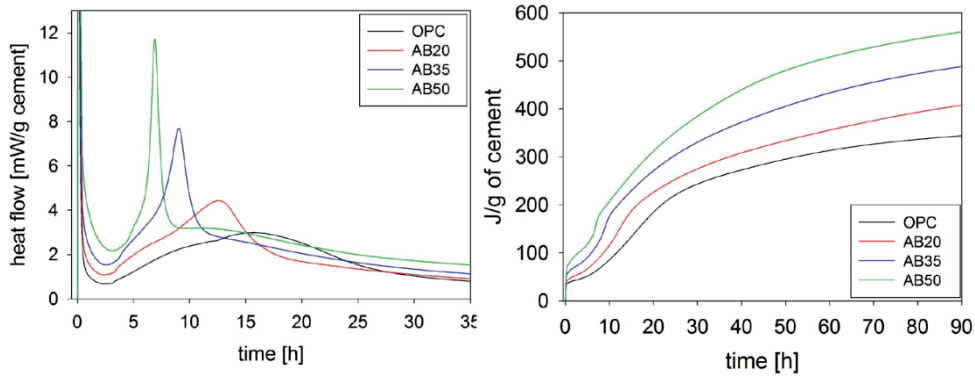

Figure 5–68: Heat flow (left) and cumulative heat (right) of hydrated OPC and cement blended with 20, 35 and 50 % calcined AB1080

The initial peak appearing after a few minutes is due to exothermic wetting accompanied with early hydration of C_3A forming ettringite and a gelatinous coating around the clinker phases. After the induction period which ends between 3-4 hours two additional exothermic peaks appear in the hydration of OPC. The first maximum is around 9-10 hours and attributed to the formation of C-S-H and

CH due to hydration reaction of the C_3S and C_2S. The second maximum in OPC hydration is at 15.3 hours and assigned to a combination of renewed ettringite formation and the conversion of AFt to AFm phases [77]. When blended with the calcined marl or clay the two maxima in the acceleration period become more distinctive and shift to earlier ages the higher the amount of calcined clay/marl in the pastes. This comes especially into effect for the pastes blended with AB1080. The times of appearance of the second maxima in the acceleration period for the different cement pastes are given in Table 5–23.

Table 5–23: Times of maximum heat flow (read out from isothermal calorimetry) in cement pastes blended with 20, 35 and 50 % calcined Søvind Marl and calcined AB1080

OPC + Søvind Marl		OPC + AB1080	
	t_{max} [h]		t_{max} [h]
OPC	15.3	**OPC**	15.3
SØ20	16.5	**AB20**	12.5
SØ35	15.1	**AB35**	9.3
SØ50	13.8	**AB50**	7.3

Moreover the time span between the two maxima in the acceleration period becomes smaller and in the cement paste blended with 50 % AB1080 the first maximum appears only as a shoulder for the second maximum. A change in the heat of hydration similar to our results was observed by other authors for cements blended with metakaolin or silica fume as well [207-209]. The change in the course of hydration is explained to be representative for an under-sulfated and C_3S depleted system. The additional reactive alumina brought into the system by the calcined clays promotes the reaction of C_3A and probably the ettringite formation as the initial heat of hydration is increased with increasing level of OPC replacement. It was stated before that the higher heat in the induction period for the blended cements as we can observe it is also associated with more ettringite formation [209]. Additionally the system is very fast depleted in sulfate ions resulting in an earlier formation of AFm phases. The induction period however is not shortened for the calcined clay blended cements, meaning that the initial setting is not accelerated.

In-situ XRD was performed on the same systems to get a better idea of early phase formations especially with regard to assumed AFm phase development. The in-situ plots that will be presented are so called level plots showing a 2D-view of the phase development over time. Different colors stand for different intensities showing decreasing or increasing peak intensities and thus directly the dissolution

or formation of new phases with time. The results of the phase development obtained with this method can be coupled to the heat flow curves of the isothermal calorimetry linking the appearance of exothermic peaks to the times of the phase formation in the XRD plots. Figure 5–69 shows the in-situ XRD plot of the reference OPC hydrated for 22 h at 20 °C. Partly dissolution of the clinker grains C_3S/C_2S and C_3A is visible in the decreasing intensities in the range between 29-42 °2θ.

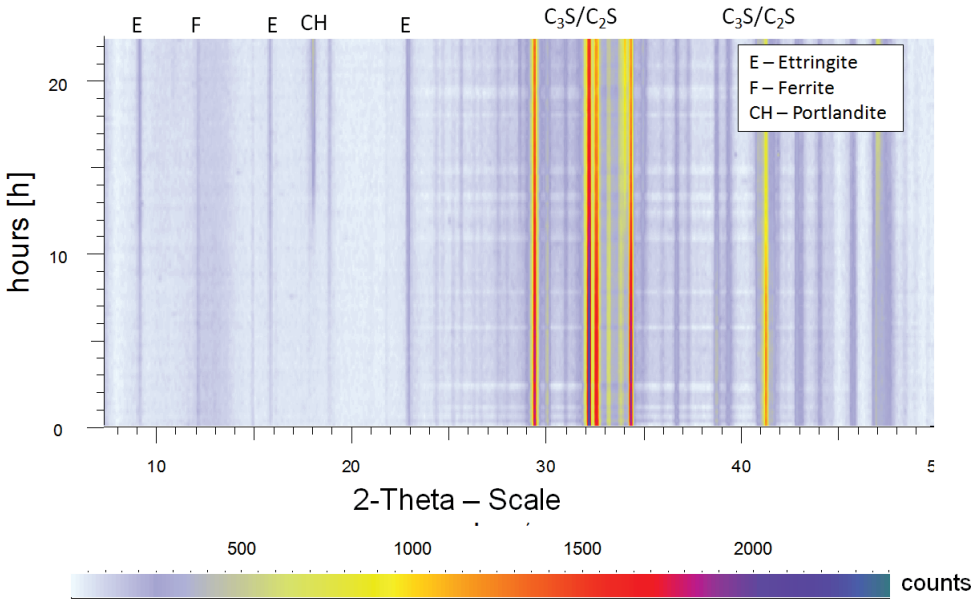

Figure 5–69: in-situ XRD Levelplot of the OPC hydration at 20 °C during the first 22 h

Continuous ettringite formation can be observed at 9.1, 15.7 and 22.9 °2θ from the first minutes. After about 11 h the formation of crystalline CH begins. This time correlates with the point of inflection between first and second maximum in the acceleration period of OPC hydration when the solution is oversaturated in Ca^{2+} ions, precipitating CH.

Figure 5–70 shows a section of the in-situ XRD Levelplot of cement blended with 20 % AB1080 hydrated at 20 °C for 24 h coupled to the heat flow of the same system.

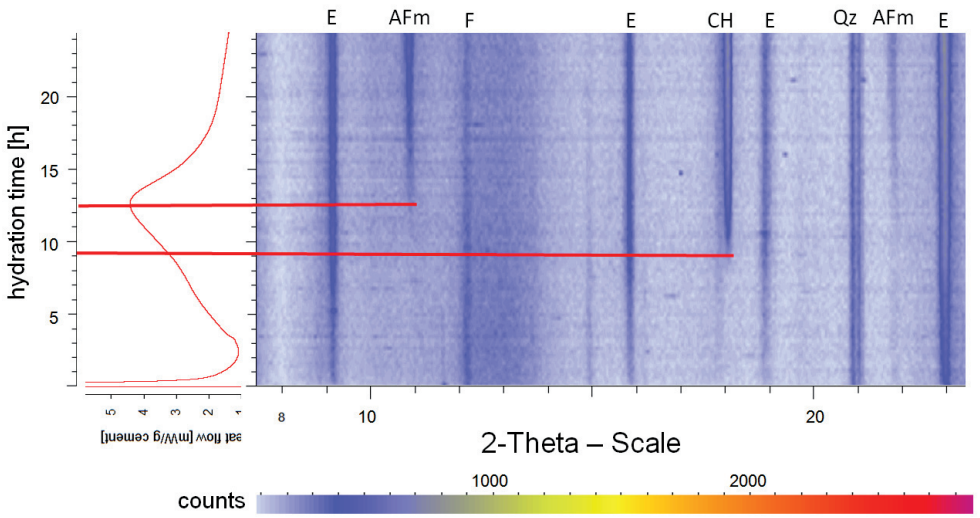

Figure 5–70: Section of the in-situ XRD Levelplot of cement blended with 20 % AB1080 hydrated at 20 °C for 24 h coupled to the heat flow of the same system

At 10.8 °2θ the formation of AFm phases is detectable from about 12.5 hours. In the pure OPC systems the formation of AFm phase could not be detected during the first 24 hours of hydration. The time of the formation of the AFm phase fits perfectly to the second peak maxima in the acceleration period of the isothermal calorimetry. Precipitation of CH takes place about 2 h earlier than in the pure cement system and again fits to the deflection point between first and second maximum.

Sections of the in-situ XRD Levelplots of cement pastes blended with 20, 35 and 50 % AB1080 hydrated at 20 °C for 24 h with special emphasis on the AFm phase formation are given in Figure 5–71. It can be seen that the AFm formation starts earlier, the higher the amount of calcined clay in the cement paste. The times of first clear detection of AFm with XRD, ~ 9 h for 35 % AB and ~7 h for 50 % AB are in agreement with the times of appearance of the second maxima in the acceleration period of the heat flow as given in Table 5–23.

Looking again at the heat flow curve of the cement blended with 50 % AB1080 (Figure 5–68) another small exothermic heat maximum can be observed at around 12-13 h of hydration after the AFm phase formation. At this high replacement levels it is possible that the reaction of the aluminates occurs before the main silicate reaction. With in-situ XRD a significant precipitation of CH could not be detected before the AFm phase formation confirming this theory (Figure 5–72).

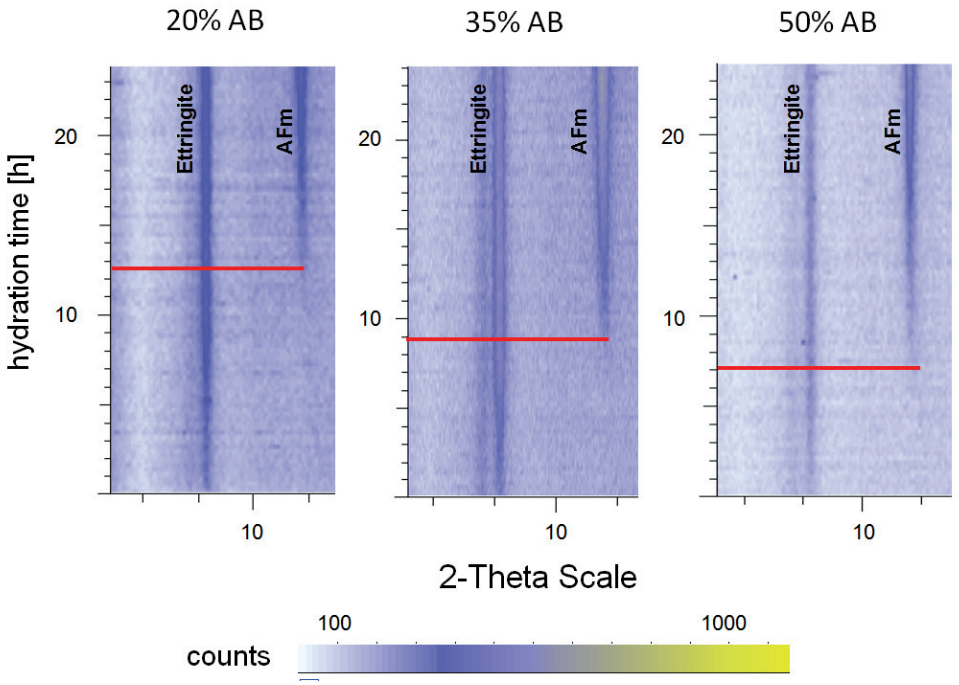

Figure 5-71: Sections of the in-situ XRD Levelplot of cement blended with 20, 35 and 50 % AB1080 hydrated at 20 °C for 24 h.

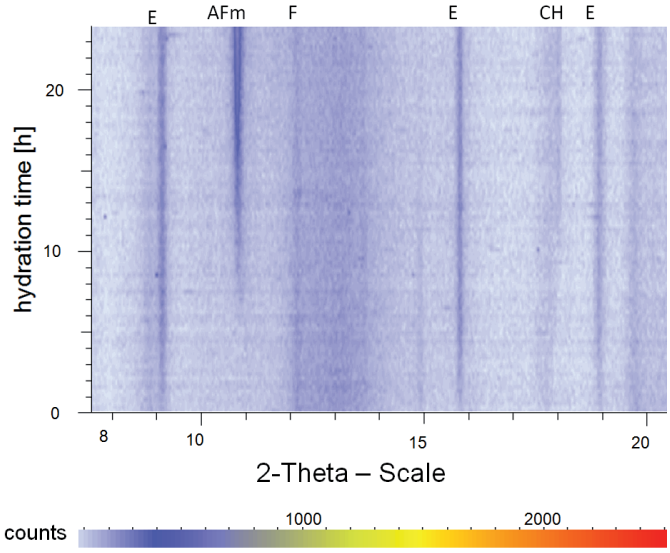

Figure 5–72: Section of the in-situ XRD Levelplot of cement blended with 50 % AB1080 hydrated at 20 °C for 24 h.

Up to 35 % replacement of OPC it seems the silicate and aluminate reaction is accelerated. Above this level of replacement the silicate reaction might be retarded again and proceed slowly over a longer period of time after the aluminate reaction.

Cement pastes blended with Søvind Marl showed similar behavior as the pastes blended with AB1080. As an example a section of the levelplot of the paste containing 35 % Søvind Marl hydrated at 20 °C for 24 h coupled to the heat flow of the same system is given in Figure 5–73.
Again the main precipitation of AFm phases is directly associated to the maximum exothermic heat peak obtained with calorimetry around 15 h of hydration. Additionally the formation of CH takes place around 11 h at the deflection point between first and second maximum in the acceleration period. Søvind Marl contains less reactive alumina than AB1080, accelerating the aluminate reaction only significantly at a replacement level of 50 %. The silicate reaction takes in all cases place before the AFm phase formation.

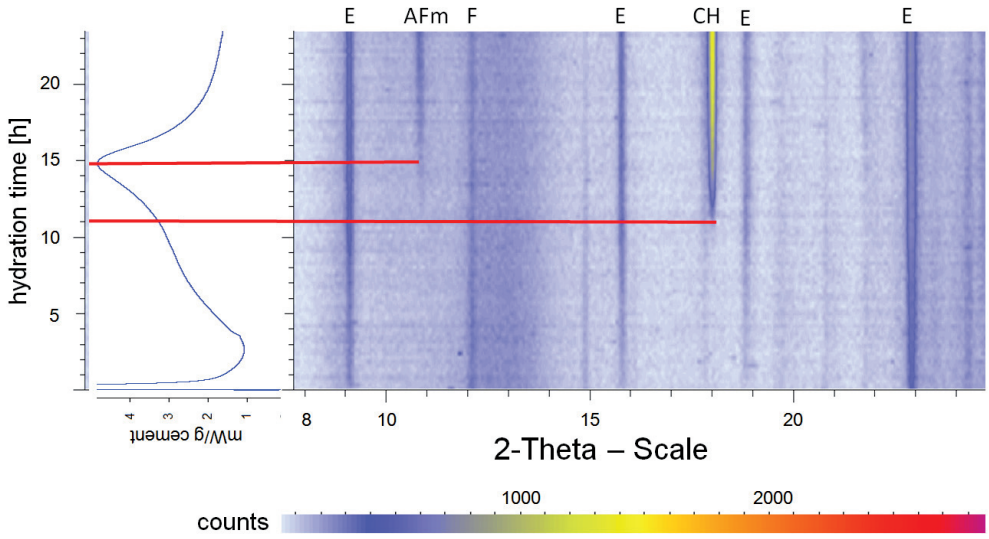

Figure 5–73: Section of the in-situ XRD Levelplot of cement blended with 35 % Søvind marl hydrated at 20 °C for 24 h coupled to the heat flow of the same system.

Based on the obtained results it could be shown that the replacement of OPC by calcined clay considerably changes the hydration of cement pastes at early ages as well as in the long term. The aluminate reaction and formation of AFm phases is more pronounced and can take place before the main silicate reaction at high replacement levels of OPC.

6 Laboratory burned clays

Small samples of the Søvind Marl and the AB1080 kaolinite rich clay from Portugal were burned at different temperatures in a laboratory electrical furnace. The aim was to test the influence of cooling rate and retention time of the samples in the furnace as well as the particle size after milling, on the pozzolanic reactivity by means of lime consumption tests.

Samples of about 15 g raw clay were put into platinum crucibles and burned in a chamber furnace from Nabertherm (Model: LH 60/14) at temperatures between 400-1100 °C. In a first trial the clays were hold for 2 h at constant temperature. While one sample was quenched in air to cool down immediately, another sample was cooled down in the furnace over night to room temperature (slow cooling).

One half of the samples was milled down to $d_{50} < 50$ µm while the other half of the samples was milled down further to a $d_{50} < 10$ µm to check the effect of particle size. The milling of the calcined samples was done by hand using an agate mortar until the desired particle size was reached.

In a next step clays were only burned for 30 min at the given temperature, shock cooled in air and milled down to a $d_{50} < 10$ µm to check the influence of retention time.

Lime consumption was tested in the same way as for the samples burned at the pilot scale installation. Pastes of clay and lime were mixed in a ratio of 1/1 with the known alkaline solution. Hydration was stopped after 28 days and the lime consumption was determined with thermal analysis.

The results obtained from these trials can be important for a potential industrialization of the two reactive clays as they might give crucial information about production parameters. Retention time in the kiln, cooling and milling of the samples can then be adjusted in an industrial installation if necessary to reach the highest reactivity. Of course the different atmospheres in the laboratory, pilot scale installation and industrial installation might influence the reactivity and burning behavior of the final material so that results cannot be directly transferred from one kiln to the other.

6.1 Effect of cooling rate

All samples were burned for 2 h at temperatures between 400-1100 °C in steps of 100 °C and milled down to a $d_{50} < 10$ µm.

For AB1080 there was no difference in crystallinity detectable with XRD between the fast and slow cooled samples. Neither was there any difference in the phase

development upon heating. Figure 6-1 shows the diffractograms of AB1080 burned in the mentioned temperature range and quenched in air. Kaolinite is dehydroxylated and transformed to metakaolin at 600 °C while the illite appears stable up to 1000 °C. Feldspar and quartz are not affected by the heat treatment up to 1000 °C. At 1100 °C recrystallization of mullite can be observed. Other new formed crystalline phases besides mullite were not detected.

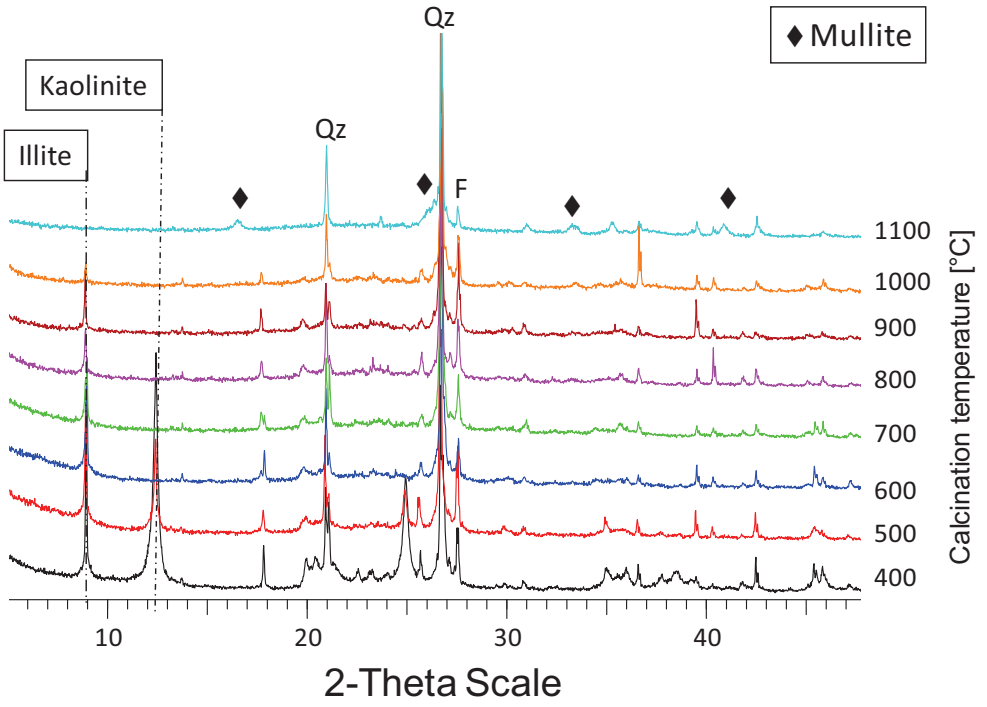

Figure 6-1: Diffractograms of the fast cooled AB1080 clay calcined between 400-1100 °C (Qz = Quartz, F = Feldspar)

In contrast to AB1080 the Søvind Marl showed small differences in the phase composition of the calcined clays when fast or slow cooled (Figure 6-2 and Figure 6-3). At 800 °C calcite is completely decomposed in both samples. The main calcite peak at 29.4 °2θ is still visible at 700 °C. Smectite is also almost completely destroyed / transformed to meta-smectite at 800 °C. When burned in the pilot scale installation some calcite was still stable after burning at 800 °C and smectite peaks were still clearly detectable. However the retention time was only 45 min in the pilot scale installation. Longer calcination times in the same temperature range can cause more complete decarbonation/dehydroxylation. Recrystallization of anorthite, diopside - wollastonite and hematite can clearly be detected from 900 °C on.

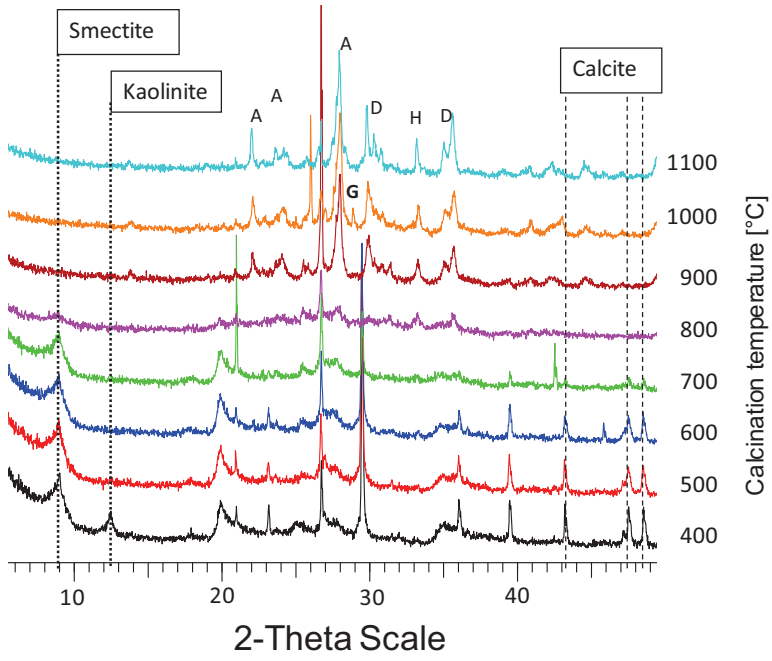

Figure 6-2: Diffractograms of the fast cooled Søvind Marl calcined between 400-1100 °C

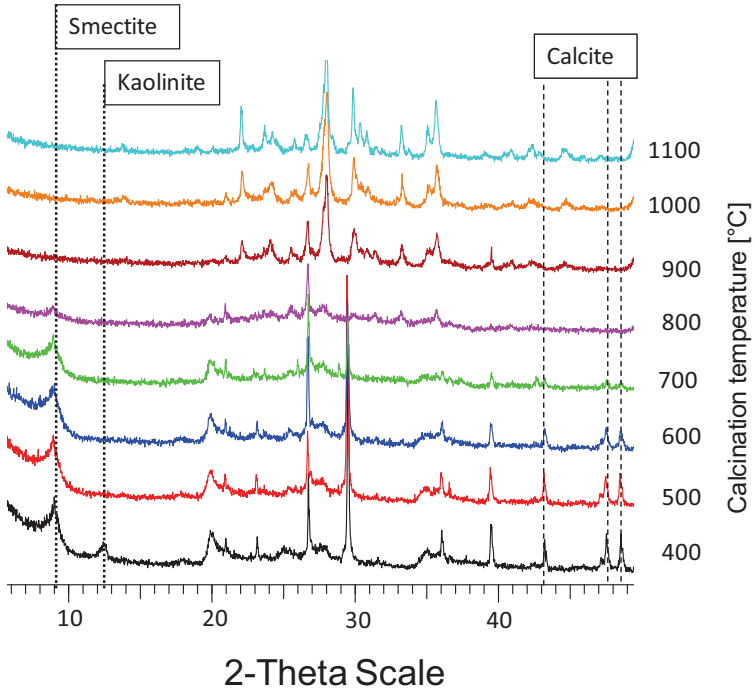

Figure 6-3: Diffractograms of the slow cooled Søvind Marl calcined between 400-1100 °C

Gehlenite could only be found as an intermediate phase at 1000 °C in the fast cooled sample. This means that crystalline gehlenite is only stable upon shock treatment. When cooled down slowly this phase either transforms back to the original phases or is present as a highly amorphous gehlenite phase.
The extreme intense peaks at ~ 21 and 43 °2θ in the fast cooled sample calcined at 700 °C belong to quartz and can be explained with an effect called spottiness. These high intensities are the result of a bigger quartz grain being in diffraction position.
The lime consumption of AB1080 and Søvind Marl burned at all temperatures is plotted in Figure 6-4 in dependence of the cooling rate.

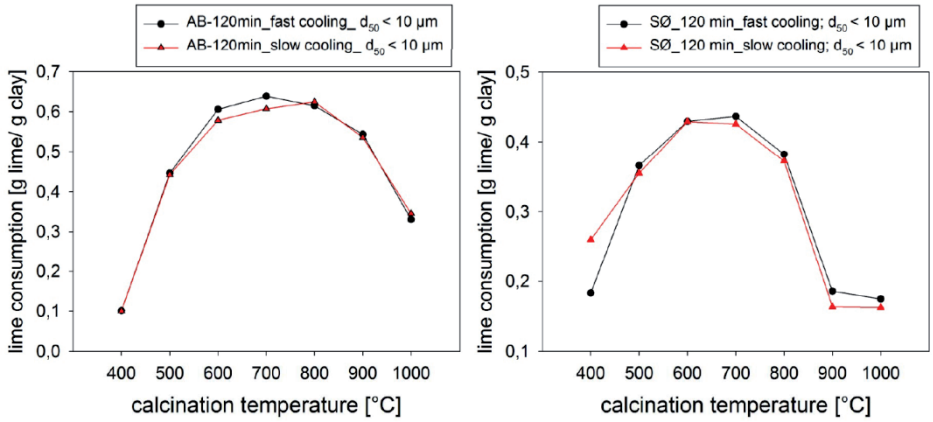

Figure 6-4: Effect of cooling rate on the lime consumption of AB1080 (left) and Søvind Marl (right)

The reactivity of both clays seems not be affected by slow or fast cooling. AB1080 shows the highest reactivity between 600-800 °C with a lime consumption between 0.61-0.64 g lime/g clay. The low reactivity at 400-500 °C is due to the not yet dehydroxylated kaolinite. At a calcination temperature higher than 900 °C the reactivity decreases as a result of starting recrystallization of new stable phases. The lime consumption at 800 °C is comparable to the samples burned in the pilot scale installation.
Earlier in this study it was already suggested that it is important to retain some calcium carbonate stable in the calcined Søvind Marl to reach maximum reactivity. Keeping that in mind we would expect a higher reactivity at 700 °C than at 800 °C for the samples burned in the electrical furnace. Looking at Figure 6-4 we can see that indeed the sample burned at 700 °C has higher lime consumption than the sample burned at 800 °C with 0.44 g lime/g clay compared to 0.38 g lime/g clay. Above 800 °C recrystallization starts, explaining the drop in reactivity.

6.2 Effect of particle size

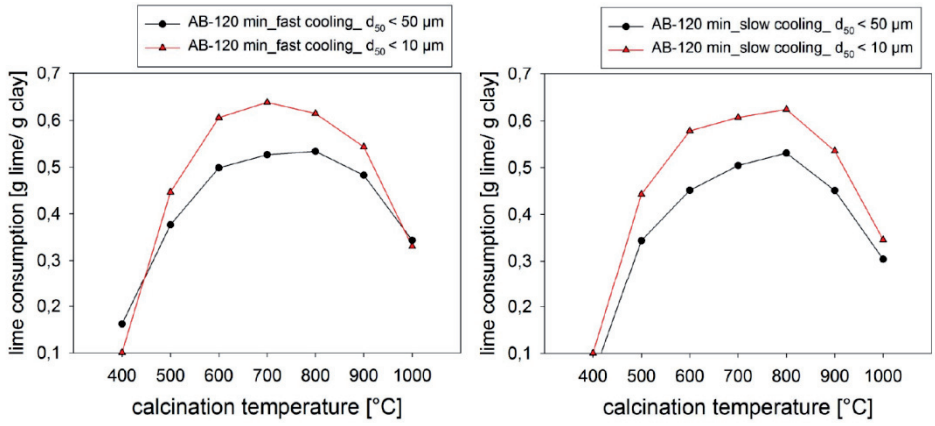

Figure 6-5: Lime consumption of fast and slow cooled AB1080 after heating at different temperatures in dependence of the particle size.

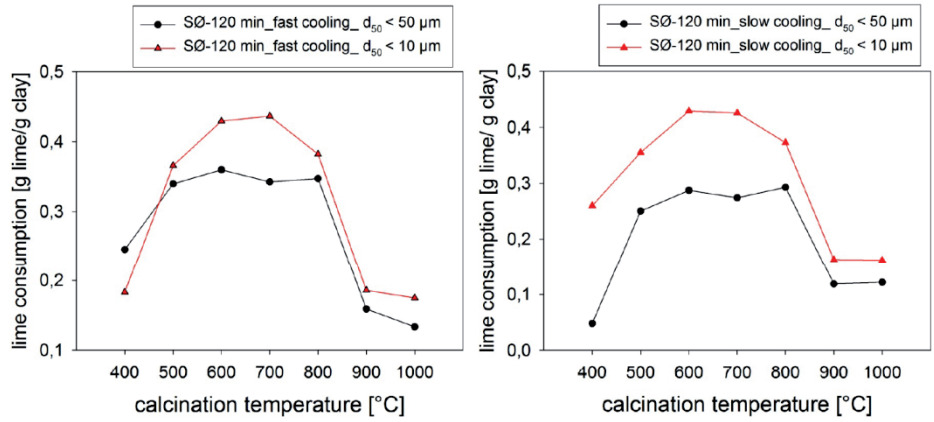

Figure 6-6: Lime consumption of fast and slow cooled Søvind Marl after heating at different temperatures in dependence of the particle size.

Figure 6-5 and Figure 6-6 show the lime consumption of slow and fast cooled AB1080 and Søvind Marl respectively as a function of their particle size. For both materials the finer ground samples show in general a higher reactivity with respect to lime consumption. In case of AB1080 the lime consumption is increased by about 0.1 g lime/g clay when the particle size is decreased from $d_{50} < 50\mu m$ to $d_{50} <$ 10 µm. For the Søvind Marl the difference in lime consumption is even higher between the fine and coarse ground samples. Also, the lime consumption is almost

constant between 500-800 °C for the Søvind Marl samples milled down to a d_{50} < 50 µm.
The effect of particle size on the reactivity of the calcined clays is obvious and no surprise since a lower particle size means higher potential reactive surface area.

6.3 Effect of retention time in the furnace

The retention time at the respective temperature in the furnace was reduced from 120 to 30 min in this trial. Samples were burned from 400-900 °C in steps of 50 °C, quenched in air and milled down to a d_{50} < 50 µm. The comparison of the lime consumption of AB1080 and Søvind Marl samples calcined for 120 min and 30 min at each temperature is plotted in Figure 6-7.

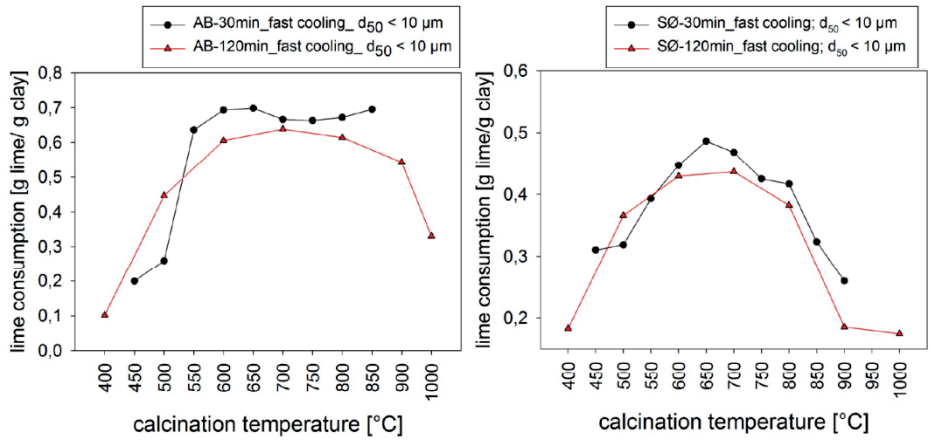

Figure 6-7: Lime consumption of fast cooled AB1080 (left) and fast cooled Søvind Marl (right) in dependence of the retention time

The reactivity with respect to lime consumption does increase by about 0.1 g lime/g clay for AB1080 in the temperature range of 550-650 °C when calcined for only 30 min compared to calcination for 120 min. It is also shown that the lime consumption is rather stable between 550 and 900 °C. If the correlation of lime consumption to mortar strength made before applies here as well, we can assume that AB1080 can be burned in this wide temperature range with a relatively short retention time in the kiln, without changing its properties in cementitious systems considerably. This can be important for production, where minor temperature variations should not have a big effect on the final product.

For the Søvind Marl the reactivity also increased slightly when calcined at lower retention times. The reactivity peaks at 650 °C and decreases continuously above that temperature. Again if this maximum lime consumption leads to the highest strength in mortars, the different calcination process compared to the pilot scale installation has an effect on the properties of the final product. The highest pozzolanic reactivity of Søvind Marl burned in the electrical furnace is reached at a temperature of 150-200 °C below the temperature of highest reactivity when burned in the pilot scale installation. The diffractograms of the Søvind Marl burned for 30 min at each temperature are given in Figure 6-8. It can be seen that calcite is more or less completely decomposed at 750 °C. The main peak at 29.4 °2θ is very small and the peaks at higher 2θ values disappeared. When burned in the pilot scale installation calcite was detectable in all cases up to 800 °C and for the H2-H4 samples from boreholes in the Søvind Marl deposit even up to 850 °C. Reason for that can be the higher partial pressure of CO_2 in the natural gas fired pilot scale kiln at IBU-Tec.

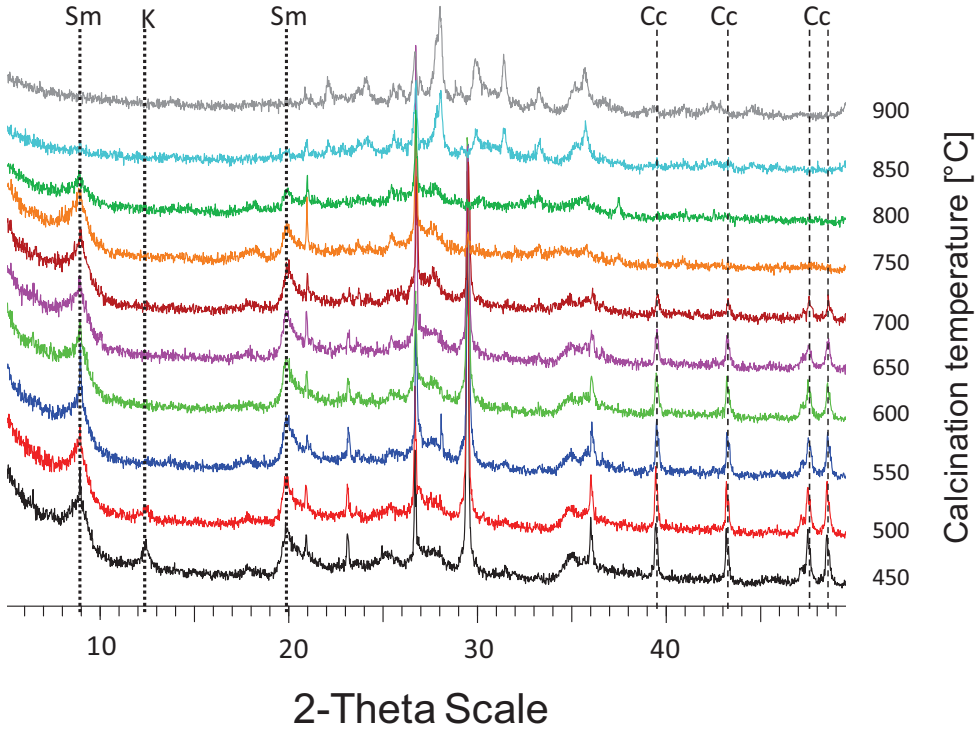

Figure 6-8: Søvind Marl calcined between 450-900 °C with a retention time of 30 min in the furnace (fast cooled). (Sm = Smectite; K = Kaolinite; Cc = Calcite

Conclusively it can be said the cooling rate does not have a significant effect on the reactivity of the calcined clay and marl with respect to lime consumption when burned in an electrical furnace. The retention time however and especially the particle size of the calcined clay/marl have a considerable effect on the reactivity. If this is transferrable to industrial production a short retention time of maximum half an hour in the hot zone can be chosen to gain a higher throughput. The cooling systems of existing plants do not have to be adjusted for special production of calcined clays which makes it possible to use Leca plant installations with free capacity.
After milling the calcined clay lumps the particle size should be controlled and have a $d_{50} \leq 10$ µm.

7 Industrial Trials

7.1 Søvind Marl - Denmark (Hinge - 12.04.2011)

7.1.1 Introduction:

From the previous investigations on the calcined Søvind Marl from pilot scale production at IBU-Tec it is known that the marl from Denmark has a rather narrow temperature window of high reactivity. The reactivity can change considerably within ± 50 ºC of the optimum calcination temperature.
One of the main goals of this industrial trial was therefore to check how stable the temperature can be held in an industrial size rotary kiln, to guarantee a calcined clay/marl product with homogeneous quality in an eventual full scale production. The aim was to produce calcined clay/marl at 5 different temperatures, with intervals of 50 ºC in the temperature range 750-950 °C, and to test the product afterwards for reactivity in terms of mortar strength and lime consumption.

This first full scale trial of calcined marl production took place in Hinge plant on April 12 2011. This a Leca producing plant from Saint-Gobain Weber. To perform this trial the production of standard expanded clay was stopped in kiln Nr. 4.

Figure 7-1: Used rotary kiln (Nr. 4) from Hinge plant in Denmark for production of calcined clay

7.1.2 General test conditions:

The only raw material used was the clay called Søvind Marl from Hinge. The clays named SØ and H2-H4 in this study are from the same pit in Hinge. Throughout the whole trial 12 samples of raw clay were taken between 12:00 and 19:00 o'clock and later investigated with regard to homogeneity, moisture and LOI values. These values are very important for the final cost calculation of the calcination process. The rotary kiln was fired with the goal to produce calcined clays at five different temperatures (750, 800, 850, 900, 950 ºC). The calcined clays were then sent to UVR-FIA for milling. The milled samples were later analyzed by means of XRD and thermal analysis and tested in standard mortars by replacing 20 % of OPC with calcined clay as well as in lime consumption tests at NTNU in Trondheim.

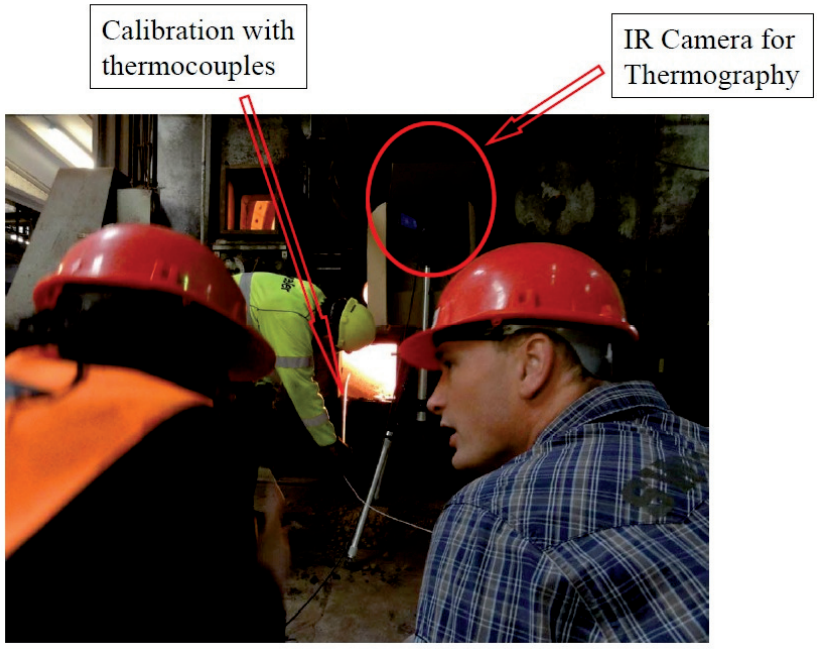

Figure 7-2: Monitoring of temperature at the kiln outlet with thermocouple and infrared camera (FLIR)

To monitor the temperature in the rotary kiln an infrared camera (FLIR) was used that pointed into the material bed just at the kiln outlet. Additionally a thermocouple was used to measure the temperature at the kiln outlet to which the infrared camera was calibrated (Figure 7-2). It has to be mentioned here that the calcined marl samples will be named with the respective temperature, but this might not

reflect the real temperature the marl has experienced in the kiln. The method of measuring the temperature is quite vague and does not reflect the real temperature profile in the kiln and thus the exact temperature of calcination as it was only measured at the kiln outlet.
Compared to standard Leca production with a clay feed of about 20-24 t/h the clay feed had to be reduced to 15 t/h. The reason for that was a higher tendency of the clay to stick together and clog the conveyer belt.
For the trial two different fuels were used:

- Natural gas 50 m^3/h
- Coal input = 40,3 % refers to 1.440 kg/h –*based on info from Hinge*

The cooler in use at kiln Nr. 4 is a so called Nimes cooler. A problem with that type of cooler is that the material is not directly transported further as in a grate cooler, meaning that some particles can remain over a long time in the cooler system. When the production of calcined marl was started it was noticed that the samples taken from the cooler were contaminated with Leca balls from the previous production days. Since it would have taken too much time to wait until the cooler is free of Leca, it was decided to take calcined clay samples direct from the kiln outlet before passing through the cooler. Doing so, the samples were spread out and cooled fast on the plant floor. At each calcination temperature three samples were taken.

7.1.3 Raw material:

The sample matrix taken from the raw clay during the industrial trial is given in Table 7-1.

Table 7-1: Samples of raw Søvind Marl taken during the day of the industrial trial in Hinge

time	12:00		14:00		16:00		17:00		18:00		19:00	
sample	1A	1B	2A	2B	3A	3B	4A	4B	5A	5B	6A	6B

Figure 7-3 shows a representative diffractogram of the raw clay with the typical clay mineral peaks. The (001) smectite peak is overlapping with the illite peak at 8.9 º2θ, because the clay was dried at 100 ºC. This causes the removal of the interlayer water, typical for smectite minerals, decreasing their d-spacing and thus shift-

ing the peaks to higher 2θ values. With XRD and TG/DTG the raw marl samples given in Table 7-1 appeared very homogeneous.
The moisture of the clays was measured by drying the different clay samples at 100 ºC for 2 h in the TG and measuring the weight loss. These dried clays were then heated up to 1100 ºC with a heating rate of 10 ºC/min to estimate the residual LOI. The LOI measured like this in a TG with N_2 atmosphere may differ from the LOI measured in an oven with air.
The average moisture and residual LOI were determined to be 29 and 18 % respectively. The residual LOI describes the LOI of the dried material (100 ºC, no moisture).

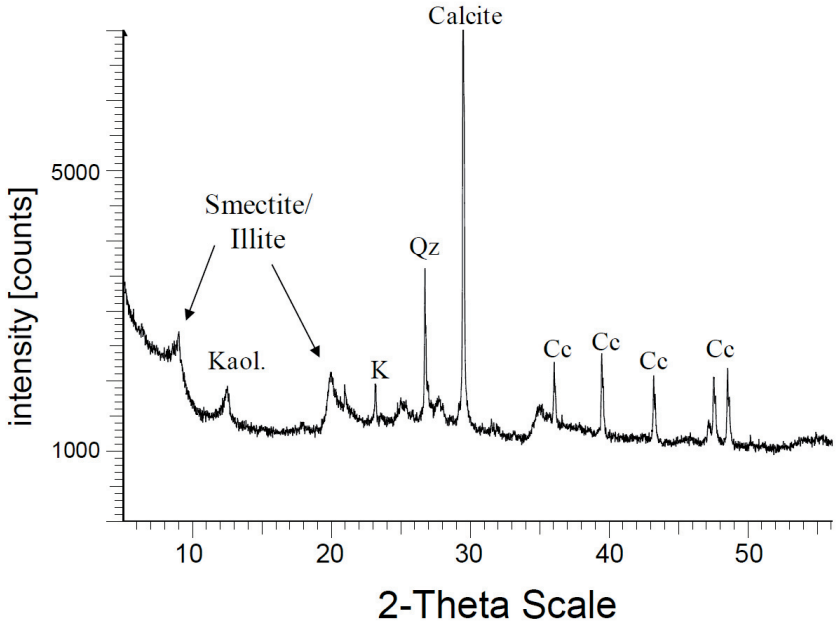

Figure 7-3: Diffractogram of a representative raw clay sample from the Søvind Marl deposit in Hinge (Denmark)

7.1.4 Calcined Clays

The raw marl was calcined at 5 different temperatures (750, 800, 850, 900, 950 ºC). 3 bags of about 20 kg calcined clay for each temperature (marked 1-3) where sent for milling to UVR-FIA. The milling time until a $d_{50} < 10$ µm was reached was recorded as it could give some information about the reactivity of the marl.
The milling time plotted against the calcination temperature can be seen in Figure 7-4.

The graph shows that the milling time increases considerably from 800 to 850 ºC before it drops again at 900 ºC. The first jump in the milling time up to almost 400 min can be explained due to sintering effects. Above 800 ºC material transport typically gives rise for densification in silicate materials [210]. Two effects are possible to take place regarding the decrease in milling time at 900 ºC. After sintering, recrystallization of new phases can occur, but a recrystallization of phases with a lower hardness is very unlikely. The typical recrystallized phases in this material like, anorthite, wollastonite or diopside possess all a higher hardness than the original clay minerals and calcite. It is more likely that the temperature treatment upon a certain point introduces lattice distortions and transformations in the material with partly amorphization and the formation of a glassy phase as described in chapter 5. These phases might be more brittle with a lot of strain helping to crack them and reducing the resistance to grinding. If that is the case and the metastable state (meta-clay) is reached at this temperature we should expect the highest reactivity for the clay burned at 900 ºC.

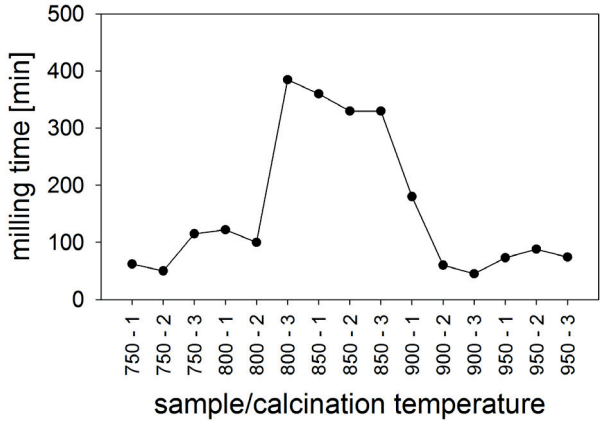

Figure 7-4: Milling time of produced calcined marl samples

Upon calcination the marl changes its color, from dark black-greenish raw clay to light brown in the calcined state. All calcined and milled clays had this light brown-ochre color, except the sample calcined at 900 degrees which had a dark brown color (Figure 7-5). Regarding the different colors it looks like the sample calcined at 750 °C is well oxidized compared to the sample calcined at 900 °C. To achieve a temperature of 750 °C in the kiln less fuel is needed which means that there is probably good excess of O_2 in the atmosphere. During the calcination process the air-flow in the kiln had to be kept high at all times to avoid sticking of the material in the inlet of the drying oven. With the same air-flow but the use of more fuel to achieve 900 °C it is likely that O_2 excess is much lower. The effect of oxida-

tion of iron on the reactivity of the calcined marl was already discussed in chapter 5.3.8. Nevertheless it appears very strange that the sample calcined at 950 ºC has the same color than the samples burned at 750 – 850 ºC. It is very unlikely that the material gets darker at 900 °C and changes back to a lighter color at 950 °C. One sample in between with a different color could also indicate that unintentionally the marking of the samples 900 and 950 was interchanged at some step of the production or milling process. Until now it is not sure what exactly happened but a new trial with optimized parameters will reveal if there is any effect of the air-flow in the kiln on the final material.

Figure 7-5: Calcined Clays at 900 and 750 ºC (measured temperature at kiln outlet)

The diffractograms of the calcined clays between 750 and 950 ºC are plotted in Figure 7-6. Between the different temperatures there is not much difference detectable. The clay mineral peaks at 8.9 and 20 º2θ do not change very much in intensity. The calcite peaks on the other hand decrease significantly but there is still a considerable amount of stable, crystalline calcite left in the clay even at 950 °C. This is especially visible at the main (001) calcite peak at around 29.4 º2θ. Recrystallization of high temperature phases could not be observed.

Although there is no significant difference visible in the different diffractograms, there is one diffractogram with noticeable higher background signal in the region between 10-40 º 2θ. By plotting only the background curves and laying them over each other it can be seen that the clay calcined at 900 ºC gives a higher background than the other clays when measured with XRD (Figure 7-7). A higher background in this 2 Theta region is probably due to a higher amorphous content in this clay sample. Taking this into account it can be expected that the clay burnt at 900 ºC has the highest reactivity. The in general high background of all diffractograms can be explained with the high iron content of about 10 % in the clay. This causes x-ray fluorescence radiation that is not filtered out.

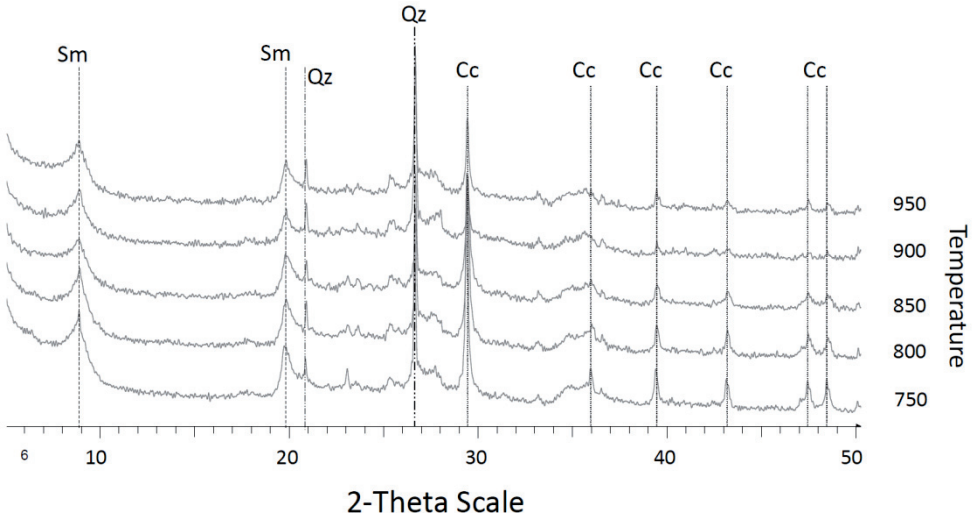

Figure 7-6: Diffractograms of calcined marl from Hinge between 750 and 950 °C (temperature measured temperature at kiln outlet; Sm = Smectite, Qz = Quartz, Cc = Calcite).

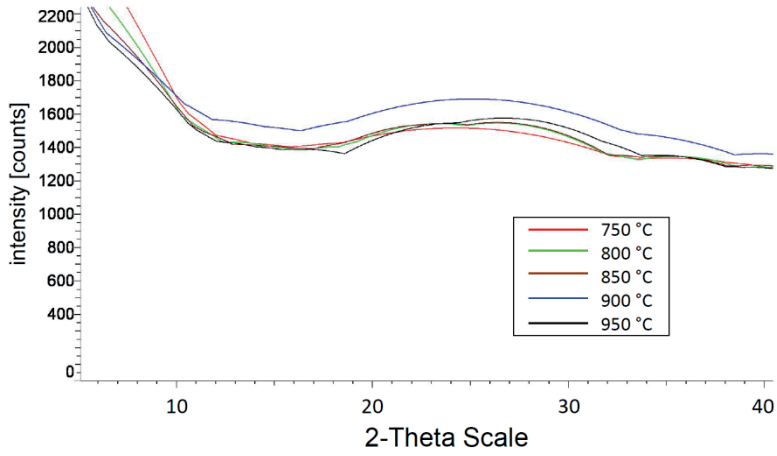

Figure 7-7: Background curves from the diffractograms of Figure 6, plotted with EVA 4.0 (Bruker)

To get accurate numbers about the calcium carbonate left in the calcined marl samples and with that a better idea about the CO_2 emissions derived from the process of calcining marl, TG measurements with coupled mass spectrometry were performed (Figure 7-8). In that way the weight loss of the samples and gas analysis for H_2O, OH^- and CO_2 can be measured simultaneously. The equipment used was a Netzsch STA 449 C TG coupled to a Netzsch QMS (quadrupole mass spectrometer) 403 C apparatus. The atmosphere during the measurements was synthetic air.

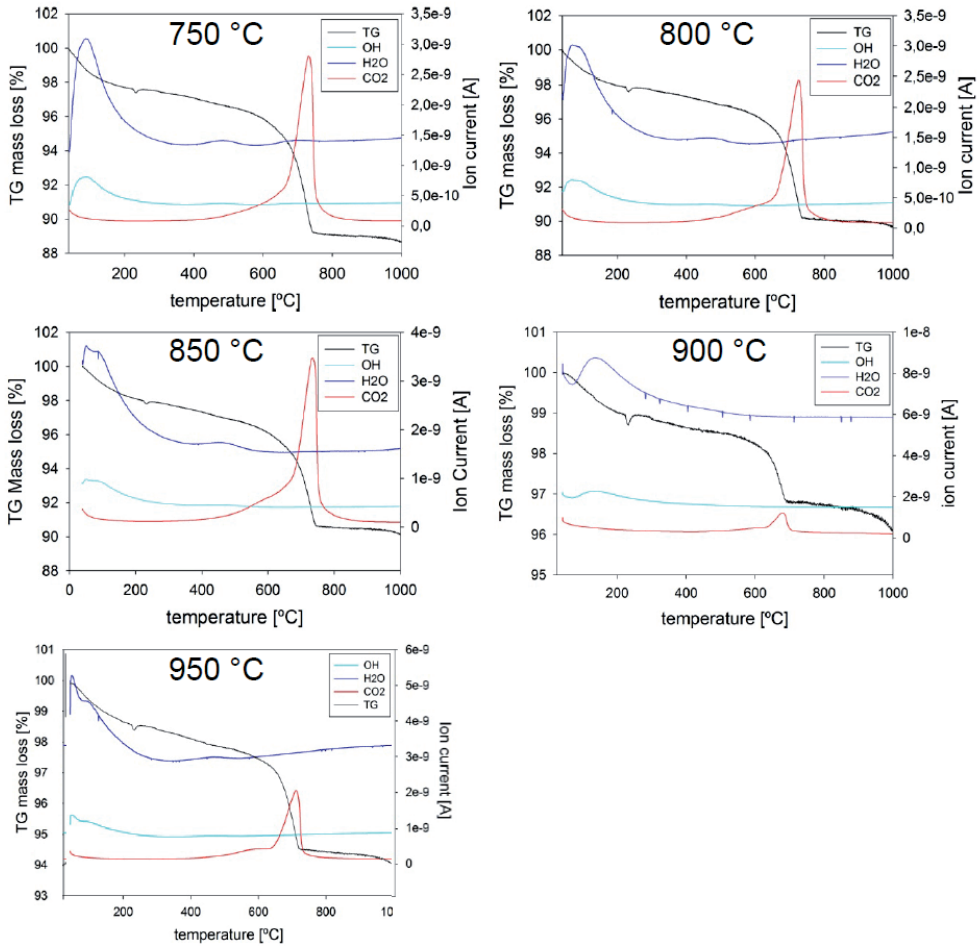

Figure 7-8: TG with coupled mass spectrometry of the calcined marl from Hinge between 750-950 °C.

It can be seen that the main weight loss in the region between 600-800 °C is only due to the release of CO_2 in all samples. In the sample named 750 the clay minerals are already almost completely dehydroxylated. All samples show a weight loss below 200 °C which is due to adsorbed water at the calcined marl surfaces during storage and some OH^- from maybe partly rehydrated clay minerals. The samples 750, 800 and 850 show furthermore a small release of water between 400 and 500 °C. This could be due to incomplete dehydroxylation during the calcination process or again due to partly rehydration of clay minerals during storage. Furthermore all samples show a small peak in the weight loss curve around 250 °C of which the origin is not yet clear. The diffuse weight loss and signals in the H_2O analysis of the sample calcined at 900 °C is probably due to an unstable balance and atmos-

phere during the measurement of this sample. The sample calcined at 900 °C releases less CO_2 than the sample calcined at 950 °C. This is not logical and another indicator that the labels of the two samples might have been mixed up.
From the graphs, the amount of CO_2 being expelled can be calculated by evaluating the mass loss between the horizontal tangents in the TG curve in the area of the calcite peak. The results are listed together with the residual LOI of the samples in Table 7-2. With the assumption that samples Hinge-900 and Hinge-950 are interchanged there is still almost 3 % not decomposed $CaCO_3$ in the clay left up to a calcination temperature of 950 ºC.

Table 7-2: Total LOI and released CO_2 of calcined marl samples from Hinge. Amount of $CaCO_3$ calculated from CO_2 release.

Sample	Total LOI [%]	Expelled CO_2 [%]	Residual $CaCO_3$ [%]
Hinge-750	11.38	6.67	15.18
Hinge-800	10.31	6.35	14.45
Hinge-850	9.82	5.93	13.50
Hinge-900	3.88	1.30	2.96
Hinge-950	5.96	2.95	6.71

One possible explanation is that the atmosphere in the kiln enhances the partial pressure of CO_2 thus increasing the decomposition temperature of calcium carbonate. Furthermore again, the given temperatures might not be exact. We know the temperature was measured only at the outlet of the kiln near the burning flame. The temperature in the other parts of the rotary kiln are hard to guess and it is also not much known about the temperature gradient throughout the kiln and the real retention time at this specific temperature.

Finally the pozzolanic reactivity was tested in lime consumption tests and mortars.
Lime consumption tests were only performed on the samples calcined at 800 °C and 900 °C as this was the best performing sample in mortar tests (Figure 7-9).
In Table 7-3 it is shown that the lime consumption is 0.42 and 0.44 g lime/g clay for the samples Hinge 800 and 900 respectively. The pozzolanic activity of the industrial produced calcined marl is slightly higher than the average pozzolanic activity of the calcined samples H2-H4 from three different boreholes of the same deposit in Hinge but produced in the pilot scale installation. However the original Søvind Marl sample calcined at pilot scale reached higher lime consumption. The best performing calcined marl burned in the electrical lab furnace reached a lime consumption of 0.49 g lime/g clay.

Table 7-3: Lime consumption of the samples calcined at 800 and 900 °C during the industrial trial in Hinge compared to the lime consumption of the best performing clays in pilot scale and lab scale production.

Marl/lime = 1/1 (20 °C)	Industrial scale		Pilot scale		Lab scale	
	Hinge 800	Hinge 900	H2-H4 850	SØ 800	SØ 700 120 min	SØ 650 30 min
CH at 0 days [%]	46.3 ± 1.3	46,1 ± 0.8	46,4 ± 1.3	47.1	46.6	46.6
CH at 28 days [%]	24.0 ± 0.9	22.5 ± 0.8	23,5 ± 1.1	19.8	22.7	20,0
Consumed CH [%] 0-28 days	48.1 ± 1.9	51.3 ± 1.7	49,0 ± 0.7	58	50.9	56,7
Consumed CH per gram clay [g]	**0.42 ± 0.02**	**0.44 ± 0.01**	**0.41 ± 0.02**	**0.52**	**0.44**	**0.49**

The results of the mortar tests where 20 % of OPC was replaced by marl calcined at each temperature during the industrial trial can be seen in Figure 7-9. The mortars were cured for 28 days at 20 °C. All mortars containing 20 % calcined marl scored a higher compressive and flexural strength than the reference mortar with no OPC replacement (black line). The sample marked Hinge-900 showed the highest reactivity in mortars with a compressive strength of 58.6 MPa after 28 days. That is 7.5 MPa higher than the reference with 51.1 MPa. Relative to the reference the strength is increased by about 14.6 % after 28 days. Consequently this industrial produced marl performs as good as or even slightly better than the calcined marl from pilot scale production.

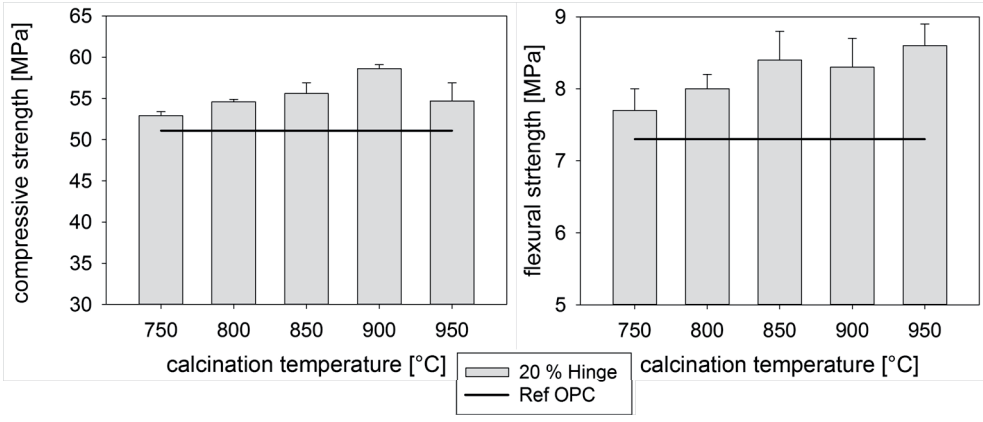

Figure 7-9: Compressive and flexural strength of standard mortars with 20 % replacement of OPC by marl calcined at the 5 different temperatures.

In chapter 5.2.4 we can see that the mortar containing 20 % H2-H4 Mix scored a compressive strength of 13.9 % higher than the reference and the mortar containing 20 % SØ scored 11.6 % higher than the reference. The samples marked 800, 850 and 950 also show good results and lie in average 3.9 MPa higher than the reference.
Regarding the flexural strength the sample marked 950 reaches the highest value with 8.6 MPa. This is 1.3 MPa higher than the flexural strength of the reference mortar. Samples 850 and 900 reach 8.4 and 8.3 MPa respectively.

Even though the absolute temperatures given from the industrial trial might not be correct there is a clear tendency that the temperature of reactivity of calcined marl increases in the order lab scale < pilot scale < industrial scale. The highest reactivity of samples burned in the electrical lab furnace was reached between 650-700 °C. From pilot scale production the marl with highest reactivity was burned at 800-850 °C and in the industrial trial the temperature of highest reactivity is around 900 °C. The partly coal fired industrial kilns produce a higher partial pressure of CO_2 thereby increasing the decomposition temperature of calcium carbonate. From previous described experiments we know that the marl reaches its highest reactivity when calcined at a temperature shortly below complete decomposition of calcium carbonate.

7.1.5 Conclusions

Except from some minor problems, like that the normal cooler could not be used for collecting samples, and some sticking of the clay that required adjustments in the kiln feeding rate, the trial was very positive. In real industrial production the cooler would be cleaned out completely and be usable in the process. With the mortar tests it could be clearly shown that it is possible to produce a reactive material by calcining the marl from Hinge on an industrial scale. Surprisingly the marl showed good reactivity over a rather wide temperature window, in compressive as well as in flexural strength tests on mortars with 20 % replacement of OPC by calcined marl, which is very positive.
The combustion process was very stable with good flame and temperature stability, showing low deviations. However the air-flow had to be kept high during the whole process and was probably higher than it would be necessary after some optimization of the calcined marl production. The trial was very encouraging for the future as it could be shown, that it is possible to produce calcined marl of its highest reactivity.

The final cost calculations for the production of calcined marl from this day, including all the numbers from the plant like fuel, energy, clay feeding etc. and the numbers from the raw material can be found in the report “Calcination Trial – Hinge Denmark” from Jan Szanser (Confidential - for internal use in Saint-Gobain only). Based on this report about 390 kg CO_2 were emitted for the production of 1 ton calcined marl during this trial. This is less than 50 % of the CO_2 emissions for the production of 1 ton OPC. Not to forget that this was the first serious trial on industrial scale to produce calcined marl. With further testing and optimization of the process parameters the CO_2 emissions and the energy consumption can be reduced further.

7.2 AB1080 – Portugal (Avelar, 30.06.2011)

7.2.1 Introduction

This trial was performed at the Leca plant of Saint-Gobain Weber in Avelar (Portugal) using the pre-treatment line 2 and kiln number 2 to produce calcined AB1080 on industrial scale. Lab scale experiments with AB1080, calcined at the pilot scale installation at IBU-Tec, showed that this clay can be highly reactive over a much wider temperature range compared to the Søvind Marl. The clay has a very good potential to be used as a binder after calcination at temperatures between 700 and 800 ºC and the possibility for industrialization at Avelar plant. For that it was very important to analyze process data, possible occurring problems and positive remarks during the first test.

Figure 7-10: Kiln nr.2 at Avelar plant in Portugal

The main goals for the industrial test were the evaluation of the possible need to change existing equipment from the usual Leca production to calcined clay production. Furthermore it was important to assess which fuels could be used, especially to check coal burning. Besides that it was crucial to find a way to check the temperature (process temperature), to produce a material with high quality and if the later described “LOI-test” can serve as a suitable process control test. Finally the calcined clay was send to the nearby company ADM which provides different mill-

ing techniques. The goal was here to investigate the influence of different milling methods (dry and wet milling) on the reactivity of the product.

7.2.2 General test conditions

Information and numbers are based on the technical report: *"Calcined Clay – Industrial Test Avelar"* from Cristina Freire.

The only raw material used was the AB1080 clay. The raw clay was pre-treated in a wet pan-mill with no addition of water. The feeding set-point had to be reduced compared to the set-point for the usual LWA-clay (50 ton/h), because the wet pan-mill started to be overloaded. The set-point for feeding the kiln was 18 ton/h with no additives and no water. Drying kiln and burning kiln speed were < 2 rpm and 4 rpm respectively with a primary air pressure of 100 mbar. Fuel Oil, Diesel and coal were used as fuels during the test.
It was intended to monitor the temperature with a pyrometer, but it had a lot of variations and the temperature was not stable. Thus it was decided to measure the temperature in the calcined clay itself with a thermocouple. For that method about ± 10 kg samples were taken from the kiln outlet and put in a metal bucket. The temperature was then recorded by putting the thermocouple inside the material until the temperature stabilized (Figure 7-11). The temperature was recorded together with the LOI of the material. The goal was to achieve a LOI (1000 ºC) of the calcined material between 1.3 and 0.5.

Figure 7-11: Employee taking out material from the kiln head (left) and measuring temperature with a thermocouple inside the material (right)

It was decided to approach three different calcination temperatures (600, 650, 730 ºC) for the clay. The calcined material was cooled in a grate cooler with four air fans and packed into bags of about 500 kg to be sent to ADM for milling. For dry milling a pendular mill and a continuous ball mill were used. For wet milling and atomization a pilot installation and an industrial installation were available and tested.

7.2.3 Notation:

Following shortcuts will be used in this chapter to describe the different samples:

MK	Metakaolin → calcined AB1080
60	600 ºC burning temperature
65	650 ºC burning temperature
73	730 ºC burning temperature
W	wet milling
I	industrial installation
D	dry milling
A	continuous ball mill
P	pendular mill

E.g. MKDP 65 = AB1080 burned at 650 ºC, dry milled with pendular mill.

Samples:

Following samples were produced in this trial and investigated with different methods at NTNU in Trondheim and at Aveiro University and ADM in Portugal.

- MKDA 60
- MKDA 65
- MKDP 73

- MKW 60
- MKW 65
- MKW 73

- MKWI 65

7.2.4 The "LOI test"

The "LOI test" is a simple test to assess the quality of the calcined clay. All calcined clays from pilot scale and lab scale production had a LOI value of < 3 % in the reactive temperature range between 650-800 °C. Furthermore the clay showed good reactivity over the whole temperature range which means it is not important to hit the temperature on target. Since the real temperature in the industrial kiln is very difficult to measure, the determination of the LOI of taken calcined clay samples might be an easy way to assess the region where the final product is reactive. The lower the LOI the more complete is the dehydroxylation and transformation to metakaolin. But the LOI should not be too low (< 0.5 %) to be sure to avoid sintering and possible recrystallization.
Calcined clay lumps with sizes of 0 to ± 10 mm are taken from the kiln outlet. When the material is cooled down it is sieved in three different fractions (0-1 mm, 2-4 mm and > 6.3 mm) and LOI was measured on all three fractions. LOI was tested by weighing the cooled samples before and after heating in a laboratory scale chamber furnace to 1000 °C in the mechanical laboratory at the production site.

7.2.5 Raw material

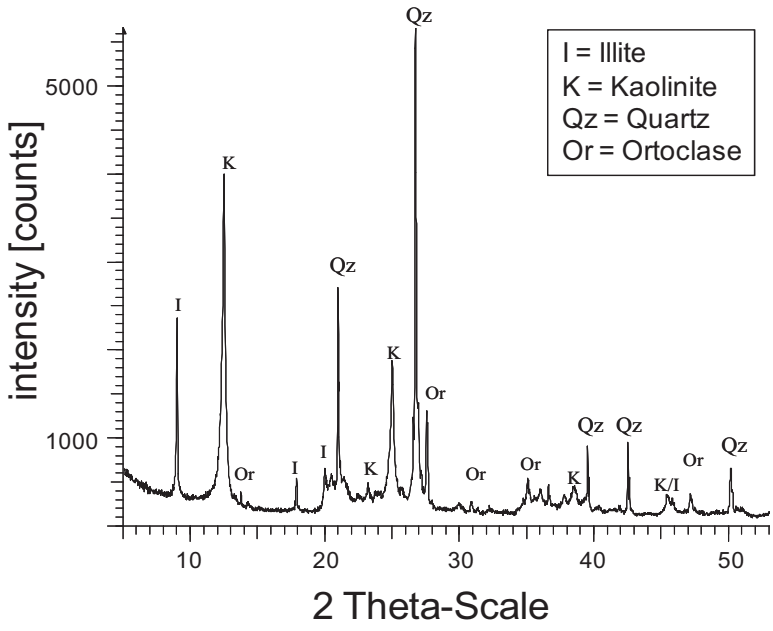

Figure 7-12: Diffractogram of the uncalcined clay AB1080 from Avelar

Figure 7-12 shows a diffractogram of the uncalcined AB1080 clay from Portugal. The average moisture (100 ºC) and the residual LOI (1100 ºC) were determined with TG to be 18 % and 9.1 % respectively.

7.2.6 Calcined Clays

It was the aim to mill down the calcined clay samples from the industrial trial to a d_{50} of at least smaller 10 µm (measurable with lasergranulometry) favourably < 3 µm. Different milling techniques were tested and the particle size was afterwards analyzed to check if it is possible to reach the goal with all mill types. Particle size distribution was measured directly in place after milling at ADM in Portugal using a sedigraph in addition to laser granulometry as well as at NTNU. The results are shown in Table 7-4. A sedigraph has a higher accuracy measuring the particle size of clay samples in particular at particle sizes below 5 µm. It can be seen that most clay samples could be milled down to a d_{50} < 3 µm as it was required. Only with the pendular mill this small particle sizes could not be reached. Due to the significantly higher particle size of the sample MKDP 73 one can expect a lower reactivity compared to the other samples.

Table 7-4: Particle size measured with a sedigraph and lasergranulometry in Portugal and at NTNU in comparison

Sample	d_{50} [µm]		
	Sedigraph	Laser granulometry	
	Portugal	Portugal	NTNU
MKDA 60	2.81	16.11	11.83
MKDA 65	2.68	7.87	8.57
MKDP 73	10.55	28.21	20.85
MKW 60	3.03	9.36	8.52
MKW 65	1.92	6.27	5.63
MKW 73	2.52	7.42	6.57
MKWI 65	2.34	11.62	6.32

Comparing the results of the laser granulometry obtained at NTNU and at ADM it can be noticed that except of the sample MKDA 65 the measured d_{50}-values from ADM are in all cases higher than the ones measured at the NTNU. Nevertheless both instruments show the same tendency and most values do not differ significantly. MKDP 73 has by far the highest d_{50}-value of all samples in agreement with the results from the sedigraph measurements. MKDA 60 has a higher particle size than

MKDA 65. Regarding the wet milled samples, sample MKW 60 has the highest particle size. The exact measurement parameters, like the dispersing agent, for the instrument at ADM are not known and can explain the differing results.
All calcined clay samples were investigated with X-ray powder diffraction to check the crystallinity and possible different phase compositions but mainly regarding the stability of the clay minerals. Sections of the diffractograms of the dry and wet milled calcined clay samples are plotted in Figure 7-13.
Regarding the dry milled samples kaolinite is almost completely decomposed at 600 ºC. There is only a very small peak left in sample MKDA 60 at 12.4 º 2Theta. The structure of the illite crystals stays stable up to 730 ºC. The higher intensity of the illite peak in the diffractogram of the MKDP sample is due to effects of preferred orientation in the (001) direction. The amount and crystallinity of feldspars and quartz is not expected to change with heat treatment in that low temperature range. Differences in the crystallinity of the dry and wet milled samples due to the different milling techniques could not be detected regarding peak widths and shoulders. In the wet milled sample calcined at 600 ºC (MKW 60), a clear kaolinite peak was detected while in the dry milled sample kaolinite was almost gone. There are two different possible explanations for that. On the one hand it could be that the kaolinite was not completely decomposed by the heat treatment at 600 ºC, but the high energy derived from the dry milling was enough to dehydroxylate the kaolinite minerals further. Depending on the milling time, delamination of the kaolinite minerals can occur together with point heating, leading to the dehydroxylation of clay minerals [211]. On the other hand it could be possible that the kaolinite structure was dehydroxylated at 600 ºC but not completely transformed or destroyed. During the wet milling process some water molecules could have been forced back into the structure, causing the kaolinite peak to reappear in the diffractogramm. Depending on the reaction temperature and time, the dehydration of kaolinite to metakaolin is claimed to be completely reversible [212-213]. The same effect is visible in the MKWI 65 sample. The diffractogram of the wet milled sample using the industrial installation shows a small kaolinite peak even for a calcination temperature of 650 ºC. In contrast to that the sample milled down with the pilot installation as well as the dry milled sample at 650 ºC show no signs of kaolinite. In addition the sample MKWI 65 shows another new peak at 9.6 º 2Theta that could not be detected in any of the other produced calcined clay samples. The peak could not be assigned to any phase yet but might represent a zeolite phase deriving from a reaction of clay and feldspars with water.

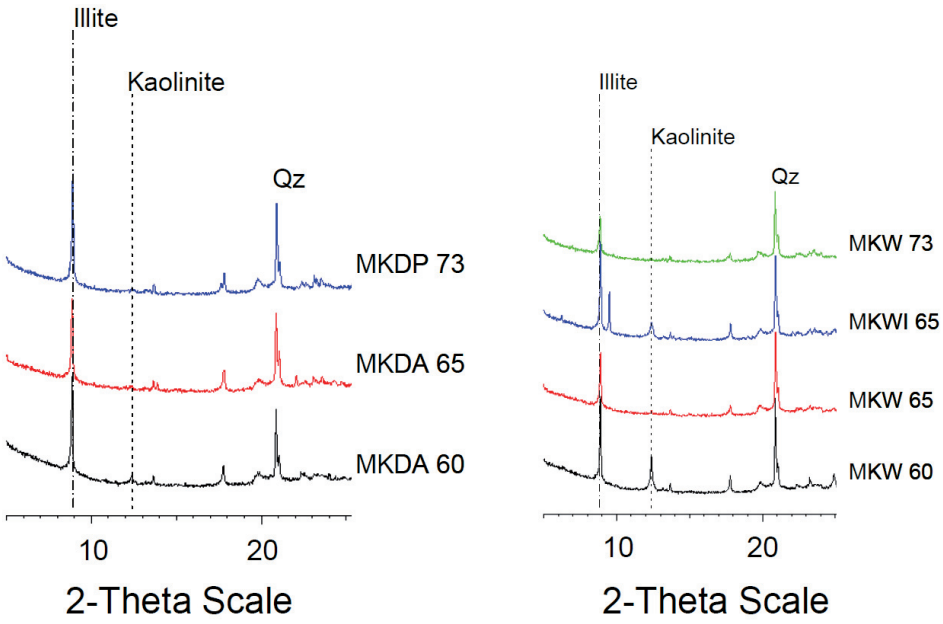

Figure 7-13: Sections of the diffractograms of dry (left) and wet (right) milled calcined clay samples from the industrial trial in Avelar

Differential thermogravimetry of the calcined clay samples from the industrial trial in Avelar could confirm the presence of kaolinite in the samples MKW 60 and MKWI 65 by the presence of a peak around 520 °C.

Data about the LOI of the calcined clay samples were collected directly at the plant after calcination and at NTNU. At the plant the LOI was collected for each burning temperature, by means of the described "LOI-test". At NTNU the LOI was taken as the weight loss measured with TG by heating the sample to 1100 ºC. The results vary quite a bit due to the different methods used. Additionally the calcined clay samples can adsorb atmospheric water during storage. At the plant the LOI was measured directly after calcination (before milling) on the calcined clay lumps taken from the kiln. Hence the samples did not contain any moisture, and the LOI values are lower than the ones measured at the NTNU. Results are given in Table 7-5.

Table 7-5: LOI of the calcined clay samples measured at the NTNU and at Avelar plant

Temperature goal	Sample	LOI NTNU	LOI Avelar
600	MKDA 60	2.66	1.63
	MKW 60	3.09	
650	MKDA 65	2.76	1.00
	MKW 65	2.62	
	MKWI 65	3.06	
730	KKDP 73	1.62	0.59
	MKW 73	1.92	

Pozzolanic activity was tested with all calcined clay samples by performing lime consumption tests and the results are given in Table 7-6. The best result was achieved with MKDA 60 reaching a lime consumption of 0.59 g lime/g clay. This is comparable to the average lime consumption of 0.63 ± 0.05 g lime/g clay achieved with the AB1080 calcined at 800 °C in the pilot scale installation. However the lime consumption reached with the clay calcined in the electrical furnace is significantly higher with up to 0.7 g lime/g clay for the sample burned at 650 °C for 30 min. Due to the atomization process after wet milling the wet milled calcined clays are present as small spherical agglomerates. These agglomerates are very difficult to disperse in the mixing process of the clay/lime pastes. Consequently the wet milled samples could not reach their full lime consumption resulting in low values like 0.4 g lime/g clay.

Table 7-6: Lime consumption of the calcined clays produced during the industrial trial in Avelar

Clay/lime = 1/1 (20 °C)	MKDA 60	MKDA 65	MKDP 73	MKW 60	MKW 65	MKW 73	MKWI 65
CH at 0 days [%]	46.6	46.6	46.6	46.6	46.6	46.6	46.6
CH at 28 days [%]	15.17	18.52	17.93	25.36	19.43	21.07	25.47
Consumed CH [%] 0-28 days	67.45	60.26	61.52	45.58	58.30	54.79	45.34
Consumed CH per gram clay [g]	**0.59**	**0.53**	**0.54**	**0.40**	**0.51**	**0.48**	**0.40**

Standard mortars were mixed with 20 % replacement of OPC by each calcined clay sample and cured for 28 days at 20 ºC. The compressive and flexural strength of the mortars after 28 days is plotted against a reference mortar with 100 % OPC in Figure 7-14.

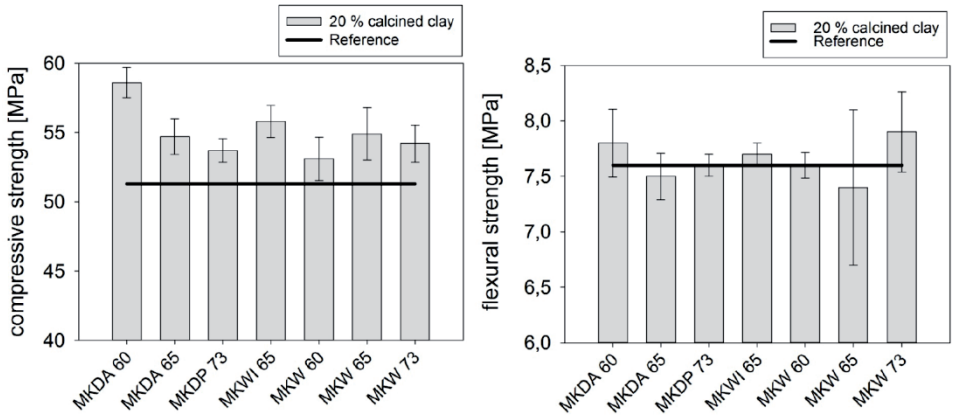

Figure 7-14: 28 days compressive (left) and flexural (right) strength of standard mortars with 20 % replacement of OPC by the respective calcined clay sample

Regarding the compressive strength all mortars containing 20 % of calcined clay score higher than the reference mortar. The highest compressive strength of 58.6 MPa was achieved at the lowest temperature with the mortar mixed with the sample MKDA 60 which also showed the highest lime consumption. The compressive strength of this sample is about 14 % higher than the compressive strength of the reference mortar with no cement replacement after 28 days. The mortar mixed with sample MKW 60, still containing some non-decomposed kaolinite, shows the lowest compressive strength with 53.1 MPa, with the simple reason that it has less reactive material with regard to metakaolin. The second lowest compressive strength is achieved with the mortar containing 20 % of the sample MKDP 73. This sample has a significantly higher particle size and is as predicted slightly less reactive than the other samples. The effect of the particle size on the reactivity was described in chapter 6.2. Nevertheless all produced clays seem to be reactive in this wide temperature window. The differences between the samples are small and between most of the samples neglectable with respect to the error bars. Regarding the flexural strength, sample MKDA 60 is performing very well again, as well as sample MKW 73. All other mortars are within the range of the flexural strength of the reference sample with 100 % OPC which reaches 7.6 MPa.

7.2.7 Conclusions

The first industrial trial was very successful. It was possible to produce a reactive calcined clay product that can be used as pozzolanic material for cementitious binders with the existing equipment at Avelar plant. Of course the process is by far not optimized yet, regarding for example the production capacity, the fuel mixture and the temperature measurement of the material. Detailed information about these parameters can be found in the mentioned report from Cristina Freire (for internal use only). The report contains also a calculation over the estimated costs of a calcined clay production.

The compressive strength after 28 days of curing, of the standard mortars with 20 % replacement of OPC by calcined clay was for all samples higher than the compressive strength of the reference mortar with 100 % OPC and in relative values compared to the reference comparable with the compressive strength of standard mortars containing calcined clay from the pilot production at IBU-Tec. Therefore it was aimed to start a second full scale trial to even increase the reactivity of the material by optimizing the process and reducing the LOI of the material slightly further.

The different milling methods can have an influence on the final product especially at calcining temperatures below 650 ºC. It could be shown that wet milling can rehydrate metakaolin to kaolinite, which could significantly reduce the reactivity of the final product on prolonged milling times. Consequently wet milling will not be the favorable choice for milling calcined AB1080 clay in future production. The pendular mill was not able to ground the calcined clay to a $d_{50} < 3$ µm. The higher particle size decreased slightly the reactivity of the sample MKDP 73 compared to the other samples. Yet the reactivity was still good enough not to exclude this milling type for a future production process. Furthermore the pendular mill lies only in a distance of 41 km from the calcination plant in Avelar. In contrast to that the continuous ball mill is located in Mangualde (FERMICA – Mangualde, MOTA Group), which is about 150 km away from the plant. In this case the lower costs for transportation can outbalance the small decrease in reactivity.

8 Compressive and flexural strength of mortars with higher replacement levels of cement by calcined clays

Based on the good results obtained with Søvind Marl and AB1080 it was decided to test both clays in mortars with higher replacement levels of OPC. Standard mortars were prepared as described in chapter 3.5 by replacing 20, 35, 50 & 65 % of OPC with calcined Søvind Marl and calcined AB1080 respectively. The mortars were cured for up to 1 year at 20 °C. The calcined marl/clay samples were chosen according to the availability in the storage.
The samples of Søvind Marl produced at the pilot scale installation at IBU-Tec were almost used up for laboratory experiments. Hence, the material marked Hinge 900 from the industrial trial was taken for this experiments. OPC was replaced with calcined marl by volume assuming a density of 2.65 g/cm^3 for calcined marl and 3.15 g/cm^3 for cement.
The mortar tests with AB1080 were performed with AB1080 clay calcined at 800 °C at pilot scale installation at IBU-Tec and the replacement was done by mass in this case. Based on calculations using a density of 2.65 g/cm^3 and 3.15 g/cm^3 for metakaolin (here AB1080) and OPC respectively a replacement of 20, 35, 50 & 65 weight % is equivalent to about 23, 39, 54 & 69 volume %, respectively.

Figure 8-1 and Figure 8-2 show the compressive and flexural strength development of standard mortars from 1 to 365 days, where 20, 35, 50 and 65 % of OPC are replaced with calcined Søvind Marl. The respective strength values with their standard deviations are given in Table 8-1and Table 8-2.
At early ages (1 & 3 days) the compressive strength of the mortars is reduced the higher the replacement level of OPC. Nevertheless the strength of the mortar with 50 % replacement by calcined marl is with about 10 MPa high enough for removing formwork of concrete in practice. But already at 7 days the compressive strength of mortars with 20 and 35 % replacement is very close to the strength of the reference mortar with no replacement. At 28 days the mortars with 20 and 35 % replacement of cement by calcined marl score higher than the reference, while 50 % replacement is almost equal to the reference. After 90 days of curing the mortars with 20 and 35 % replacement have still a higher compressive strength than the reference mortar with 100 % OPC. After 1 year the mortar containing 35 %

calcined marl has about the same strength as the reference while with 20 % replacement the compressive strength is still higher. Even with 50 % replacement of cement the compressive strength is very close to that of the reference after 365 days of curing.

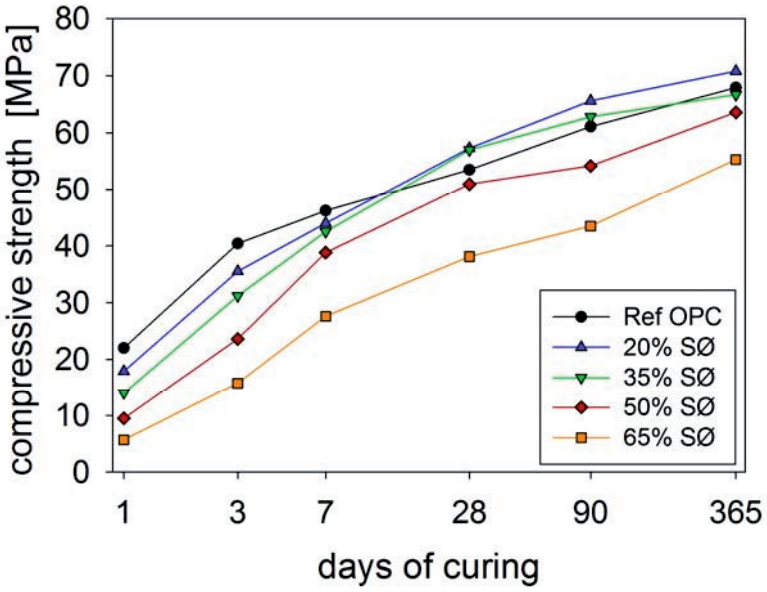

Figure 8-1: Compressive strength of standard mortars with 20, 35, 50 and 65 % replacement of OPC by volume with calcined Søvind Marl, cured for 1, 3, 7, 28, 90 and 365 days at 20 °C

Table 8-1: Compressive strength development for mortar mixes where cement is replaced with marl on a volume basis

Cement replacement by marl [%]	Average compressive strength ± standard deviation [MPa] at different ages [days]					
	1	3	7	28	90	365
0 (Reference)	22.0 ± 0.3	40.4 ± 1.0	46.2 ±1.0	53.5 ± 0.6	61.1 ± 1.6	67.9 ± 0.9
20	17.9 ± 0.4	35.5 ± 0.5	44.0 ± 1.0	57.3 ± 1.3	65.6 ± 0.9	70.8 ± 1.3
35	14.0 ± 0.1	31.2 ± 0.4	42.5 ± 0.6	57.0 ± 0.8	62.8 ± 1.6	66.7 ± 3.7
50	9.5 ± 0.2	23.6 ± 0.3	38.8 ± 0.4	51.0 ± 1.2	54.2 ± 1.1	63.6± 1.3
65	5.7 ± 0.1	15.8 ± 0.3	27.6 ± 0.1	38.1 ± 1.2	43.5 ± 1.0	55.3 ± 2.0

With 65 % replacement of cement by calcined marl the strength of mortars is constantly below that of the reference. This is probably due to a lot of unreacted clay particles since calcium hydroxide is depleted. This may also be indicated by the fact that the reference strength continues to increase from 28 to 90 days, while the increase is lower in the same period for 50 % replacement of cement by calcined marl. Figure 8-3 shows BSE images of the standard mortars with 35, 50 and 65 % replacement of OPC by calcined marl hydrated for 28 days at 20 °C compared to the reference mortar with no replacement of OPC (Figure 8-3a). In the reference mortar (Figure 8-3a) calcium hydroxide (CH) particles are clearly visible all over the matrix while one can hardly find CH in the mortars with 50 and 65 % replacement of OPC by calcined marl. This is supported by the results described in Chapter 5.4.3 about cement pastes containing calcined marl or AB1080. In the mortar containing 65 % calcined marl a lot of unreacted clay particles are visible in the matrix explaining the low strength development at these high replacement levels even though their similar grey values to the cement paste makes it difficult to spot with the naked eye.

Even though calcium hydroxide is depleted after 28 days there is still a significant further strength increase in the mortars with high replacement levels between 90 and 365 days. One reason for that might be a transformation of hydration products leading to higher stability instead of forming further new phases during an ongoing pozzolanic reaction at long curing times. Such a transformation of hydration products could not be directly detected with XRD and DTG in the clay/lime pastes. It could be an ongoing reaction of CAH phases with the calcium carbonate, continuously forming more stable carboaluminate hydrate phases. Also at a hydration temperature of 38 °C the formation of hydrogarnet (C_3AH_6) was observed. The transformation of calcium aluminate hydrate phases into more stable hydrogarnet is a phenomenon also known to occur after longer curing times. In Calcium Aluminate Cements (CAC) this transformation reaction was investigated in detail and it is well known that it can actually lead to higher porosity resulting in a strength decrease due to the higher density of C_3AH_6 compared to other calcium aluminate hydrates. However during the transformation reaction water is also set free which can react with yet unreacted cement to form further hydration products at long ages. If the water to cement ratio is sufficiently low, and unreacted cement is still present the transformation does not necessarily lead to a strength decrease.

In case there is transformation reaction setting free water, yet unreacted cement can react further to form additional CH which would then be available for a late pozzolanic reaction with the unreacted calcined clay particles.

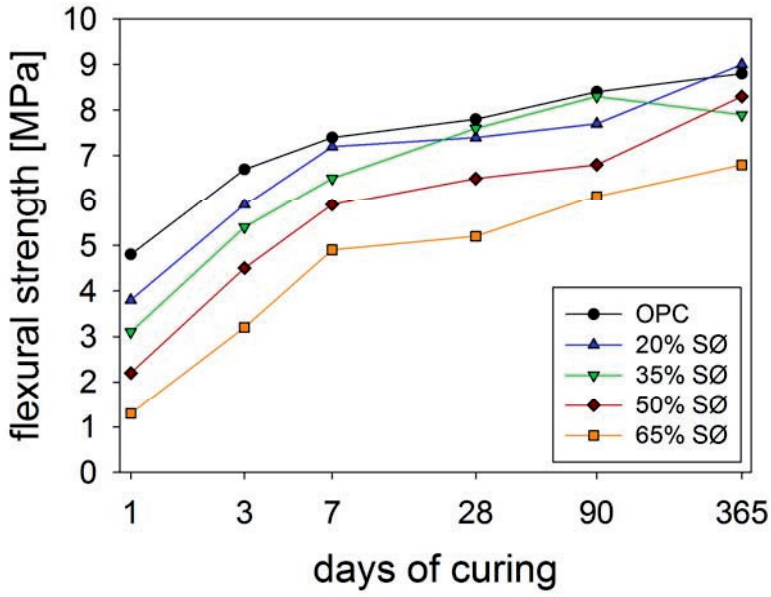

Figure 8-2: Flexural strength of standard mortars with 20, 35, 50 and 65 % replacement of OPC by volume with calcined Søvind Marl, cured for 1, 3, 7, 28, 90 and 365 days at 20 °C

Table 8-2: Flexural strength development for mortar mixes where cement is replaced with marl on a volume basis

Cement replacement by marl [%]	Average flexural strength ± Standard deviation [MPa] at different ages [days]					
	1	3	7	28	90	365
0 (Reference)	4.8 ± 0.1	6.7 ± 0.4	7.4 ± 1.0	7.8 ± 0.3	8.4 ± 0.4	8.8 ± 0.4
20	3.8 ± 0.3	5.9 ± 0.2	7.2 ± 0.2	7.4 ± 0.2	7.7 ± 0.6	9.0 ± 0.5
35	3.1 ± 0.1	5.4 ± 0.2	6.5 ± 0.2	7.6 ± 0.5	8.3 ± 0.2	7.9 ± 0.2
50	2.2 ± 0.1	4.5 ± 0.2	5.9 ± 0.3	6.5 ± 0.3	6.8 ± 0.4	8.3 ± 0.9
65	1.3 ± 0.1	3.2 ± 0.1	4.9 ± 0.2	5.2 ± 0.4	6.1 ± 0.3	6.8 ± 0.4

The flexural strength of mortars where OPC is replaced by calcined marl is reduced at all times compared to the reference except after 365 days where the mortar containing 20 % calcined marl scores a higher strength. However with 20 and 35 % replacement of OPC the flexural strength comes very close to the reference strength from 7 days onwards. 35 % replacement of OPC by calcined marl seems

to be the optimum between 28 and 90 days before decreasing again in performance after 1 year, but the decrease is only within 2 times the standard deviation and is hardly significant.

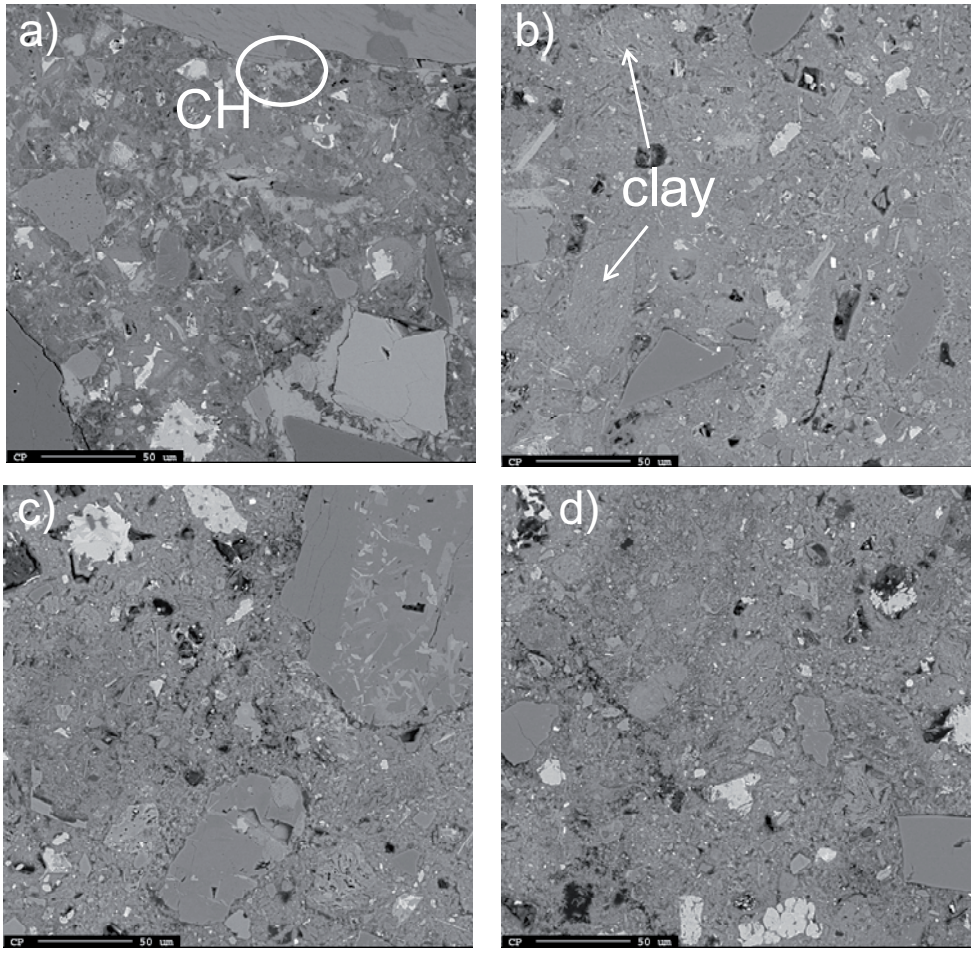

Figure 8-3: BSE images of standard mortars with 0 % (a-Reference), 35 % (b), 50 % (c) and 65 % (d) calcined marl as replacement for OPC, hydrated for 28 days at 20 °C.

Figure 8-4 and Figure 8-5 show the compressive and flexural strength development of standard mortars from 1 to 90 days, where 20, 35, 50 and 65 % of OPC are replaced with calcined AB1080 clay. The respective strength values with their standard deviations are given in Table 8-3 and Table 8-4.

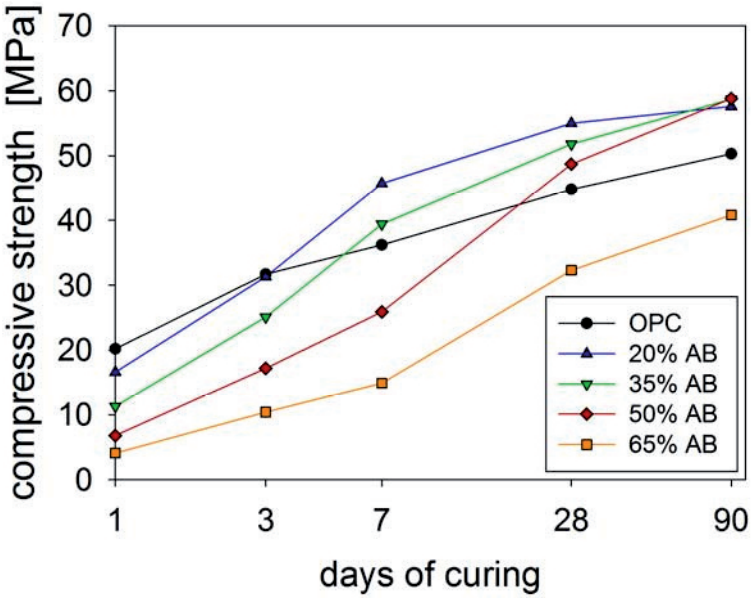

Figure 8-4: Compressive strength of standard mortars with 20, 35, 50 and 65 % replacement of OPC by volume with calcined AB1080, cured for 1, 3, 7, 28, 90 and 365 days at 20 °C

Table 8-3: Compressive strength development for mortar mixes where cement is replaced with calcined AB1080 on a mass basis

Cement replacement by marl [%]	Average compressive strength ± standard deviation [MPa] at different ages [days]				
	1	3	7	28	90
0 (Reference)	20.2 ± 1.1	31.7 ± 0.6	36.2 ± 0.7	44.8 ± 0.3	50.3 ± 1.4
20	16.6 ± 0.4	31.3 ± 0.5	45.7 ± 0.6	55.0 ± 2.1	57.6 ± 1.3
35	11.3 ± 0.2	25.1 ± 0.2	39.5 ± 0.3	51.8 ± 2.1	58.7 ± 1.0
50	6.8 ± 0.1	17.2 ± 0.2	25.9 ± 0.5	48.7 ± 0.5	58.8 ± 1.1
65	4.1 ± 0.1	10.4 ± 0.20	14.9 ± 0.8	32.3 ± 0.4	40.8 ± 1.2

The strength of the reference mortar with 100 % OPC is lower compared to the tests made with Søvind Marl as it passed some time between the two test series and hence different batches of cement were used. At 1 day curing the compressive strength of the mortars is reduced with increasing replacement level of OPC. But already after 3 days the mortar with 20 % replacement of OPC by calcined AB1080 scores a higher compressive strength than the reference. After 7 days mortars with 20 and 35 % calcined AB1080 perform better than the reference. The strength development between 7 and 28 days of the mortar containing 50 and 65 % calcined AB1080 is faster than the strength development of mortars with lower OPC replacement levels. Consequently, after 28 days also the mix containing 50 % calcined AB1080 is catching up and gaining a higher strength than the reference. After curing for 90 days the mortars with 20, 35 and 50 % replacement of OPC by calcined marl achieve about the same strength with about 58 MPa. This is about 15 % higher than the reference strength. The compressive strength of the mortars containing 65 % calcined AB1080 is at all ages below the compressive strength of the reference. Even though the relative strength increase between 7 and 28 days is faster for the mortars with 50 and 65 % replacement of OPC by calcined clay compared to the other mixes, it is slower at earlier ages. This shows that the strength development in the mortars is retarded for the higher replacement levels of OPC. It seems to take some time before sufficient CH is produced to react with the high amounts of calcined clay. In fact between 7 and 28 days and between 28 and 90 days the percentage increase in compressive strength of the mortars containing cement blended with calcined clay is increased the higher the replacement level of cement. The compressive strength of the mortar with 20 % replacement of OPC by calcined AB1080 does not increase significantly after 28 days considering the standard deviations while the percentage strength increase in mortars containing 50 and 65 % calcined AB1080 by mass of cement is about 20 and 26 %. It seems that after 28 days of curing the limiting factor for further percentage strength increase is the amount of clay. In the mortar with 20 % replacement of OPC by calcined AB1080 almost all the available clay seems to have already reacted with CH. The strength of the reference mortar is still increasing (higher percentage increase than with 20 % replacement) after 28 days producing more CH. At late ages the pozzolanic reaction can take place more significant the more clay is available to react with the CH. On the other hand we showed with DTG and XRD that after a hydration for 28 days in cement pastes containing 50 % calcined AB1080 almost all CH was already consumed (Chapter 5.4.3). Assuming that more or less all CH produced from the cement hydration is consumed in the mortars with 50 and 65 % replacement of OPC by calcined AB1080 after 28 days the further high strength

increase might not only be due to the pozzolanic reaction. As explained before for the mortar tests with Søvind Marl a transformation of hydration products to more stable phases at later ages is a further possibility for the observed strength increase. The formation of hydrogarnet was only clearly observed in calcined clay/lime pastes hydrated at 38 °C (Chapter 5.4.2.2). But it is also known that the occurrence of hydrogarnet is associated with the presence of clay minerals at long curing times [58]. As mentioned the transformation reaction of calcium aluminate hydrates to hydrogarnet sets free water that can react further with yet unreacted clinker grains to form more CH which can be used in the pozzolanic reaction.

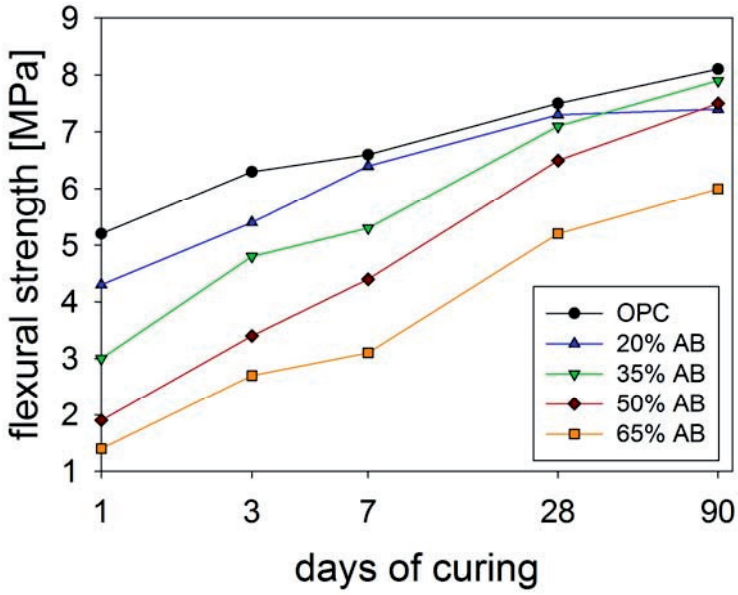

Figure 8-5: Flexural strength of standard mortars with 20, 35, 50 and 65 % replacement of OPC by volume with calcined AB1080, cured for 1, 3, 7, 28, 90 and 365 days at 20 °C

Again the flexural strength of mortars where OPC is replaced by calcined clay is reduced at all times compared to the reference. However the strength of mortars containing 20 % of calcined clay comes very close to the reference strength at 7 and 28 days. 35 % replacement of OPC by calcined marl seems to be the optimum replacement level after 90 days.

It is known that cements blended with natural pozzolanas have a higher water demand than OPC alone depending on the specific surface of the pozzolanas [58]. As described already in chapter 5.2.4 the use of a superplasticizer was therefore neces-

sary to keep a constant flow and good workability of the mortar mixes during mixing and casting. As expected the amount of superplasticizer increases with increasing amount of calcined marl/clay in our tests. The amount of superplasticizer used given in percent of the total dry weight is given in Table 8-5. It can be seen that the mortars containing calcined AB1080 need more than double as much superplasticizer as the mortar mixes with calcined Søvind Marl. One reason can be the higher specific surface of AB1080.

Table 8-4: Flexural strength development for mortar mixes where cement is replaced with calcined AB1080 on a mass basis

Cement replacement by marl [%]	Average flexural strength ± standard deviation [MPa] at different ages [days]				
	1	3	7	28	90
0 (Reference)	5.2 ± 0.3	6.3 ± 0.2	6.6 ± 0.2	7.5 ± 0.3	8.1 ± 0.2
20	4.3 ± 0.1	5.4 ± 0.2	6.4 ± 0.2	7.3 ± 0.2	7.4 ± 0.3
35	3.0 ± 0.2	4.8 ± 0.1	5.3 ± 0.1	7.1 ± 0.4	7.9 ± 0.4
50	1.9 ± 0.2	3.4 ± 0.2	4.4 ± 0.2	6.5 ± 0.2	7.5 ± 0.1
65	1.4 ± 0.1	2.7 ± 0.6	3.1 ± 0.3	5.2 ± 0.2	6.0 ± 0.1

Table 8-5: Amount of superplasticizer in percent of total dry binder weight (cement + calcined clay) for the mortar mixes with 20, 35, 50 and 65 % replacement of OPC by Søvind Marl and AB1080 respectively

Replacement level [%]	Søvind Marl	AB1080
20	0.18	0.40
35	0.35	0.77
50	0.52	1.55
65	0.91	2.24

9 Conclusions

Pozzolanicity tests measuring the lime consumption of different calcined clays in clay/lime pastes by means of thermal analysis as well as the compressive and flexural strength in mortar tests revealed a clear dependency of the reactivity of the calcined clays on their respective mineralogy. In terms of the main mineral phases of the different clays under investigation the reactivity increased in the following order:

(Illite) < (Smectite) < (Illite, Calcite) < (Smectite, Calcite) < (Kaolinite, Feldspar)

From literature it is known that illite is the least reactive and kaolinite the most reactive clay mineral with regard to pozzolanic reactivity. This tendency is also clearly prevailing in natural clays with substantial amounts of accessory non clay minerals. A minimum amount of < 30% kaolinite (Kal-Sorgila from Portugal) in the clay proved to be sufficient to give good pozzolanic activity after calcination. However it seems that the presence of calcite can boost the reactivity of illite and smectite rich clays as the clays containing mixtures of those two minerals are more reactive than the clays containing illite or smectite alone. Reason for that is probably the formation of a more reactive vitreous phase upon calcination in calcium carbonate rich clays. Nevertheless as the addition of calcite to AB1080 did not increase the reactivity in lime consumption as well as mortar tests of this kaolinite rich clay, the reactivity in combination with calcite might also be dependent on the actual source of calcium carbonate.
A reason for the high reactivity of Søvind Marl might be that the main calcium carbonate content is derived from coccoliths. The minute calcite crystals from biomineral origin seem to decompose earlier than calcite of inorganic origin. Although up to 5 % calcite are left in the most reactive state of Søvind Marl when calcined at 800-850 °C coccoliths could not be detected in the calcined marl and it was shown with SEM that coccoliths were completely decomposed. With XRD, DTG and FT-IR it was shown that crystalline calcite is left but the only calcium carbonate phases found under the SEM were inorganic calcite grains from a different origin. The Ca from the decomposed coccoliths together with the dehydroxylated meta-clay minerals seems to form a reactive glass phase of similar composition as the original raw marl.

The mineralogy of the different clays plays a much bigger role than the specific surface of the calcined materials. It was shown that the two clays with the highest

specific surface area when calcined are the two least reactive clays when it comes to lime consumption or strength development in mortars. For the Søvind Marl it was shown that the strength development in mortars can be very sensitive to the right temperature treatment but also the mineralogical composition. However at the optimum calcination temperature mortars with 20 % replacement of OPC by marl samples from three different boreholes (H2, H3, H4) had about the same strength within the standard deviations. This showed that despite minor variations in the mineralogy within the Søvind Marl deposit, it is possible to produce calcined marl of homogeneous quality.

XRD and DTG served as good methods to observe the degree of dehydroxylation and decomposition of clay and carbonate minerals. Together with FT-IR and SEM structural and micro-structural changes upon calcination like amorphization could be observed and help to explain why some clays are more reactive than others.
The two most reactive clays which experienced significant structural changes due to the heat treatment are the Søvind Marl and AB1080. The emphasis of this chapter lies therefore on these two clays.

In the most reactive state of the Søvind Marl all clay minerals are completely dehydroxylated but only kaolinite is completely transformed to metakaolin. From XRD data it seemed that the structures of smectite and illite are not completely destroyed as the main peaks partly remain although major structural changes were observed with other spectroscopical methods. Additionally the calcium carbonate is not completely decomposed. As explained above the calcium carbonate in Søvind Marl derives from two different sources. While the calcium carbonate of the coccoliths is completely decomposed, inorganic calcite grains partly remain stable upon calcination. The decomposing calcium carbonate of the coccoliths helps to form a vitreous reactive phase in the calcined clay. The remaining calcite however also plays an important role in the final product with regard to the pozzolanic reaction in clay/lime pastes and blended cements with the calcined marl. During the hydration of the calcined clay with calcium hydroxide C-S-H and C-A-H phases are formed which react further with the remaining calcite to form carboaluminate hydrate phases.
Observing the remaining calcium carbonate in the calcined marl is also a simple test method to guarantee the reactivity of the final product. It was shown that as soon also the inorganic calcite is completely decomposed recrystallization of new stable phases like anorthite, wollastonite, diopside, gehlenite etc. begins resulting in an immediate loss of reactivity. In all calcination tests (laboratory, pilot scale and industrial scale) the marl had a residual LOI (measured with TG) between 4-2

% in its most reactive state. This remaining LOI (after drying the sample) was entirely due to calcium carbonate confirming that about 8-4 % of calcite is left in the sample. Applying the described "LOI test", the residual LOI should be monitored during production and not get much lower than 2 % to guarantee good product quality. If the LOI becomes too small there is a high risk of recrystallization and decreased reactivity.

In the calcined marl the presence of increased amorphous content was confirmed with XRD, FT-IR and SEM. With WDX analysis it could be shown that the composition of the vitreous amorphous phase has a composition similar to that of the original clay material but with somehow higher Fe_2O_3 contents. As a result of the formation of these glassy particles the BET surface decreased considerably upon calcination, but is still very high with ~ 15 m^2/g.
HR-ICP-MS results showed increased release of Al ions but decreased release of Si ions in the calcined state. The Søvind Marl is the only investigated material where the release of silicon decreased from the raw to the calcined state. A separation of the tetrahedral and octahedral layer in the calcined clay minerals as observed with FT-IR spectroscopy might explain the increased release of Al ions due to increased exposure of the octahedral units, while the silicon is possibly more fixed in the new glassy phase as a network former. Infrared Spectroscopy, ^{27}Al-MAS-NMR and Mössbauer spectroscopy together revealed extensive structural changes and distortions beginning in the octahedral sheet of the clay minerals but also affecting the tetrahedral sheet leading to a highly disorganized metaclay. Almost all octahedrally coordinated Al is converted to tetrahedrally coordinated Al. With Mössbauer spectroscopy it was shown that the oxidation of iron during the calcination process results in strong distortions of the octahedral layer of the calcined clay mineral structure. Due to the redistribution of the octahedral charge the clay mineral changes from a tri-octahedral clay mineral containing Fe^{2+} to a dioctahedral clay mineral containing mainly Fe^{3+} in the structure. Accompanied with the inclusion of an extra oxygen atom in the structure for every second iron oxidized this leads to a relocation of oxygen atoms in the octahedral layer and thus to significant changes in the ligand structure of iron. Quadrupole splitting values and isomer shifts indicated that the coordination of Fe^{3+} is changing towards 5 and 6 while the coordination of Fe^{2+} is changing more towards 4-fold. As the iron is mainly located in the octahedrons of clay minerals substituted for Al, the observed changes are also representative for the changes in the Al environment.
The induced distortions in the octahedral layer do affect the tetrahedral layer as well probably resulting in a bending of the tetrahedra and changes of the bond length between different tetrahedral units. It could be shown the Al-O-Si bonds

may break up partly leading to separated Al and Si phases in the reactive marl state. But not only the connectivity between tetrahedral and octahedral sheet also the connectivity of the tetrahedra itself seems to be affected by the heat treatment as the intensity of the Si-O-Si deformation band decreased significantly.

In the AB1080 clay the only mineral that undergoes major changes upon heating seems to be kaolinite. Besides the dehydroxylation of illite this phase seems to be rather stable as XRD and SEM could show. Quartz and feldspars are also not affected by the short heat treatment. Nevertheless these non-clay minerals may play an important role for the overall good performance of this material. They may act as filler compounds in mortar and concrete and it could be shown that they serve as nucleation sites for hydration products and even are actively participating in the pozzolanic reaction.
Kaolinite is completely dehydroxylated and the transformation to metakaolin is completed already at temperatures around 700 °C. The BET surface area of the clay did not change much upon calcination. The BET surface area of about 19 m^2/g is in the same range as for silica fume, ensuring high reactivity. An increased background in the XRD diffractograms and the respective signals of FT-IR spectroscopy showed the presence of a phase of low crystallinity, probably reflecting metakaolin. While pure metakaolin compounds could be detected under the SEM there were no signs of a new vitreous phase. The formation of a vitreous phase seems to be only associated with the presence of calcium carbonate in clays as it was also observed for the Gniew clay and Søvind Marl. The metakaolin particles were very small with about 2-10 µm and it seemed like the clay sheets are separating from each other. A lower degree of connectivity of tetrahedral and octahedral sheet was moreover again observed with FT-IR for this material, too. In combination with ^{27}Al-MAS-NMR spectroscopy significant structural distortions and changes in the local environment of Al and Si were detected in the calcined state. In the metakaolin Al is present in 4, 5 and 6-fold coordination whereas 5 is the dominant coordination number. As a result of this disorganized metastable structure the release of Al and Si ions increased considerably upon calcination, which may increase the rate of the pozzolanic reaction in blended cementitious systems.

The calcium hydroxide consumption of the calcined clays under investigation in clay/lime pastes after 28 days of curing could be directly correlated to the 28 days strength of mortars where 20 % of OPC was replaced by the respective calcined clay. The results showed that the clays are mainly contributing to the strength gain

by pozzolanic reaction. Despite the high amounts of non-clay minerals like quartz and feldspars a filler effect of the materials seems to play only a minor role. As mentioned above some results indicated that the feldspars and quartz actually contribute to the pozzolanic reaction. Due to the high amount of non-clay minerals in natural clays the total sum of $SiO_2 + Al_2O_3 + Fe_2O_3$ cannot directly be correlated to the pozzolanic activity as it is described in the standards.

The main hydration products formed during the pozzolanic reaction of the calcined clays with calcium hydroxide are C-S-H phases with incorporation of Al, calcium aluminate hydrates like C_4AH_{13} and C_3AH_6 as well as strätlingite (C_2ASH_8) in case of hydration with AB1080. In the presence of calcite (Søvind Marl, Gniew, Rascoia and Sorgila) carboaluminate hydrate phases were the main crystalline hydration product as a result of the reaction of the calcium aluminate hydrates with calcium carbonate. When AB1080 was mixed with calcium carbonate the equilibrium also shifted from strätlingite towards carboaluminate hydrates with increasing calcium carbonate content. Substitution of iron from the clay minerals for aluminum was common in AFm and calcium aluminate hydrate phases. The formation of C_3AH_6 (hydrogarnet) is mainly associated with higher hydration temperatures (38 °C) or long curing times and is probably the result of a transformation reaction from unstable calcium aluminate hydrates to the more stable cubic C_3AH_6. The hydrogarnet included some silicon and katoite seemed to be the dominating phase.
The main calcium hydroxide consumption in clay/lime pastes took place during the first 28 days while the most reactive clay already reached the same lime consumption after 1 day as the least reactive clay after 28 days.

In cement/clay pastes with a calcined clay content of up to 50 % it was shown that after hydration for 28 days only about 2-5 % of calcium hydroxide was left in the different systems. In the cement pastes with Søvind Marl carboaluminate hydrates and ettringite were the main crystalline hydration products. Ettringite is still stable after 28 days and a transformation to monosulphate phases was not detected. The stabilization of ettringite might be induced by the favored formation of carboaluminate hydrate phases. In cement pastes with AB1080 strätlingite was only stable at a hydration temperature of 20 °C.
The early hydration of cement pastes blended with calcined Søvind Marl and calcined AB1080 was monitored with isothermal calorimetry and in-situ XRD. Early hydration is influenced by the additional aluminate brought into the system with increasing calcined marl/clay content, accelerating the formation of AFm

phases. The first appearance of CH and thus the silicate reaction also seems to take place at earlier times. However the induction period is not shortened so that the first setting of the cement pastes is not accelerated.

In a test series with calcined clays burned in the laboratory furnace it could be shown that the particle size distribution can have a significant effect on the reactivity of the final material while the cooling rate does not influence the reactivity at all. A short retention time of 30 min in the furnace at the respective temperature seems to increase the reactivity compared to a longer retention time of 2 h.

In two separate full scale industrial trials it was proven that both calcined Søvind Marl and calcined AB1080 can be produced on a large scale with very good quality. In case of Søvind Marl the atmosphere in the kiln does influence the temperature of highest reactivity. With increasing partial pressure of CO_2 the decomposition temperature of calcite increases and thus the temperature of best reactivity.
With further optimization of the production parameters both materials have great potential to be introduced into the market as pozzolanas for cementitious based binders.
Both clays can be considered as “industrial pozzolan” within the European cement standard (EN-197-1) and maybe feasible to make portland pozzolan cements with up to 55 % clinker replacement (CEM IV/B), considering the 28 day strength and sufficient early strength.

10 Future Work

Early hydration of blended cements with calcined clay as well as the early strength development of mortar and concrete specimens are very important issues and should be investigated in more detail. Especially the use of accelerators for good early strength even with high replacement levels of OPC by calcined clays should be a topic for future investigations. Actually one experiment was performed testing a "3-component admixture" [142] as accelerator for mortars containing cement blended with calcined Søvind Marl. In this test the 1 day compressive strength of mortars with 20 % replacement of OPC by calcined Søvind Marl increased from 10.9 without admixture to 15.8 MPa with the admixture.
Besides that a good workability of such systems is also very important for industrial use. Therefore further research should also look into rheology studies and the interaction of superplasticizers in calcined clay blended cements.
During this study concrete application were not tested. In order to get closer to the application and to confirm the results obtained for mortars, the reactivity of the calcined clays should be tested in concrete as well.

Nevertheless one must not forget the long term performance of mortars or concrete structures containing calcined clay blended cements. Durability measurements including, chloride ingress, sulfate attack, resistance to carbonation, resistivity measurements as well as capillary suction and saturation tests are currently performed for the Søvind Marl within the COIN-group (www.coinweb.no) and first results were already presented at international conferences. Future investigations should also cover the calcined AB1080 clay from Portugal.

The characterization of the raw and calcined clays is very fundamental and some of the presented methods could be used in more detail to gain further information. Besides ^{27}Al-MAS-NMR, ^{29}Si-MAS-NMR could help to complete the understanding of structural changes going on in the clay minerals upon calcination. However it was tried to measure and for the Søvind Marl the signal to noise ratio for ^{29}Si-MAS-NMR was too high to get a quality spectra that allows interpretation. XRD and FT-IR could be used additionally for quantitative investigations besides the qualitative phase development. Especially the quantification of the amorphous content in the calcined clays could be very interesting to follow and thus also the exact composition of the amorphous phases present in the calcined clays.

Different SEM techniques could be used to get a better insight of microstructural changes in calcined clay blended cements and mortars. Significant changes are to expect in the pore structure and interfacial transition zones etc.

The hydration products formed in calcined clay blended cements differ in most cases considerably from those formed in ordinary Portland cement. Especially the incorporation of elements deriving from the clay minerals might influence the stability of some phases. For example the incorporation of alkali and earth-alkali ions in different phases, iron in AFm-phases and aluminum in the C-S-H phase. Especially the shape and structural changes in the C-S-H phase should stand in more focus. A higher degree of polymerization and connectivity could explain the high strength and further strength gain at long ages in mortars with high replacement levels even when calcium hydroxide is already consumed.

A small additional lab scale experiment showed that a dry mix of calcined marl, calcium hydroxide and gypsum mixed to a paste with an alkaline solution hardened and formed substantial amounts of ettringite as main crystalline phase. Such systems could be suitable for ettringite based cementitious free binders and could be of interest as ready mix products for Saint-Gobain Weber. This topic will also be further pursued in COIN.

Full scale industrial trials showed that it is possible to produce calcined marl/clay with existing equipment in Leca plants. Nevertheless there were minor problems with the temperature measurement, air flow and fuel adjustments. The right temperature in the kiln is very important for the product quality and at temperatures below 800 °C the use of biofuels like raps oil can be an option. After further trials and more knowledge about the optimum production parameters it is maybe worth considering energy optimized custom build kilns for calcined clays with for example integrated thermocouples in different areas and more stable atmospheric control.

Literature

1. Cement Industry Energy and CO2 Performance - "Getting the numbers right". *WBCSD - World Business Council for Sustainable Development - The cement sustainability initiative* (2011).
2. Cement Technology Roadmap 2009 - Carbon emissions reduction up to 2050. *WBCSD - World Business Council for Sustainable Development* (2009).
3. Oss, H.G.v. Cement - Annual Publication 2012. in *Mineral Commodity Summaries, Cement Statististics and Information* (USGS - U.S. Geological Survey, 2012).
4. World Cement Production 2011. *European Cement Association* (2012).
5. Kurdowski, W. Cement Manufacture. in *Structure and Performance of Cements - 2nd Ed.* (eds. Benstedt, J. & Barnes, P.) (Taylor & Francis, New York, 2009).
6. Stark, J. & Wicht, B. *Zement und Kalk*, (Birkhäuser verlag, Basel, 2000).
7. Pöllmann, H. Composition of cement phases. in *Structure and Performance of Cements* (eds. Benstedt, J. & Barnes, P.) (Taylor & Frabcis, New York, 2009).
8. Worrel, E., Price, L., Martin, N., Hendriks, C. & Meida, L.O. Carbon Dioxide Emissions From The Global Cement Industry. *Annual Review of Energy and Environment* **26**, 303-329 (2001).
9. Mehta, P.K. Concrete Technology for Sustainable Development. *Concrete International* **21**, 47-53 (1999).
10. Schneider, M., Romer, M., Tschudin, M. & Bolio, H. Sustainable cement production—present and future. *Cement and Concrete Research* **41**, 642-650 (2011).
11. Damtoft, J.S., Lukasik, J., Herfort, D., Sorrentino, D. & Gartner, E.M. Sustainable development and climate change initiatives. *Cement and Concrete Research* **38**, 115-127 (2008).
12. Gartner, E. Industrially interesting approaches to “low-CO2” cements. *Cement and Concrete Research* **34**, 1489-1498 (2004).
13. Fernandez, R., Martirena, F. & Scrivener, K.L. The origin of the pozzolanic activity of calcined clay minerals: A comparison between kaolinite, illite and montmorillonite. *Cement and Concrete Research* **41**, 113-122 (2011).
14. Bergaya, F. & Lagaly, G. General Introduction: Clays, Clay Minerals, and Clay Science. in *Handbook of Clay Science*, Vol. 1 (eds. Bergaya, F., Theng, B.K.G. & Lagaly, G.) (Elsevier, Developments in Clay Science, 2006).
15. Guggenheim, S. & Martin, R.T. Definition of clay and clay minerals: Joint report of the AIPEA nomenclature and CMS nomenclature committeess. *Clays and Clay Minerals* **43**, 255-256 (1995).

16. Moore, D.M. & Reynolds, R.C. *X-Ray Diffraction and the Identification and Analysis of Clay Minerals*, (Oxford University Press, Inc, New York, 1989).
17. Wentworth, C.K. A Scale of Grade and Class Terms for Clastic Sediments. *The Journal of Geology* **30**, 377-392 (1922).
18. Alling, H.L. A Metric Grade Scale for Sedimentary Rocks. *The Journal of Geology* **51**, 259-269 (1943).
19. Heim, D. *Tone und Tonminerale - Grundlagen der Sedimentologie und Mineralogie*, (Ferdinand Enke Verlag, Stuttgart, 1990).
20. Murray, H.H. *Applied Clay Mineralogy - Occurences, Processing and Application of Kaolins, Bentonites, Palygorskite-Sepiolite, and Common Clays*, (Elsevier, Developments in Clay Science, 2, 2007).
21. Galán, E. Genesis of Clay Minerals. in *Handbook of Clay Science*, Vol. 1 (eds. Bergaya, F., Theng, B.K.G. & Lagaly, G.) (Elsevier Ltd., 2006).
22. Okrusch, M. & Matthes, S. *Mineralogie - Eine Einführung in die spezielle Mineralogie, Petrologie und Lagerstättenkunde*, (Springer Verlag, Berlin Heidelberg, 2005).
23. De Carlo, E.H., McMurtry, G.M. & Yeh, H.-W. Geochemistry of hydrothermal deposits from Loihi submarine volcano, Hawaii. *Earth and Planetary Science Letters* **66**, 438-449 (1983).
24. Kristmannsdottir, H. Alteration of Basaltic Rocks by Hydrothermal-Activity at 100-300°C. in *Developments in Sedimentology*, Vol. Volume 27 (eds. Mortland, M.M. & Farmer, V.C.) 359-367 (Elsevier, 1979).
25. Marumo, K. & Hattori, K.H. Seafloor hydrothermal clay alteration at Jade in the back-arc Okinawa Trough: mineralogy, geochemistry and isotope characteristics. *Geochimica et Cosmochimica Acta* **63**, 2785-2804 (1999).
26. McMurtry, G.M., Chung-Ho, W. & Hsueh-Wen, Y. Chemical and isotopic investigations into the origin of clay minerals from the Galapagos hydrothermal mounds field. *Geochimica et Cosmochimica Acta* **47**, 475-489 (1983).
27. Press, F. & Siever, R. *Allgemeine Geologie - Einführung in das System Erde*, (Spektrum Akademischer Verlag, Heidelberg, 2003).
28. www.mindat.org.
29. Brigatti, M.F., Galan, E. & Theng, B.K.G. Structures and Mineralogy of Clay Minerals. in *handbook of Clay Science*, Vol. 1 (Elsevier Ltd., 2006).
30. Rösler, H.J. *Lehrbuch der Mineralogie*, (VEB Deutscher Verlag für Grundstoffindustrie, Leipzig, 1987).
31. http://pubs.usgs.gov/of/2001/of01-041/htmldocs/clays/kaogr.htm. (U.S. Geological Survey).
32. Kumar, S.*, et al.* Mechanical activation of granulated blast furnace slag and its effect on the properties and structure of portland slag cement. *Cement and Concrete Composites* **30**, 679-685 (2008).

33. Murgier, S., Zanni, H. & Gouvenot, D. Blast furnace slag cement: a 29Si and 27Al NMR study. *Comptes Rendus Chimie* **7**, 389-394 (2004).
34. Pal, S.C., Mukherjee, A. & Pathak, S.R. Investigation of hydraulic activity of ground granulated blast furnace slag in concrete. *Cement and Concrete Research* **33**, 1481-1486 (2003).
35. Yeau, K.Y. & Kim, E.K. An experimental study on corrosion resistance of concrete with ground granulate blast-furnace slag. *Cement and Concrete Research* **35**, 1391-1399 (2005).
36. Lothenbach, B., Scrivener, K. & Hooton, R.D. Supplementary cementitious materials. *Cement and Concrete Research* **41**, 1244-1256 (2011).
37. Mueller, C.J., PhD Thesis, Pozzolanic activity of natural clay minerals with respect to environmental geotechniques, ETH Zuerich, No. 16299 (2005).
38. Kosmatka, S.H., Kerkhoff, B. & Panarese, W.C. Fly Ash, Slag, Silica Fume, and Natural Pozzolans. in *Design and Control of Concrete Mixtures* (Portland Cement Association, 2003).
39. Massaza, F. Pozzolanic Cements. *Cement and Concrete Composites* **15**, 185-214 (1993).
40. Mielenz, R.C., Witte, L.P. & Glantz, O.J. Effect of Calcination on Natural Pozzolans. in *Symposium on Use of Pozzolanic Materials in Mortars and Concrete* (American Society for Testing Materials, Baltimore, 1949).
41. García, R., Vigil de la Villa, R., Vegas, I., Frías, M. & Sánchez de Rojas, M.I. The pozzolanic properties of paper sludge waste. *Construction and Building Materials* **22**, 1484-1490 (2008).
42. Paya, J., MOnzo, J., Borrachero, M.V., Diaz-Pinzon, L. & Ordonez, L.M. Sugar-cane bagasse ash (SCBA): studies on its properties for reusing in concrete production. *Journal of Chemical Technology and Biotechnology* **77**, 321-325 (2002).
43. Villar-Cociña, E., Morales, E.V., Santos, S.F., Savastano Jr, H. & Frías, M. Pozzolanic behavior of bamboo leaf ash: Characterization and determination of the kinetic parameters. *Cement and Concrete Composites* **33**, 68-73 (2011).
44. ASTM. C618 - Standard Specification for Coal Fly Ash and Raw or Calcined Natural Pozzolan for Use in Concrete. (2012).
45. Sabir, B.B.W., S.; Bai, J. Metakaolin and calcined clays as pozzolans for concrete: a review. *Cement and Concrete Research* **23**, 441-454 (2001).
46. He, C., Osbaeck, B. & Makovicky, E. Pozzolanic reactions of six principal clay minerals: Activation, reactivity assessments and technological effects. *Cement and Concrete Research* **25**, 1691-1702 (1995).
47. Buchwald, A., Hohmann, M., Posern, K. & Brendler, E. The suitability of thermally activated illite/smectite clay as raw material for geopolymer binders. *Applied Clay Science* **46**, 300-304 (2009).

48. He, C., Makovicky, E. & Osbæck, B. Thermal stability and pozzolanic activity of raw and calcined mixed-layer mica/smectite. *Applied Clay Science* **17**, 141-161 (2000).
49. Bauer, A. & Berger, G. Kaolinite and smectite dissolution rate in high molar KOH solutions at 35° and 80°C. *Applied Geochemistry* **13**, 905-916 (1998).
50. Stumm, W. & Morgan, J.J. *Aquatic Chemistry - Chemical Equlibria and rates in Natural Water*, (John Wiley & Sons, Inc., 1996).
51. Madsen, F.T. & Müller-Vonmoos, M. Das Quellverhalten der Tone. in *Tonmineralogie und Bodenmechanik*, Vol. 133 39-50 (Lang, Zurich, 1988).
52. Shi, C. An overview on the activation of reactivity of natural pozzolans. *Canadian Journal of Civil Engineering* **28**, 778-786 (2001).
53. Baudet, G., Perrotel, V., Seron, A. & Stellatelli, M. Two dimensions comminution of kaolinite clay particles. *Powder Technology* **105**, 125-134 (1999).
54. Vdovic, N., Jurina, I., Skapin, S.D. & Sondi, I. The surface properties of clay minerals modified by intensive dry milling -- revisited. *Applied Clay Science* **48**, 575-580 (2010).
55. Komadel, P. Chemically modified smectites. *Clay Minerals* **38**, 127-138 (2003).
56. Panda, A.K., Mishra, B.G., Mishra, D.K. & Singh, R.K. Effect of sulphuric acid treatment on the physico-chemical characteristics of kaolin clay. *Colloids and Surfaces A: Physicochemical and Engineering Aspects* **363**, 98-104 (2010).
57. Önal, M., Sarikaya, Y. & Alemdaroglu, T. The Effect of Acid Activation on some physicochemical Properties of a Bentonite. *Turkish Journal of Chemistry* **26**, 409-416 (2002).
58. Massaza, F. Properties and applications of natural pozzolanas. in *Structure and Performance of Cements* (eds. Benstedt, J. & Barnes, P.) (Taylor & Francis, New York, 2009).
59. Ramachandran, V.S., Paroli, R.M., Beaudoin, J.J. & Delgado, A.H. Handbook of Thermal Analysis of Construction Materials. (William Andrew Publishing/Noyes, 2002).
60. Heller-Kalai, L. Thermally modified clay minerals. in *Handbook of Clay Science* (eds. Bergaya, F., Theng, B.K.G. & Lagaly, G.) (Elsevier Ltd., 2006).
61. Ambroise, J., Maximilien, S. & Pera, J. Properties of Metakaolin blended cements. *Advanced Cement Based Materials* **1**, 161-168 (1994).
62. Badogiannis, E., Kakali, G., Dimopoulou, G., Chaniotakis, E. & Tsivilis, S. Metakaolin as a main cement constituent. Exploitation of poor Greek kaolins. *Cement and Concrete Composites* **27**, 197-203 (2005).
63. Pera, J. Metakaolin and calcined clays. *Cement and Concrete Composites* **23**, iii (2001).

64. Vu, D.D., Stroeven, P. & Bui, V.B. Strength and durability aspects of calcined kaolin-blended Portland cement mortar and concrete. *Cement and Concrete Composites* **23**, 471-478 (2001).
65. Jones, T.R. Metakaolin as a pozzolanic addition to concrete. in *Structure and Performance of Cements* (eds. Benstedt, J. & Barnes, P.) (Taylor & Francis, New York, 2009).
66. Forrester, J.A. Burnt clay pozzolans. in *Proceedings of the meeting on small-scale manufacture of cement materials* 53-59 (Intermed Technological Publications, London, 1974).
67. Bleam, W., Dec, S. & Frye, J. ²⁷Al Solid-state nuclear magnetic resonance study of five-coordinate aluminum in augelite and senegalite. *Physics and Chemistry of Minerals* **16**, 817-820 (1989).
68. He, C., Makovicky, E. & Osbaeck, B. Thermal treatment and pozzolanic activity of Na- and Ca-montmorillonite. *Applied Clay Science* **10**, 351-368 (1996).
69. He, C., Makovicky, E. & Osbæck, B. Thermal stability and pozzolanic activity of calcined kaolin. *Applied Clay Science* **9**, 165-187 (1994).
70. He, C., Makovicky, E. & Øsbæck, B. Thermal stability and pozzolanic activity of calcined illite. *Applied Clay Science* **9**, 337-354 (1995).
71. Østnor, T. "Alternative Pozzolans" as supplementary cementitious materials in concrete. in *SINTEF Report* (SINTEF Building and Infrastructure, Trondheim, 2007).
72. Mota, L.*, et al.* Thermally treated soil clays as ceramic raw materials: Characterization by X-ray diffraction, photoacoustic spectroscopy and electron spin resonance. *Applied Clay Science* **43**, 243-247 (2009).
73. Trindade, M.J., Dias, M.I., Coroado, J. & Rocha, F. Mineralogical transformations of calcareous rich clays with firing: A comparative study between calcite and dolomite rich clays from Algarve, Portugal. *Applied Clay Science* **42**, 345-355 (2009).
74. Rathossi, C., Tsolis-Katagas, P. & Katagas, C. Technology and composition of Roman pottery in northwestern Peloponnese, Greece. *Applied Clay Science* **24**, 313-326 (2004).
75. Henning, O. & Knöfel, D. *Baustoff Chemie - Eine Einführung für Bauingenieure und Architekten*, (Bauverlag, Verlag für Bauwesen, Berlin, 1997).
76. Gartner, E.M., Young, J.F., Damidot, D.A. & jawed, I. Hydration of Portland Cement. in *Structure and Performance of Cements* (eds. Bendstedt, J. & Barnes, P.) (Taylor & Francis, New York, 2009).
77. Taylor, H.F.W. *Cement Chemistry*, (Thomas Telford Publishing, London, 1997).
78. Skrivener, K.L. & Capmas, A. Calcium Aluminate Cements. in *Lea's Chemistry of Cement and Concrete* (Elsevier Ltd., 2003).

79. Frías, M. & Cabrera, J. Pore size distribution and degree of hydration of metakaolin–cement pastes. *Cement and Concrete Research* **30**, 561-569 (2000).
80. Kostuch, J.A., Walters, G.V. & Jones, T.R. *High Performance concrete incorporating metakaolin - a review*, (University of Dundee, 1993).
81. Davis, R.E. A review of pozzolanic materials and their use in concrete. in *Symposium on use of pozzolanic materials in mortars and concrete* (American Society for testing Materials, 1949).
82. Wild, S., Khatib, J.M. & Jones, A. Relative strength, pozzolanic activity and cement hydration in superplasticised metakaolin concrete. *Cement and Concrete Research* **26**, 1537-1544 (1996).
83. Aras, A., Albayrak, M., Arikan, M. & Sobolev, K. Evaluation of selected kaolin clays as a raw material for the turkish cement and concrete industry.
84. Al-Ajeel, A.W.A., Abdul-Hameed, F.F., Al-Dahan, D.K., Abdul-Qadir, M.Q. & Ahmed, S.a.K. Evaluation of Al-Amij and Al-Hussainiyat Claystones (Iraqi western desert) for the Production of Pozzolana. *Iraqi Bulletin of Geology and Mining* **8**, 59-73 (2012).
85. Chakchouk, A., Samet, B. & Mnif, T. Study on the potential use of Tunisian clays as pozzolanic material. *Applied Clay Science* **33**, 79-88 (2006).
86. Ilic, B.R., Mitrovic, A.A. & Milicic, L.R. Thermal Treatment of Kaolin Clay to obtain Metakaolin. (ed. Materials, I.f.T.) (Belgrade, 2010).
87. Tironi, A., Trezza, M.A., Scian, A.N. & Irassar, E.F. Kaolinitic calcined clays: Factors affecting its performance as pozzolans. *Construction and Building Materials* **28**, 276-281 (2012).
88. Al-Rawas, A.A., Hago, A.W., Al-Lawati, D. & Al-Battashi, A. The Omani Artificial Pozzolans (Sarooj). *Cement, Concrete and aggregates* **23**, 19-26 (2001).
89. Østnor, T.D.W., K. Optimization of calcined clay. in *SINTEF Report* (SINTEF Building and Infrastructure, Trondheim, 2009).
90. Jenkins, R. & Snyder, R. *Introduction to X-Ray Powder Diffractometry*, (Wiley-Interscience, New York, 1996).
91. RSC. *Powder Diffraction: Theory and Practice*, (RSC, 2008).
92. CEN. Norsk Standard NS-EN 196-1. in *Methods of testing cement Part1: Determination of strength* (Standard Norge, 2005).
93. J.Sanz. Nuclear Magnetic Resonance Spectroscopy. in *Handbook of Clay Science*, Vol. 1 (eds. Bergaya, F., Theng, B.K.G. & G.Lagaly) (Developments in Clay Science, 2006).
94. Skipsted, J., Mägi, M. & Tarmak, M. Nuclear magnetic resonance spectroscopy and magnetic resonance imaging of cements and cement-based materials. in *Structure and Performance of Cements* (eds. Bendsted, J. & Barnes, P.) (Taylor & Francis, 2002).

95. Hore, P.J. *Nuclear magnetic Resonance*, (Oxford University Press, 1995).
96. Lippmaa, E., Mägi, M., Tarmak, M., Wieker, W. & Grimmer, A.R. A high resolution 29Si NMR study of the hydration of tricalciumsilicate. *Cement and Concrete Research* **12**, 597-602 (1982).
97. Müller, D., Gessner, W., Behrens, H.J. & Scheler, G. Determination of the aluminium coordination in aluminium-oxygen compounds by solid-state high-resolution 27AI NMR. *Chemical Physics Letters* **79**, 59-62 (1981).
98. Slichter, C.P. *Principles of magnetic resonance*, (Springer, Berlin, 1990).
99. Andrew, E.R., Bradbury, A. & Eades, R.G. Nuclear Magnetic Resonance Spectra from a Crystal rotated at High Speed. *Nature* **182**, 1659-1659 (1958).
100. Murad, E. Mössbauer Spectroscopy of Clays and Clay MInerals. in *Handbook of Clay Science*, Vol. 1 (eds. Bergaya, F., Theng, B.K.G. & Lagaly, G.) (Elsevier, 2006).
101. Tolchard, J. PhD Thesis, Structural, Electrochemical and Magnetic Studies of some Lithium Titanates and Lithium Titanium Ferrites, University of St. Andrews (2001).
102. Maddock, A.G. *Mössbauer Spectroscpy - Principles and Applications of the Techniques*, (Horwood Publishing, 1997).
103. Justnes, H. Mechanisms of calcined clay as pozzolana. in *SINTEF Report* (SINTEF Building and Infrastructure, Trondheim, 2010).
104. Oliviera, V. & Fiebiger, W. China Clays for the Sanitaryware Production from Portugal. *DKG* **84**, E 64-65 (2007).
105. Rocha, F. & Gomes, C. Palaeoenvironment of the Aveiro region of Portugal during the Cretaceous, based on clay mineralogy. *Cretaceous Research* **16**, 187-194 (1995).
106. Wilson, I.R. Kaolin deposits of Western Iberia. *Geoscience in south-west England* **9**, 214-217 (1998).
107. Prudêncio, M.I., *et al.* Clay mineral assemblages in weathered basalt profiles from central and southern Portugal: climatic significance. *CATENA* **49**, 77-89 (2002).
108. Heilmann-Clausen, C., Nielsen, O.B. & Gersner, F. Lithostratigraphy and depositional environments in the Upper Paleocene and Eocene of Denmark. *Bulletin of the geological society of Denmark* **33**, 287-323 (1985).
109. Hugget, J. Petrology and diagenesis of Paleogene clays from Ølst and Ålbækhoved, Denmark. *Bulletin of the geological society of Denmark* (1992).
110. Grønbech, G.L., Nielsen, B.N. & Ibsen, L.B. Comparison of Plasticity Index of Søvind Marl found by use of Casagrande Cup, Fall Cone apparatus and Loss on Ignition. in *DCE Technical Report* (University of Aalborg, 2010).

111. Okkels, N. & Juul, K. Søvindmergel. *GEO, Danmark*.
112. Blaszkiewicz, M. & Gruszka, B. Development and infill of Vistulian glacial Lake Gniew (N Poland): a sedimentological analysis. *Geological Quaterly* **49**, 449-462 (2005).
113. Galazka, D. & marks, L. Geology of the Lower Vistulia Region, Northern Poland. *Polish geological Institute Special Papers* **25**, 13-20 (2009).
114. J. Ambroise, M. Murat & Pera, J. Investigations on synthetic binders obtained by middle-temperature thermal dissociation of clay minerals. *Silicate Industries* **7**, 99-107 (1986).
115. Siddique, R. & Klaus, J. Influence of metakaolin on the properties of mortar and concrete: A review. *Applied Clay Science* **43**, 392-400 (2009).
116. van Aardt, J.H.P. & Visser, S. Reaction of Ca(OH)2 and of Ca(OH)2 + CaSO4.2H2O at various temperatures with feldspars in aggregates used for concrete making. *Cement and Concrete Research* **8**, 677-681 (1978).
117. Ramachandran, V.S. & Phil, D. *Applications of Differential Thermal Analysis in Cement Chemistry*, (Chemical Publishing Company, Inc., New York, 1969).
118. Tschegg, C., Ntaflos, T. & Hein, I. Thermally triggered two-stage reaction of carbonates and clay during ceramic firing -- A case study on Bronze Age Cypriot ceramics. *Applied Clay Science* **43**, 69-78 (2009).
119. Duminuco, P., Messiga, B. & Riccardi, M.P. Firing process of natural clays. Some microtextures and related phase compositions. *Thermochimica Acta* **321**, 185-190 (1998).
120. Schomburg, J. Thermal reactions of clay minerals: their significance as "archaeological thermometers" in ancient potteries. *Applied Clay Science* **6**, 215-220 (1991).
121. Bayliss, P. & Warne, S.S.J. DIFFERENTIAL THERMAL ANALYSIS OF SIDERITE-KAOLINITE MIXTURES. *American Mineralogist* **57**, 960-966 (1972).
122. Gallagher, P.K. & Warne, S.S.J. Thermomagnetometry and thermal decomposition of siderite. *Thermochimica Acta* **43**, 253-267 (1981).
123. Jaboyedoff, M., Bussy, F., Kübler, B. & Thelin, P. ILLITE "CRYSTALLINITY" REVISITED. *Clays and Clay Minerals* **49**, 156-167 (2001).
124. Sperinck, S., Raiteri, P., Marks, N. & Wright, K. Dehydroxylation of kaolinite to metakaolin-a molecular dynamics study. *Journal of Materials Chemistry* **21**, 2118-2125 (2011).
125. Lee, Y.J., Carr, S.W. & Parise, J.B. Phase transition upon K+ ion exchange into Na low silica X: Combined NMR and synchrotron X-ray powder diffraction study. *Chemical Materials* **10**, 2561-2570 (1998).

126. Rowland, R.A. Differential Thermal Analysis of Clays and Carbonates. 151-163 (Explorationa and Production Technical Division, Shell Oil Co., Houston).
127. Grim, R.E. & R.A., R. Differential Thermal Analysis of Clay Minerals and Other Hydrous Materials. Part 1. *American Mineralogist* **27**, 746-761 (1942).
128. Kakali, G., Perraki, T., Tsivilis, S. & Badogiannis, E. Thermal treatment of kaolin: the effect of mineralogy on the pozzolanic activity. *Applied Clay Science* **20**, 73-80 (2001).
129. Grim, R.E. & Rowland, R.A. Differential Thermal Analysis of Clay Minerals and Other Hydrous Materials. Part 2
American Mineralogist **27**, 801-811 (1942).
130. Justnes, H. Condensed silica fume as a cement admixture. in *Structure and Performance of Cements* (eds. Bensted, J. & Barnes, P.) (Taylor & Francis, 2009).
131. Tite, M.S. & Maniatis, Y. Examination of ancient pottery using the scanning electron microscope. *Nature* **257**, 122-123 (1975).
132. Nodari, L., Marcuz, E., Maritan, L., Mazzoli, C. & Russo, U. Hematite nucleation and growth in the firing of carbonate-rich clay for pottery production. *Journal of the European Ceramic Society* **27**, 4665-4673 (2007).
133. Eshel, G., Levy, G.J., Mingelgrin, U. & Singer, M.J. Critical Evaluation of the Use of Laser Diffraction for Particle-Size Distribution Analysis. *Soil Sci. Soc. Am. J.* **68**, 736-743 (2004).
134. Michot, L.J. & Villieras, F. Surface Area and Porosity. in *Handbook of Clay Science* (eds. Bergaya, F., B.K.G., T. & Lagaly, G.) (2006).
135. Dow, C. & Glasser, F.P. Alkali releases from crushed minerals and thermally activated constituents of metakaolin. *Advances in Cement Research* **15**, 137-143 (2003).
136. Scott, A.D., Ismail, F.T. & Locatis, R.R. Changes in interlayer potassium exchangeability induced by heating micas. in *International Clay Conference* (ed. Serratosa, J.M.) 467-479 (Division Ciencias CSIC, Madrid, 1972).
137. Seiffarth, T., Hohmann, M., Posern, K. & Kaps, C. Effect of thermal pre-treatment conditions of common clays on the performance of clay-based geopolymeric binders. *Applied Clay Science* (2012).
138. Aylward, G.H. & Findlay, T.J.V. *SI Chemical Data*, (Milton, 2002).
139. Berner, R.A. Distribution and diagenesis of sulfur in some sediments from the Gulf of California. *Marine Geology* **1**, 117-140 (1964).
140. Grønbech, G.L., Ibsen, L.B. & Nielsen, B.N. Chloride concentration and pHs influence on the Atterberg limits of Søvind Marl. in *DCE Technical Report No. 088* (Aalborg University
Department of Civil Engineering
Geotechnical Engineering Group, Aalborg, 2010).

141. SCHOONHEYDT, R.A. & JOHNSTON, C.T. SURFACE AND INTERFACE CHEMISTRY OF CLAY MINERALS. in *Handbook of Clay Science* (eds. F. Bergaya, Theng, B.K.G. & Lagaly, G.) (2006).
142. Hoang, K.D., Hardening Accelerator for Fly Ash Blended Cement, NTNU - Norwegian University of Science and Technology (2012).
143. Gadsden, J.A. *Infrared Spectra of Minerals and Related Inorganic Compounds* (Butterworth & Co, London, 1975).
144. Madejova, J. & Komadel, P. Baseline Studies of Clay Minerals Society Clays: Infrared Methods. *Clays and Clay Minerals* **49**, 410-432 (2001).
145. Schroeder, P.A. Infrared Spectroscopy in Clay Science. *CMS Workshop Lectures* **11**, 181-206 (2002).
146. Madejova, J. FTIR techniques in clay mineral studies. *Vibrational Spectroscopy* **31**, 1-10 (2003).
147. Chakchouk, A., Trifi, L., Samet, B. & Bouaziz, S. Formulation of blended cement: Effect of process variables on clay pozzolanic activity. *Construction and Building Materials* **23**, 1365-1373 (2009).
148. Bich, C., Ambroise, J. & Péra, J. Influence of degree of dehydroxylation on the pozzolanic activity of metakaolin. *Applied Clay Science* **44**, 194-200 (2009).
149. Wang, L., Zangh, M., Redfern, S.A.T. & Zangh, Z. Dehydroxylation and Transformation of the 2:1 Phyllosilicate Pyrophyllite at Elevated Temperatures: An Infrared Spectroscopy Study. *Clays and Clay Minerals* **50**, 272-283 (2002).
150. Ferone, C., Colangelo, F., Cioffi, R., Montagnaro, F. & Santoro, L. Use of reservoir clay sediments as raw materials for geopolymer binders. *Advances in Applied Ceramics* (2012).
151. Young, J.R. & Henriksen, K. Biomineralization within vesicles: The calcite of coccoliths. *Reviews in mineralogy and geochemistry* **54**, 189-215 (2003).
152. Brandl, P. Skype conversation about coccoliths and foraminifera. (University Erlangen-Nuremberg, Geozentrum Nordbayern, 2012).
153. Cölfen, H. & Antonietti, M. Mesocrystals: Inorganic Superstructures Made by Highly Parallel Crystallization and Controlled Alignment. *Angewandte Chemie International Edition* **44**, 5576-5591 (2005).
154. Zollfrank, C. e-mail conversation about element substitution in coccoliths. (TUM - Technische Universität München, Biogene Polymere, 2012).
155. Lauf, R.J., Harris, L.A. & Rawlston, S.S. Pyrite framboids as the source of magnetite spheres in fly ash. *Environmental Science & Technology* **16**, 218-220 (1982).
156. Bond, D.P.G. & Wignall, P.B. Pyrite framboid study of marine Permian–Triassic boundary sections: A complex anoxic event and its relationship to contemporaneous mass extinction. *Geological Society of America Bulletin* **122**, 1265-1279 (2010).

157. Czerewko, M.A., Cripps, J.C., Reid, J.M. & Duffell, C.G. The development of a new testing protocol for sulphur compounds in structural backfills. *Quarterly Journal of Engineering Geology and Hydrogeology* **36**, 133-142 (2003).
158. Schieber, J. & Baird, G. On the Origin and Significance of Pyrite Spheres in Devonian Black Shales of North America. *Journal of Sedimentary Research* **71**, 155-166 (2001).
159. Mozley, P.S. Relation between depositional environment and the elemental composition of early diagenetic siderite. *Geology* **17**, 704-706 (1989).
160. Carroll, D.L., Kemp, T.F., Bastow, T.J. & Smith, M.E. Solid-state NMR characterisation of the thermal transformation of a Hungarian white illite. *Solid State Nuclear Magnetic Resonance* **28**, 31-43 (2005).
161. Brown, I.W.M., MacKenzie, K.J.D. & Meinhold, R.H. The thermal reactions of montmorillonite studied by high-resolution solid-state ^{29}Si and ^{27}Al NMR. *Journal of Materials Science* **22**, 3265-3275 (1987).
162. Drachman, S.R., Roch, G.E. & Smith, M.E. Solid state NMR characterisation of the thermal transformation of Fuller's Earth. *Solid State Nuclear Magnetic Resonance* **9**, 257-267 (1997).
163. Sanz, J. Nuclear Magnetic Resonance Spectroscopy. in *Handbook of Clay Science*, Vol. 1 (eds. F. Bergaya, Theng, B.K.G. & Lagaly, G.) (Elsevier Ltd., 2006).
164. Skibsted, J., Report, ^{27}Al MAS NMR investigation of three clay samples. (Aarhus University - Department of Chemistry, 2011).
165. Rocha, J. & Klinowski, J. ^{29}Si and ^{27}Al magic-angle-spinning NMR studies of the thermal transformation of kaolinite. *Physics and Chemistry of Minerals* **17**, 179-186 (1990).
166. Singh, P., Bastow, T. & Trigg, M. Structural studies of geopolymers by 29Si and 27Al MAS-NMR. *Journal of Materials Science* **40**, 3951-3961 (2005).
167. Liu, Q., Spears, D.A. & Liu, Q. MAS NMR study of surface-modified calcined kaolin. *Applied Clay Science* **19**, 89-94 (2001).
168. MacKenzie, K.J.D., Brown, I.W.M., Meinhold, R.H. & Bowden, M.E. Outstanding Problems in the Kaolinite-Mullite Reaction Sequence Investigated by 29Si and 27Al Solid-state Nuclear Magnetic Resonance: I, Metakaolinite. *Journal of the American Ceramic Society* **68**, 293-297 (1985).
169. Zhou, L., Guo, J., Yang, N. & Li, L. Solid-state nuclear magnetic resonance and infrared spectroscopy of alkali feldspars. *Science in China (Series D)* **40**, 159-165 (1997).
170. Häggström, L. Report of a mössbauer spectroscopic study of calcinated clay. (University Uppsala, Department of Physics and Astronomy, Uppsala, 2011).

171. Murad, E. & Wagner, U. Clays and Clay Minerals: The firing products. *Hyperfine Interact*, 337-356 (1998).
172. Helgason, Ö., Gunnlaugsson, H., Steinthorsson, S. & Mørup, S. High temperature stability of maghemite in partially oxidized basalt lava. *Hyperfine Interact* **70**, 981-984 (1992).
173. Sidhu, P.S. Transformation of Trace Element-Substituted Maghemite to hematite. *Clays and Clay Minerals* **36**, 31-38 (1988).
174. Murad, E. & Cashion, J. *Mössbauer Spectroscopy of Environmental Materials*, (Kluwer Academic Press, 2004).
175. Takeda, M., Kawakami, O. & Tominaga, T. 57Fe Mössbauer Spectroscopic Studies of Structural Changes of Montmorillonite on Heating in Reduced Atmosphere. *Journal de Physique; Colloque C2; supplément au nr.3*, C2-472 (1979).
176. MacKenzie, K.J.D. & Rogers, D.E. Thermal and Mössbauer studies of iron-containing hydrous silicates : I. Nontronite. *Thermochimica Acta* **18**, 177-196 (1977).
177. Miller, J.G. Oxidizing Power of the Surface of Attapulgite Clay. in *12th Conference on Clays and Clay Minerals* 381-395 (Pergamon Press, New York, 1965).
178. Simopoulos, A., Kostikas, A. & Sigalas, I. Mössbauer Study of Transformations Induced in Clay by Firing. *Clays and Clay Minerals* **23**(1975).
179. Tichit, D.F., F.; Figueras,F.; Ducourant, B.; Mascherpa, G.; Gueguen, C.; Bousquet, J. Sintering of Montmorillonites pillared by Hydroxy-aluminium species. *Clazs and Clay Minerals* **36**, 369-375 (1988).
180. Schroeder, P.A. Far infrared, X-Ray powder diffraction, and chemical investigation of potassium micas. *American Mineralogist* **75**, 983-991 (1990).
181. Justnes, H. Hydraulic binders based on condensed silica fume and slaked lime. in *The 9th International Congress on the Chemistry of Cement*, Vol. 3 284-290 (New Dehli, India, 1992).
182. Bushnell-Watson, S.M. & Sharp, J.H. The detection of the carboaluminate phase in hydrated high alumina cements by differential thermal analysis. *Thermochimica Acta* **93**, 613-616 (1985).
183. Bonavetti, V.L., Rahhal, V.F. & Irassar, E.F. Studies on the carboaluminate formation in limestone filler-blended cements. *Cement and Concrete Research* **31**, 853-859 (2001).
184. Ipavec, A., *et al.* Carboaluminate phases formation during the hydration of calcite-containing portland cement. *Journal of the American Ceramic Society* **94**, 1238-1242 (2011).
185. DeWeerdt, K., Justnes, H., Kjellsen, K.O. & Sellevold, E. Fly Ash-Limestone Ternary Composite Cements: Synergy Effect at 28 days. *Nordic Concrete Research* **42**, 51-70 (2010).

186. Kuzel, H.J. & Pöllmann, H. Hydration of C3A in the presence of Ca(OH)2, CaSO4·2H2O and CaCO3. *Cement and Concrete Research* **21**, 885-895 (1991).
187. Dilnesa, B.Z., PhD Thesis, Fe-containing hydrates and their fate during cement hydration: thermodynamic data and experimental study, École Polytechnique Fédérale de Lausanne EPFL, (2011).
188. Midgley, H.G. Measurement of High-Alumina Cement - Calcium Carbonate Reactions using DTA. *Clay Minerals* **19**, 857-864 (1984).
189. Gabrovsek, R., Vuk, T. & Kaucic, V. The Preparation and Thermal Behavior of Calcium Monocarboaluminate. *Acta Chimica Slovenica* **55**, 942-950 (2008).
190. Andersen, M.D., Jakobsen, H.J. & Skibsted, J. A new aluminium-hydrate species in hydrated Portland cements characterized by 27Al and 29Si MAS NMR spectroscopy. *Cement and Concrete Research* **36**, 3-17 (2006).
191. Andersen, M.D., Jakobsen, H.J. & Skibsted, J. Incorporation of Aluminum in the Calcium Silicate Hydrate (C−S−H) of Hydrated Portland Cements: A High-Field 27Al and 29Si MAS NMR Investigation. *Inorganic Chemistry* **42**, 2280-2287 (2003).
192. Faucon, P., Delagrave, A., Richet, C., Marchand, J.M. & Zanni, H. Aluminum Incorporation in Calcium Silicate Hydrates (C−S−H) Depending on Their Ca/Si Ratio. *The Journal of Physical Chemistry B* **103**, 7796-7802 (1999).
193. Skibsted, J., Henderson, E. & Jakobsen, H.J. Characterization of calcium aluminate phases in cements by aluminum-27 MAS NMR spectroscopy. *Inorganic Chemistry* **32**, 1013-1027 (1993).
194. Murat, M. Hydration reaction and hardening of calcined clays and related minerals. 1. Preliminary investigations on metakaolinite. *Cement and Concrete Research* **13**, 259-266 (1983).
195. Frías, M. & Cabrera, J. Influence of MK on the reaction kinetics in MK/lime and MK-blended cement systems at 20°C. *Cement and Concrete Research* **31**, 519-527 (2001).
196. Frías, M. & Cabrera, J. The effect of temperature on the hydration rate and stability of the hydration phases of metakaolin–lime–water systems. *Cement and Concrete Research* **32**, 133-138 (2002).
197. Morsy, M.S. Effect of Temperature on Hydration Kinetics and Stability of Hydration Phases of Metakaolin-Lime Sludge-Silica Fume System. *Ceramics - Silikaty* **49**, 225-229 (2005).
198. Gameiro, A.L., Silva, A.S., Veiga, M.R. & Velosa, A.L. Lime-Metakaolin Hydration Products: A Microscopy Analysis. *Materials and Technology* **46**, 145-148 (2012).
199. Silva, P.S.D. & Glasser, F.G. Pozzolanic activation of metakaolin. *Advances in Cement Research* **4**, 167-178 (1992).

200. Love, C.A., Richardson, I.G. & Brough, A.R. Composition and structure of C–S–H in white Portland cement–20% metakaolin pastes hydrated at 25 °C. *Cement and Concrete Research* **37**, 109-117 (2007).
201. Kwan, S., LaRosa, J. & Grutzeck, M.W. 29Si and 27Al MASNMR Study of Stratlingite. *Journal of the American Ceramic Society* **78**, 1921-1926 (1995).
202. Sun, G.K., Young, J.F. & Kirkpatrick, R.J. The role of Al in C–S–H: NMR, XRD, and compositional results for precipitated samples. *Cement and Concrete Research* **36**, 18-29 (2006).
203. Mechti, W., Mnif, T., Samet, B. & Rouis, M.J. Effects of the Secondary Minerals on the Pozzolanic Activity of Calcined Clay: Case of Quartz. *International Journal of research and reviews in Applied Science* **12**, 61-71 (2012).
204. DeWeerdt, K., Kjellsen, K.O., Sellevold, E. & Justnes, H. Synergy between fly ash and limestone powder in ternary cements. *Cement and Concrete Composites* **33**, 30-38 (2010).
205. Lothenbach, B., Le Saout, G., Gallucci, E. & Scrivener, K. Influence of limestone on the hydration of Portland cements. *Cement and Concrete Research* **38**, 848-860 (2008).
206. Rojas, M.F., amp, x, as & Sánchez de Rojas, M.I. The effect of high curing temperature on the reaction kinetics in MK/lime and MK-blended cement matrices at 60 °C. *Cement and Concrete Research* **33**, 643-649 (2003).
207. Rahhal, V. & Talero, R. Calorimetry of Portland cement with metakaolins, quartz and gypsum additions. *Journal of Thermal Analysis and Calorimetry* **91**, 825-834 (2008).
208. Talero, R. & Rahhal, V. Calorimetric comparison of portland cements containing silica fume and metakaolin. *Journal of Thermal Analysis and Calorimetry* **96**, 383-393 (2009).
209. Fernandez, R., Calcined Clayey Soils as a Potential Replacement for Cement in Developing Countries, Ecole Polytechnique Federale De Lausanne EPFL (2009).
210. Greil, P., Glass and Ceramics: 1. Structure and Mechanical Properties, University of Erlangen-Nuernberg (2002).
211. Horváth, E., Frost, R.L., Makó, É., Kristóf, J. & Cseh, T. Thermal treatment of mechanochemically activated kaolinite. *Thermochimica Acta* **404**, 227-234 (2003).
212. Frost, R.L., Horváth, E., Makó, É., Kristóf, J. & Rédey, Á. Slow transformation of mechanically dehydroxylated kaolinite to kaolinite—an aged mechanochemically activated formamide-intercalated kaolinite study. *Thermochimica Acta* **408**, 103-113 (2003).

213. Rocha, J., Adams, J.M. & Klinowski, J. The rehydration of metakaolinite to kaolinite: Evidence from solid-state NMR and cognate techniques. *Journal of Solid State Chemistry* **89**, 260-274 (1990).

Appendix

Geological time scale:

The vast expanse of geological time has been separated into eras, periods, and epochs. The numbers included below refer to the beginnings of the division in which the title appears. The numbers are in millions of years.

Era	Period	Epoch	Plant and Animal Development
Cenozoic	Quaternary	Holocene (.01)	Humans develop
		Pleistocene (1.8)	
	Tertiary	Pliocene (5.3)	
		Miocene (23.8)	"Age of mammals"
		Oligocene (33.7)	
		Eocene (54.8)	
		Paleocene (65.0)	Extinction of dinosaurs and many other species.
Mesozoic	Cretaceous (144)	"Age of Reptiles"	First flowering plants
	Jurassic (206)		
	Triassic (248)		First birds Dinosaurs dominant.
Paleozoic	Permian (290)	"Age of Amphibians"	Extinction of trilobites and many other marine animals
	Carboniferous: Pennyslvanian (323)		First reptiles
	Carboniferous: Mississippian (354)		Large coal swamps Large Amphibians abundant.

	Devonian (417)	"Age of Fishes"	First insect fossils
	Silurian (443)		Fishes dominant First land plants
	Ordovician (490)	"Age of Invertibrates"	First fishes
	Cambrian (540)		Trilobites dominant First organisms with shells
Precambrian - comprises about 88% of geologic time (4500)			First multicelled organisms First one-celled organisms Origin of Earth

Adapted from Lutgens and Tarbuck. They cite the Geological Society of America as the source of the data

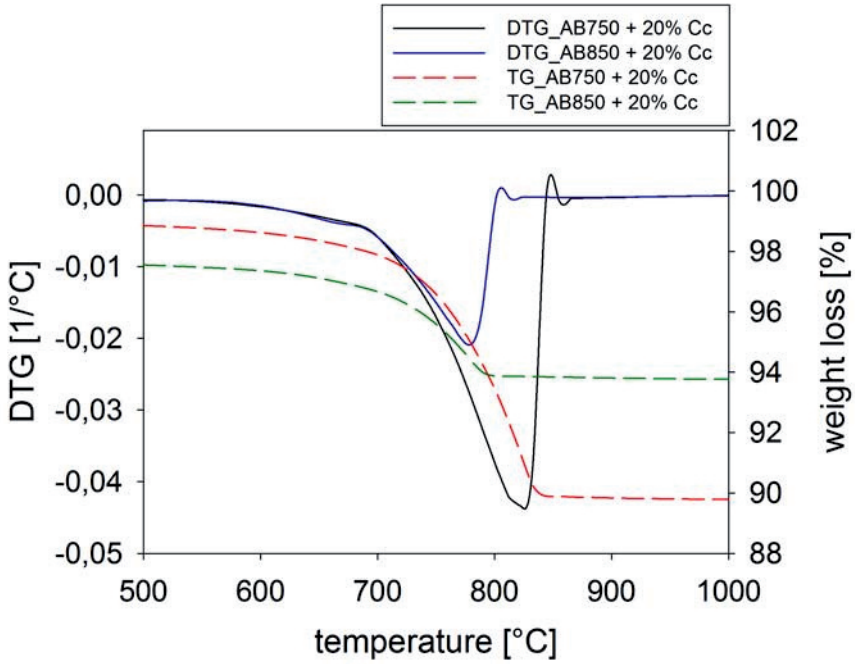

TG/DTG curves of AB1080 mixed with 20 % Calcite and calcined at 750 and 850 °C

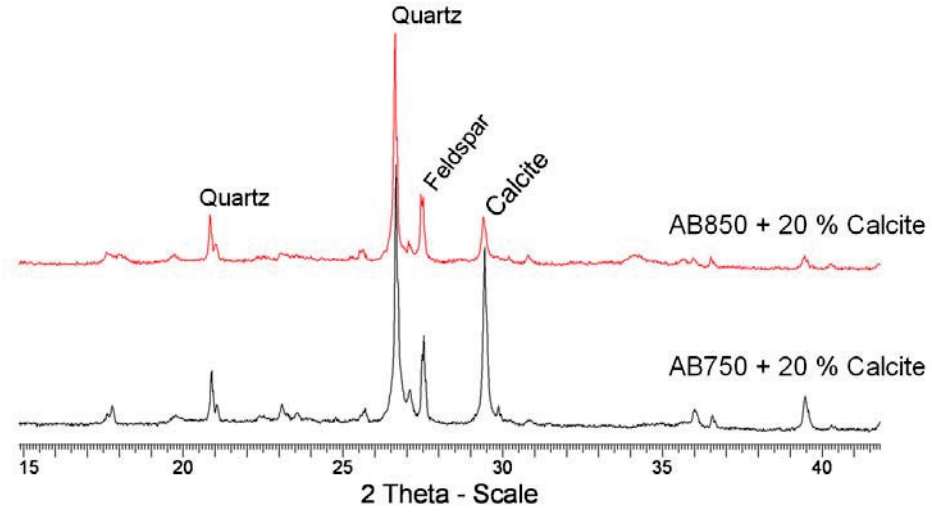

Diffractograms of AB1080 mixed with 20 % Calcite before calcination at 750 and 850 °C

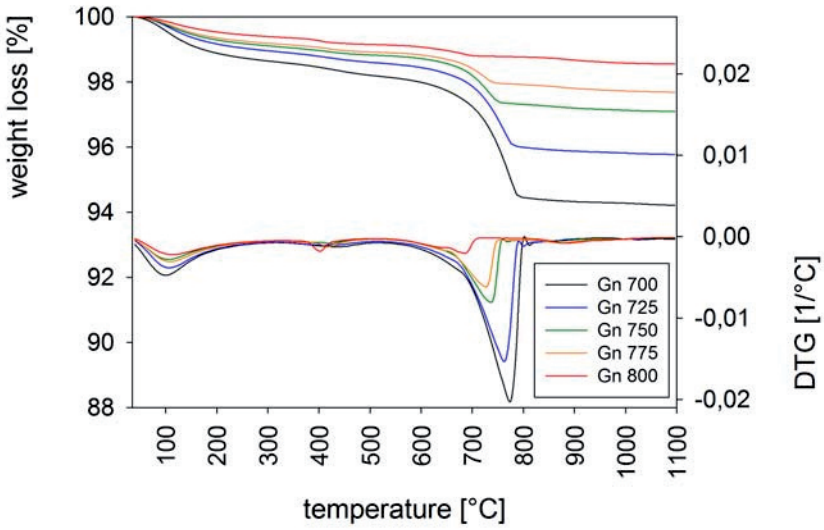

TG/DTG curves of Gniew clay calcined between 700 -800 °C

Solubility Calculations:

$K_{sp}\ CaCO_3 = 3.3 \times 10^{-9}$ mol/l
$K_{sp}\ Ca(OH)_2 = 6.4 \times 10^{-6}$ mol/l

$CaCO_3 \leftrightarrow Ca^{2+} + CO_3^{2-}$
$K_{sp} = [Ca^{2+}] \times [CO_3^{2-}]$ $\quad [Ca^{2+}] = [CO_3^{2-}]$
$K_{sp} = [Ca^{2+}]^2$
$[Ca^{2+}] = \sqrt{Ksp} = \sqrt{3.3 \times 10^{-9}} = 5.74 \times 10^{-5}$ mol/l
$[Ca^{2+}] = 5.74 \times 10^{-5}$ mol/l $\times$ 40.08 g/mol = **2.3 *mg/l***
(measured 8 mg/l)

$Ca(OH)_2 \leftrightarrow Ca^{2+} + 2OH^-$
$K_{sp} = [Ca^{2+}] \times [OH^-]^2$ $\quad [OH^-] = 2[Ca^{2+}]$
$K_{sp} = [Ca^{2+}]^3$
$[Ca^{2+}] = \sqrt[3]{Ksp}$
$[Ca^{2+}] = 0.019$ mol/l
$[Ca^{2+}] = 0.019$ mol/l $\times$ 40.08 g/mol = **744 mg/l**
(measured 73 mg/l)

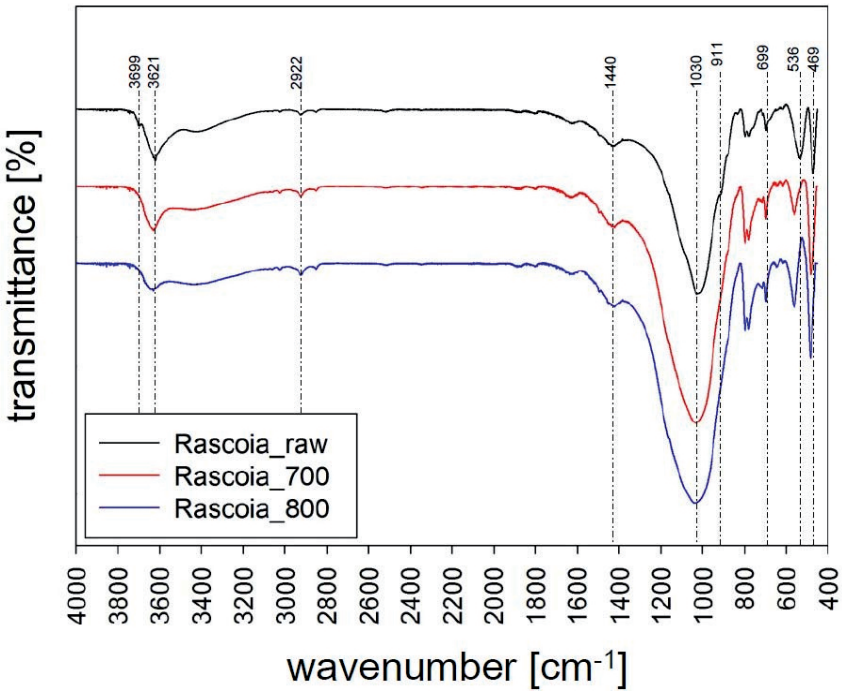

FT-IR spectra of Argila Rascoia in the raw and calcined state

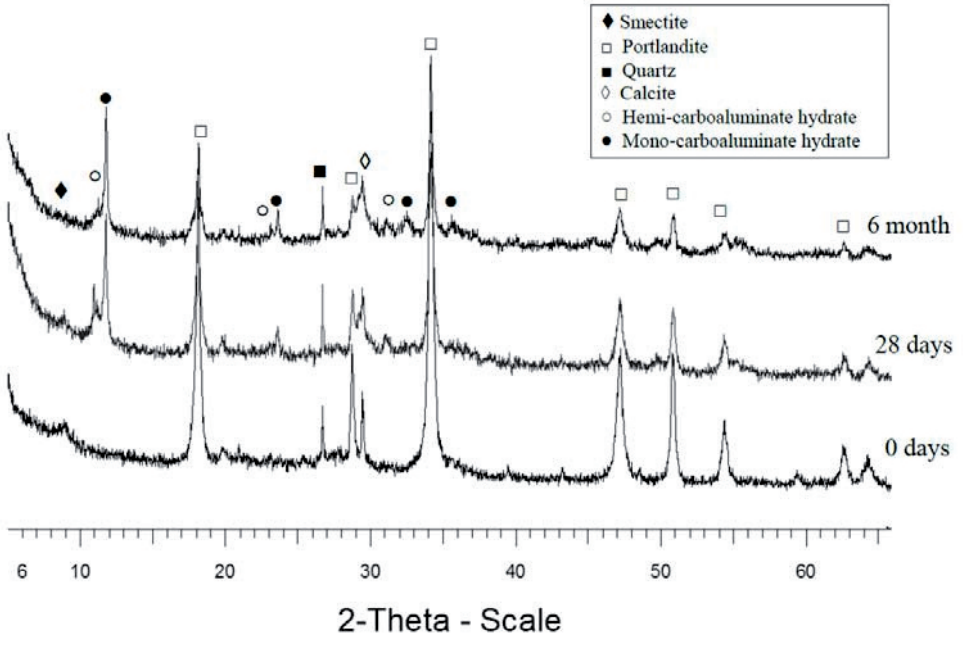

XRD of the calcined Søvind Marl/lime pastes hydrated for 28 days and 6 month at 20 and 38 °C

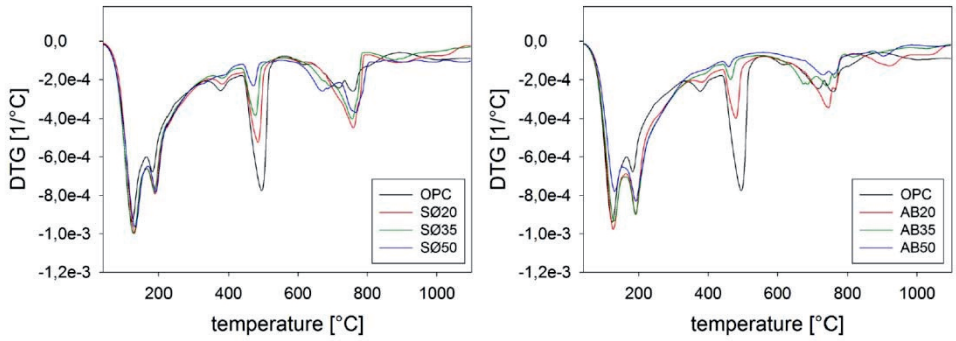

DTG of calcined clay/cement pastes with 20, 35 and 50 % calcined AB1080 (left) and calcined Søvind Marl (right), hydrated for 28 days at 38 °C